Université de Lille 1 SCIENCES ET TECHNOLOGIES

HABILITATION A DIRIGER DES RECHERCHES
UNIVERSITE DE LILLE 1 SCIENCES ET TECHNOLOGIES

N° d'ordre :

NOM/PRENOM DU CANDIDAT : LEMONNIER LOIC

Ecole doctorale : Biologie Santé
Laboratoire/Etablissement : Laboratoire de Physiologie Cellulaire, INSERM U1003, Université de Lille 1, Sciences et Technologies
Discipline : Sciences Naturelles

TITRE DE L'HDR :

Rôle des canaux ioniques dans le cancer de la prostate

JURY :

- Garant de l'habilitation : Pr Natalia Prevarskaya

- Rapporteurs : Pr Halima Ouadid-Ahidouch
  Pr Morad Roudbaraki
  Dr OlivierSoriani

- Examinateurs : Dr Dominique Collard
  Dr Thierry Capiod

SOUTENANCE : 22 Décembre 2017, 15h, Salle Pasteur (SN3)

Remerciements

L'exercice de style est obligatoire en pareilles circonstances, mais j'ai effectivement une longue liste de personnes à remercier pour l'aide qu'elles m'ont apporté durant ce long parcours m'amenant aujourd'hui à soutenir mon HDR.

Tout d'abord, merci aux membres de mon jury pour avoir accepté de prendre le temps de lire ce manuscrit, et de venir m'écouter en cette fin d'année 2017. Halima et Morad, nous nous connaissons depuis presque 20 ans, donc je compte sur vous pour glisser quelques anecdotes durant la soutenance ! Un grand merci pour votre aide durant toutes ces années ! Olivier, le hasard et une dégustation de vins de la région de Würtzburg nous ont amené à travailler ensemble : in vino veritas ? J'espère que cette collaboration donnera bientôt le jour à de jolis articles, et à un financement INCa ! Thierry, je te remercie d'avoir accepté de participer à ma soutenance, et je te fais confiance pour me poser quelques questions en rapport avec le CaR ! Dominique, un grand merci pour tes conseils littéraires, ainsi que pour ton aide dans le développement de nouvelles collaborations avec le Japon. C'est déjà grâce à toi que Lucile part 3 mois chez le Pr Sakai, et j'espère avoir la chance de rejoindre le laboratoire du Pr Takeuchi en avril prochain. Last but not least, un immense merci à Natacha pour son soutien indéfectible durant toute ma carrière ! C'est grâce à vous que je suis là aujourd'hui, 20 ans après notre première rencontre sur les bancs de la fac. Je vous souhaite un bon rétablissement !

Je remercie évidemment également tous mes collègues, passés et présents, en France et aux USA (Mohamed, Guillermo, Rebecca, Gary, Jim). La liste serait trop longue pour tous vous citer individuellement (coucou au club café !), mais sachez que si j'ai passé d'aussi bons moments et que j'ai continué jusqu'à aujourd'hui ce métier de chercheur, c'est grâce à vous ! Certains d'entre vous sont devenus de véritables amis (Stéphanie, Diana, Alexis, Marie, Sandra …), et vous êtes toujours les bienvenus si vous passez en France ! Je vais aussi faire une mention spéciale pour mes grands collaborateurs de ces dernières années, Mirto et Gabriel, en espérant que nous allons continuer à travailler ensemble encore quelques temps ! Je tiens également à remercier Lucile Noyer, la principale cause de ma soutenance

d’HDR, et ma première thésarde. J’espère que mes prochains étudiants seront aussi doués que toi (et je ne parle pas que de tes gâteaux au chocolat) !

Enfin, mes derniers remerciements vont à ma famille qui m’a soutenu dès le lycée dans mon projet fou de devenir un jour chercheur. Nous savons tous à quel point les chances de succès étaient faibles, et malgré tout, vous avez toujours cru en moi, et vous m’avez donné l’opportunité de pouvoir le tenter. C’est grâce à vous que je suis là aujourd’hui, c’est aussi votre réussite !

TABLE DES MATIERES

Quelques mots d'introduction	page 5
Curriculum vitae	page 7
Travaux de thèse	page 15
Travaux post-doctoraux	page 26
Travaux depuis mon retour en France	page 31
Conclusion	page 38
Bibliographie	page 40
Articles	page 43

Quelques mots d'introduction…

Bonjour à toi, ami lecteur !
Tout d'abord, un grand merci de prendre un peu de ton temps afin de lire ce manuscrit. Nous sommes aujourd'hui à l'heure d'un nouveau bilan, 13 ans après ma thèse (j'espère que tu n'es pas superstitieux !), et 9 ans après mon recrutement à l'Inserm. Qu'il est loin maintenant le temps où le jeune stagiaire que j'étais venait hanter les couloirs du Laboratoire de Physiologie Cellulaire, il y a presque 20 ans de cela ! Seuls nos « anciens » s'en souviennent, et ne manqueront pas de vous raconter une anecdote ou deux de cette époque, bien avant la labélisation de l'équipe par l'Inserm. Dire que j'ai changé est une évidence, mais de savoir si ce fut pour le pire ou pour le meilleur, ce sera à mes camarades et collègues de répondre. Aujourd'hui, le but est pour moi de passer un nouveau cap, et de pouvoir encadrer « officiellement » mes propres étudiants. Il était temps, me diras-tu ? Et oui, tu n'as pas tort, mais j'attendais (en vain) que l'HDR disparaisse. Il en est toujours question, mais au rythme où les choses évoluent, je ne verrais probablement pas son abrogation, donc me voilà à devoir la passer à mon tour… Bah, ce sera mon dernier bizutage par le système universitaire Français, donc autant en profiter !

Avant de te laisser commencer ta lecture, patient lecteur, voici quelques mots afin de te donner les éléments nécessaires à la compréhension de ce manuscrit. Tout d'abord, il n'est pas question de trouver un recueil exhaustif de mes travaux : j'ai en effet eu la chance de pouvoir être impliqué dans de nombreux projets collaboratifs, et ce dès le début de ma thèse. Je ne serai jamais assez reconnaissant envers les Pr Prevarskaya et Skryma qui m'ont donné cette opportunité dès mes débuts dans leur équipe, et sans laquelle je n'aurais probablement pas pu être recruté à l'Inserm. J'ai poursuivi cette démarche à travers les différentes étapes de ma carrière, et encore aujourd'hui, tu verras mon nom apparaître dans des articles ne portant pas directement sur mes sujets de recherche. Donc, si tu as besoin d'aide pour des expériences de patch-clamp ou d'imagerie calcique, n'hésites pas à me le dire : il y a toujours moyen que nous collaborions !

Le deuxième point sur lequel je veux insister, c'est que ce manuscrit ne contiendra pas non plus une longue introduction passant en détail la liste des canaux ioniques

sur lesquels j'ai travaillé et leurs propriétés respectives. D'autres avant moi ont déjà fait ce travail, probablement mieux que je ne le pourrais, et je te renvoie donc à leurs publications si tu intéressé par des détails complémentaires. En effet, ces 17 dernières années, j'ai étudié les canaux VRAC, les TRP, le SOC, les canaux potassiques (dans une moindre mesure) : cela ferait beaucoup de choses à couvrir, et pour toi une liste peu palpitante. Je te donnerai toutefois aux endroits stratégiques les dernières revues sur les domaines que je vais couvrir ici, et libre à toi d'en apprendre plus si tu le désires !

Le dernier point de ce prologue concerne le choix des articles qui seront présentés ici. En effet, je ne vais parler que des résultats « majeurs » que j'ai obtenus, ou tout du moins de ceux qui me semblent les plus importants ou représentatifs de ce que j'ai fait depuis mes débuts en Sciences. L'idée est également de mettre en évidence le fil conducteur de mon parcours, car oui, il existe une certaine logique dans le cheminement intellectuel m'ayant conduit jusqu'à aujourd'hui, même s'il a fortement été influencé par différentes rencontres et collaborations. Il est maintenant plus que temps de commencer ensemble ce voyage dans le passé, en nous replongeant au tout début du XXIème siècle, après une petite phase de présentations…

CURRICULUM VITAE

Etat-civil

Loïc LEMONNIER
Né le 10 août 1977 à Lille

Adresse professionnelle
Laboratoire de Physiologie Cellulaire, U1003
Bâtiment SN3, Université de Lille 1, Sciences et Technologies
59655 Villeneuve d'Ascq cedex
Tel : 03 20 43 68 38

Date de recrutement à l'INSERM : 2009 (CR2)
Date de nomination au grade actuel : 2013 (CR1)
Langues : Français (langue maternelle), Anglais

Diplômes

2000-2004 : **Doctorat ès Sciences obtenu en 2004** (Université des Sciences et Technologies de Lille ; Ecole doctorale Biologie et Santé de Lille, **Laboratoire de Physiologie Cellulaire INSERM EMI 0228**).
Mention très honorable avec les félicitations unanimes du Jury.
Intitulé de la soutenance : Caractérisation moléculaire et fonctionnelle des canaux chlorures volume-dépendants : implication dans la cancérogenèse prostatique.
Directeur de thèse : Pr Roman Skryma
Date de la soutenance : 11/06/2004

1999-2000 : **DEA Vie et Santé** obtenu (Université des Sciences et Technologies de Lille) avec la **mention Bien** (classé 5ème sur 42)

1998-1999 : **Maîtrise de biologie cellulaire**, mention physiologie cellulaire (Université des Sciences et Technologies de Lille) obtenue avec la mention Bien (classé 1er sur 126)

1997-1998 : **Licence de Biologie**, mention Biologie Cellulaire et Physiologie (Université des Sciences et Technologies de Lille) obtenue avec la mention Assez-bien.

1995-1997 : **D.E.U.G. Sciences de la Vie** (filière biologie, Université des Sciences et Technologies de Lille) obtenu avec la mention Assez-Bien.

1994-1995 : **Baccalauréat général série S** (scientifique) obtenu avec la mention Bien.

Formation complémentaire en France et à l'étranger

2006-2008 : **CDD 3-5 ans INSERM** au sein de l'unité INSERM U800.
Intitulé du projet : Implication du canal TRPM8 dans les physiopathologies prostatiques.

2004-2006 : **Stage post-doctoral** au Laboratory of Signal Transduction, Ca^{2+} regulation group (*NIEHS, Research Triangle Park, North Carolina, USA*) sous la responsabilité scientifique du **Dr. James W. PUTNEY Jr**.
Sujet : Caractérisation des mécanismes d'activation et de régulation des canaux TRPC.
Financement : NIEHS.

Situation actuelle

2009-présent : **Chargé de Recherche INSERM** au sein de l'unité INSERM U1003.

Activités d'enseignement universitaire

2012-2017 : Participation (10 heures/an) aux journées thématiques organisées par mon équipe d'accueil pour les étudiants de Master 2 Biologie-Santé de Lille.

Encadrement

2010-2011 : Encadrement à 50% du Dr. Diaw pendant son année de Master 2 Biologie-Santé (Lille 1)

2014-2015 : Encadrement à 100% de Mme Noyer pendant son année de Master 2 Biologie-Santé (Lille 1)

2015-2017 : Co-tutelle de Mme Noyer pendant sa thèse

Publications

Publications originales dans des revues à comité de lecture,

1. Genova T, GP. Grolez, C. Camillo, M. Bernardini, A. Bokhobza, E. Richard, M. Scianna, **L. Lemonnier**, D. Valdembri, L. Munaron, MR. Philips, V. Mattot, G. Serini, N. Prevarskaya, D. Gkika, AF. Pla. 2017. TRPM8 inhibits endothelial cell migration via a non-channel function by trapping the small GTPase Rap1. ***J Cell Biol***. 216(7):2107-2130.

2. Vancauwenberghe E, L. Noyer, S. Derouiche, **L. Lemonnier**, P. Gosset, LR. Sadofsky, P. Mariot, M. Warnier, A. Bokhobza, C. Slomianny, B. Mauroy, JL.

Bonnal, E. Dewailly, P. Delcourt, L. Allart, E. Desruelles, N. Prevarskaya, M. Roudbaraki. 2017. Activation of mutated TRPA1 ion channel by resveratrol in human prostate cancer associated fibroblasts (CAF). ***Mol Carcinog***. 56(8):1851-1867.

3. Borowiec AS, B. Sion, F. Chalmel, AD. Rolland, **L. Lemonnier**, T. De Clerck, A. Bokhobza, S. Derouiche, E. Dewailly, C. Slomianny, C. Mauduit, M. Benahmed, M. Roudbaraki, B. Jégou, N. Prevarskaya, G. Bidaux. 2016. Cold/menthol TRPM8 receptors initiate the cold-shock response and protect germ cells from cold-shock-induced oxidation. ***FASEB J***. Jun 17.

4. Bidaux G, AS. Borowiec, C. Dubois, P. Delcourt, C. Schulz, FV. Abeele, G. Lepage, E. Desruelles, A. Bokhobza, E. Dewailly, C. Slomianny, M. Roudbaraki, L. Héliot, JL. Bonnal, B. Mauroy, P. Mariot**, L. Lemonnier,** N. Prevarskaya. 2016. Targeting of short TRPM8 isoforms induces 4TM-TRPM8-dependent apoptosis in prostate cancer cells. ***Oncotarget***. Apr 9.

5. Bidaux G, M. Sgobba, **L. Lemonnier**, AS. Borowiec, L. Noyer, S. Jovanovic, AV. Zholos, S. Haider. 2015. Functional and Modeling Studies of the Transmembrane Region of the TRPM8 Channel. ***Biophys J***. 109(9):1840-51.

6. Bidaux G, AS. Borowiec, D. Gordienko, B. Beck, GG. Shapovalov, **L. Lemonnier**, M. Flourakis, M. Vandenberghe, C. Slomianny, E. Dewailly, P. Delcourt, E. Desruelles, A. Ritaine, R. Polakowska, J. Lesage, M. Chami, R. Skryma, N. Prevarskaya. 2015. Epidermal TRPM8 channel isoform controls the balance between keratinocyte proliferation and differentiation in a cold-dependent manner. ***Proc Natl Acad Sci U S A***. 112(26):E3345-54.

7. Gkika D*, **L. Lemonnier***, G. Shapovalov*, D. Gordienko, C. Poux, M. Bernardini, A. Bokhobza, G. Bidaux, C. Degerny, K. Verreman, B. Guarmit, M. Benahmed, Y. de Launoit, R.J. Bindels, A. Fiorio Pla, N. Prevarskaya. (* co-auteurs) 2015. TRP channel-associated factors are a novel protein family that regulates TRPM8 trafficking and activity. ***J Cell Biol***. 208(1):89-107.

8. Kondratska K, A. Kondratskyi, M. Yassine, **L. Lemonnier**, G. Lepage, A. Morabito, R. Skryma, N. Prevarskaya. 2014 Orai1 and STIM1 mediate SOCE and contribute to apoptotic resistance of pancreatic adenocarcinoma. ***Biochim Biophys Acta***. 1843(10):2263-9.

9. Bidaux G, B. Beck, A. Zholos, D. Gordienko, **L. Lemonnier**, M. Flourakis, M. Roudbaraki, AS. Borowiec, J. Fernández, P. Delcourt, G. Lepage, Y. Shuba, R. Skryma, N. Prevarskaya. 2012. Regulation of activity of transient receptor potential melastatin 8 (TRPM8) channel by its short isoforms. ***J Biol Chem***. 287(5):2948-62.

10. Firlej V, JR. Mathieu, C. Gilbert, **L. Lemonnier**, J. Nakhlé, C. Gallou-Kabani, B. Guarmit, A. Morin, N. Prevarskaya, NB. Delongchamps, F. Cabon. 2011. Thrombospondin-1 triggers cell migration and development of advanced prostate tumors. ***Cancer Res.*** 71(24):7649-58.

11. Gkika D, M. Flourakis, **L. Lemonnier**, N. Prevarskaya. 2010. PSA reduces prostate cancer cell motility by stimulating TRPM8 activity and plasma membrane expression. ***Oncogene***. 29(32):4611-6.

12. **Lemonnier L**.*, M. Trebak*, B.J. Wedel, G.S. Bird, J.W. Putney Jr. (* co-auteurs). 2009. Complex functions of phosphatidylinositol 4,5-bisphosphate in regulation of TRPC5 cation channels. ***Pflugers Arch.*** 457(4):757-69.

13. **Lemonnier L**.*, M. Trebak*, J.W. Putney Jr**.** (* co-auteurs). 2007. Complex regulation of the TRPC3, 6 and 7 channel subfamily by diacylglycerol and phosphatidylinositol-4,5-bisphosphate. ***Cell Calcium***.

14. Beck, B, G. Bidaux, A. Bavencoffe, **L. Lemonnier**, S. Thebault, Y. Shuba, G. Barrit, R. Skryma, N. Prevarskaya. 2007. Prospects for prostate cancer imaging and therapy using high-affinity TRPM8 activators. ***Cell Calcium***. 41:285-294. (ISI Impact Factor 2010: **3.553**).

15. **Lemonnier L**, M. Trebak, J.P. Lievremont, G.S. Bird, J.W. Putney Jr. 2006. Protection of TRPC7 cation channels from calcium inhibition by closely associated SERCA pumps. ***Faseb J.***, 20:503-505.

16. Smyth, J.T., **L. Lemonnier**, G. Vazquez, G.S. Bird, J.W. Putney Jr. 2006. Dissociation of regulated trafficking of TRPC3 channel to the plasma membrane from their activation by phospholipase C. ***J Biol Chem.*** 281:11712-11720.

17. Lievremont J.P., T. Numaga, G. Vazquez, **L. Lemonnier**, Y. Hara, E. Mori, M. Trebak, S.E. Moss, G.S. Bird, Y. Mori, J.W. Putney Jr. 2005. The role of canonical transient receptor potential 7 in B-cell receptor-activated channels. ***J Biol Chem*** 280:35346-35351.

18. **Lemonnier L.***, S. Thebault*, G. Bidaux*, M. Flourakis, A. Bavencoffe, D. Gordienko, M. Roudbaraki, P. Delcourt, Y. Panchin, Y. Shuba *et al.* (* co-auteurs). 2005. Novel Role of Cold/Menthol-sensitive Transient Receptor Potential Melastatine Family Member 8 (TRPM8) in the Activation of Store-operated Channels in LNCaP Human Prostate Cancer Epithelial Cells. ***J Biol Chem*** 280 39423-39435.

19. **Lemonnier, L.**, R. Lazarenko, Y. Shuba, S. Thebault, M. Roudbaraki, G. Lepage, N. Prevarskaya, and R. Skryma. 2005. Alterations in the regulatory volume decrease (RVD) and swelling-activated Cl- current associated with neuroendocrine differentiation of prostate cancer epithelial cells. ***Endocr Relat Cancer***. 12:335-349.

20. Zholos, A., B. Beck, V. Sydorenko, **L. Lemonnier**, P. Bordat, N. Prevarskaya, and R. Skryma. 2005. Ca(2+)- and volume-sensitive chloride currents are differentially regulated by agonists and store-operated Ca2+ entry. ***J Gen Physiol*.** 125:197-211.

21. **Lemonnier, L**., N. Prevarskaya, J. Mazurier, Y. Shuba, and R. Skryma. 2004. 2-APB inhibits volume-regulated anion channels independently from intracellular calcium signaling modulation. ***FEBS Lett***. 556:121-126.

22. **Lemonnier, L**., Y. Shuba, A., Crepin, M. Roudbaraki, C. Slomianny, B. Mauroy, B. Nilius, N. Prevarskaya, and R. Skryma. 2004. Bcl-2-dependent modulation of swelling-activated Cl- current and ClC-3 expression in human prostate cancer epithelial cells. ***Cancer Res*.** 64:4841-4848.

23. Vanden Abeele, F., **L. Lemonnier**, S. Thebault, G. Lepage, J.B. Parys, Y. Shuba, R. Skryma, and N. Prevarskaya. 2004. Two types of store-operated Ca2+ channels with different activation modes and molecular origin in LNCaP human prostate cancer epithelial cells. ***J Biol Chem*.** 279:30326-30337.

24. Ivanov, D.V., T.V. Tyazhelova, **L. Lemonnier**, N. Kononenko, A.A. Pestova, E.A. Nikitin, N. Prevarskaya, R. Skryma, Y.V. Panchin, N.K. Yankovsky, and A.V. Baranova. 2003. A new human gene KCNRG encoding potassium channel regulating protein is a cancer suppressor gene candidate located in 13q14.3**.** ***FEBS Lett*.** 539:156-160.

25. Thebault, S., M. Roudbaraki, V. Sydorenko, Y. Shuba, **L. Lemonnier**, C. Slomianny, E. Dewailly, J.L. Bonnal, B. Mauroy, R. Skryma, and N. Prevarskaya. 2003. Alpha1-adrenergic receptors activate Ca(2+)-permeable cationic channels in prostate cancer epithelial cells. ***J Clin Invest*.** 111:1691-1701.

26. Vanden Abeele, F., Y. Shuba, M. Roudbaraki, **L. Lemonnier**, K. Vanoverberghe, P. Mariot, R. Skryma, and N. Prevarskaya. 2003. Store-operated Ca2+ channels in prostate cancer epithelial cells: function, regulation, and role in carcinogenesis. ***Cell Calcium***. 33:357-373.

27. **Lemonnier, L**., N. Prevarskaya, Y. Shuba, F. Vanden Abeele, B. Nilius, J. Mazurier, and R. Skryma. 2002. Ca2+ modulation of volume-regulated anion channels: evidence for colocalization with store-operated channels. ***Faseb J***. 16:222-224.

28. **Lemonnier, L**., Y. Vitko, Y.M. Shuba, F. Vanden Abeele, N. Prevarskaya, and R. Skryma. 2002. Direct modulation of volume-regulated anion channels by Ca(2+) chelating agents. ***FEBS Lett*.** 521:152-156.

29. Rybalchenko, V., N. Prevarskaya, F. Van Coppenolle, G. Legrand, **L. Lemonnier**, X. Le Bourhis, and R. Skryma. 2001. Verapamil inhibits proliferation of LNCaP human prostate cancer cells influencing K+ channel gating. ***Mol Pharmacol*.** 59:1376-1387.

30. Shuba, Y.M., N. Prevarskaya, **L. Lemonnier**, F. Van Coppenolle, P.G. Kostyuk, B. Mauroy, and R. Skryma. 2000. Volume-regulated chloride conductance in the LNCaP human prostate cancer cell line. ***Am J Physiol Cell Physiol*.** 279:C1144-1154.

Publications de revue dans des livres ou ouvrages

Trebak M, **L. Lemonnier**, J.T. Smyth, G. Vazquez, J.W. Putney Jr. 2007. Phospholipase C-coupled receptors and activation of TRPC channels. ***Handb Exp Pharmacol.*** 179:593-614.

Publications effectuées dans le cadre de congrès internationaux

Schwab, A., C. Stock, P. Swietach, A. Hulikova, R. Vaughan-Jones, SF. Pedersen, AD. Andersen, E. Hoffmann, I. Novak, S. Reshkin, N. Prevarskaya, **L. Lemonnier**, AS. Borowiec, A. Arcangeli, F. Zanieri, M. D'Amico, SP. Fraser, MB. Djamgoz, F. Alves, H. Kalthoff, L. Pardo, W. Stuehmer, 2010. Ion transport proteins control pancreatic ductal adenocarcinoma. ***ONKOLOGIE***. Volume: 33 Supplement: 6 Pages: 269-269.

Lemonnier L., G. Bidaux, O. Guenard, N. Prevarskaya. 2009. Growth factors regulate positively TRPM8 channel through a protein tyrosine kinase-dependent pathway. ***JOURNAL OF PHYSIOLOGICAL SCIENCES*** Volume: 59 Supplement: 1 Pages: 398-398.

Skryma R; **L. Lemonnier**; Y. Shuba. 2005. Alterations in the calcium homeostasis and regulatory volume decrease associated with neuroendocrine differentiation of prostate cancer epithelial cells 49th Annual Meeting of the Biopysical-Society Location: Long Beach, CA Date: FEB 12-16, 2005.

Skryma R**, L. Lemonnier**; Y. Shuba, N. Prevarskaya. 2004 Bcl-2-dependent modulation of swelling-activated Cl- current 48th Annual Meeting of the Biophysical Society Location: Baltimore, MD Date: FEB 14-18, 2004

Lemonnier L., Y. Shuba; A. Crepin, M. Roudbaraki, C. Slomianny, B. Mauroy, B. Nilius, N. Prevarskaya, N. Preavarskaya. 2003. Bcl-2-dependent modulation of swelling-activated Cl- current and ClC-3 expression in human prostate cancer epithelial cells 57th Annual Meeting of the Society-of-General-Physiologists Location: MARINE BIOL LAB, WOODS HOLE, MASSACHUSETTS Date: SEP 03-07, 2003

Lemonnier L., Vitko Y; Shuba Y, F. Vanden Abeele, N. Prevarskaya, R. Skryma. 2003. Direct modulation of volume-regulated anion channels by Ca2+ chelating agents. 47th Annual Meeting of the Biophysical-Society Location: SAN ANTONIO, TEXAS Date: MAR 01-05, 2003

Thebault S; Sidorenko V; Shuba Y, **L. Lemonnier**, C. Slomianny, B. Mauroy, R. Skryma, N. Prevarskaya. 2003. Involvement of Ca2+-permeable (TRP-type) cationic channels in a1-adrenoreceptor signaling and in the control of proliferation of human prostate cancer epithelial cells 47th Annual Meeting of the Biophysical-Society Location: SAN ANTONIO, TEXAS Date: MAR 01-05, 2003

Shuba YM, N. Prevarskaya, **L. Lemonnier**, F. Van Coppenolle, PG. Kostyuk, B. Mauroy, R. Skryma. 2000. Volume-regulated chloride conductance in the LNCaP human prostate cancer cell line. ***AMERICAN JOURNAL OF PHYSIOLOGY-CELL PHYSIOLOGY.*** Volume: 279 Issue: 4 Pages: C1144-C1154.

Communications orales sans actes dans un congrès international ou national

Lemonnier L. Roles of TRPM8 in prostate cancer. Conférence plénière durant le « patch-club » 2014 (Montpellier, France)

Lemonnier L. Implication du canal TRPM8 dans la cancérogenèse prostatique. Présentation orale pendant la journée des doctorants cancer (Lille, juin 2012)

Lemonnier L. Roles of TRPM8 in prostate carcinogenesis. Conférence plénière durant le « France-Korea meeting » de 2009 (Villeneuve d'Ascq, France).

Communications par affiche dans un congrès international ou national

Kondratska K, A. Kondratskyi, M. Yassine, **L. Lemonnier**, G. Lepage, A. Morabito, R. Skryma, N. Prevarskaya. Orai1 and STIM1 mediate SOCE and contribute to apoptotic resistance of pancreatic adenocarcinoma. Présentation d'un poster à l'INCA 2015 (Londres, UK).

Lemonnier L., D. Gkika, N. Prevarskaya. TCAF as newly identified regulatory proteins of TRPM8 channel. Présentation d'un poster à l'ITC 2012 (Würzburg, Allemagne).

Lemonnier L., D. Gkika, N. Prevarskaya. TCAF as newly identified regulatory proteins of TRPM8 channel. Présentation d'un poster à la 17ème conférence CaBP en 2011 (Pékin, Chine).

Activité d'animation et de rayonnement

Collaborations :

- Service d'Urologie de l'hôpital St Philibert de Lille (Pr. Mauroy).
- U837 (Dr Polakowska et Pr Quesnel, Lille), dans le cadre de mon travail sur les cellules souches cancéreuses prostatiques.
- iBV, Nice (Dr Soriani), dans le cadre du projet sur le rôle du S1R dans le cancer de la prostate.
- phLAM, Lille (Dr Héliot), également pour l'étude du rôle du S1R.
- Department of Human and Animal Biology (Dr Fiorio Pla, University of Torino, Italy), dans le cadre du projet sur l'angiogenèse.
- Institut für Physiologie II (Pr Schwab, Muenster, Germany). Le Pr Schwab est le coordinateur du projet européen IonTraC auquel je participe.

- Institute of Industrial Science, University of Tokyo, Japan (Pr Sakai) dans le cadre d'un travail sur les cellules souches hépatiques (financement JSPS).

Implication dans des réseaux locaux et internationaux :

- Expert pour l'ARC depuis Janvier 2017 (CN4 Signalisation, Métabolisme cellulaire, Cibles thérapeutiques, Pharmacologie)
- Participation au Labex ICST (http://www.labex-icst.fr/fr)
- Participation au réseau européen IonTraC (Marie Curie ITN, http://www.iontrac.uni-muenster.de/)
- Participation au SIRIC ONCOLille
- Participation à la SFR « Cancer » de Lille
- Participation au réseau « Canaux ioniques et Cancer » du CNO

Financements récents :

- 2014-2015 : 50000 euros, La Ligue contre le Cancer, comité du Septentrion. Projet : Les cellules souches cancéreuses, un nouveau rôle pour les canaux calciques ?
- 2016 : Attribution d'une bourse (1500 euros) par l'ambassade de France à Tokyo, programme exploration Japon, sciences de la vie.
- 2017-2018 : 50000 euros, La Ligue contre le Cancer, comité du Septentrion. Projet : Le récepteur Sigma 1, un nouveau partenaire des canaux calciques dans le cancer de la prostate.

Evaluation d'articles :

Reviewer pour les revues Acta Pharmaceutica Sinica B, Cell Calcium, BBA biomembranes, Cancer Research, Cancer Letters, Molecular Cancer Research,

Fonctions d'intérêt collectif :

Responsable de la salle de culture L2 du laboratoire U1003.

TRAVAUX DE THESE (2000-2004)

Caractérisation moléculaire et fonctionnelle des canaux chlorures volume-dépendants : implication dans la cancérogenèse prostatique.

A - Contexte international et hypothèse de travail

Le cancer de la prostate est une maladie fréquente touchant plus de 53000 hommes chaque année en France. Véritable problème de santé publique, cette pathologie présente la particularité d'être seulement partiellement sensible aux chimiothérapies. Depuis la découverte de l'androgéno-dépendance du cancer de la prostate, les traitements visent à empêcher l'action des androgènes sur cet organe. Ces traitements ont malheureusement une efficacité limitée dans le temps, et les patients développent un cancer dit « androgéno-indépendant » dont l'issue est souvent fatale. Certains de ces cancers prostatiques androgéno-indépendants présentent une différenciation neuroendocrine, considérée comme mauvais pronostic clinique. La compréhension des mécanismes modulant la croissance cellulaire (prolifération et apoptose) et la différenciation neuroendocrine des cellules cancéreuses prostatiques constitue donc un enjeu considérable dans le développement à long terme de thérapies innovantes permettant d'améliorer la qualité de vie des patients.

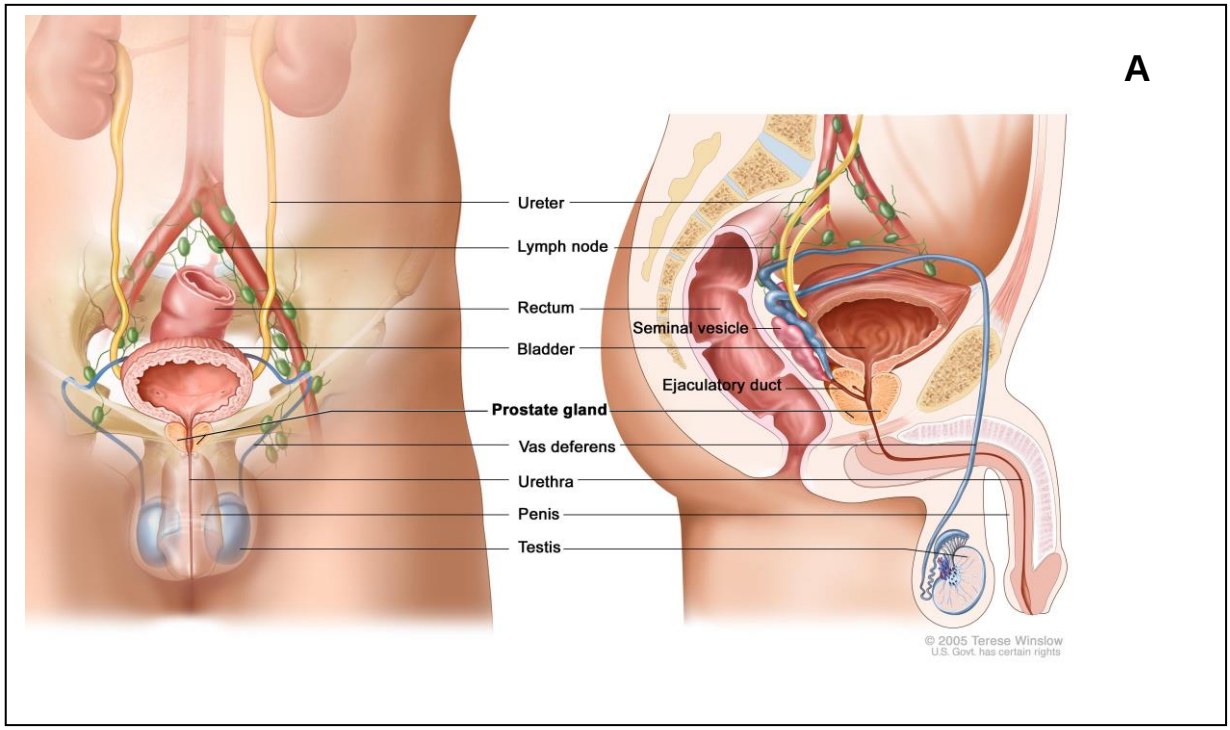

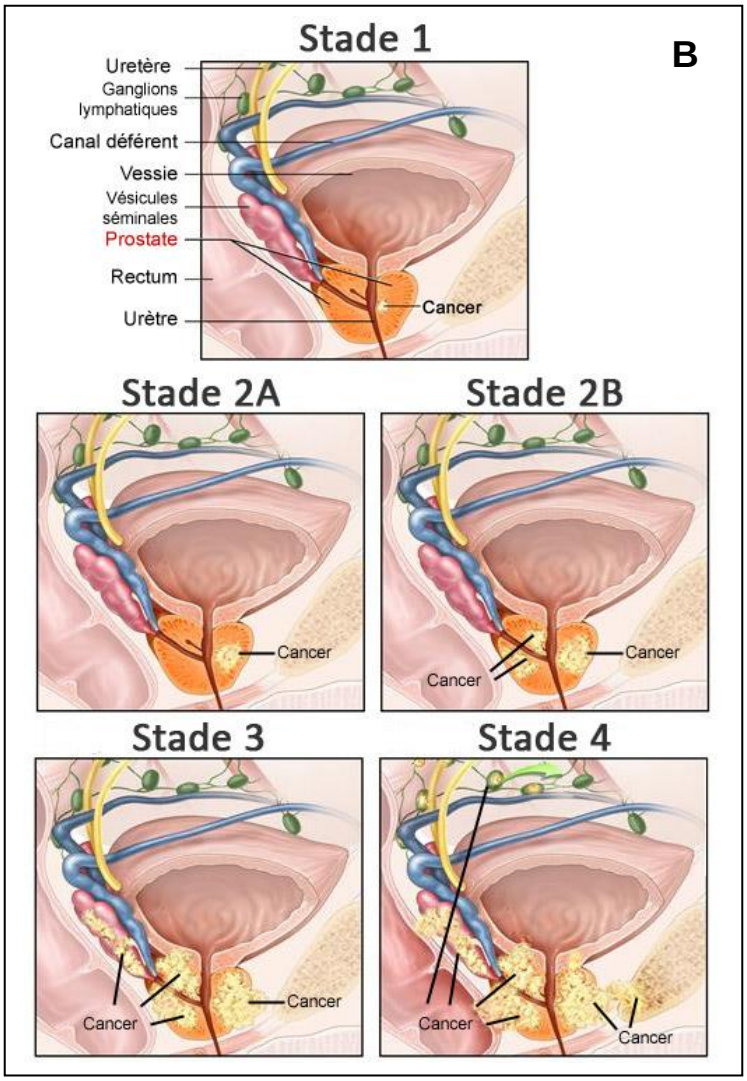

Figure 1 :
A. Localisation anatomique de la prostate (source : Terese Winslow, 2005).
B. Les 4 grands stades de progression du cancer de la prostate (source : France-oncology.com).

Le cancer de la prostate représente la troisième cause de mortalité par cancer chez l'homme, avec près de 8700 décès associés en 2015 (source : e-cancer.fr). La croissance et le développement de la prostate sont sous contrôle androgénique. Malgré l'efficacité des traitements visant à diminuer les taux d'androgènes circulants, ceux-ci se révèlent incapables à long terme d'empêcher la progression des tumeurs vers l'androgéno-indépendance et l'échappement thérapeutique. Il est donc évident que d'autres facteurs interviennent lors la cancérogenèse prostatique, et différents mécanismes ont été suggérés. Au cours de ma thèse, je me suis plus particulièrement intéressé au phénomène de résistance à l'apoptose. En effet, le défaut d'apoptose rend inefficace les chimiothérapies, ce qui conduit à l'échappement thérapeutique des cancers de la prostate. Ces cancers androgéno-indépendants se caractérisent notamment par l'apparition de cellules tumorales surexprimant des protéines de la famille Bcl-2 (Raffo et al., 1995) et de cellules cancéreuses différenciées en cellules neuroendocrines (Fixemer et al., 2002), ces

deux types cellulaires présentant un défaut d'apoptose. J'ai donc fait de l'étude de ces deux phénomènes la priorité de ma thèse, les mécanismes cellulaires à l'origine de la résistance à l'apoptose représentant un enjeu majeur dans la lutte contre le cancer de la prostate.

Or, il a été démontré que les canaux chlorures volume-dépendants ou VRAC (Volume-Regulated Anion Channels) sont impliqués dans le processus apoptotique (Okada et al., 2001), tout comme d'importantes altérations de l'homéostasie calcique (Carafoli, 2004). Il est en effet connu que l'apoptose implique de profonds remaniements dans l'organisation cellulaire, notamment en conduisant à une diminution du volume cellulaire lors de la formation de corps apoptotiques. Ce phénomène, appelé AVD (Apoptotic Volume Decrease), a été récemment démontré comme faisant intervenir les VRAC (Maeno et al., 2000). Malgré l'importance de ces canaux, et en dépit des recherches effectuées ces quinze dernières années, l'identité moléculaire des VRAC reste mystérieuse. Parmi les protéines candidates, les canaux de la famille ClC, et plus particulièrement ClC-3, restent des cibles d'intérêts malgré des rapports controversés quant à leur implication dans la formation des VRAC (Duan et al., 1997). Par ailleurs, il a été montré que les canaux VRAC sont modulés de manière très variable par le calcium selon les modèles cellulaires, son effet allant de l'inhibition à l'activation. Or il a été prouvé par notre équipe que la vidange des stocks calciques intracellulaires, ainsi que la subséquente entrée capacitive via les canaux calciques de type SOC (Store Operated Channels), jouent un rôle crucial dans l'initiation de l'apoptose (Skryma et al., 2000).

Malgré ces informations capitales, aucune étude n'a démontré la présence des canaux de type VRAC ou n'a établi l'existence d'une régulation de ces canaux par le calcium dans la prostate. De plus, la nature moléculaire, la régulation et le rôle des canaux VRAC lors de la cancérogenèse prostatique et de son évolution vers l'androgéno-indépendance sont inconnues. Ces éléments ont conduit mon projet de recherche vers l'identification des VRAC et de leur régulation dans la prostate, ainsi que vers l'étude des éventuelles modifications d'expression et de régulation de ces canaux au cours du développement des tumeurs de la prostate et de leur évolution vers l'androgéno-indépendance.

B - Résultats

I. Identification et caractérisation des canaux chlorures volume-dépendants (VRAC) dans les cellules cancéreuses de la prostate humaine.

La première étape de ma thèse a consisté à caractériser les canaux de type VRAC dans un modèle de cellules cancéreuses épithéliales prostatiques humaines (cellules LNCaP). Cette étude, reposant sur l'utilisation des techniques électrophysiologiques (patch-clamp dans les configurations « whole-cell » et « courant unitaire »), m'a conduit à mettre en évidence pour la première fois dans les cellules prostatiques la présence de canaux de type VRAC activés par l'augmentation du volume cellulaire. Cette étude a impliqué la caractérisation des canaux de type VRAC par l'utilisation d'inhibiteurs pharmacologiques, ainsi qu'une mise en évidence de leur régulation par les protéines tyrosine kinases. Par la suite, lors d'une étude complémentaire, j'ai montré la sensibilité de ces canaux au 2-APB, un inhibiteur classique des canaux calciques et des récepteurs IP_3.

Ces résultats mettent en évidence la présence de canaux VRAC dans les cellules prostatiques présentant un profil de régulation caractéristique pour cette lignée cellulaire (Lemonnier et al., 2004; Shuba et al., 2000). Ces études constituent donc une première étape incontournable avant une potentielle mise en évidence de mécanismes de régulation propres à la prostate.

II. Mise en évidence de la régulation des canaux chlorures volume-dépendants par l'entrée capacitive de calcium via les canaux de type SOC dans les cellules cancéreuses de la prostate humaine (article n°1).

Comme indiqué précédemment, les canaux de type VRAC présentent un profil de régulation par le calcium des plus remarquables dans le sens ou il ne semble pas exister de motif unique : chaque modèle cellulaire semble présenter une sensibilité variable aux fluctuations de la concentration calcique dans les milieux intra- et extracellulaires. Or, il a été montré par notre équipe que la perturbation de l'homéostasie calcique, et plus précisément la vidange des stocks calciques intracellulaires, conduit à l'entrée en apoptose des cellules prostatiques humaines. Ces deux observations m'ont donc amenées dans un premier temps à étudier de manière générale la sensibilité au calcium des canaux de type VRAC dans les cellules cancéreuses de la prostate humaine. Dans un second temps, je me suis

plus particulièrement concentré sur la possible interaction existant entre les canaux de type VRAC et les mécanismes d'induction de l'apoptose en réponse à la vidange des stocks calciques intracellulaires. En effet, l'existence d'une telle interaction offrirait de nouvelles possibilités thérapeutiques en désignant les canaux de type VRAC comme une cible potentielle dans le traitement du cancer de la prostate.

1. Les canaux de type VRAC sont insensibles aux variations de la concentration calcique extracellulaire, mais sont inhibés par les chélateurs calciques. Le recours à la technique du patch-clamp dans sa configuration « whole-cell » m'a permis de montrer l'absence d'effet du calcium extracellulaire sur l'amplitude du courant chlorure volume-dépendant (I_{Cl}). Durant cette étude, afin de contrôler précisément la concentration calcique dans le milieu extracellulaire, j'ai utilisé différents chélateurs calciques. Mes résultats ont montré que ces chélateurs sont des inhibiteurs de I_{Cl}, probablement en interagissant directement avec le pore du canal (Lemonnier et al., 2002a). Cette étude met en évidence le besoin de réévaluer certains résultats obtenus précédemment concernant la sensibilité des canaux de type VRAC au calcium extracellulaire, et fourni un nouvel outil pharmacologique pour la caractérisation des canaux de type VRAC.

Ces résultats ont un impact sur la recherche fondamentale dédiée aux canaux de type VRAC en fournissant une nouvelle caractéristique de ces canaux, ainsi qu'un nouveau moyen de réguler leur activité.

2. Régulation de l'activité des canaux de type VRAC par l'entrée capacitive via les canaux de type SOC. Ayant montré l'absence d'effet direct du changement de la concentration calcique extracellulaire sur I_{Cl}, je me suis ensuite intéressé à la possible régulation de ce courant par des variations de la concentration calcique intracellulaire. Il avait précédemment été prouvé au laboratoire que la vidange des stocks calciques intra-réticulaires induit l'entrée en apoptose des cellules prostatiques humaines (Skryma et al., 2000). Une vidange réticulaire a également été décrite comme activant dans nos cellules une entrée dite « capacitive » de calcium via les canaux de type SOC (Vanden Abeele et al., 2002). Ces deux phénomènes conduisant à une élévation de la concentration calcique intracellulaire et se retrouvant lors de l'induction de l'apoptose, il était intéressant de voir leur éventuelle influence sur I_{Cl}. Dans un premier temps, j'ai vérifié l'effet d'une augmentation globale de la concentration calcique intracellulaire sur I_{Cl} en augmentant la quantité de calcium présente dans la solution intracellulaire utilisée

durant mes expériences de patch-clamp. Le changement de la concentration calcique intracellulaire s'est toutefois révélé sans influence sur I_{Cl}, tout comme cela avait été montré pour le calcium extracellulaire. Dans un deuxième temps, j'ai eu recours à un outil pharmacologique, la thapsigargine, afin de déterminer l'effet de la vidange réticulaire et de l'entrée capacitive sur I_{Cl}. En effet la thapsigargine, en inhibant de manière irréversible les pompes SERCA (Sarcoplasmic Endoplasmic Reticulum Calcium ATPase), conduit à la vidange passive des stocks calciques réticulaires via des canaux de fuite constamment ouverts dans la membrane du réticulum endoplasmique. Cette vidange va induire par un mécanisme inconnu l'ouverture sur la membrane plasmique de canaux de type SOC laissant rentrer du calcium en vue de remplir à nouveau le réticulum endoplasmique. L'utilisation conjointe des techniques de patch-clamp et d'imagerie calcique m'a amené à montrer l'absence d'effet de la vidange réticulaire sur I_{Cl}. Cependant, ces mêmes techniques m'ont permis de montrer que l'entrée de calcium via les canaux de type SOC est à même de prévenir l'activation des canaux de type VRAC en réponse à un stimulus hypotonique.

Ces observations m'ont conduit à proposer un modèle dans lequel les canaux de type VRAC et SOC sont localisés dans une même structure membranaire. Selon ce modèle, l'entrée de calcium via les canaux de type SOC induit une augmentation locale de la concentration calcique dans un compartiment sous-membranaire autrement inaccessible aux augmentations globales du taux de calcium intracellulaire. A ce titre, cette étude constitue une première mise en évidence de la potentielle interaction existant entre les canaux de type VRAC et SOC, deux structures participant au processus apoptotique, et fournit également une explication élégante au manque de cohérence dans les précédents rapports concernant la sensibilité de I_{Cl} aux variations globales de la concentration intracellulaire. De manière intéressante, alors que de précédentes études ont montré dans d'autres modèles cellulaires que l'inhibition des canaux de type VRAC prévient l'entrée en apoptose (Okada et al., 2001), je montre ici que dans la prostate l'entrée en apoptose pourrait impliquer l'inhibition de ces canaux suite à l'ouverture des canaux de type SOC situés dans une même structure membranaire (Lemonnier et al., 2002b).

Ces résultats constituent une première mise en évidence du rôle potentiel des canaux de type VRAC dans le processus apoptotique des cellules cancéreuses de la

prostate humaine. Ils mettent également en avant le potentiel intérêt thérapeutique de l'inhibition de ces canaux lors de traitements visant à promouvoir l'apoptose des cellules tumorales prostatiques.

III. Implication des canaux chlorures volume-dépendants dans la cancérogenèse prostatique et la différenciation neuroendocrine (article n°2).

1.Modulation de l'activité des canaux chlorures volume-dépendants par l'oncoprotéine Bcl-2. L'oncoprotéine Bcl-2 est connue pour être surexprimée dans un grand nombre de cancers, notamment lors du cancer de la prostate. Dans ce cas particulier, il a été montré que la surexpression de Bcl-2 est associée à l'acquisition d'un phénotype androgéno-indépendant par les cellules cancéreuses prostatiques, conduisant à la perte de réponse de ces cellules au principal traitement du cancer de la prostate : l'hormonothérapie. La prostate étant une glande dont la croissance est favorisée par les androgènes, le principal traitement consiste en une castration chimique visant à diminuer les taux d'androgènes circulant. Etant donné le rôle fondamental de Bcl-2 lors de la cancérogenèse et de l'échappement thérapeutique du cancer de la prostate, ainsi que le rôle potentiel des canaux de type VRAC en tant qu'inhibiteurs de l'apoptose dans ce modèle, j'ai cherché à déterminer la présence d'une possible relation entre Bcl-2 et les canaux de type VRAC. Dans ce but, j'ai utilisé deux différentes lignées cellulaires fournies par le Dr. Buttyan (Raffo et al., 1995) : les cellules LNCaP-neo transfectées stablement avec un plasmide vide, ainsi que les cellules LNCaP-Bcl-2 transfectées stablement avec un plasmide contenant le gène codant pour l'oncoprotéine Bcl-2.

Grâce à une approche reposant sur la technique de patch-clamp, ainsi qu'à des collaborations au sein de mon laboratoire impliquant le recours aux techniques de biologie cellulaire et moléculaire, j'ai montré que les cellules surexprimant Bcl-2 présentent un doublement de l'amplitude de I_{Cl}. Afin de confirmer cette observation dans un modèle plus physiologique de surexpression de Bcl-2, j'ai traité les cellules LNCaP avec de l'EGF (Epidermal Growth Factor). Il a en effet été montré au laboratoire que ce traitement induit une augmentation de l'expression de Bcl-2 dans les cellules prostatiques (Legrand et al., 2001). En agrément avec ma précédente observation, l'augmentation d'expression de Bcl-2 induite par l'EGF se traduit également par le doublement de l'amplitude de I_{Cl}. Quelle que soit la méthode employée, l'augmentation d'amplitude de ce courant s'accompagne d'une

augmentation du niveau d'expression de la protéine ClC-3, un candidat potentiel pour le rôle de canal VRAC. L'utilisation d'un anticorps dirigés contre ClC-3 m'a permis de confirmer l'implication de ce canal dans I_{Cl} : l'introduction de l'anticorps dans la cellule via la pipette de patch-clamp prévient le développement de I_{Cl}. Mes résultats montrent donc que la surexpression de Bcl-2 conduit à l'augmentation de l'activité et/ou de l'expression des canaux de type VRAC dans les cellules cancéreuses prostatiques humaines. L'augmentation concomitante de l'expression de ClC-3, un candidat au rôle de VRAC, et la mise en évidence de son implication dans le développement de I_{Cl} tendent à prouver que la surexpression de Bcl-2 induit l'augmentation de I_{Cl} via une augmentation du nombre de canaux ClC-3 exprimés à la surface cellulaire.

Une étude réalisée en parallèle au laboratoire a montré que la surexpression de Bcl-2 conduit à une altération des mécanismes présidant à l'homéostasie calcique cellulaire. Plus précisément, les cellules LNCaP-Bcl-2 présentent une diminution de leur stocks calciques intra-réticulaires, ainsi qu'une diminution du nombre de canaux SOC (Vanden Abeele et al., 2002). Ce phénotype se traduit par une résistance accrue de ces cellules à l'apoptose induite par la vidange des stocks calciques intra-réticulaires. Ayant précédemment montré une relation entre les canaux de type VRAC, SOC et le réticulum endoplasmique, j'ai voulu savoir comment cette relation était affectée par la surexpression de Bcl-2. Mes résultats montrent que l'inhibition de I_{Cl} liée à l'activation des canaux de type SOC est fortement diminuée dans les cellules surexprimant Bcl-2. Cela signifie que lors de la surexpression de Bcl-2, que l'on retrouve dans la majorité des cancers prostatiques, les canaux de type VRAC qui ont ici un potentiel rôle protecteur vis à vis de l'apoptose sont surexprimés. Dans le même temps, le contenu calcique intra-réticulaire ainsi que le nombre de canaux SOC membranaires, que j'ai prouvé avoir un rôle inhibiteur sur les canaux de type VRAC, sont diminués.

Je montre donc qu'il existerait au cours de la cancérogenèse prostatique une série d'événements initiés par la surexpression de Bcl-2 conduisant à la favorisation de la survie cellulaire, notamment en augmentant le nombre de canaux de type VRAC exprimés à la surface cellulaire, et en diminuant l'expression des canaux de type SOC qui interviennent dans l'inhibition de I_{Cl}.

2.Modulation de l'activité des canaux chlorures volume-dépendants lors de la différenciation neuroendocrine. Ayant montré que la surexpression de Bcl-2, qui est connue pour induire l'androgéno-indépendance des cellules cancéreuses prostatiques humaines, conduit à une forte augmentation de l'activité des canaux de type VRAC, je me suis par la suite intéressé aux variations de cette activité dans un modèle cellulaire reproduisant le phénomène de différenciation neuroendocrine. Il a en effet été montré que l'échappement thérapeutique du cancer de la prostate (perte de réponse aux chimiothérapies et hormonothérapies) s'accompagne d'une augmentation du nombre de cellules neuroendocrines observées dans cette glande (Vashchenko and Abrahamsson, 2005). Ces cellules, associées à un mauvais pronostique quant à la survie du patient, sont insensibles à la suppression des androgènes circulants. Afin de déterminer si mes précédentes observations concernant les canaux de type VRAC et leur régulation par les canaux de type SOC étaient affectées de la même manière par la surexpression de Bcl-2 et par la différenciation neuroendocrine, j'ai soumis la lignée LNCaP à deux types de traitements connus pour induire la différenciation neuroendocrine (Mariot et al., 2002). J'ai ainsi montré que, quelle que soit la méthode utilisée, l'amplitude de I_{Cl} est deux fois plus grande dans les cellules différenciées que dans les cellules contrôles. Dans ces conditions, la différenciation s'accompagne d'une augmentation de l'expression de ClC-3, ce qui tend à confirmer l'idée selon laquelle ClC-3 est impliqué dans la formation des canaux de type VRAC dans la prostate. Cependant, la différenciation neuroendocrine des cellules LNCaP intervient sans aucun changement dans le niveau d'expression de Bcl-2. Couplé au fait que les cellules différenciées montrent une résistance accrue à l'entrée en apoptose, cet absence de changement d'expression de Bcl-2 renforce mon hypothèse selon laquelle la surexpression des canaux de type VRAC constitue en elle-même un mécanisme de défense des cellules prostatiques contre l'entrée en apoptose.

Une étude réalisée en parallèle au laboratoire a montré que les cellules différenciées présentent une altération de leur homéostasie calcique similaire à celle observée dans les cellules surexprimant Bcl-2, à savoir une diminution de la concentration calcique dans le réticulum endoplasmique ainsi qu'une diminution du nombre de canaux de type SOC exprimés à la surface cellulaire (Vanoverberghe et al., 2004). De manière similaire, j'ai montré que les cellules différenciées présentent une perte d'inhibition de I_{Cl} en réponse à une entrée de calcium via les canaux de

type SOC. Mes résultats montrent donc qu'il existerait au cours de la cancérogenèse prostatique et de la différenciation neuroendocrine une série de phénomènes communs conduisant au même phénotype de diminution du potentiel apoptotique. Ces phénomènes incluent une augmentation de l'expression des canaux de type VRAC, ainsi qu'une diminution du nombre de canaux de type SOC connus pour participer au processus apoptotique dans la prostate et que j'ai montré avoir un rôle inhibiteur sur l'activité des canaux de type VRAC. Je propose donc que, contrairement aux précédentes observations réalisées dans d'autres modèles cellulaires où ces canaux sont nécessaires à l'entrée en apoptose, les canaux de type VRAC auraient dans la prostate un rôle protecteur vis à vis de l'entrée en apoptose. Je montre également que ce rôle est soumis au contrôle des canaux de type SOC, des acteurs reconnus dans l'entrée en apoptose des cellules prostatiques, et que ce contrôle disparaît au cours de la cancérogenèse et de la différenciation neuroendocrine. Enfin, mes résultats suggèrent que le canal ClC-3 participe à la formation des canaux de type VRAC dans la prostate, ouvrant ainsi la voie à de nouvelles thérapies ciblant la prostate, les canaux ClC-3 étant généralement trouvés dans d'autres modèles cellulaires au niveau des endosomes (Lemonnier et al., 2005).

C - Conclusion

L'exposé de mes résultats dans le contexte de la recherche médicale montre le rôle fondamental des canaux chlorures volume-dépendants dans la résistance à l'apoptose des tumeurs prostatiques androgéno-indépendantes incurables. Ces canaux ioniques pourraient donc servir d'une part de marqueurs potentiels du cancer de la prostate et d'autre part de cibles pharmacologiques éventuellement utilisables en thérapeutique.

Ces travaux auront également permis une meilleure compréhension des mécanismes de régulation de ces canaux, notamment par les canaux calciques de type SOC, ainsi que la détermination de leur nature moléculaire dans les cellules tumorales prostatiques. Ces résultats sont de toute première importance car ils permettent de mieux appréhender les mécanismes ioniques accompagnant la cancérogenèse prostatique et son évolution vers des stades tardifs résistant aux

traitements actuels. Ils mettent également en évidence l'existence d'un lien entre les canaux de type VRAC et l'un des plus mystérieux mécanismes de la signalisation calcique, l'entrée capacitive de calcium, dont le rôle crucial dans la physiologie de la cellule n'est plus à démontrer.

C'est à ce point que s'est achevée ma thèse, avec l'idée que le ClC-3 participait aux activités du VRAC dans les cellules cancéreuses prostatiques. A cette période, nous ne disposions pas des outils et connaissances qui nous auraient permis d'aller plus loin dans cette étude, ce qui explique notamment pourquoi j'ai commencé à m'intéresser dès cette époque à une autre famille de canaux ioniques, les TRP, et plus particulièrement à TRPM8 dont l'activité était à même d'initier l'entrée capacitive dans nos cellules. Cependant, en 2014, une nouvelle famille de canaux a été découverte : LRRC8. Cette famille comprend 5 membres (LRRC8 A-E), et de nombreux travaux montrent que ces protéines constituent la base moléculaire du VRAC (pour revue, Pasantes-Morales, 2016). Avec la découverte en 2005-2006 de la nature moléculaire des canaux SOC (Frischauf et al., 2016), il semble clair que mes travaux de thèse pourraient maintenant reprendre, afin notamment de confirmer la nature moléculaire exacte des canaux VRAC dans nos cellules. De plus, les progrès technologiques aidant, il serait possible de suivre en temps réel l'association des VRAC et SOC dans nos modèles, et d'observer l'éventuel remodelage de ces interactions lors des différents stades de développement de la maladie. J'espère pouvoir un jour relancer cette thématique, sous réserve de trouver les fonds et le personnel nécessaire à l'étude d'une classe de canaux trop souvent ignorée par les électrophysiologistes.

TRAVAUX POST-DOCTORAUX (2004-2006)

Suite à ma thèse, j'ai rejoint le Laboratory of Signal Transduction (NIEHS, North Carolina, USA) dirigé par le Dr. J. W. Putney qui est à l'origine de la découverte du phénomène d'entrée capacitive suite à la vidange des stocks calciques intra-réticulaires. Au sein de ce laboratoire, j'ai eu l'occasion d'étudier les mécanismes d'activation et de régulation de différents canaux TRPC (Transient Receptor Potential « canonical ») qui constitueraient la base moléculaire de l'entrée capacitive et joueraient un rôle crucial dans l'homéostasie calcique.

A - Contexte international et hypothèse de travail

Les canaux de la famille TRP sont actuellement l'objet de nombreuses études et controverses. A l'origine, ces canaux ont été mis en évidence dans la transduction du signal lumineux chez la Drosophile (Peretz et al., 1994), et possèdent la particularité d'être activés par la PLC (Phospholipase C). Par la suite, la recherche de molécules homologues chez les Mammifères a conduit à l'identification d'un nombre toujours croissant de canaux TRP classés en plusieurs sous-familles aux propriétés distinctes (pour revue, (Montell, 2005)). Les TRPC ou TRP « canoniques » sont les plus proches structurellement du TRP initialement cloné chez la Drososphile, et conservent la propriété d'être activés par la voie de signalisation de la PLC. Des études complémentaires ont rapidement montré que la surexpression de ces canaux dans plusieurs modèles cellulaires induisait l'augmentation de l'entrée capacitive, ce qui a conduit à l'idée maintenant généralement acceptée que les canaux TRPC contribuent à la formation des canaux de type SOC. TRPC7, le dernier membre identifié de la famille TRPC, présente tout comme TRPC3 et TRPC6 la particularité de pouvoir être directement activé par le DAG (diacylglycerol), l'un des produits de dégradation du PIP2 (phosphatidylinositol-4,5-bisphosphate) par la PLC. Il a également été montré que TRPC7 peut jouer le rôle de canal de type SOC quand il est surexprimé, bien que ce point reste sujet à controverse (Okada et al., 1999; Riccio et al., 2002).

Malgré ces études, les connaissances concernant TRPC7 et la régulation de son activité restent parcellaires. Ainsi, les mécanismes de régulation de ce canal par le calcium sont méconnus, et son comportement lors de l'induction de l'entrée capacitive n'a jamais été étudié. Mon principal axe de recherche a donc consisté en

une mise en évidence des mécanismes de régulation de TRPC7 par le calcium et de leur altération lors de l'induction de l'entrée capacitive.

B - Synergie du stage post-doctoral avec mon parcours professionnel

J'ai choisi de rejoindre l'équipe du Dr. J. W. Putney pour de multiples raisons :

- Au cours de ma thèse, j'ai mis en évidence la colocalisation des canaux VRAC et SOC, ce qui m'a amené à m'intéresser au phénomène d'entrée capacitive correspondant à l'ouverture des canaux de type SOC. De nombreux travaux effectués ces 15 dernières années ont montré que les canaux de type TRP peuvent constituer la base moléculaire des canaux de type SOC. Or, le Dr. Putney représente une figure de renommée internationale dans le domaine des mécanismes d'entrée capacitive et des canaux TRP. Son équipe constitue donc un environnement des plus propices à l'étude de ces canaux en proposant une approche multidisciplinaire combinant la biologie moléculaire, la biochimie, l'imagerie calcique et les techniques électrophysiologiques.

- De par sa haute visibilité au niveau international, le laboratoire du Dr. Putney offre la chance de pouvoir établir de nombreux contacts avec les principaux acteurs de la recherche dans le domaine des canaux TRP et SOC en favorisant les collaborations ainsi que les échanges lors des grands congrès internationaux ou des nombreux séminaires qu'il organise.

- Cette équipe s'est spécialisée depuis plusieurs années dans l'expression hétérologue des canaux TRP. Ayant jusqu'à présent uniquement travaillé dans des modèles où ces canaux sont exprimés de manière endogène, rejoindre cette équipe m'a permis de me familiariser avec les techniques d'expression hétérologue dans les principaux modèles cellulaires rencontrés en laboratoire (HEK 293, Jurkat, DT40, RBL 2H3). L'acquisition de ces techniques est un pré requis à la plupart des études électrophysiologiques, puisqu'elles permettent de faciliter la caractérisation des propriétés biophysiques et des principaux mécanismes de régulation d'un canal d'intérêt, ainsi que de mettre en évidence d'éventuelles particularités liées à l'expression de différentes isoformes tissus-spécifiques. Il est également plus aisé d'étudier le rôle d'un canal au cours du processus apoptotique dans un tel contexte que lorsque plusieurs protéines d'une même famille sont exprimées de manière endogène. Ces techniques sont donc directement transposables à l'étude des

canaux exprimés dans la prostate. Mon projet reposant également sur l'emploi d'ARN interférentiels, j'ai eu l'occasion de me familiariser avec cette technique de choix permettant d'inhiber spécifiquement l'expression d'une protéine d'intérêt.

C - Résultats

I. Mise en évidence d'une interaction entre le canal TRPC7 et les pompes SERCA (article 3).

Au cours de mon stage post-doctoral, j'ai identifié un nouveau mécanisme de régulation du canal TRPC7 par le calcium. Mes résultats confirment que lorsqu'il est surexprimé dans les cellules HEK 293, le canal TRPC7 présente deux modes de fonctionnement faisant probablement intervenir deux populations distinctes de canaux : il peut être activé soit par la vidange des stocks calciques intra-réticulaires (ce qui confirme que TRPC7 peut former un canal de type SOC), soit par l'activation de la voie de transduction de la PLC (Lievremont et al., 2004). Bien que ces résultats soient connus depuis longtemps grâce à l'imagerie calcique, j'ai pu montrer l'existence d'un courant induit par la thapsigargine (un inhibiteur des pompes SERCA) correspondant à une population de canaux TRPC7 sensibles à la vidange réticulaire. Par ailleurs, j'ai voulu savoir s'il existait une relation fonctionnelle entre la composante de TRPC7 activée par la vidange et celle activée par la voie de signalisation de la PLC. Pour cela, j'ai traité les cellules avec différents inhibiteurs des pompes SERCA (thapsigargine, acide cyclopiazonique) avant d'appliquer de l'OAG (1-oleoyl-2-acetyl-*sn*-glycerol), un analogue perméant du DAG. Alors que l'OAG induit dans les conditions contrôles l'activation du canal TRPC7, la présence d'inhibiteurs des pompes SERCA prévient cette activation. Mes résultats suggèrent que cette inhibition résulte directement de l'inactivation des pompes SERCA réticulaires : dans les conditions contrôles, les pompes SERCA sont localisées à proximité des canaux TRPC7 et leur activité prévient l'accumulation locale de calcium. Leur inhibition conduirait donc à une forte augmentation locale de la concentration calcique cytosolique. J'ai également montré que la désorganisation du cytosquelette, qui induirait la perte de l'association TRPC7-SERCA, prévient à elle seule l'activation des canaux TRPC7. Ce résultat, en plus de renforcer l'idée d'une co-localisation entre TRPC7 et les pompes SERCA, suggère qu'il existerait en permanence un rétrocontrôle négatif de l'activité des canaux TRPC7 par le calcium entrant par le canal lui-même. Cette association fonctionnelle entre TRPC7 et les

pompes SERCA renforce également l'idée selon laquelle TRPC7 est un canal de type SOC : une interaction directe entre le canal et les pompes SERCA qui contrôlent le niveau de calcium réticulaire fournirait un mécanisme élégant d'activation de l'entrée capacitive.

Il a été montré par Shi et al. que la calmoduline est très probablement à l'origine de la sensibilité du canal TRPC7 aux variations de la concentration calcique cytoplasmique (Shi et al., 2004). En accord avec cette observation, j'ai montré que l'inactivation de la calmoduline prévient l'inhibition du canal TRPC7 liée à la présence de thapsigargine. Je propose donc un modèle où les canaux TRPC7 sont étroitement associés avec les pompes SERCA. La perte d'activité de ces pompes, tout comme l'augmentation de la distance TRPC7-SERCA, conduisent à l'inactivation du canal TRPC7, probablement suite à une augmentation locale de la concentration calcique favorisant la fixation de la calmoduline sur le canal au niveau du domaine CIRB (Calmodulin IP3 Receptor Binding).

II. Mécanismes d'activation du canal TRPC5 (article 4).

En sus de ma thématique principale, j'ai initié au sein de mon laboratoire plusieurs collaborations. L'une d'elle a porté sur les mécanismes d'activation du canal TRPC5, un autre candidat potentiel au rôle de SOC. Alors que le DAG a été identifié comme étant l'activateur des canaux TRPC3, 6 et 7 suite à la stimulation de la PLC, il n'existe pas d'intermédiaire connu entre la PLC et les canaux TRPC1, 4 et 5. Grâce à une approche associant l'imagerie calcique et les techniques électrophysiologiques, nous avons montré que l'activation du canal TRPC5 résulte de la dégradation du PIP2 suite à l'activation de la PLC dans un modèle de cellules HEK 293 exprimant stablement TRPC5. Plus précisément, la PLC clive le PIP2 en IP_3 et DAG qui sont généralement associés à l'activation des canaux TRPC3, 6 et 7. Cependant, nous montrons que ces deux seconds messagers sont incapables d'activer TRPC5. L'utilisation d'inhibiteurs de la voie de synthèse du PIP2, qui induisent la déplétion des stocks membranaires de PIP2, provoquent ici l'ouverture des canaux TRPC5. J'ai montré que cet effet peut-être prévenu par l'inclusion dans la pipette de patch-clamp du PIP2 ou de son précurseur le PIP (phosphatidylinositol-4-phosphate). Nous proposons donc que le canal TRPC5 est activé par la PLC suite

à la dégradation des stocks de PIP2 qui exercent autrement un rôle répresseur vis à vis de l'ouverture du canal.

D- Conclusion

Les travaux que j'ai entrepris au sein de l'équipe du Dr. Putney ont conduit à la découverte de nouveaux mécanismes de régulation et d'activation de canaux TRPC qui sont par ailleurs proposés comme constituant la base moléculaire des canaux de type SOC. Ces travaux fondamentaux sont de toute première importance car ils ouvrent de nouvelles voies de recherche pour la compréhension des phénomènes physiologiques liés aux voies de signalisation calcique impliquant les TRPC exprimés de manière endogène dans les cellules primaires ou tissus d'intérêts. De plus, cette étude met en évidence de nouveaux mécanismes et interactions potentiellement fondamentaux dans la physiologie cellulaire normale ou pathologique, et à ce titre fourni de nouvelles pistes pour mieux comprendre les mécanismes de carcinogenèse et de résistance à l'apoptose.

Ce séjour aux USA a donc été riche en enseignements, et m'a donné l'occasion de travailler sur une régulation plus fondamentale des canaux ioniques dans un environnement scientifique particulièrement propice. En effet, j'ai pu interagir avec des spécialistes mondialement reconnus dans notre domaine. Ainsi, le laboratoire du Dr Birnbaumer, qui a initialement cloné les canaux TRP chez les Mammifères, se trouvait dans le même département que le nôtre. J'ai également eu l'occasion de monter mon premier poste de patch-clamp, ainsi que de réaliser des enregistrements en conditions unitaires. Par ailleurs, cette période correspond à la publication de la nature moléculaire des canaux SOC. Il a donc été particulièrement stimulant de pouvoir vivre la dynamique de recherche que cette découverte a engendré dans le laboratoire qui a décrit ce phénomène en premier. J'ai cependant décidé de revenir en France au bout de deux ans, grâce à l'obtention d'un premier financement par l'INSERM correspondant à un CDD de 3 ans.

TRAVAUX DEPUIS MON RETOUR EN FRANCE ET LE RECRUTEMENT A L'INSERM (2006-…)

A Hypothèses de travail

Les données bibliographiques et nos résultats préliminaires nous permettent de supposer que le canal cationique TRPM8 joue un rôle dans la physiologie de la prostate et que sa dérégulation peut favoriser la progression du cancer. Au cours de ma thèse, j'ai notamment caractérisé fonctionnellement une isoforme androgéno-indépendante du canal TRPM8 prostatique, et montré sa présence au niveau du réticulum endoplasmique où elle peut induire la vidange des stocks calciques réticulaires et ainsi provoquer l'ouverture des canaux SOC à l'origine de l'entrée capacitive de calcium dans la cellule. Plus récemment, en collaboration avec le Dr Bidaux, nous avons commencé à caractériser d'autres isoformes plus courtes de TRPM8 (notamment celles de 6 et 18 kDa, (Bidaux et al., 2012)). Ces isoformes font actuellement l'objet de plusieurs études au sein de notre équipe de par leurs fonctions modulatrices de l'activité du canal TRPM8, mais aussi en raison de leur impact sur l'homéostasie calcique réticulaire qui, comme nous l'avons montré dans de nombreux travaux préliminaires, est cruciale dans le devenir des cellules cancéreuses prostatiques. Nous avons par ailleurs démontré que le gène *trpm8* est régulé par le récepteur aux androgènes dans les cellules de la prostate humaine. Cette régulation stricte de TRPM8 par les androgènes fait de cette protéine un possible facteur pronostique du cancer avancé de la prostate. En plus de ce rôle prometteur, la ou les fonction(s) physiologique(s) et physiopathologique(s) de ce canal dans la prostate n'est (ne sont) toujours pas complétement élucidée(s). A la suite de la publication d'un premier travail sur la régulation de TRPM8 par la PSA (Gkika et al., 2010), je me suis intéressé à la dépendance du canal TRPM8 vis-à-vis de protéines partenaires pour son fonctionnement normal et pathologique dans la prostate. Il a en effet été montré pour d'autres canaux TRPs que la présence de telles protéines est indispensable pour leur bon adressage membranaire et/ou leur activation. Cette étude s'inscrit donc dans ma volonté de mieux comprendre les nombreux facteurs pouvant contrôler la fonction du canal TRPM8 et de ses isoformes dans le cadre de la cancérogenèse prostatique.

B. Résultats

I Rôle du canal calcique membranaire TRPM8 dans la cancérogenèse prostatique (article 5)

Une première identification/caractérisation d'isoformes courtes de TRPM8 a été publiée (Bidaux et al., 2012). Ce que nous montrons, c'est qu'il existe un épissage alternatif de TRPM8 qui donne naissance à deux protéines tronquées correspondant à l'extrémité N-terminale du canal. Ces deux isoformes sont retrouvées dans les cellules cancéreuses prostatiques, et l'une de leurs fonctions consiste à moduler la fonction du canal TRPM8 dans la membrane plasmique en interagissant directement avec son extrémité C-terminale. Plus précisément, nous montrons que les isoformes stabilisent le canal dans une conformation « fermée », rendant ainsi le canal moins susceptible de s'ouvrir en réponse à ses agonistes. Cette étude initiale s'est prolongée par la recherche d'autres isoformes du canal TRPM8 présentes dans les cellules prostatiques cancéreuses et saines, ainsi que par l'identification des effets physiologiques de ces isoformes dans nos modèles (Bidaux et al., 2016). Cette recherche ne s'est cependant pas limitée au seul tissu épithélial prostatique (Bidaux et al., 2015a)(Genova et al., 2017). En ce qui concerne la forme classique de TRPM8, en collaboration avec un groupe Irlandais, nous avons construit un modèle décrivant les domaines transmembranaires du canal, et mis en évidence les éléments clés de cette structure. Afin de valider ce modèle, des mutations ponctuelles ont été réalisées, et j'ai effectué les expériences de patch-clamp permettant de déterminer leurs impacts fonctionnels sur l'activité du canal (Bidaux et al., 2015b).

Pour ce qui est de l'axe de recherche sur les protéines partenaires de TRPM8, en collaboration avec le Dr Gkika, nous avons identifié 6 protéines partenaires putatives du canal. Après avoir testé fonctionnellement l'effet de ces partenaires sur le canal dans un modèle d'expression hétérologue (utilisation de siRNA/surexpression du partenaire étudié), nous avons sélectionné la protéine EAPA2 comme étant la plus prometteuse. En effet, cette protéine présomptive chez l'Homme est exprimée exclusivement au niveau prostatique, et sa suppression inhibe totalement l'activité du canal qui n'est plus exporté à la membrane plasmique. De plus, sa seule surexpression suffit à augmenter le nombre de canaux présents

dans la membrane plasmique. Peu de temps après avoir obtenu ces résultats, ma collègue a identifié dans les bases de données une deuxième protéine présomptive apparentée à EAPA2 et présentant une délétion de sa partie C-terminale qui possède une homologie avec la PI3-kinase. Nous avons mis en ligne ces séquences, et nous avons nommé les protéines humaines correspondantes TCAFs (TRP Channel Associated Factor). Mes observations montrent que la forme tronquée (notée TCAF2), qui est exprimée dans les cellules prostatiques, possède une fonction inhibitrice de l'activité du canal TRPM8. Des expériences complémentaires (co-immunoprécipitations, FRET) ont permis de prouver la colocalisation de TRPM8 avec les TCAFs. Nous avons également montré, en utilisant un mutant de TCAF1 dépourvu de son domaine PI3K, que cette activité est absolument cruciale pour le fonctionnement du canal. Parallèlement, ma collègue a montré des variations d'expression de ces deux protéines en fonction du stade de la maladie grâce à la technique de PCR en temps réel. Ces observations sont concordantes avec nos précédentes publications qui avaient montré une augmentation de l'expression de TRPM8 dans les phases précoces du cancer pour ensuite retomber dans les stades tardifs plus agressifs. Nos résultats permettent donc d'expliquer ces variations, et sachant que TRPM8 est actuellement utilisé pour le diagnostic du cancer de la prostate, nous pourrions à terme proposer un affinage de ces tests en utilisant la balance de ces deux protéines. Ces résultats sont présentés dans l'article 5.

II Implication des canaux SOC dans le contrôle de la quiescence des cellules souches cancéreuses prostatiques (article 6)

Une autre thématique sur laquelle je suis impliqué à l'heure actuelle concerne l'étude des cellules souches cancéreuses (CSC). En effet, un nombre croissant d'études suggèrent que, de manière générale, le cancer pourrait être initié par un type cellulaire ayant des propriétés identiques à celles des cellules souches (auto-renouvellement, capacité à induire une tumeur), ce qui a conduit à l'hypothèse de l'existence d'une «cellule souche cancéreuse». Selon cette hypothèse, l'échec des thérapies conventionnelles s'expliquerait par la présence de ces CSC qui seraient insensibles aux traitements. Bien que cette hypothèse ait été validée dans plusieurs tissus, peu de choses sont connues sur le cancer de la prostate. Il est par ailleurs bien établi que le calcium a une fonction vitale dans la physiologie cellulaire, et que

des altérations touchant les canaux calciques peuvent perturber les fonctions cellulaires et favoriser le cancer. En collaboration avec l'U837 à Lille, nous avons entamé une étude de l'expression et de l'activité des canaux calciques en nous intéressant au modèle du cancer de la prostate ainsi qu'à celui du mélanome sur lequel travaille cette équipe. Après une longue étape de mise au point des conditions permettant d'isoler ces populations de CSC, nos résultats ont montré une claire diminution de l'expression et de l'activité des canaux calciques SOC dans les CSC par rapport aux cellules non-souches. Par ailleurs, nous avons pu mettre en évidence dans les CSC une diminution du taux de calcium cytoplasmique associée à une plus faible activité du facteur de transcription NFAT. L'article 6 montre les résultats de cette étude par laquelle j'ai obtenu un financement de La Ligue contre le cancer (2014-2015). A l'heure actuelle, nous sommes en train de réaliser des expériences complémentaires afin d'adresser les principales critiques que nous avons reçus après avoir soumis ce travail. La plus grande critique concernant la validation de nos modèles de CSCs, nous allons procéder à des tests in vivo afin de montrer que la population de CSCs est capable de générer des tumeurs après injection à faible densité (<10000 cellules), contrairement aux cellules non-souches.

III Le Sigma 1 récepteur, un nouveau partenaire des canaux SOC ?

A l'heure actuelle, et avec l'aide d'une étudiante en thèse que j'encadre, nous avons démarré une nouvelle étude portant sur le rôle du récepteur sigma 1 (S1R) en tant que protéine partenaire des canaux SOC dans le cadre du cancer de la prostate. Ce travail est réalisé en étroite collaboration avec le Dr. Olivier Soriani (IBV, Nice), un spécialiste Français du S1R. Ce projet est financé par La Ligue contre le cancer pour la période 2017-2018.

Initialement identifié comme un récepteur aux opioïdes, le récepteur Sigma 1 (S1R) répond en réalité à de nombreuses molécules exogènes naturelles ou synthétiques. Ce récepteur possède au moins un segment transmembranaire permettant son insertion dans les membranes cellulaires (Schmidt et al., 2016). Ainsi, il peut être retrouvé au niveau de la membrane plasmique, mais aussi au niveau des membranes du réticulum endoplasmique et de la mitochondrie. Bien que l'implication de ce récepteur ait été retrouvée dans différentes pathologies principalement neurologiques, de nombreuses études ont associé le S1R au cancer.

Des auteurs ont ainsi montré une augmentation de l'expression de la protéine proportionnellement à l'agressivité de différents cancers, notamment celui de la prostate (Aydar et al., 2006). Malgré ces observations prometteuses, aucun rôle précis n'a été attribué à ce récepteur dans le contexte du cancer. Par ailleurs, il existe un nombre croissant d'études montrant son rôle de protéine partenaire. Ce récepteur est en effet capable de moduler de nombreuses protéines cibles, dont les canaux ioniques (Crottès et al., 2013). Il n'existe cependant pour le moment aucune donnée montrant l'interaction de ce récepteur avec les canaux SOC. Le but de cette étude est donc de mettre en évidence dans le cancer de la prostate le rôle du S1R et de ses ligands.

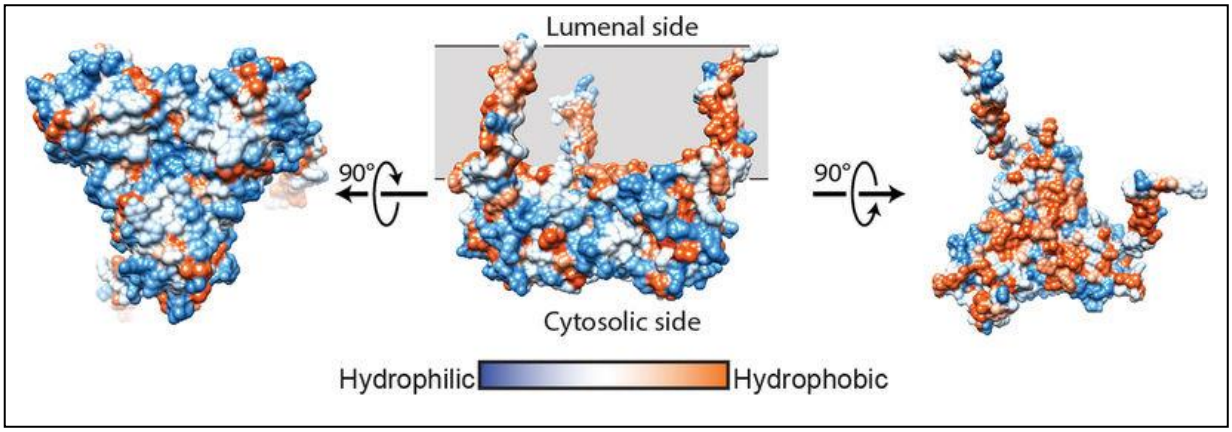

Figure 2 : Structure du S1R et intégration dans la membrane du réticulum endoplasmique (Schmidt et al., 2016).

Il a été montré par de nombreuses équipes que l'expression du S1R augmente dans différents cancers, notamment celui de la prostate, en corrélation avec l'agressivité. La première étape du projet a donc consisté à mesurer l'expression du récepteur dans le modèle du cancer de la prostate. Pour cela, nous avons réalisé des RT-qPCR sur des prélèvements humains sains et cancéreux obtenus grâce à une collaboration avec le Pr Vandier (Inserm UMR1069, Tours). Nous avons ainsi pu confirmer les données de la littérature qui indiquent une augmentation de l'expression du récepteur S1R dans le cancer de la prostate. Parallèlement, nous avons réalisé des RT-qPCR et des Western Blot afin de quantifier le taux d'ARNm et de protéine du récepteur dans différentes lignées cellulaires représentatives des principaux stades de la cancérogenèse prostatique. Par ces expériences, nous avons confirmé la surexpression du S1R dans les cellules cancéreuses prostatiques

androgéno-dépendantes LNCaP. Cependant, les cellules cancéreuses prostatiques androgéno-indépendantes PC3 n'expriment que faiblement le S1R. Ces résultats suggèrent l'existence d'une possible régulation de l'expression du récepteur par les androgènes que nous sommes en train de vérifier.

Un point important de cette étude concerne la localisation cellulaire du S1R. En effet, ce récepteur est connu pour son rôle de protéine chaperonne dans le réticulum endoplasmique. Cependant, il existe plusieurs travaux suggérant que le S1R pourrait également se trouver dans la membrane plasmique où il interagirait directement avec certains canaux ioniques. Par des expériences d'immunofluorescence, nous avons pu mettre en évidence la présence du récepteur dans le réticulum endoplasmique, ainsi que dans la membrane plasmique. Ces expériences sont actuellement complétées par des cinétiques de stimulation des canaux SOC afin de voir s'ils entraînent une redistribution du S1R dans la membrane plasmique. Pour cela, nous collaborons avec le Dr Héliot (phLAM, Université Lille1) ainsi qu'avec le Dr. Touil et la plateforme de cytométrie et de tri cellulaire de Lille (N. Jouy, IRCL).

Comme indiqué précédemment, un nombre croissant d'études montrent que le S1R est une protéine partenaire de canaux ioniques, et qu'il peut à ce titre moduler leur activité et leur localisation. La deuxième étape de ce projet consiste donc à déterminer si ce récepteur peut interagir avec nos canaux d'intérêts, mais aussi à étudier la modulation des canaux calciques SOC par le S1R et ses ligands. Pour ces études fonctionnelles, nous utilisons principalement les techniques de patch-clamp et d'imagerie calcique, afin de mesurer l'activité des canaux calciques étudiés. Nos premiers résultats montrent une modulation de l'activité de ces canaux lors de la surexpression du S1R. Ainsi, l'activité des canaux SOC est augmentée dans des cellules prostatiques cancéreuses surexprimant S1R. L'utilisation d'un siRNA dirigé contre le S1R a l'effet inverse sur l'activité de ces canaux calciques, ce qui suggère un lien étroit entre l'expression du récepteur et l'activité des canaux. Par ailleurs, des agonistes du S1R tels que l'igmésine, et des antagonistes tels que le BD-1063 reproduisent les effets de la surexpression et de l'inhibition de son expression.

Par la suite, nous allons étudier l'impact physiopathologique des modulations mises en évidence précédemment, notamment sur la prolifération et la résistance à l'apoptose des cellules cancéreuses prostatiques. Nos résultats montrent un impact clair de la modulation du S1R sur la prolifération liée à l'activité basale des canaux

SOC, et nous allons entamer d'ici peu nos premières études in vivo afin de valider ces observations.

CONCLUSION

Nous voilà donc à la fin de ce manuscrit. Comme indiqué dans l'introduction, ceci n'est pas une description exhaustive de mon travail. Je n'ai par exemple rien dit de ma participation au réseau européen IonTraC (https://campus.uni-muenster.de/iontrac/home/) portant sur l'étude du cancer du pancréas, ou sur d'autres collaborations internes et externes au laboratoire. Ce n'est évidemment pas un jugement de valeur sur ces autres travaux, mais j'ai préféré mettre l'accent sur les thématiques où je me suis le plus directement impliqué.

Pour dire quelques mots de mes projets à court terme, je suis actuellement en train de développer quelques collaborations avec le Japon. En effet, le site Lillois a eu la chance de voir se développer la thématique des BioMEMs en partenariat avec l'université de Tokyo, sous la houlette du Dr Collard. Dans ce cadre, et grâce à la recommandation de Dominique, j'ai pu établir un contact direct avec les équipes de Tokyo lors d'un voyage réalisé en Novembre 2016. Depuis, la doctorante dont je m'occupe a obtenu un financement de la JSPS afin de réaliser un séjour de 3 mois dans le laboratoire du Pr Sakai (IIS, UTokyo). Dans ce cadre, nous allons réaliser une première étude de l'expression des canaux calciques exprimés dans leurs modèles de iPS hépatocytaires à différentes étapes de leur différenciation en hépatocytes matures. Par ailleurs, je suis actuellement en attente d'une réponse concernant une demande de financement par la JSPS d'un séjour de 2 mois dans le laboratoire du Pr Takeuchi (IIS, UTokyo). En cas d'obtention de ce financement, j'irai réaliser dans son laboratoire des expériences d'électrophysiologie concernant le rôle du S1R en tant que partenaire des canaux calciques. En effet, ce laboratoire a mis au point des systèmes microfluidiques permettant de fusionner des vésicules lipidiques durant un enregistrement électrophysiologique. Ceci me permettrait de suivre en temps réel l'effet du S1R sur l'activité de mes canaux d'intérêt. J'espère également que ces échanges avec le Japon constitueront une base pour de futures demandes de financement de grande ampleur entre nos équipes.

Il est maintenant plus que temps de te laisser, ami lecteur, retourner à tes activités habituelles. Merci à toi pour ta patience, et pour le temps que tu as bien voulu consacrer à la lecture de mes pérégrinations scientifiques. Nous ne nous croiserons probablement plus par manuscrit interposé, sauf invention d'une nouvelle forme de diplôme universitaire (je vais croiser les doigts pour que cela n'arrive pas !). Bonne chance dans tes travaux de recherche et tes demandes de financement, et rappelle-toi que si tu as besoin d'aide pour des expériences en fonctionnel, je ne suis jamais bien loin !

BIBLIOGRAPHIE

Aydar, E., Onganer, P., Perrett, R., Djamgoz, M.B., and Palmer, C.P. (2006). The expression and functional characterization of sigma (σ) 1 receptors in breast cancer cell lines. Cancer Lett. *242*, 245–257.

Bidaux, G., Beck, B., Zholos, A., Gordienko, D., Lemonnier, L., Flourakis, M., Roudbaraki, M., Borowiec, A.-S., Fernandez, J., Delcourt, P., et al. (2012). Regulation of activity of transient receptor potential melastatin 8 (TRPM8) channel by its short isoforms. J. Biol. Chem. *287*, 2948–2962.

Bidaux, G., Borowiec, A., Gordienko, D., Beck, B., Shapovalov, G.G., Lemonnier, L., Flourakis, M., Vandenberghe, M., Slomianny, C., Dewailly, E., et al. (2015a). Epidermal TRPM8 channel isoform controls the balance between keratinocyte proliferation and differentiation in a cold-dependent manner. Proc. Natl. Acad. Sci. U. S. A. *112*, E3345–E3354.

Bidaux, G., Sgobba, M., Lemonnier, L., Borowiec, A.-S., Noyer, L., Jovanovic, S., Zholos, A.V., and Haider, S. (2015b). Functional and Modeling Studies of the Transmembrane Region of the TRPM8 Channel. Biophys. J. *109*, 1840–1851.

Bidaux, G., Borowiec, A.-S., Dubois, C., Delcourt, P., Schulz, C., Abeele, F.V., Lepage, G., Desruelles, E., Bokhobza, A., Dewailly, E., et al. (2016). Targeting of short TRPM8 isoforms induces 4TM-TRPM8-dependent apoptosis in prostate cancer cells. Oncotarget.

Carafoli, E. (2004). The ambivalent nature of the calcium signal. J. Endocrinol. Invest. *27*, 134–136.

Crottès, D., Guizouarn, H., Martin, P., Borgese, F., and Soriani, O. (2013). The sigma-1 receptor: a regulator of cancer cell electrical plasticity? Membr. Physiol. Membr. Biophys. *4*, 175.

Duan, D., Winter, C., Cowley, S., Hume, J.R., and Horowitz, B. (1997). Molecular identification of a volume-regulated chloride channel. Nature *390*, 417–421.

Fixemer, T., Remberger, K., and Bonkhoff, H. (2002). Apoptosis resistance of neuroendocrine phenotypes in prostatic adenocarcinoma. The Prostate *53*, 118–123.

Frischauf, I., Fahrner, M., Jardin, I., and Romanin, C. (2016). The STIM1: Orai Interaction. Adv. Exp. Med. Biol. *898*, 25–46.

Genova, T., Grolez, G.P., Camillo, C., Bernardini, M., Bokhobza, A., Richard, E., Scianna, M., Lemonnier, L., Valdembri, D., Munaron, L., et al. (2017). TRPM8 inhibits endothelial cell migration via a non-channel function by trapping the small GTPase Rap1. (United States).

Gkika, D., Flourakis, M., Lemonnier, L., and Prevarskaya, N. (2010). PSA reduces prostate cancer cell motility by stimulating TRPM8 activity and plasma membrane expression. Oncogene *29*, 4611–4616.

Legrand, G., Humez, S., Slomianny, C., Dewailly, E., Vanden Abeele, F., Mariot, P., Wuytack, F., and Prevarskaya, N. (2001). Ca2+ pools and cell growth. Evidence for sarcoendoplasmic Ca2+-ATPases 2B involvement in human prostate cancer cell growth control. J. Biol. Chem. *276*, 47608–47614.

Lemonnier, L., Vitko, Y., Shuba, Y.M., Vanden Abeele, F., Prevarskaya, N., and Skryma, R. (2002a). Direct modulation of volume-regulated anion channels by Ca(2+) chelating agents. FEBS Lett. *521*, 152–156.

Lemonnier, L., Prevarskaya, N., Shuba, Y., Vanden Abeele, F., Nilius, B., Mazurier, J., and Skryma, R. (2002b). Ca2+ modulation of volume-regulated anion channels: evidence for colocalization with store-operated channels. FASEB J. Off. Publ. Fed. Am. Soc. Exp. Biol. *16*, 222–224.

Lemonnier, L., Prevarskaya, N., Mazurier, J., Shuba, Y., and Skryma, R. (2004). 2-APB inhibits volume-regulated anion channels independently from intracellular calcium signaling modulation. FEBS Lett. *556*, 121–126.

Lemonnier, L., Lazarenko, R., Shuba, Y., Thebault, S., Roudbaraki, M., Lepage, G., Prevarskaya, N., and Skryma, R. (2005). Alterations in the regulatory volume decrease (RVD) and swelling-activated Cl- current associated with neuroendocrine differentiation of prostate cancer epithelial cells. Endocr. Relat. Cancer *12*, 335–349.

Lievremont, J.-P., Bird, G.S.J., and Putney, J.W.J. (2004). Canonical transient receptor potential TRPC7 can function as both a receptor- and store-operated channel in HEK-293 cells. Am. J. Physiol. Cell Physiol. *287*, C1709–C1716.

Maeno, E., Ishizaki, Y., Kanaseki, T., Hazama, A., and Okada, Y. (2000). Normotonic cell shrinkage because of disordered volume regulation is an early prerequisite to apoptosis. Proc. Natl. Acad. Sci. U. S. A. *97*, 9487–9492.

Mariot, P., Vanoverberghe, K., Lalevee, N., Rossier, M.F., and Prevarskaya, N. (2002). Overexpression of an alpha 1H (Cav3.2) T-type calcium channel during neuroendocrine differentiation of human prostate cancer cells. J. Biol. Chem. *277*, 10824–10833.

Montell, C. (2005). The TRP superfamily of cation channels. Sci. STKE Signal Transduct. Knowl. Environ. *2005*, re3.

Okada, T., Inoue, R., Yamazaki, K., Maeda, A., Kurosaki, T., Yamakuni, T., Tanaka, I., Shimizu, S., Ikenaka, K., Imoto, K., et al. (1999). Molecular and functional characterization of a novel mouse transient receptor potential protein homologue TRP7. Ca(2+)-permeable cation channel that is constitutively activated and enhanced by stimulation of G protein-coupled receptor. J. Biol. Chem. *274*, 27359–27370.

Okada, Y., Maeno, E., Shimizu, T., Dezaki, K., Wang, J., and Morishima, S. (2001). Receptor-mediated control of regulatory volume decrease (RVD) and apoptotic volume decrease (AVD). J. Physiol. *532*, 3–16.

Pasantes-Morales, H. (2016). Channels and Volume Changes in the Life and Death of the Cell. Mol. Pharmacol. *90*, 358–370.

Peretz, A., Sandler, C., Kirschfeld, K., Hardie, R.C., and Minke, B. (1994). Genetic dissection of light-induced Ca2+ influx into Drosophila photoreceptors. J. Gen. Physiol. *104*, 1057–1077.

Raffo, A.J., Perlman, H., Chen, M.W., Day, M.L., Streitman, J.S., and Buttyan, R. (1995). Overexpression of bcl-2 protects prostate cancer cells from apoptosis in vitro and confers resistance to androgen depletion in vivo. Cancer Res. *55*, 4438–4445.

Riccio, A., Medhurst, A.D., Mattei, C., Kelsell, R.E., Calver, A.R., Randall, A.D., Benham, C.D., and Pangalos, M.N. (2002). mRNA distribution analysis of human TRPC family in CNS and peripheral tissues. Brain Res. Mol. Brain Res. *109*, 95–104.

Schmidt, H.R., Zheng, S., Gurpinar, E., Koehl, A., Manglik, A., and Kruse, A.C. (2016). Crystal structure of the human sigma1 receptor. Nature *532*, 527–530.

Shi, J., Mori, E., Mori, Y., Mori, M., Li, J., Ito, Y., and Inoue, R. (2004). Multiple regulation by calcium of murine homologues of transient receptor potential proteins TRPC6 and TRPC7 expressed in HEK293 cells. J. Physiol. *561*, 415–432.

Shuba, Y.M., Prevarskaya, N., Lemonnier, L., Van Coppenolle, F., Kostyuk, P.G., Mauroy, B., and Skryma, R. (2000). Volume-regulated chloride conductance in the LNCaP human prostate cancer cell line. Am. J. Physiol. Cell Physiol. *279*, C1144–C1154.

Skryma, R., Mariot, P., Bourhis, X.L., Coppenolle, F.V., Shuba, Y., Vanden Abeele, F., Legrand, G., Humez, S., Boilly, B., and Prevarskaya, N. (2000). Store depletion and store-operated Ca2+ current in human prostate cancer LNCaP cells: involvement in apoptosis. J. Physiol. *527 Pt 1*.

Vanden Abeele, F., Skryma, R., Shuba, Y., Van Coppenolle, F., Slomianny, C., Roudbaraki, M., Mauroy, B., Wuytack, F., and Prevarskaya, N. (2002). Bcl-2-dependent modulation of Ca(2+) homeostasis and store-operated channels in prostate cancer cells. Cancer Cell *1*, 169–179.

Vanoverberghe, K., Vanden Abeele, F., Mariot, P., Lepage, G., Roudbaraki, M., Bonnal, J.L., Mauroy, B., Shuba, Y., Skryma, R., and Prevarskaya, N. (2004). Ca2+ homeostasis and apoptotic resistance of neuroendocrine-differentiated prostate cancer cells. Cell Death Differ. *11*, 321–330.

Vashchenko, N., and Abrahamsson, P.-A. (2005). Neuroendocrine differentiation in prostate cancer: implications for new treatment modalities. Eur. Urol. *47*, 147–155.

Article 1

The FASEB Journal express article 10.1096/fj.01-0383fje. Published online December 14, 2001.

Ca^{2+} modulation of volume-regulated anion channels: evidence for colocalization with store-operated channels

Loïc Lemonnier, Natalia Prevarskaya, Yaroslav Shuba,* Fabien Vanden Abeele, Bernd Nilius,† Joël Mazurier, and Roman Skryma

Laboratoire de Physiologie Cellulaire, INSERM EPI 9938, Bâtiment SN3, USTL, 59655 Villeneuve d'Ascq, France

Permanent addresses: *Bogomoletz Institute of Physiology, Bogomoletz Str., 4, 01024 Kiev-24, Ukraine. †KU Leuven, Laboratorium voor Fysiologie, B-3000 Leuven, Belgium

Corresponding author: Roman Skryma, Laboratoire de Physiologie Cellulaire, INSERM EPI 9938, Bâtiment SN3, Université des Sciences et Technologies de Lille, 59655 Villeneuve d'Ascq, France. E-mail: phycel@univ-lille1.fr

ABSTRACT

Ca^{2+} regulation of Cl^- current induced by cell swelling ($I_{Cl,swell}$) in response to hypotonicity was studied in human prostate cancer epithelial cells (LNCaP) by using the patch-clamp technique. Increase of global intracellular Ca^{2+} ($[Ca^{2+}]_{in}$) to 1 μM as well as variations of the extracellular Ca^{2+} ($[Ca^{2+}]_{out}$) in the 0 to 10 mM range did not affect time course of the development, maximal amplitude, rectification properties, and kinetics of $I_{Cl,swell}$. However, the presence of 0.1 μM thapsigargin (TG), an inhibitor of endoplasmic reticulum (ER) Ca^{2+} pump, resulted in a more than 50% inhibition of $I_{Cl,swell}$. The blockade of plasma membrane store-operated channels (SOCs), activated in the presence of TG, by 2 mM Ni^{2+} prevented TG-conferred $I_{Cl,swell}$ inhibition by extracellular Ca^{2+}. In the presence of TG and Ca^{2+}, the cells failed to exhibit regulatory volume decrease. We conclude that interaction between volume-regulated anion channels (VRACs) carrying $I_{Cl,swell}$ and Ca^{2+} occurs in the microdomains from the inner surface of the membrane that are not accessible to the changes in $[Ca^{2+}]_{in}$, but can be readily reached by Ca^{2+} entering the cell via plasma membrane, especially through SOCs. Preferred access of SOC-transported Ca^{2+} to VRAC suggests colocalization of these channels in the cell membrane.

Key words: calcium • capacitative entry • chloride channels • regulatory volume decrease

Activation of the chloride current in response to cell swelling ($I_{Cl,swell}$) is one of the major mechanisms via which cells tend to restore their volume following hypoosmotic stress. At normal resting potentials, this current provides for the loss of intracellular Cl^- and some other anions, thereby decreasing intracellular osmolarity to counteract water inflow that would otherwise lead to increased cell volume. This process is known as regulatory volume decrease (RVD). Extracellular osmotic perturbations are not the only reason for the alterations of the cell volume. At constant extracellular osmolarity, such processes as active solute uptake (1), action of the hormones (2), proliferation (3, 4), differentiation (5, 6), and

apoptosis (4, 7, 8) at some point are all associated with changes in cell volume, implying activation of $I_{Cl,swell}$ and concomitantly the role of this current in the regulation of these processes.

The molecular nature of the channels underlying $I_{Cl,swell}$ is unknown; therefore, we denote them generally as volume-regulated anion channels (VRACs). These channels are described in many cell types, where they exhibit such common properties as volume sensitivity, cytosolic ATP dependency, moderate outward rectification, characteristic selectivity to halogens, and distinct pharmacology. They also have variable patterns of regulation by intracellular second-messenger systems and somewhat different single-channel conductance (for reviews, see refs 9–14). There is no consensus on the mechanisms via which cell volume signals are transducted into activation of VRACs. These data strongly suggest that VRACs may have complex molecular structures, with cell-specific subunit expression, and that different auxiliary subunits may exert strong modulatory effects on the channel's function.

Ca^{2+} is known to be a universal second messenger regulating many cellular processes and several ion channels, including Cl^- channels. In general, intracellular Ca^{2+} may participate in VRAC regulation indirectly via activation of Ca^{2+}-dependent protein kinases such as protein kinase C (PKC) and Ca^{2+}/calmoduline-dependent protein kinase II (CaM kinase II) as well as via direct interaction with the channel. The reported modes of VRAC regulation involving Ca^{2+} are diverse and cell specific, and it is not always clear whether the effect is direct or mediated by a kinase activity. Both PKC (15–20) and CaM kinase II (21, 22) have been shown to modulate $I_{Cl,swell}$ at least in some cell types, whereas in a vast majority of cells, simple variations of global intracellular Ca^{2+} were found to exert no effects on $I_{Cl,swell}$ (for a review, see ref 11). Only in a few preparations was activation of $I_{Cl,swell}$ shown to be facilitated in response to an increase in intracellular Ca^{2+} (16, 23, 24). The spectrum of the reported effects of extracellular Ca^{2+} on $I_{Cl,swell}$ is also broad, including no effects (16, 25), down-regulation (6, 26, 27), up-regulation (28, 29), and changing kinetics of the VRAC development (29) and of voltage-dependent inactivation (6, 26, 27). In addition, a mechanism involving G-protein-coupled Ca^{2+}-sensing receptors has recently been proposed for mediating the up-regulating action of extracellular Ca^{2+} on $I_{Cl,swell}$ in human epithelial intestine 407 cells (30).

The diversity of the results on Ca^{2+}-dependent regulation of $I_{Cl,swell}$ may be attributed on one hand to the cell-specific properties of VRACs, but on the other hand it may also be explained by various degrees of accessibility of VRACs to the changes in global intracellular Ca^{2+} and/or by colocalization of VRACs with various Ca^{2+}-transporting structures in different cell types. Distinguishing between these possibilities in different cells is a subject of physiological importance.

We have recently described VRAC-mediated $I_{Cl,swell}$ in a human prostate cancer epithelial cell line, LNCaP (lymph node carcinoma of the prostate), and showed its susceptibility to the regulation via protein tyrosine phosphorylation (31). Given the role that Ca^{2+} plays in the physiology of the prostate epithelial cells (32, 33), here we focused on possible modes and mechanisms of the direct VRAC regulation by Ca^{2+} in these cells and show that although variations of both intracellular and extracellular global Ca^{2+} concentrations had no visible effects on $I_{Cl,swell}$, transmembrane Ca^{2+} influx strongly modulates it. Our data suggest that interaction

between VRAC and Ca^{2+} occurs in the confined compartments from the inner surface of the membrane that are not accessible to the changes of global intracellular Ca^{2+}, but can be readily reached by Ca^{2+} entering the cell via plasma membrane, especially through the store-operated Ca^{2+} channels.

MATERIALS AND METHODS

Cell cultures

LNCaP cells from the American Type Culture Collection (Manassas, VA) were cultured in RPMI 1640 medium (Biowhittaker, Fontenay sous Bois, France) supplemented with 5mM L-glutamine (Sigma, L'Isle d'Abeau, France) and 10% fetal bovine serum (Seromed, Poly-Labo, Strasbourg, France). The culture medium also contained 50,000 IU/l penicillin and 50 mg/l streptomycin. Cells were routinely grown in 50-ml flasks (Nunc, Poly-Labo, Strasbourg, France) and kept at 37°C in a humidified incubator in an air/CO_2 (95%/5%) atmosphere. For electrophysiological experiments, the cells were subcultured in petri dishes (Nunc) and used after 3–6 days.

Electrophysiology and solutions

Macroscopic membrane ionic currents in LNCaP cells (average whole-cell membrane capacitance, C_m=25.5±1.2 pF, *n*=46) were recorded in the whole-cell configuration of the patch-clamp technique with the use of computer-controlled EPC-9 amplifier (HEKA Electronic, Lambrecht/Pfalz,Germany). Because LNCaP cells have voltage-activated, tetraethylammonium (TEA)-sensitive K^+ current (34), to prevent $I_{Cl,swell}$ contamination with this current, we used TEA as a major cation in our experimental extracellular solutions. The composition of the normal and TEA-based isotonic (310 mosmol/l) and hypotonic (190 mosmol/l) extracellular solutions is presented in Table 1. The basic intracellular pipette solution (osmolarity 290 mosmol/l) contained (in mM) K gluconate, 100; KCl, 50; $MgCl_2$, 1; $CaCl_2$, 0.5; HEPES, 10; EGTA, 8; pH, 7.2. Using the WinMaxc 1.7 program (35), we estimated the concentration of free Ca^{2+} in this solution to be 10^{-8} M. Unless specified otherwise, this basic intracellular solution was used in all experiments. To adjust free Ca^{2+} concentration to 1 μM, $CaCl_2$ content in the basic intracellular solution was raised to 6.6 mM. The resistance of the pipette varied between 3 and 5 MΩ, and series resistance compensation was used to improve voltage-clamp performance. Necessary supplements were added directly to the respective solutions, in concentrations that could not significantly change the osmolarity. Changes of the external solutions were carried out using a multibarrel puffing micropipette with common outflow that was positioned in close proximity to the cell under investigation. During the experiment, the cell was continuously superfused with the solution via puffing pipette to reduce possible artifacts related to the switches from static to moving solution and vise versa. Complete external solution exchange was achieved in <1 s.

Flow cytometry and $[Ca^{2+}]_{in}$ measurements

The estimations of the changes of cell volume during the RVD process were performed on a FACScalibur flow cytometer (Becton-Dickinson, San Jose, CA) with the use of Q Cell Quest

software for data analysis (36). The light-scatter channels were set on linear gains. Cells in suspension in normal or Hypo-TEA solutions were gated for forward-angle scatters, and 5000 particles of each gated population were analyzed.

Fluorescence $[Ca^{2+}]_{in}$ measurements were conducted on fura-2AM (5 μM) loaded (30 min) LNCaP cells, using a photomultiplier-based system (Photon Technologies, Princeton, NJ) and double wavelength (340 and 380 nM) excitation protocol to quantify the absolute value of Ca^{2+} concentration (37).

RESULTS

Effects of global intra- and extracellular Ca^{2+} on $I_{Cl,swell}$

To determine whether or not either intra- or extracellular Ca^{2+} is capable of modulating properties of $I_{Cl,swell}$, we performed three series of experiments. In the first series, the cells were dialyzed with our basic intracellular solution with free Ca^{2+} concentration ($[Ca^{2+}]_{in}$) adjusted to 10^{-8} M, and $I_{Cl,swell}$ was elicited by cell exposure to the hypo-TEA solution containing standard extracellular Ca^{2+} concentration ($[Ca^{2+}]_{out}$) of 2 mM (2/Ca Hypo-TEA, see Table 1). These conditions were considered as control and were used to evaluate baseline properties of $I_{Cl,swell}$. In the second series of experiments, aimed to determine the effects of extracellular Ca^{2+}, its concentration in the hypo-TEA solution was elevated to 10 mM (10/Ca Hypo-TEA, see Table 1) while using the same basic intracellular solution for cells dialysis. The third series of experiments was undertaken to test for the effects of intracellular Ca^{2+} by using Ca^{2+}/EGTA buffer to adjust $[Ca^{2+}]_{in}$ in the pipette solution to 1 μM while eliciting $I_{Cl,swell}$ with the standard 2/Ca Hypo-TEA. In all experiments, $I_{Cl,swell}$ was evoked by hypotonic exposure after at least 5 min of cell dialysis with the intracellular pipette solution to make sure that Ca^{2+} concentration inside the cell reached the value of that in the dialyzing solution.

Figure 1 presents cumulative results of these three series of experiments (6–9 cells in each series): normalized time courses of $I_{Cl,swell}$ development at pulse potential (V_m) +50 mV and holding potential (V_h) –50 mV in response to hypotonic exposure (Fig. 1A , time courses for each individual cell were normalized to the maximal $I_{Cl,swell}$ value at V_m = +50 mV and then averaged), averaged current-voltage (I-V) relationships for $I_{Cl,swell}$ current densities (Fig. 1B), and original $I_{Cl,swell}$ recordings obtained in representative cells under three experimental conditions (Fig. 1C). The time courses shown in Figure 1A and the I-Vs in Figure 1B basically are superimposed, suggesting that variations of $[Ca^{2+}]_{out}$ or $[Ca^{2+}]_{in}$ did not noticeably affect either the temporary parameters of $I_{Cl,swell}$ activation in response to hypotonicity or the size and rectification properties of $I_{Cl,swell}$. Original tracings of $I_{Cl,swell}$ shown in Figure 1C also suggest that kinetics of the current at different voltages is not sensitive to the external or internal Ca^{2+}. Thus, our data allow one to conclude that variations in global intracellular or extracellular Ca^{2+} are not capable of modulating $I_{Cl,swell}$ in LNCaP cells.

We have also verified whether osmotic swelling of LNCaP cells results in an increase in intracellular Ca^{2+} concentration, as has been shown in some other cell types (38–41). The lower part of Figure 1A shows the time dependence of $[Ca^{2+}]_{in}$ monitored in fura-2-loaded LNCaP cells exposed to the hypotonic 2/Ca Hypo-TEA solution. Within the time span that is sufficient for

full $I_{Cl,swell}$ activation (upper part of Fig. 1A), $[Ca^{2+}]_{in}$ stays basically constant, suggesting that swelling of LNCaP cells and concomitant $I_{Cl,swell}$ activation do not interfere with intracellular Ca^{2+} homeostasis.

Thapsigargin confers $I_{Cl,swell}$ sensitivity to the regulation by extracellular Ca^{2+}

Several Ca^{2+}-regulated processes take place in a confined space to which Ca^{2+} ions either released from intracellular organelles or entering the cell via specific plasma membrane pathways have preferred access (42, 43). Having demonstrated that changes in global extra- or intracellular Ca^{2+} exert no effects on VRAC function in prostatic LNCaP cells, we were interested if Ca^{2+}/VRAC interaction may occur in the subcellular compartments with limited access to global Ca^{2+}.

We have recently shown that LNCaP cells have Ca^{2+}-release stores, Ca^{2+} content of which can be effectively manipulated with the use of thapsigargin (TG), an inhibitor of the SERCA Ca^{2+} pump of endoplasmic reticulum (ER) (33). Application of the TG in these cells causes depletion of Ca^{2+} stores followed by Ca^{2+} entry from extracellular space via plasma membrane store-operated channels (SOCs) (33). Thus, by using TG, we can raise intracellular Ca^{2+} by two physiologically relevant means: release from intracellular stores and entry via plasma membrane SOCs. Therefore, our next series of experiments was aimed to examine whether or not influencing intracellular Ca^{2+} homeostasis with TG can in any way alter Ca^{2+} sensitivity of $I_{Cl,swell}$.

Figure 2A shows the time course of $I_{Cl,swell}$ development in the representative cell in response to the hypotonic solutions supplemented with 0.1 μM TG. In the presence of TG (for almost 8 min), 10/Ca Hypo-TEA failed to evoke a statistically significant elevation of $I_{Cl,swell}$. However, complete removal of external Ca^{2+} in the presence of TG, that is, switching to TG-supplemented 0/Ca Hypo-TEA (see Table 1), elicited the development of typical $I_{Cl,swell}$.

We have also performed experiments in which $I_{Cl,swell}$ was first evoked by standard 2/Ca Hypo-TEA, and after the development of maximal current, the solution was switched either to 0/Ca Hypo-TEA plus TG (Fig. 2B) or to 10/Ca Hypo-TEA plus TG (Fig. 2C). Depending on the extracellular Ca^{2+} content, the consequences of TG inclusion appeared to be very different: If in the absence of Ca^{2+}, inclusion of TG produced almost no change of $I_{Cl,swell}$ (Fig. 2B) and in the presence of 10 mM $Ca^{2+,}$ it resulted in a dramatic $I_{Cl,swell}$ inhibition (Fig. 2C).

Lower concentrations of extracellular Ca^{2+} in the presence of TG produced less $I_{Cl,swell}$ inhibition. This is documented in Figure 2D, which shows original traces of $I_{Cl,swell}$ in the representative cell sequentially exposed to 0/Ca Hypo-TEA, 2/Ca Hypo-TEA, and 10/Ca Hypo-TEA in the presence of 0.1 μM TG. Figure 2E also demonstrates averaged I-V relationships for $I_{Cl,swell}$ current density in the respective solutions. In the presence of TG, the degree of inhibition at V_m = +50 mV increased from 37±6% (*n*=4) to 50.5±6.5% (*n*=7) in response to the elevation of $[Ca^{2+}]_{out}$ from 2 mM to 10 mM.

Thus, our results with TG coapplication unequivocally demonstrate that TG confers VRAC sensitivity to the inhibition by extracellular Ca^{2+}. The ineffectiveness of TG itself under zero $[Ca^{2+}]_{out}$ conditions argues against its possible direct action on VRAC and suggests the

involvement of TG-induced changes in the intracellular Ca^{2+} homeostasis in the mechanism of its action.

Which Ca^{2+} is more important?

As was previously mentioned, the inhibition of the SERCA pump by TG produces liberation of Ca^{2+} from intracellular stores followed by Ca^{2+} entry via plasma membrane SOCs that become activated by stores depletion. Ca^{2+} from which source (liberated from stores or entered via SOCs) plays a primary role in the TG-conferred VRAC sensitivity to the extracellular Ca^{2+}? Because TG confers sensitivity to VRAC, particularly to the extracellular Ca^{2+}, and this sensitivity becomes $[Ca^{2+}]_{out}$-dependent, whereas at 0 mM $[Ca^{2+}]_{out}$, TG produces no effects, we hypothesized that Ca^{2+} entering from the extracellular space via activated SOCs is a primary player in VRAC regulation.

To test this hypothesis, we conducted experiments with the use of Ni^{2+}, a blocker of store depletion-activated Ca^{2+} entry in LNCaP cells (33). Figure 3A shows the result of the experiment in the representative cell in which $I_{Cl,swell}$ was first elicited by a standard 2/Ca Hypo-TEA solution. After its maximal activation, the solution was changed to 10/Ca Hypo-TEA supplemented with 0.1 μM TG and 2 mM Ni^{2+}. In sharp contrast to what has been observed in 10/Ca Hypo-TEA with TG alone (see Fig. 2C), additional inclusion of Ni^{2+} completely prevented the downward trend of $I_{Cl,swell}$, consistent with the idea that indeed Ca^{2+} entering via SOCs is primarily responsible for the inhibition of VRAC.

Ca^{2+} current transported via SOCs is characterized by pronounced inward rectification; therefore, if this particular Ca^{2+} is responsible for the interaction with VRACs, one would expect stronger $I_{Cl,swell}$ inhibition at more negative holding potentials. To verify whether this is the case, we evoked $I_{Cl,swell}$ by exposing the cell to the standard 2/Ca Hypo-TEA, But before the administration of TG-supplemented 10/Ca Hypo-TEA, we increased the holding potential from regular –50 mV to 0 mV, at which SOC-mediated Ca^{2+} entry should be minimal. Consistent our expectations, the application of TG at this holding potential provoked only a tiny $I_{Cl,swell}$ inhibition (Fig. 3B). However, subsequent shift of the holding potential to –80 mV, at which Ca^{2+} influx via SOCs is facilitated, induced enhanced $I_{Cl,swell}$ rundown, which leveled at about 35% of its pre-TG amplitude (Fig. 3B), thus providing additional strong argument in favor of the SOC-Ca^{2+}-VRAC interaction hypothesis.

The activation of SOC-mediated Ca^{2+} entry in the presence of TG was confirmed by our fluorescence measurements of $[Ca^{2+}]_{in}$ in fura-2 loaded LNCaP cells, which are documented in Figure 3C. In the absence of extracellular Ca^{2+}, TG elicited transient elevation of $[Ca^{2+}]_{in}$ associated with the depletion of intracellular stores under conditions of inhibited uptake. Switching from Ca^{2+}-free to Ca^{2+}-containing extracellular medium in the continuing presence of TG produced a rapid increase in $[Ca^{2+}]_{in}$. This increase was $[Ca^{2+}]_{out}$-dependent, and at a given $[Ca^{2+}]_{out}$, it showed very little time-dependence, suggesting constant Ca^{2+} influx from extracellular space via activated SOCs.

Passive stores depletion in response to the cell's dialysis with high concentrations of Ca^{2+} buffers (EGTA or BAPTA) is also capable of activating SOCs (44). However, our control experiments

under conditions that allow passage of large Na^+ current via SOCs (45, 46) to permit its better resolution have shown that introduction of our basic intracellular solution (10^{-8} M free Ca^{2+} and 1 mM Mg^{2+}; see Materials and Methods) into LNCaP cells during dialysis is by itself not sufficient to activate SOCs (data not shown). Thus, in our experiments on Ca^{2+}-dependent regulation of VRACs, TG was the only intervention that could activate SOC-mediated Ca^{2+} influx.

To exclude specific actions of TG, which are not related to the activation of SOCs, and to confirm the necessity of Ca^{2+} entry, we have also performed experiments with the use of Ca^{2+} ionophore ionomycin (IM) instead of TG. By incorporating into the membranes and being able to transport Ca^{2+}, IM depletes the stores, thereby producing the effects on Ca^{2+} homeostasis qualitatively similar to those of TG (47). Again, inclusion of 1 μM IM in the 10/Ca Hypo-TEA solution caused $I_{Cl,swell}$ inhibition, whereas adding it to the 0/Ca Hypo-TEA had no effect. Moreover, the levels of steady-state $I_{Cl,swell}$ inhibition by 10 mM Ca^{2+} in the presence of 1 μM IM were similar to those achieved in the presence of 0.1 μM TG (see Fig. 4A). Similar to TG the effects of IM were $[Ca^{2+}]_{out}$-dependent. Figure 3D illustrates original $I_{Cl,swell}$ recordings from a representative cell obtained first in the control 2/Ca Hypo-TEA and then in 2/Ca Hypo-TEA and 10/Ca Hypo-TEA solutions supplemented with 1 μM IM, demonstrating enhanced current down-regulation with increasing extracellular Ca^{2+} concentration. The overall appearance of these recordings was hardly changed by inhibition, suggesting that inhibition is not associated with noticeable alterations in the $I_{Cl,swell}$ kinetics. The averaged I-V relationships for $I_{Cl,swell}$ current densities in the same solutions (Fig. 3E) show that IM-conferred inhibition by Ca^{2+} does not affect channel rectification properties. Not only qualitatively, but also quantitatively similar, results to IM were obtained with another Ca^{2+} ionophore A23187 (data not shown).

To exclude the possibility that the described effects may at least in part be related to the modification by TG of a signaling pathway from extracellular Ca receptor to VRAC, we performed a series of tests using Ca receptor agonists La^{3+}, neomycin, and spermine administered under the experimental protocols described by Shimizu et al. (30). The application of any of these agonists, with or without TG, produced no appreciable effects on $I_{Cl,swell}$ in LNCaP cells, suggesting that in these cells Ca receptor is either insignificantly expressed or lacks a functional link with VRAC.

Figure 4A summarizes the effects of major interventions used in this study to manipulate Ca^{2+} homeostasis on the density of $I_{Cl,swell}$ in LNCaP cells. Taken together, these results strongly suggest that Ca^{2+} entering the cell via plasma membrane SOCs is the most crucial element for VRAC modulation.

Effects of TG on RVD process

Having demonstrated that interventions that lead to the activation of SOCs confer Ca^{2+} sensitivity on VRAC, we were interested in finding whether these interventions are also capable of altering the RVD process that is largely determined by activation of VRAC-mediated $I_{Cl,swell}$. To test this, we measured relative changes of the cell volume at different times following the cells exposure to the 0.1 μM TG-supplemented 0/Ca or 2/Ca Hypo-TEA solutions. The measurements were conducted using flow cytometry, which allows volume to be estimated on at

least 5000 cells at a time. The results of these experiments are presented in Figure 4B. Exposure of the cells to 0/Ca Hypo-TEA and TG resulted in a rapid increase of relative cell volume to the peak value of 30% followed by its slow decline due to development of $I_{Cl,swell}$-mediated RVD. Virtually complete cell volume relaxation in the group of cells exposed to 0/Ca Hypo-TEA and TG occurred in about 15 min (Fig. 4B, gray bars). The overall behavior of cell volume in this group of cells was not much different from the control group, which was treated with regular 2/Ca Hypo-TEA in the absence of TG (Fig. 4B, inset, gray bars), suggesting that TG per se does not interfere with the normal course of the RVD process. In sharp contrast to such behavior, inclusion of TG to 2/Ca Hypo-TEA resulted in a somewhat higher increase of maximal cell volume, but most important, in a significant slowdown of the volume relaxation phase, such that after 15 min, it decreased from a peak value of about 37% to only about 26% (Fig. 4B, light gray bars). Such a dramatic difference with 0/Ca conditions indicates that only when extracellular Ca^{2+} is present is TG able to impair the RVD process, consistent with TG-conferred down-regulation of $I_{Cl,swell}$ by extracellular Ca^{2+}. The inhibition of RVD by TG was very similar to the inhibition observed in the presence of the Cl^- channel blocker NPPB (100 μM) (Fig. 4B, inset, light gray bars), suggesting that both interventions target the Cl^- efflux via VRACs.

DISCUSSION

In many cell types, osmotic cell swelling has been shown to be associated with an increase in $[Ca^{2+}]_{in}$ (38–41), with cell-specific contributions from a variety of sources. Therefore, if intracellular Ca^{2+} would have any effect on VRACs activity, it would essentially affect the RVD process. However, in contrast to clearly established Ca^{2+} dependence of K^+ channels involved in RVD, activation of VRACs in the vast majority of cell types was found to be independent of intracellular Ca^{2+} (41, 48). However, there were some exceptions. For instance, $I_{Cl,swell}$ activation in human neuroblastoma cells (23), in rat insulinoma cells (16), and in bovine endothelial cells (24) was found to depend on $[Ca^{2+}]_{in}$. We believe that inconsistencies in the reported modes of $I_{Cl,swell}$ regulation by intracellular Ca^{2+} in various cell types may reflect different degrees of intracellular compartmentalization that prevent free access of global Ca^{2+} to the interaction site(s) with VRACs. Indeed, evidence exists that in the human neuroblastoma CHP-100 cell line, for instance, $I_{Cl,swell}$ is particularly sensitive to the Ca^{2+} entering via P-type Ca^{2+} channels (23).

In our experiments in prostate cancer epithelial cells, we were also unable to demonstrate any significant influence of global $[Ca^{2+}]_{in}$ and $[Ca^{2+}]_{out}$ on the characteristics of hypotonicity-evoked $I_{Cl,swell}$. However, under conditions that allow Ca^{2+} influx via plasma membrane SOCs, the sensitivity of VRAC to the extracellular Ca^{2+} became obvious. Because the necessary prerequisite for SOC activation is the depletion of intracellular stores, any interventions that result in store depletion are able to confer Ca^{2+} sensitivity of VRAC. In our experiments on stores depletion, we used an inhibitor of the SERCA Ca^{2+} pump of the ER, TG, and two Ca^{2+} ionophores, ionomycin and A23187. Despite different mechanisms of store depletion, all three agents produced similar effects on the regulation of $I_{Cl,swell}$ by extracellular Ca^{2+}, that is, increasing levels of $[Ca^{2+}]_{out}$ evoked progressive $I_{Cl,swell}$ inhibition.

The following line of evidence supports our notion that the inhibition of $I_{Cl,swell}$ is due to VRAC interaction with Ca^{2+} entering via SOCs and not Ca^{2+} released from the stores or due to direct effects of store-depleting agents on VRACs. First, $I_{Cl,swell}$ inhibition never occurred in response

to the application of store-depleting agents in the absence of extracellular Ca^{2+}. Second, blockade of SOCs by Ni^{2+} prevented $I_{Cl,swell}$ inhibition by Ca^{2+} in the presence of store-depleting agents, whereas increasing SOC-mediated Ca^{2+} influx by more negative holding potentials enhanced it. Third, TG-, ionomycin-, and A23187-confered $I_{Cl,swell}$ inhibition was $[Ca^{2+}]_{out}$-dependent. All this evidence, together with $I_{Cl,swell}$ insensitivity to the rise in global $[Ca^{2+}]_{in}$ and to the Ca^{2+} liberated from the stores, suggest that Ca^{2+} entering the cell via SOCs has preferred access to VRACs and implies close colocalization of these two channel types in the plasma membrane. Our data on VRAC regulation by SOC-transported Ca^{2+} seem to be consistent with previous studies in endothelial cells showing that activation of VRACs requires permissive intracellular Ca^{2+} concentration (24). Indeed, high buffering of intracellular Ca^{2+} used in these studies could activate SOCs due to a passive Ca^{2+} leak from the ER, resulting in VRAC inhibition while increasing the intracellular Ca^{2+} above a particular level that would prevent ER depletion. Concomitant activation of SOCs would render VRACs available.

Ca^{2+} is a universal intracellular messenger regulating many processes. Therefore, spatial compartmentalization of the structures subjected to Ca^{2+} regulation is one of the necessary prerequisites for the specificity of its action. In this respect, Ca^{2+} regulation of VRAC is reminiscent of Ca^{2+}-induced inactivation of Ca^{2+} channels, also proven to take place in the confined subcellular domains (43). An inverse correlation between the Ca^{2+} influx and $I_{Cl,swell}$ in prostate cancer epithelial cells is opposite to the facilitating role of Ca^{2+} found in other preparations (16, 23, 24). The physiological significance of such a mode of Ca^{2+}-dependent regulation and of the underlying colocalization of SOCs and VRACs on prostatic cells is not clear. As this study shows, the depletion of intracellular Ca^{2+} stores and the concomitant activation of SOCs by TG strongly impair the normal course of RVD process. One can assume that in the presence of any hormonal stimuli acting through cell surface receptors and resulting in liberation of Ca^{2+} and store depletion, the VRACs-mediated RVD process would be inhibited as well. In our recent study (33), we demonstrated that the depletion of intracellular stores, and not the rise in $[Ca^{2+}]_{in}$, is the primary reason for apoptotic LNCaP cell death in a TG-induced apoptosis model. Depletion of stores during the progression to apoptosis would activate Ca^{2+} entry via SOCs and would increase cytosolic Ca^{2+} and the down-regulation of VRACs. Concomitant inhibition of the VRAC-mediated RVD process would lead to the enhanced vesiculation and formation of apoptotic blebs in response to any osmotic perturbations, and together with increased cytosolic Ca^{2+}, it would result in accelerated apoptotic cell death.

Recently, it has been shown that expression of a highly Ca^{2+}-permeable CaT1 channel in prostate carcinoma cells (including LNCaP cells) correlates with the tumor grade of prostate cancers (49). By having functional properties very similar to the native SOCs, this channel is a likely candidate for mediating store-operated Ca^{2+} influx (50). Thus, functional interaction between SOC-mediated Ca^{2+} entry tumor growth and activity of VRACs may provide novel targets for therapy and diagnosis of prostate cancers.

ACKNOWLEDGMENTS

We are grateful to A. Dub and I. Spadone for excellent technical assistance. This work was supported by grants from INSERM, La Ligue Nationale Contre le Cancer and l'ARC (France), and INTAS-99-01248. Y. M. Shuba was supported by the Ministry of Science of France.

REFERENCES

1. MacLeod, R. J., and Hamilton, J. R. (1991) Volume regulation initiated by Na^+-nutrient cotransport in isolated mammalian villus enterocytes. *Am. J. Physiol.* **260,** G26–G33

2. Haussler, U., Rivet-Bastide, M., Fahlke, Ch., Müller, D., Zachar, E., and Rüdel, R. (1994) Role of the cytoskeleton in the regulation of $C1^-$ channels in human embryonic skeletal muscle cells. *Pflügers Arch.* **428,** 323–330

3. Dubois, J. M., and Rouzaire-Dubois, B. (1993) Role of potassium channels in mitogenesis. *Prog. Biophys. Mol. Biol.* **59,** 1–21

4. Lang, F., Ritter, M., Gamper, N., Huber, S., Fillon, S., Tanneur, V., Lepple-Wienhues, A., Szabo, I., and Gulbins, E. (2000) Cell volume in the regulation of cell proliferation and apoptotic cell death. *Cell Physiol. Biochem.* **10,** 417–428

5. Voets, T., Szucs, G., Droogmans, G., and Nilius B. (1995) Blockers of volume-activated Cl^- currents inhibit endothelial cell proliferation. *Pflügers Arch.* **431**, 132–134

6. Voets, T., Wei, L., De Smet, P., Van Driessche, W., Eggermont, J., Droogmans, G., and Nilius, B. (1997) Downregulation of volume-activated $C1^-$ currents during muscle differentiation. *Am. J. Physiol.* **272,** C667–C674

7. Maeno, E., Ishizaki, Y., Kanaseki, T., Hazama, A. and Okada, Y. (2000) Normotonic cell shrinkage because of disordered volume regulation is an early prerequisite to apoptosis. *Proc. Natl. Acad. Sci. USA* **97,** 9487–9492

8. Okada, Y., Maeno, E., Shimizu, T., Dezaki, K., Wang, J., and Morishima, S. (2001) Receptor-mediated control of regulatory volume decrease (RVD) and apoptotic volume decrease (AVD). *J. Physiol.* **532,** 3–16

9. Strange, K., Emma, F., and Jackson, P. S (1996) Cellular and molecular physiology of volume-sensitive anion channels. *Am. J. Physiol.* **270,** C711–C730

10. Jackson, P. S., and Strange, K. (1996) Single channel properties of a volume sensitive anion channel: lessons from noise analysis. *Kidney Int.* **49,** 1695–1699

11. Okada, Y. (1997) Volume expansion-sensing outward-rectifier Cl^- channel: fresh start to the molecular identity and volume sensor. *Am. J. Physiol.* **273,** C755–C789

12. Okada, Y. (1998) Cell volume-sensitive chloride channels. *Contrib. Nephrol.* **123,** 21–33.

13. Nilius, B., Eggermont, J., Voets, T., Buyse, G., Manolopoulos, V., and Droogmans G. (1997) Properties of volume-regulated anion channels in mammalian cells. *Prog. Biophys. Mol. Biol.* **68,** 69–119

14. Perlman, D. F., and Goldstein L. (1999) Organic osmolyte channels in cell volume regulation in vertebrates. *J. Exp. Zool.* **283,** 725–733

15. Robson, L., and Hunter, M. (1994) Role of cell volume and protein kinase C in regulation of a Cl^- conductance in single proximal tubule cells of *Rana temporaria*. *J. Physiol.* **480,** 1–7

16. Verdon, B., Winenny, J. P., Whitfield, K. J., Argent, B. E., and Gray, M. A. (1995) Volume-activated chloride currents in pancreatic duct cells. *J. Membr. Biol.* **147,** 173–183

17. Mayer, K., and Korbmacher, C. (1996) Cell swelling activates ATP-dependent voltage-gated chloride channels in M-1 mouse cortical collecting duct cells. *J. Gen. Physiol.* **108,** 177–193

18. Chou, C. Y., Shen, M. R., Hsu, K. S., Huang, H. Y., and Lin, H. C. (1998) Involvement of PKC-alpha in regulatory volume decrease responses and activation of volume-sensitive chloride channels in human cervical cancer HT-3 cells. *J. Physiol.* **15,** 435–448

19. Roman, R. M., Bodily, K. O., Wang, Y., Raymond, J. R., and Fitz, J. G. (1998) Activation of protein kinase C alpha couples cell volume to membrane Cl^- permeability in HTC hepatoma and Mz-ChA-1 cholangiocarcinoma cells. *Hepatol.* **28,** 1073–1080

20. Duan, D., Cowley, S., Horowitz, B., and Hume, J. R. (1999) A serine residue in ClC-3 links phosphorylation-dephosphorylation to chloride channel regulation by cell volume. *J. Gen. Physiol.* **113,** 57–70

21. Sarkadi, B., Cheung, R., Mack, E., Grinstein, S., Gelfand, E. W., and Rothstein, A. (1985) Cation and anion transport pathways in volume regulatory response of human lymphocytes to hypoosmotic media. *Am. J. Physiol.* **248,** C480–C487

22. Hoffmann, E. K., Lambert, I. H., and Simonsen L. O. (1986) Separate, Ca^{2+}-activated K^+ and Cl^- transport pathways in Ehrlich ascites tumor cells. *J. Membr. Biol.* **91,** 227–244

23. Basavappa, S., Chartouni, V., Kirk, K., Prpic, V., Ellory, J. C., and Mangel, A. W. (1995) Swelling-induced chloride currents in neuroblastoma cells are calcium dependent. *J. Neurosci.* **15,** 3662–3666

24. Szucs, G., Heinke, S., Droogmans, G., and Nilius, B. (1996) Activation of the volume-sensitive chloride current in vascular endothelial cells requires a permissive intracellular Ca^{2+} concentration. *Pflugers Arch.* **431,** 467–469

25. Wu, J., Zhang, J. J., Koppel, H., and Jacob, T. J. (1996) P-glycoprotein regulates a volume-activated chloride current in bovine non-pigmented ciliary epithelial cells. *J. Physiol.* **491,** 743–755

26. Anderson, J. W., Jirsch, J. D., and Fedida, D. (1995) Cation regulation of anion current activated by cell swelling in two types of human epithelial cancer cells. *J. Physiol.* **483,** 549–557

27. Braun, A. P., and Schulman, H. (1996) Distinct voltage-dependent gating behaviours of a swelling-activated chloride current in human epithelial cells. *J. Physiol.* **495,** 743–753

28. Sakai, H., Nakamura, F., and Kuno, M. (1999) Synergetic activation of outwardly rectifying Cl^- currents by hypotonic stress and external Ca^{2+} in murine osteoblasts. *J. Physiol.* **515,** 157–168

29. Shi, C., Ryan, J. S., French, A. S., Coca-Prados, M., and Kelly, M. E. (1999) Hyposmotically activated chloride channels in cultured rabbit non-pigmented ciliary epithelial cells. *J. Physiol.* **521,** 57–67

30. Shimizu, T., Morishima, S., and Okada, Y. (2000) Ca^{2+}-sensing receptor-mediated regulation of volume-sensitive Cl^- channels in human epithelial cells. *J. Physiol.* **528,** 457–472

31. Shuba, Y. M., Prevarskaya, N., Lemonnier, L., Van Coppenolle F., Kostyuk, P. G., Mauroy, B., and Skryma, R. (2000) Volume-regulated chloride conductance in the LNCaP human prostate cancer cell line. *Am. J. Physiol.* **279,** C1144–C1154

32. Skryma, R. N., Van Coppenolle, F., Dufy-Barbe, L., Dufy, B., and Prevarskaya, N. B. (1999) Characterization of Ca^{2+}-inhibited potassium channels in the LNCaP human prostate cancer cell line. *Recept. Chan.* **6,** 241–253

33. Skryma, R. N., Mariot, P., Le Bourhis, X., Van Coppenolle, F., Shuba, Y., Vanden Abeele, F., Legrand, G., Humez, S., Boilly, B., and Prevarskaya, N. (2000) Store depletion and store-operated Ca^{2+} current in human prostate cancer LNCaP cells: involvement in apoptosis. *J. Physiol.* **527,** 73–83

34. Skryma, R. N., Prevarskaya, N. B., Dufy-Barbe, L., Odessa, M. F., Audin, J., and Dufy, B. (1997) Potassium conductance in the androgen-sensitive prostate cancer cell line, LNCaP: involvement in cell proliferation. *Prostate* **32**, 112–122

35. Brooks, S. P., and Storey, K. B. (1992) Bound and determined: a computer program for making buffers of defined ion concentrations. *Anal. Biochem.* **14,** 119–126

36. Bratosin, D., Mazurier, J., Slomianny, C., Aminoff, D., and Montreuil, J. (1997) Molecular mechanisms of erythrophagocytosis: flow cytometric quantitation of in vitro erythrocyte phagocytosis by macrophages. *Cytometry* **30,** 269–274

37. Grynkiewicz, G., Poenie, M., and Tsien, R. Y. (1985) A new generation of Ca^{2+} indicators with greatly improved fluorescence properties. *J. Biol. Chem.* **260,** 3440–3450

38. Hazama, A., and Okada, Y. (1990) Involvement of Ca^{2+}-induced Ca^{2+} release in the volume regulation of human epithelial cells exposed to a hypotonic medium. *Biochem. Biophys. Res. Commun.* **167,** 287–293

39. Wu, X., Yang, H., Iserovich, P., Fischbarg, J., and Reinach, P. S. (1997) Regulatory volume decrease by SV40-transformed rabbit corneal epithelial cells requires ryanodine-sensitive Ca^{2+}-induced Ca^{2+} release. *J. Membr. Biol.* **158,** 127–136

40. McCarty, N. A., and O'Neil, R. G. (1992) Calcium signaling in cell volume regulation. *Physiol. Rev.* **72,** 1037–1061

41. Pasantes-Morales, H., and Morales, M. S. (2000) Influence of calcium on regulatory volume decrease: role of potassium channels. *Nephron* **86,** 414–427

42. Llinas, R., Sugimori, M., and Silver, R. B. (1995) The concept of calcium concentration microdomains in synaptic transmission. *Neuropharmacol.* **34,** 1443–1451

43. Adachi-Akahane, S., Cleemann, L., and Morad, M. (1996) Cross-signaling between L-type Ca^{2+} channels and ryanodine receptors in rat ventricular myocytes. *J. Gen. Physiol.* **108,** 435–454

44. Hoth, M., and Penner, R. (1993) Calcium release-activated calcium current in rat mast cells. *J. Physiol.* **465,** 359–386

45. Kerschbaum, H. H., and Cahalan, M. D. (1998) Monovalent permeability, rectification, and ionic block of store-operated calcium channels in Jurkat T lymphocytes. *J. Gen. Physiol.* **111,** 521–537

46. Kerschbaum, H. H., and Cahalan, M. D. (1999) Single-channel recording of a store-operated Ca^{2+} channel in Jurkat T lymphocytes. *Science* **283,** 836–839

47. Huang, Y., and Putney, J. W. (1998) Relationship between intracellular calcium store depletion and calcium release-activated calcium current in mast cell line (RBL-1). *J. Biol. Chem.* **273,** 19554–19559

48. Hazama, A., and Okada, Y. (1988) Ca^{2+} sensitivity of volume-regulatory K^+ and Cl^- channels in cultured human epithelial cells. *J. Physiol.* **402,** 687–702

49. Peng, J-B., Zhuang, L., Berger, U. V., Adam, R. M., Williams, J., Brown, E. M., Hediger, M. A., and Freeman, M. R. (2001) CaT1 expression correlates with tumor grade in prostate cancer. *Biochem. Biophys. Res. Com.* **282,** 729–734

50. Yue, L., Peng, J-B., Hediger, M. A., and Clapham, D. E. (2001) CaT1 manifests the pore properties of the calcium-release-activated calcium channel. *Nature* **410,** 705–70

Received July 17, 2001; revised August 18, 2001.

Table 1

Composition of the extracellular solutions[a]

	Normal	Iso-TEA	0/Ca Hypo-TEA	2/Ca Hypo-TEA	10/Ca Hypo-TEA
NaCl	140	—	—	—	—
KCl	5	—	—	—	—
$CaCl_2$	2	2	0	2	10
$MgCl_2$	2	2	2	2	2
Na_2HPO_4	0.3	—	—	—	—
KH_2PO_4	0.4	—	—	—	—
$NaHCO_3$	4	—	—	—	—
Glucose	5	10	10	10	10
HEPES	10	10	10	10	10
TEA-Cl	—	145	84	80	64
D-mannitol	—	—	—	2	10

[a]Concentration is given in millimoles; pH of all solutions was adjusted to 7.3.

Fig. 1

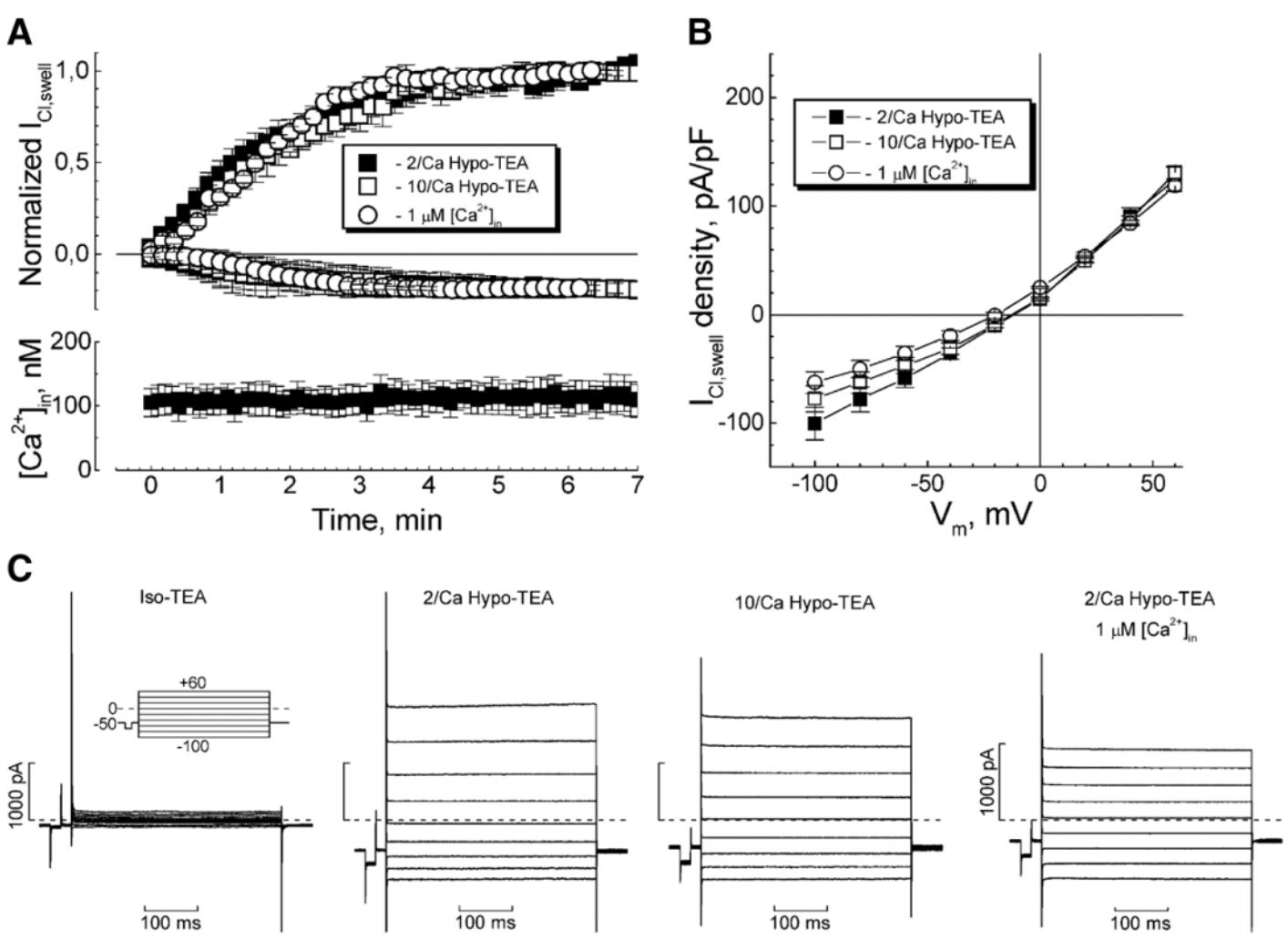

Figure 1. Variations of global extra- and intracellular Ca^{2+} do not affect current $(I)_{Cl,swell}$ in human prostate cancer epithelial cells (LNCaP). A) Upper graph: Averaged (mean ±SE, *n*=6–9) normalized time courses of $I_{Cl,swell}$ development in response to hypotonic Hypo-TEA solution containing 2 mM (filled squares and open circles) and 10 mM (open squares) $[Ca^{2+}]_{out}$ during cell dialysis with 10 nM (open and filled squares) and 1 μM (open circles) $[Ca^{2+}]_{in}$. Here and on all other similar plots, points above and below the zero line represent $I_{Cl,swell}$ amplitude measured at voltage-clamp pulse potential +50 mV and holding potential –50 mV, respectively. Lower graph: Changes in $[Ca^{2+}]_{in}$ (averaged data for 10 cells) during application of 2/Ca Hypo-TEA. For both graphs, time 0 corresponds to the moment of hypotonic exposure. **B)** Averaged current-voltage relationships for the fully developed $I_{Cl,swell}$ current density (pA/pF) under the same experimental conditions. **C)** From left to right: Original traces of the baseline current and of the fully developed $I_{Cl,swell}$ obtained in 10 nM $[Ca^{2+}]_{in}$-dialyzed representative cell in isotonic Iso-TEA, 2/Ca Hypo-TEA, and 10/Ca Hypo-TEA solutions and of the fully developed $I_{Cl,swell}$ obtained in another 1 μM $[Ca^{2+}]_{in}$-dialyzed representative cell in 2/Ca Hypo-TEA. Voltage-clamp protocol used to elicit the currents is shown in the inset to the baseline currents.

Fig. 2

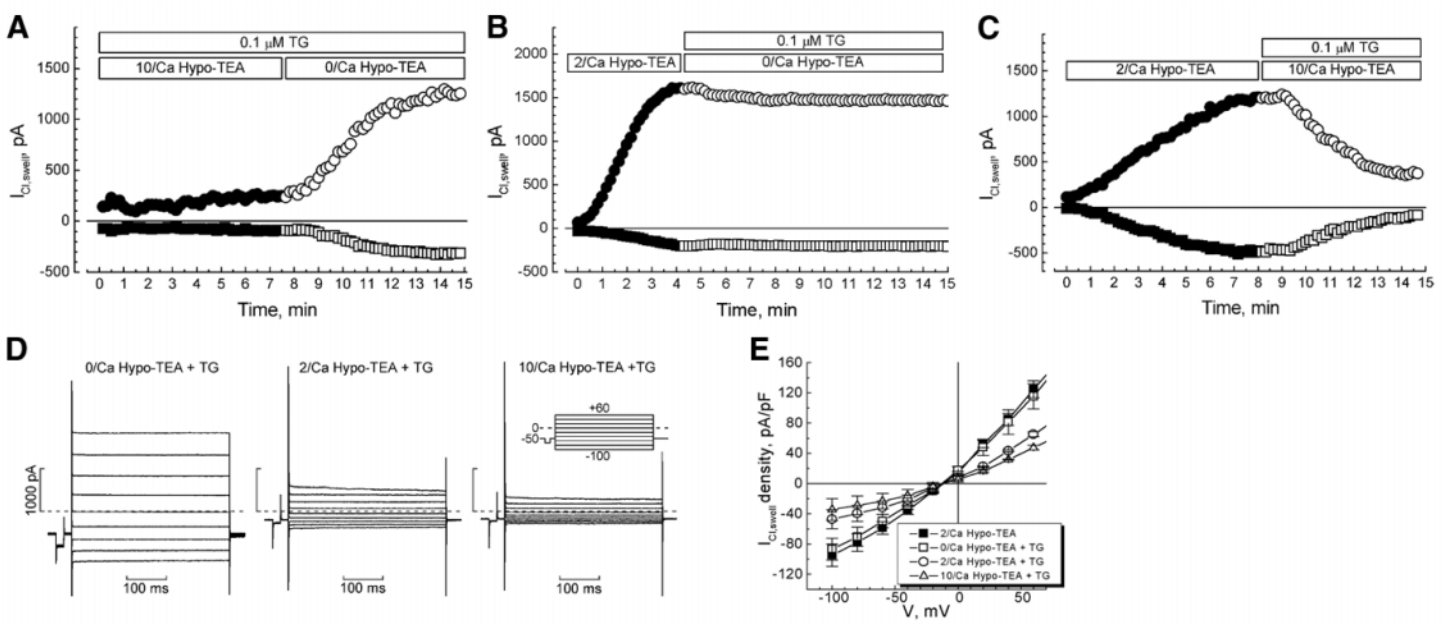

Figure 2. Effects of thapsigargin (TG) on Ca^{2+}-sensitivity of $I_{Cl,swell}$ in human prostate cancer epithelial cells (LNCaP). A) Time course of $I_{Cl,swell}$ development in a representative cell in response to the consecutive exposure to 10/Ca Hypo-TEA and 0/Ca Hypo-TEA in the presence of 0.1 μM TG. **(B** and **C)** The changes of $I_{Cl,swell}$ initially evoked by 2/Ca Hypo-TEA in two representative cells in response to 0/Ca **(B)** and 10/Ca **(C)** Hypo-TEA solutions co-applied with 0.1 μM TG. Time «0» on A, B, and C correspond to the moment of hypotonic exposure, and the horizontal bars mark respective interventions. **D)** From left to right: Original traces of the fully developed $I_{Cl,swell}$ obtained in a representative cell in the 0/Ca Hypo-TEA solution in the presence of 0.1 μM TG, following the addition of 2 mM $[Ca^{2+}]_{out}$ to this solution and an increase of $[Ca^{2+}]_{out}$ in Hypo-TEA to 10 mM in the presence of 0.1 μM TG. Voltage-clamp protocol used to elicit the currents is shown in the inset to the far-right set of currents. **E)** Averaged current-voltage relationships (I-Vs) for the fully developed $I_{Cl,swell}$ current density (pA/pF) (mean ± SE, *n*=4–7) in 0/Ca (open squares), 2/Ca (open circles), and 10/Ca (open triangles) Hypo-TEA solutions in the presence of 0.1 μM TG. For comparison, the averaged I-V in the control 2/Ca Hypo-TEA from **Figure 1B** is also shown (filled squares).

Fig. 3

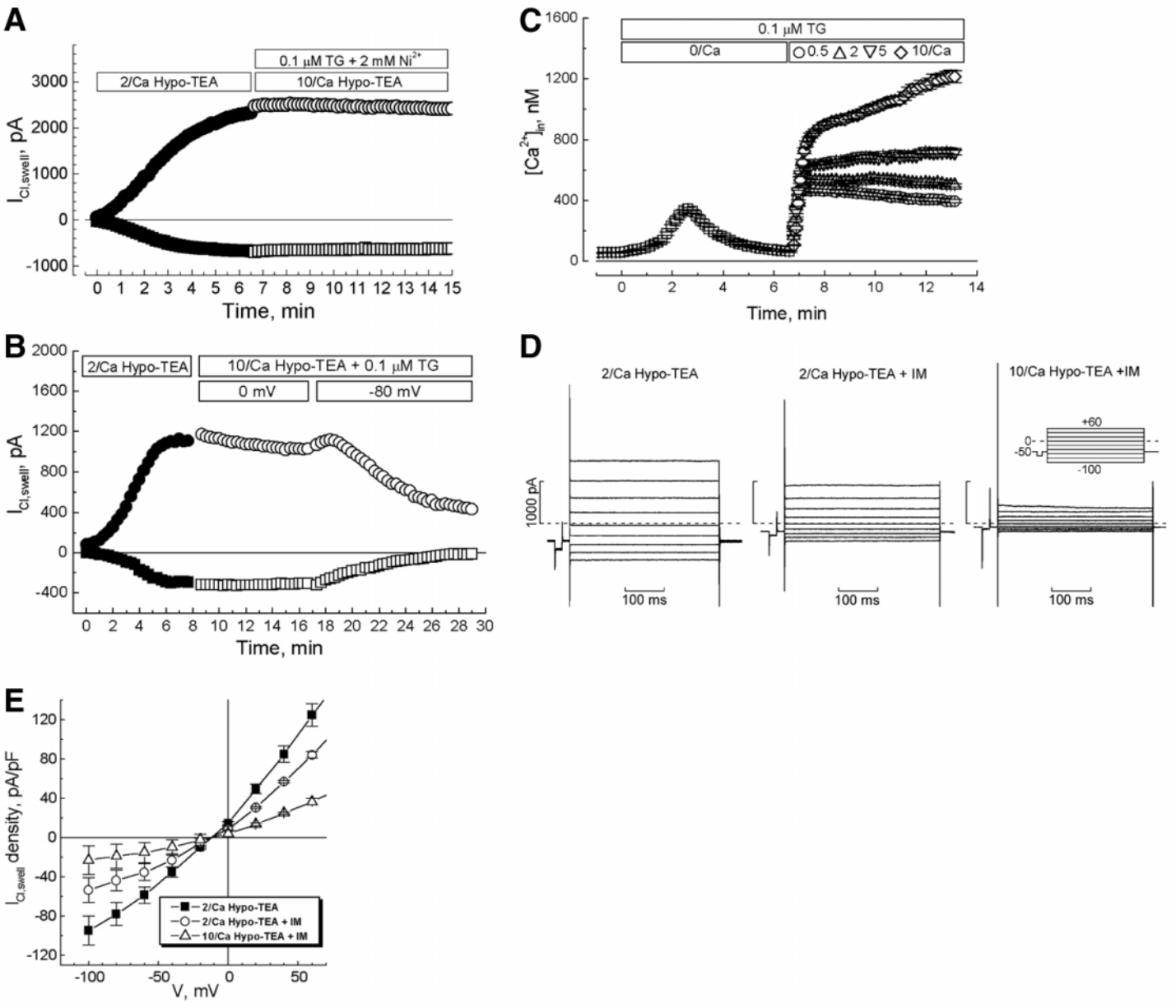

Figure 3. Ca^{2+}-sensitivity of $I_{Cl,swell}$ in human prostate cancer epithelial cells (LNCaP) requires transmembrane Ca^{2+} entry. A) The changes of $I_{Cl,swell}$ initially evoked by 2/Ca Hypo-TEA exposure in a representative cell in response to 10/Ca Hypo-TEA solution supplemented with 0.1 μM TG and 2 mM Ni^{2+}: Points above and below the zero line represent $I_{Cl,swell}$ amplitude measured at voltage-clamp pulse potential +50 mV and holding potential –50 mV, respectively. Time «0» corresponds to the moment of hypotonic exposure; horizontal bars mark respective interventions. **B)** The time course showing enhanced TG-conferred $I_{Cl,swell}$ inhibition at holding potential –80 mV compared with 0 mV. **C)** Averaged (mean ±SE, *n*=7–10) time courses of the changes of $[Ca^{2+}]_{in}$ following exposure to 0.1 μM TG in the presence of various $[Ca^{2+}]_{out}$; respective interventions are marked by horizontal bars. Circles, up-triangles, down-triangles, and diamonds correspond to 0.5, 2, 5, and 10 mM $[Ca^{2+}]_{out}$, respectively. **D)** From left to right: original traces of the fully developed $I_{Cl,swell}$ obtained in a representative cell in the control 2/Ca Hypo-TEA and then sequentially exposed to 2/Ca and 10/Ca Hypo-TEA solutions supplemented with 1 μM IM. Voltage-clamp protocol used to elicit the currents is shown in the inset to the far right set of currents. **E)** Averaged current-voltage relationships for the fully developed $I_{Cl,swell}$ current density (pA/pF) (mean ± SE, *n*=4–7) in 2/Ca Hypo-TEA solution (filled squares), 2/Ca (open circles), and 10/Ca Hypo-TEA solutions in the presence of 1 μM IM (open triangles).

Fig. 4

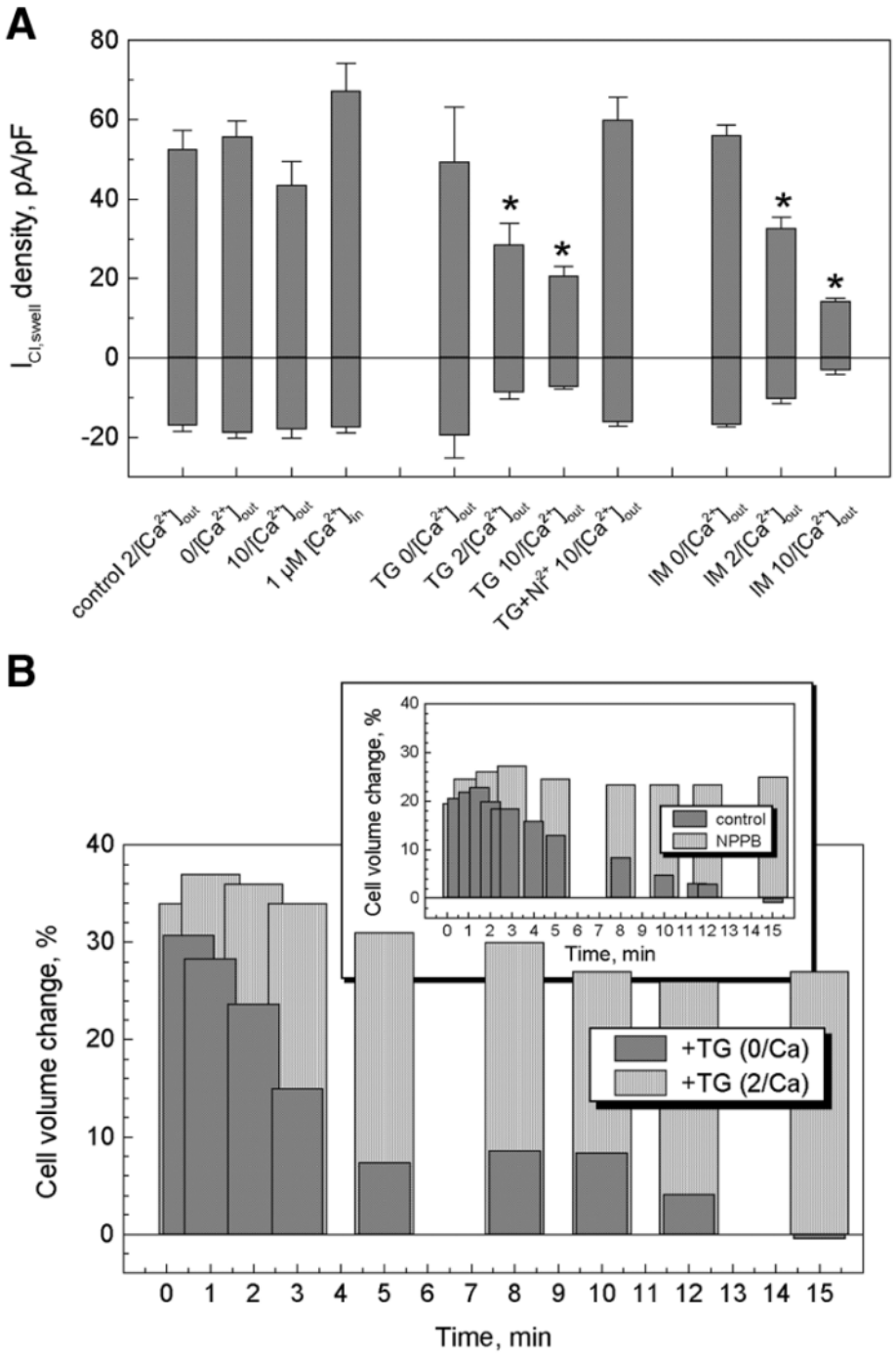

Figure 4. Ca^{2+}-dependent regulation of $I_{Cl,swell}$ and regulatory volume decrease (RVD) process in human prostate cancer epithelial cells (LNCaP). A) Bar graph summarizing the effects of major interventions used to manipulate Ca^{2+} homeostasis (indicated under each bar) on $I_{Cl,swell}$ density at +50 mV (upward bars above zero line) and –50 mV (downward bars below zero line); the size of the bars represents mean ± SE, *n* = 4–16; *, statistically significant difference (*P*<0.05, Student's *t* test) compared with the control. **B)** RVD process in LNCaP cells exposed to thapsigargin - supplemented (0.1 μM) 0/Ca (gray bars) and 2/Ca (light gray bars) Hypo-TEA solutions. Inset shows RVD under control conditions (i.e., exposure to 2/Ca Hypo-TEA, gray bars) following the addition of Cl^- channel blocker 5-nitro-2-(3-phenylpropylamino)benzoic acid (100 μM) to 2/Ca Hypo-TEA (light gray bars). Hypotonic solution was applied at time 0; the height of each bar represents the average percentage of cell volume change at a given time measured on a flow cytometer on at least 5000 cells.

Article 2

[CANCER RESEARCH 64, 4841–4848, July 15, 2004]

Bcl-2-Dependent Modulation of Swelling-Activated Cl^- Current and ClC-3 Expression in Human Prostate Cancer Epithelial Cells

Loïc Lemonnier, Yaroslav Shuba, Alexandre Crepin, Morad Roudbaraki, Christian Slomianny, Brigitte Mauroy, Bernd Nilius, Natalia Prevarskaya, and Roman Skryma

Laboratoire de Physiologie Cellulaire, Institut National de la Santé et de la Recherche Médicale EMI 0228, Villeneuve d'Ascq, France

ABSTRACT

Cell shrinkage is an integral part of apoptosis. However, intimate mechanisms linking apoptotic events to the alterations in cell volume homeostasis remain poorly elucidated. We investigated how overexpression of Bcl-2 oncoprotein, a key antiapoptotic regulator, in lymph node carcinoma of the prostate (LNCaP) prostate cancer epithelial cells interferes with the volume-regulated anion channel (VRAC), a major determinant of regulatory volume decrease. Bcl-2 overexpression resulted in the doubling of VRAC-carried swelling-activated Cl^- current ($I_{Cl,swell}$) and weakened $I_{Cl,swell}$ inhibition by store-operated Ca^{2+} channel (SOC)-transported Ca^{2+}. This also was accompanied by substantial up-regulation of ClC-3 protein, a putative molecular candidate for the role of VRAC. ClC-3-specific antibody suppressed $I_{Cl,swell}$ in the wild-type and Bcl-2-overexpressing LNCaP cells. Epidermal growth factor treatment of wild-type LNCaP cells, promoting their proliferation, resulted in the enhancement of endogenous Bcl-2 expression and associated increases in ClC-3 levels and $I_{Cl,swell}$ magnitude. We conclude that Bcl-2-induced up-regulation of $I_{Cl,swell}$, caused by enhanced expression of ClC-3 and weaker negative control from SOC-transported Ca^{2+}, would strengthen the ability of the cells to handle proliferative volume increases and thereby promote their survival and diminish their proapoptotic potential.

INTRODUCTION

Apoptosis is an orderly physiologic process that allows the elimination of cells that have already completed or for any reason are incapable of performing their physiologic function and therefore are no longer necessary. The antiapoptotic Bcl-2 protein helps to withstand apoptosis by preventing the release of mitochondrial apoptogenic factors, presumably via interaction with the mitochondrial porin channel (1, 2). Although thus far the mitochondrial action of Bcl-2 has received great attention, there is increasing evidence suggesting extramitochondrial localization and other possible roles of Bcl-2 (3–5), especially in the regulation of intracellular Ca^{2+} homeostasis (5, 6). A number of reports recently have appeared claiming the additional involvement of Bcl-2 in the regulation of several types of plasma membrane ion channels. In particular, overexpression of Bcl-2 has been shown to exert cell type-specific inhibition (7) or enhancement of transmembrane capacitative Ca^{2+} entry (8, 9) to inhibit voltage-gated K^+ channels in vascular smooth muscle cells (10). The last observation contrasts with their enhancement by Bcl-2-related mcl-1 protein in murine myeloblastic FDC-P1 cells (11) and to increased swelling-activated Cl^- channel activity in MDCK cells (9).

In our recent study, we have shown that Bcl-2 overexpression in androgen-dependent lymph node carcinoma of the prostate (LNCaP; Ref. 12) prostate cancer epithelial cells, transforming them to androgen-independent phenotype, down-regulates store-operated Ca^{2+} current by decreasing the number of functional plasma membrane store-operated channels (SOCs). We also have suggested that this phenomenon may be characteristic of a progression to hormone-insensitive prostate cancer (13). In the different studies we also have discovered volume-regulated anion channels (VRACs) in LNCaP cells (14), which carry swelling-activated Cl^- current ($I_{Cl,swell}$), involved in regulatory volume decrease (RVD) in response to hypoosmotic stress. It consequently has been shown that Ca^{2+} entering the cell via closely colocalized SOCs in the plasma membrane can effectively regulated these channels (15).

Given that, on one hand, proliferation and apoptosis are associated with normotonic alterations of cell volume (16) and, conversely, there is strong evidence that the processes of normotonic apoptotic volume decrease (AVD) and RVD may be coupled (17, 18), in the present study we examined whether Bcl-2 overexpression in LNCaP cells is capable of affecting VRACs and the RVD process. We also were interested in whether down-regulation of SOCs, associated with Bcl-2 overexpression, impacts the type and manner of $I_{Cl,swell}$ Ca^{2+}-dependent regulation. Using direct patch-clamp recording of hypotonicity-evoked $I_{Cl,swell}$ combined with immunodetection techniques, we show that an elevation of Bcl-2 levels, irrespectively of whether it was achieved by heterologous overexpression or exposure to mitogens, augments $I_{Cl,swell}$, increases the endogenous levels of ClC-3 mRNA and protein—one of the molecular candidates for the role of VRAC (19) involved, as we show, in $I_{Cl,swell}$ in LNCaP cells—and weakens Ca^{2+}-dependent inhibition of $I_{Cl,swell}$ by SOC-transported Ca^{2+}. Our results demonstrate a new role of the antiapoptotic Bcl-2 protein in cancer cells: the cell volume regulation via $I_{Cl,swell}$ enhancement and the promotion of ClC-3 expression. Given that $I_{Cl,swell}$ and cell volume homeostasis are involved in the potential apoptotic signaling pathway, ClC-3 protein could represent a potential new target for cancer therapy.

MATERIALS AND METHODS

Cell Cultures, Electrophysiology, and Solutions. The procedures of original LNCaP (12) cells (American Type Culture Collection, Manassas, VA), LNCaP cells stably transfected with human Bcl-2 (LNCaP/Bcl-2; Ref. 20), and with control neomycin-selectable pBK-CMV plasmid (LNCaP/neo; the latter two provided by Dr. R. Buttyan, Department of Urology, College of Physicians and Surgeons of Columbia University, New York, NY) are detailed in our previous article (20).

Macroscopic membrane ionic currents were recorded using the patch-clamp technique in the whole-cell configuration described elsewhere (20). The resistance of the patch pipettes, filled with the basic pipette solution (in mM): K(OH), 100; KCl, 40; $MgCl_2$, 1; $CaCl_2$, 3.1; HEPES, 10; and EGTA, 8 (pH 7.3; adjusted with glutamic acid), varied between 4–6 MΩ. Series resistance compensation was used to improve voltage-clamp performance during recording of the whole-cell currents. Normal extracellular solution contained (in mM) NaCl, 120; KCl, 5; $CaCl_2$, 2; $MgCl_2$, 2; glucose, 5; and HEPES, 10 [pH 7.3; adjusted with Na(OH)]. For the recording of uncontaminated swelling-activated Cl^- current ($I_{Cl,swell}$), we eliminated all of the other possible currents by using TEA-based isotonic (300 mosM) and hypotonic (170 mosM) extracellular solutions of the following composition (in mM): TEA-Cl, 145 (or 100); $CaCl_2$,

Received 10/14/03; revised 4/5/04; accepted 5/19/04.

Grant support: INSERM, La Ligue Nationale Contre le Cancer and l'ARC (France), and INTAS-99–01248. L. Lemonnier was supported by ARC (France). Y. M. Shuba was supported by INSERM and the French Ministry of Science.

The costs of publication of this article were defrayed in part by the payment of page charges. This article must therefore be hereby marked *advertisement* in accordance with 18 U.S.C. Section 1734 solely to indicate this fact.

Note: Y. Shuba is currently at the Bogomoletz Institute of Physiology, Kiev, Ukraine; B. Nilius is currently at the KU Leuven, Laboratorium voor Fysiologie, Leuven, Belgium.

Requests for reprints: Roman Skryma, Laboratoire de Physiologie Cellulaire, INSERM EMI 0228, Université des Sciences et Technologies de Lille, Bāt. SN3, 59655 Villeneuve d'Ascq, France. Phone: 33-3-2033-6018; Fax: 33-3-2043-4066; E-mail: Roman.Skryma@univ-lille1.fr.

2; $MgCl_2$, 2; glucose, 10; and HEPES, 10 [pH 7.3; adjusted with TEA(OH)]. Necessary supplements in concentrations that would not significantly change the osmolarity were added directly to the respective solutions. All of the chemicals were from Sigma (St. Louis, MO).

The currents were analyzed offline using Pulse/PulseFit (HEKA Electronik, Lambrecht/Pfalz, Germany) and Origin 6 (OriginLab Corporation, Northampton, MA) software. Results were expressed as mean ± SE where appropriate. Each experiment was repeated several times. Student's *t* test was used for statistical comparison among means, and differences with $P < 0.05$ were considered significant.

Reverse Transcription-PCR analysis of ClC-3 Expression. Reverse transcription-PCR analysis was performed on mRNA extracts from various types of LNCaP cells using standard procedures described elsewhere (20). The PCR primers used to amplify the reverse transcription-generated ClC-3 cDNAs were designed based on established GenBank sequences. Invitrogen (Carlsbad, CA) synthesized the primers. The primers for human ClC-3 cDNA were 5′-GGCAGCATTAACAGTTCTACAC-3′ (nucleotides 675–696; GenBank accession no. NM 001829) and 5′-TTCCAGAGCCACAGGCATATGG-3′ (nucleotides 1207–1188). The expected DNA length of the PCR product generated by these primers is 533 bp. To confirm the identity of the amplified product, restriction analysis was carried out on PCR products using specific restriction enzymes.

Bcl-2 Hybrid Depletion. The LNCaP cells were treated for up to 48 h with either 0.5 μM phosphorothioate antisense oligodeoxynucleotides (ODNs; Eurogentec, Seraing, Belgium) targeted to the coding region of the human Bcl-2 and 2.5 μM cytofectin (GS 3815 to DOPE at a 2:1 molar ration, unsized; Eurogentec) or sense ODNs by adding them directly to the culture medium. The 18-mer ODNs used in these experiments had the following sequences: 5′-TCTCCCAGCGTGCGCCAT-3′ for antisense ODNs and 5′-ATGGCG-CACGCTGGGAGA-3′ for sense ODNs.

Western Blot Analysis of Bcl-2 and ClC-3. Western blot analysis of protein expression was performed as described previously (12). Anti-ClC-3 was from Alomone Labs Ltd. (Jerusalem, Israel) and anti-Bcl-2 was from Santa Cruz Biotechnology (Santa Cruz, CA). The intensity of the signals was evaluated by densitometry and semiquantified using the relationship between the protein of interest value divided by actin value for each experiment. Each presented experiment was repeated at least two times.

RESULTS

In this study we used LNCaP human prostate cancer cells stably transfected with human Bcl-2 (LNCaP/Bcl-2; Ref. 20) and compared the results with those obtained in LNCaP cells transfected with an empty vector (LNCaP/neo), which served as a control. Both cell types were originally created and provided to us by Dr. R. Buttyan (Columbia University, New York, NY; Ref. 20). As shown in our previous work, various mixed populations of individual LNCaP/Bcl-2 or

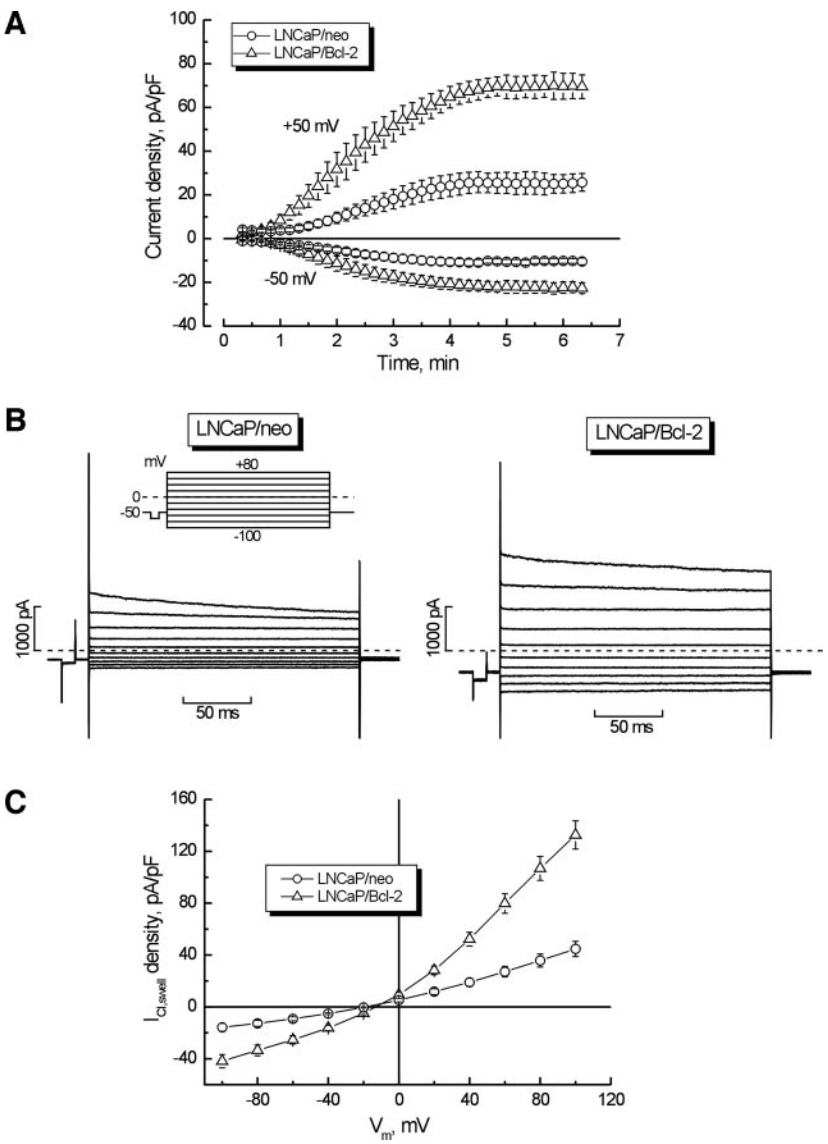

Fig. 1. Bcl-2 overexpression increases swelling-activated Cl^- current ($I_{Cl,swell}$) in lymph node carcinoma of the prostate (*LNCaP*) prostate cancer epithelial cells. *A*, averaged time courses of $I_{Cl,swell}$ in response to hypotonic exposure in the control (LNCaP/neo; ○) and Bcl-2-overexpressing (LNCaP/Bcl-2; △) cells (mean ± SE; $n = 20$ and 12, respectively); $I_{Cl,swell}$ amplitudes were measured at ±50 mV and normalized to membrane capacitance. *B*, representative traces of $I_{Cl,swell}$ at different pulse potentials (*inset*) in the control (LNCaP/neo) and Bcl-2-overexpressing (LNCaP/Bcl-2) cells. *C*, averaged I-V relationships of $I_{Cl,swell}$ (mean ± SE) in the control (LNCaP/neo; ○; $n = 20$) and Bcl-2-overexpressing (LNCaP/Bcl-2; △; $n = 12$) cells.

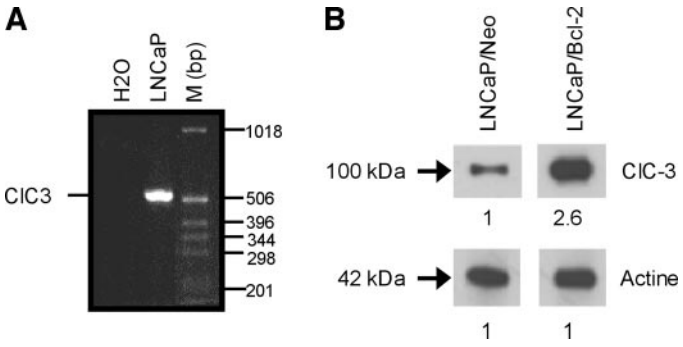

Fig. 2. Bcl-2 overexpression enhances ClC-3 levels in lymph node carcinoma of the prostate (*LNCaP*) prostate cancer epithelial cells. *A*, reverse transcription-PCR analysis of the expression of human ClC-3 transcript in LNCaP/neo cells. *B*, semiquantitative Western blots with ClC-3-specific antibody showing 2.6-fold higher ClC-3 in LNCaP/Bcl-2 compared with LNCaP/neo cells; actin expression was used as control.

LNCaP/neo clones showed no difference in the patterns of protein expressions (including Bcl-2) and the magnitudes of the recorded currents (13). To rule out clonal heterogeneity in each of our experiments, we used two mixed populations of LNCaP/Bcl-2 and LNCaP/neo cells, and because no differences between populations were found, the respective results were pooled for statistical purposes. Overexpression of Bcl-2 in LNCaP/Bcl-2 cells was confirmed by us (13) and by others (20) with immunocytochemical, Northern blot, and reverse transcription-PCR techniques.

Bcl-2-Overexpressing LNCaP Cells Show Higher $I_{Cl,swell}$. In our previous work, we showed that exposure of the whole-cell patch-clamped LNCaP cells to hypotonic extracellular solution elicits the development of the membrane Cl^- current, the magnitude of which correlates with the extent of hypotonicity-induced cell swelling ($I_{Cl,swell}$; Ref. 14). We also proved that by providing for the loss of Cl^- at normal resting potential, this current participates in the RVD process of intact LNCaP cells subjected to hypo-osmotic challenge (15). With no difference to these observations in the wild-type LNCaP cells (LNCaP/wt), a similar current also could be activated in LNCaP/neo and LNCaP/Bcl-2 cells. Fig. 1*A* compares average time courses of $I_{Cl,swell}$ development at +50 and −50 mV in two cell types exposed to hypo-TEA solution at time "0." As one can see, although generally following comparable time courses, $I_{Cl,swell}$ in LNCaP/Bcl-2 cells reached considerably higher maximal density (65 ± 7.6 and −28.2 ± 3.4 pA/pF at +50 and −50 mV, respectively; $n = 12$) compared with LNCaP/neo cells (29.1 ± 3.3 and −17.1 ± 1.7 pA/pF at +50 and −50 mV, respectively; $n = 20$). The augmentation of maximal current in LNCaP/Bcl-2 cells was not accompanied by notable alterations of $I_{Cl,swell}$ waveform at different step voltages (Fig. 1*B*) and was not voltage dependent (Fig. 1*C*). This would indicate that no change occurred in the inactivation and rectification properties of underlying VRACs and suggests that Bcl-2 overexpression most probably affects open probability, unitary conductance, or the number of active channels.

ClC-3 Levels in LNCaP Cells Directly Correlate with Bcl-2 Expression. It is becoming more evident that probably any of the cloned membrane proteins, capable of forming Cl^- conducting pathways, when taken alone cannot represent the endogenous VRAC in all of its hallmark properties (for the most recent critical reviews see Refs. 21–23). However, ClC-3, a volume-sensitive member of the ClC family of Cl^- channels, is believed to be involved in RVD and

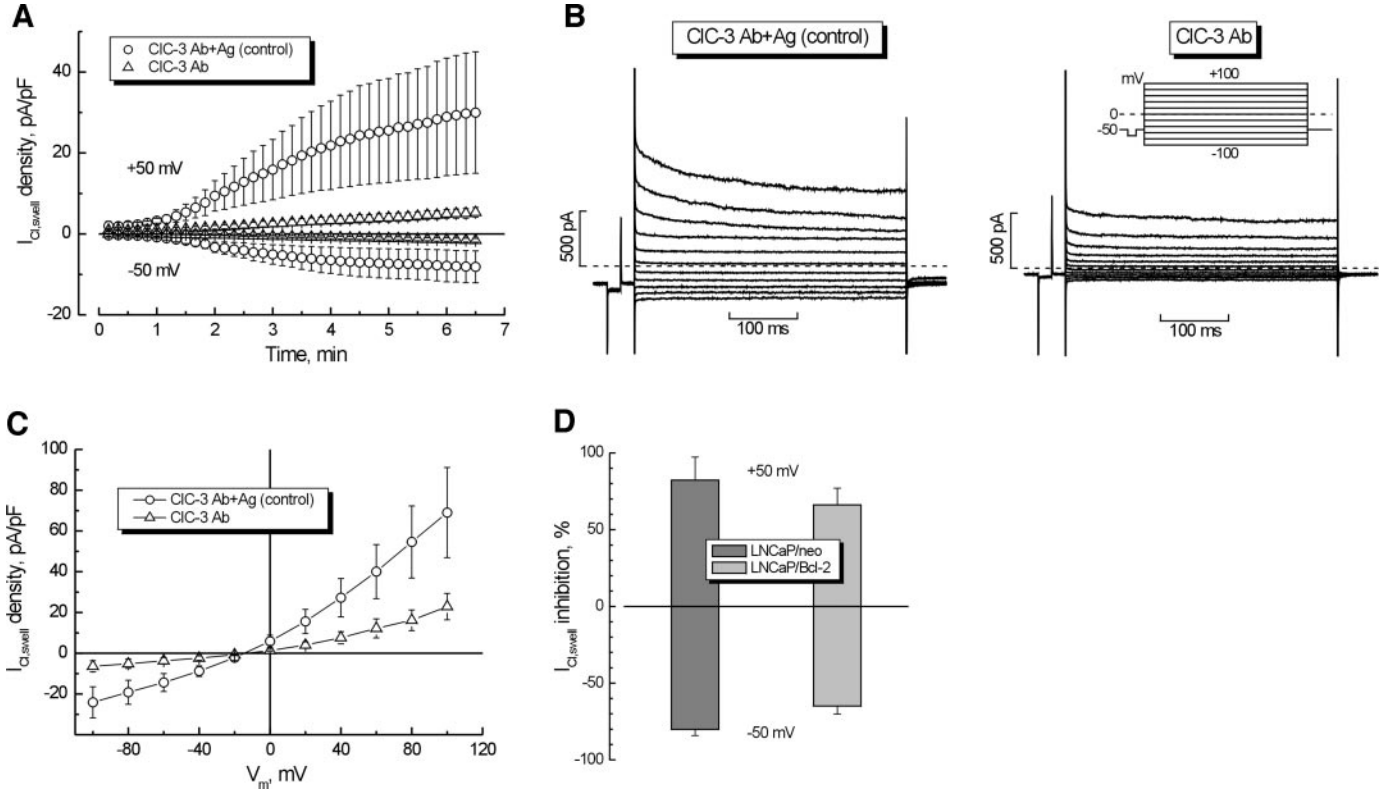

Fig. 3. ClC-3-specific antibody suppresses swelling-activated Cl^- current ($I_{Cl,swell}$) in lymph node carcinoma of the prostate (*LNCaP*) prostate cancer epithelial cells. *A*, averaged time courses of $I_{Cl,swell}$ (mean ± SE) in response to hypotonic exposure showing decreased $I_{Cl,swell}$ in LNCaP cells dialyzed with ClC-3-specific antibody (0.04 μg/μl; ClC-3 Ab; △; $n = 6$) and antagonizing of suppressive antibody effect by ClC-3 antigen (0.08 μg/μl; ClC-3 Ab+Ag; ○; $n = 8$); $I_{Cl,swell}$ amplitudes were measured at ±50 mV and normalized to membrane capacitance. *B*, representative traces of $I_{Cl,swell}$ at different pulse potentials (*inset*) in LNCaP cells dialyzed with ClC-3-specific antibody plus antigen (ClC-3 Ab+Ag, control) and antibody alone (ClC-3 Ab). *C*, averaged I-V relationships of $I_{Cl,swell}$ (mean ± SE) in LNCaP cells dialyzed with ClC-3-specific antibody plus antigen (ClC-3 Ab+Ag; control; $n = 8$) and antibody alone (ClC-3 Ab; $n = 6$). *D*, quantification of the ClC-3-specific antibody suppressive effect on $I_{Cl,swell}$ (mean ± SE) in LNCaP/neo (*dark gray columns*; $n = 6$) and LNCaP/Bcl-2 (*light gray columns*; $n = 6$) cells at ±50 mV.

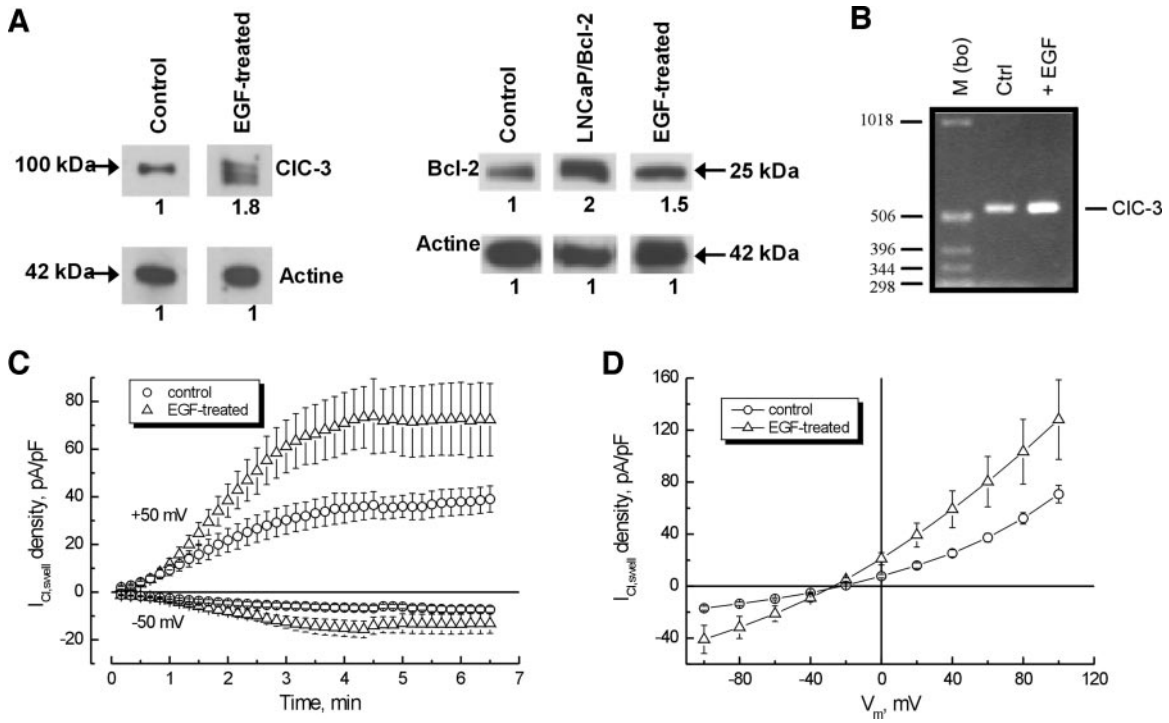

Fig. 4. Epidermal growth factor (*EGF*) treatment enhances Bcl-2 and ClC-3 expression and augments swelling-activated Cl^- current ($I_{Cl,swell}$) in lymph node carcinoma of the prostate (*LNCaP*) prostate cancer epithelial cells. *A*, semiquantitative Western blots with ClC-3- and Bcl-2-specific antibodies showing 1.8- and 1.5-fold enhancement of ClC-3 and Bcl-2, respectively, in EGF-treated LNCaP cells compared with control; treatment with 2 ng/ml EGF for 72 h. As previously shown, Bcl-2 level enhancement was twofold in LNCaP/Bcl-2 cells. *B*, reverse transcription-PCR analysis of the expression of human ClC-3 transcript in control LNCaP/neo cells (*ctrl*) and after a 3-day treatment with 2 ng/ml EGF (*+EGF*). *C*, averaged time courses of $I_{Cl,swell}$ (mean ± SE) in response to hypotonic exposure in the control (○; $n = 10$) and EGF-treated (△; $n = 7$) LNCaP cells; $I_{Cl,swell}$ amplitudes were measured at ±50 mV and normalized to membrane capacitance. *D*, averaged I-V relationships of $I_{Cl,swell}$ (mean ± SE) in the control (○; $n = 10$) and EGF-treated (△; $n = 7$) LNCaP cells.

therefore may potentially be a part of multimeric endogenous VRAC in at least some cell types (19, 24–28). Therefore, we examined ClC-3 transcript presence and protein expression in LNCaP cells with variable Bcl-2 levels using semiquantitative Western blot analysis with a ClC-3-specific antibody.

Fig. 2, *A* and *B*, shows that ClC-3 transcript and protein are notably expressed in LNCaP/neo cells. However, its expression further increases by a factor of 2.6 in LNCaP/Bcl-2 cells (Fig. 2*B*), suggesting a direct correlation between Bcl-2 and ClC-3 levels. Such a pattern of ClC-3 expression prompted us to conclude that (*a*) ClC-3 probably plays a functional role in LNCaP cells; (*b*) given reported ClC-3 volume sensitivity and Cl^- permeation, this functional role may be related to $I_{Cl,swell}$ transfer and RVD; and (*c*) the enhancement of $I_{Cl,swell}$ in Bcl-2-overexpressing LNCaP cells may be associated with the increased levels of ClC-3 in these cells. The next series of experiments was aimed at verifying these conclusions.

ClC-3 Is Involved in $I_{Cl,swell}$ Transfer in LNCaP Cells. We first sought to examine whether ClC-3 knockout is capable of influencing $I_{Cl,swell}$ in the wild-type LNCaP cells. To do so, we used an anti-ClC-3-specific antibody, which has been shown in previous study to effectively inhibit the function of recombinant ClC-3 expressed in NIH/mouse fibroblast cells cells, and endogenous VRACs in a number of cell types (24). This antibody was introduced into the cell via a patch pipette, whereas $I_{Cl,swell}$ simultaneously was monitored in the whole-cell patch-clamp configuration. To make sure that the concentration of antibody inside the cell balanced the one in the pipette and that the antibody effectively interacts with endogenous ClC-3, we dialyzed the cell for at least 10 min before activating $I_{Cl,swell}$ by hypotonic exposure. As control in this series of experiments, we used cell dialysis with a pipette solution containing inactivated anti-ClC-3 by means of a control antigen (premixed 1 h before the experiment to ensure complete antibody inactivation). Fig. 3 demonstrates the cumulative results of these experiments. As one can see, the introduction of anti-ClC-3 into LNCaP cells almost completely prevented $I_{Cl,swell}$ development in response to hypo-TEA (Fig. 3*A*): if under control conditions, with inactivated antibody, the maximal density of $I_{Cl,swell}$ at +50 and −50 mV reached 29.8 ± 14.9 and −8.1 ± 3.9 pA/pF, respectively, then in the presence of active intracellular anti-ClC-3, it decreased to only 5.3 ± 1.2 and −1.6 ± 0.4 pA/pF, respectively. The elimination of anti-ClC-3 effects by its specific antigen rules out nonspecific antibody action on $I_{Cl,swell}$.

Dramatic $I_{Cl,swell}$ down-regulation following anti-ClC-3 dialysis was not accompanied by any change in $I_{Cl,swell}$ overall appearance at various step voltage pulses (Fig. 3*B*), its reversal potential, and rectification properties (Fig. 3*C*), suggesting a simple scaling down of the original current without alterations to its biophysical properties.

A similar inhibitory effect of anti-ClC-3 dialysis on $I_{Cl,swell}$ also was observed in LNCaP/Bcl-2 cells. Fig. 3*D* presents the summary of $I_{Cl,swell}$ changes in response to anti-ClC-3 or anti-ClC-3 plus antigen dialysis in these cell types. The same experiments were realized with the anti-ClC-2 antibody and its specific antigen, and we have never obtained any significant changes in $I_{Cl,swell}$ amplitude and properties in LNCaP/neo and LNCaP/Bcl-2 (data not shown). These results prompted us to conclude that ClC-3 is involved in $I_{Cl,swell}$.

To further prove the association between ClC-3 and $I_{Cl,swell}$, we performed artificial transient overexpression of human hClC-3 in LNCaP cells. This experiment conflicted with our mainline results in the respect that hClC-3-transfected cells exhibited reduced $I_{Cl,swell}$ compared with the control ones. However, we believe that such outcome cannot be used as an argument against the role of endogenous ClC-3 in VRAC in LNCaP cells because there is evidence that endogenous and overexpressed channels may not only behave differ-

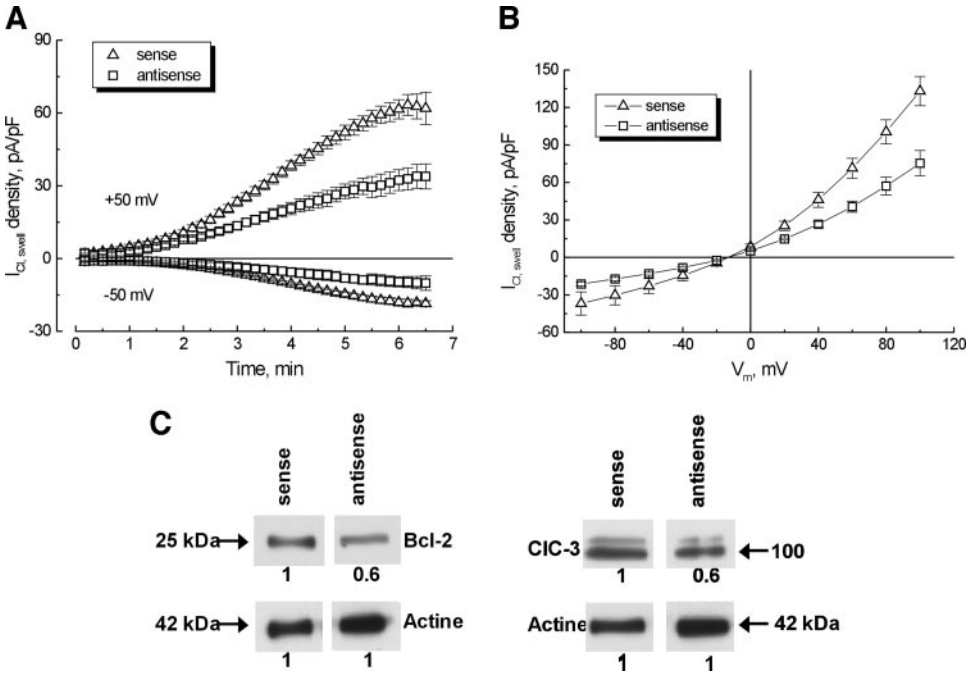

Fig. 5. Bcl-2 hybrid depletion counteracts epidermal growth factor (EGF)-induced augmentation of swelling-activated Cl^- current ($I_{Cl,swell}$). *A*, averaged time courses of hypotonic-induced $I_{Cl,swell}$ (mean ± SE) in lymph node carcinoma of the prostate (LNCaP) cells treated for 3 days with EGF in the presence of sense (△; $n = 6$) and antisense (□; $n = 5$) Bcl-2 oligonucleotides; $I_{Cl,swell}$ amplitudes were measured at ±50 mV and normalized to membrane capacitance. *B*, averaged I-V relationships of $I_{Cl,swell}$ (mean ± SE) in the 3-day EGF-treated LNCaP cells exposed to sense (△; $n = 6$) and antisense (□; $n = 5$) Bcl-2 oligonucleotides. *C*, semiquantitative Western blot analysis with Bcl-2- and ClC-3-specific antibodies showing decreased Bcl-2 (*left*) and ClC-3 (*right*) protein expression in EGF-treated (2 ng/ml for 3 days) LNCaP cells subjected to Bcl-2 mRNA hybrid depletion with antisense oligonucleotides compared with control.

ently but also the behavior of the latter often depends on the level of the expression (29). Together with the probability of extra plasmalemmal ClC-3 localization, this makes the results on overexpression difficult to interpret (30).

EGF Treatment Enhances Bcl-2 and ClC-3 Expression and Augments $I_{Cl,swell}$ in LNCaP Cells. To further confirm direct correlation between Bcl-2, ClC-3 levels, and the magnitude of $I_{Cl,swell}$, we sought another, more physiologic means of increasing the endogenous expression of Bcl-2 in LNCaP cells. For example, there is evidence that some growth factors may inhibit apoptosis by up-regulating Bcl-2 expression (31). Because the epidermal growth factor (EGF) is known to promote the proliferation of LNCaP prostate cancer cells (32) and to protect them from apoptosis (33), we first focused on this agent as a potential stimulus that can elevate the endogenous Bcl-2 levels in LNCaP cells.

Semiquantitative Western blot analysis showed that pretreatment of the wild-type LNCaP cells with EGF (2 ng/ml) for 3 days enhanced Bcl-2 expression by 1.5-fold (Fig. 4*A*) and that this enhancement was paralleled by a 1.8-fold increase in the endogenous ClC-3 level (Fig. 4*A*). This result was confirmed by the reverse transcription-PCR technique; we observed an increase in ClC-3 mRNA after the treatment with EGF (Fig. 4*B*). Moreover, exposure of EGF-treated cells (Fig. 4*C*) to hypotonic solution in the whole-cell patch-clamp experiments revealed an $I_{Cl,swell}$ density about twice as high as that of the control (72.4 ± 15.2 *versus* 39 ± 5.5 pA/pF and −13.3 ± 4.1 *versus* −6.4 ± 2.1 pA/pF at +50 and −50 mV, respectively; $n = 7$–10). This augmentation was not accompanied by any alterations in the appearance of the voltage step-evoked current (data not shown), its reversal potential, or rectification (Fig. 4*D*), suggesting simple $I_{Cl,swell}$ scaling up in EGF-treated cells without changing any properties or activating new currents.

The involvement of Bcl-2 in the EGF-induced $I_{Cl,swell}$ enhancement was further confirmed in a series of hybrid depletion experiments. In these experiments, 3-day EGF (2 ng/ml) treatment of LNCaP cells was performed in the presence of either Bcl-2 sense or antisense ODNs, of which only the latter are capable of reducing endogenous Bcl-2 mRNA levels. As shown in Fig. 5*A*, EGF-treated LNCaP cells with Bcl-2 mRNA depleted by means of antisense ODNs exhibited almost twofold lower $I_{Cl,swell}$ density (34.4 ± 4.8 pA/pF and −10.3 ± 2.4 pA/pF at +50 and −50 mV, respectively; $n = 5$) compared with the cells exposed to Bcl-2 sense ODNs, which served as control (63.3 ± 5.1 pA/pF and −18.6 ± 0.8 pA/pF at +50 and −50 mV, respectively; Fig. 5*A*; $n = 6$). Again, the reduction of $I_{Cl,swell}$ density was not associated with any changes in the kinetics of the current (data not shown), its reversal potential, or apparent rectification (Fig. 5*B*). Semiquantitative Western blot analysis confirmed 40% reduction of Bcl-2 and ClC-3 protein levels in response to antisense Bcl-2 depletion (Fig. 5*C*), which together with the decreased $I_{Cl,swell}$ established direct cause-effect relationship between endogenous Bcl-2, on one hand, and ClC-3/$I_{Cl,swell}$ expression, on the other. These results also support the notion that EGF may influence volume homeostasis of prostate cancer epithelial cells via Bcl-2-mediated enhancement of ClC-3/$I_{Cl,swell}$.

Bcl-2 Overexpression Modulates Ca^{2+} Sensitivity of VRACs. In our two recent studies we showed that (*a*) $I_{Cl,swell}$-carrying VRACs in LNCaP cells are effectively inhibited by Ca^{2+} entering the cell via SOCs, which implies spatial colocalization of two channel types in the plasma membrane (15); and (*b*) Bcl-2 overexpression down-regulates store-operated current (I_{SOC}) in these cells, which is most probably because of a reduction in the number of active SOCs (13). Together, these results suggest that apart from the ClC-3 enhancement and $I_{Cl,swell}$ augmentation demonstrated previously, Bcl-2 overexpression also may alter the mode of Ca^{2+}-dependent regulation of $I_{Cl,swell}$. To verify this, we used the same experimental approach as in the original study (15), namely, exposure of the cell generating $I_{Cl,swell}$ to SERCA pump inhibitor thapsigargin (TG), which facilitates the depletion of the intracellular Ca^{2+} store and thereby induces Ca^{2+} entry from extracellular space via activated SOCs.

Fig. 6*A* shows that in agreement with the previously postulated mechanism of Ca^{2+}-dependent regulation (15), exposure of LNCaP/neo and LNCaP/Bcl-2 cells to 0.1 μM TG in the presence of 5 mM $[Ca^{2+}]_{out}$ caused $I_{Cl,swell}$ inhibition. However, quantification of the steady levels of this inhibition at +50 and −50 mV (Fig. 6*B*) showed that if in LNCaP/neo cells it constituted 49.4 ± 6.9% and 47.4 ± 7.5%, respectively ($n = 5$), then in LNCaP/Bcl-2 cells it decreased to only 22.6 ± 2.3% and 29.4 ± 1.4%, respectively ($n = 4$). Such a reduction in TG-induced $I_{Cl,swell}$ inhibition in LNCaP/Bcl-2 cells is consistent with our previous finding that Bcl-2 overexpression

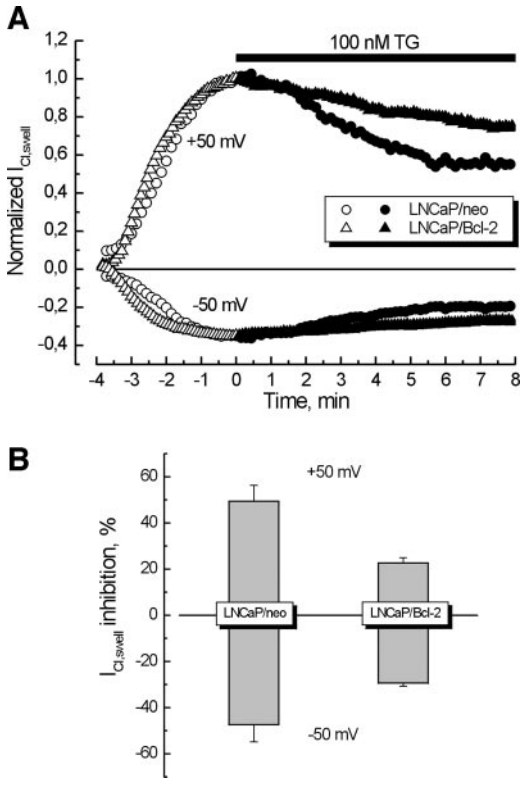

Fig. 6. Bcl-2 overexpression decreases swelling-activated Cl^- current ($I_{Cl,swell}$) inhibition by thapsigargin (*TG*)-induced Ca^{2+} influx in lymph node carcinoma of the prostate (*LNCaP*) prostate cancer epithelial cells. *A*, superimposed normalized time courses of hypotonically evoked $I_{Cl,swell}$ from representative LNCaP/neo (*circles*) and LNCaP/Bcl-2 (*triangles*) cells exposed to 100 nM TG at time "0" in the presence of 5 mM extracellular Ca^{2+}; $I_{Cl,swell}$ amplitudes were measured at ±50 mV and normalized to the immediate pre-TG value at +50 mV. *B*, quantification of TG-conferred $I_{Cl,swell}$ inhibition (mean ± SE) in LNCaP/neo ($n = 5$) and LNCaP/Bcl-2 ($n = 4$) cells at ±50 mV.

down-regulates store-operated Ca^{2+} influx and provides additional proof of spatial colocalization and functional interaction of VRAC and SOC channels (13).

DISCUSSION

In the present article, we report on three major findings: (*a*) overexpression of antiapoptotic oncoprotein Bcl-2 in androgen-dependent prostate cancer epithelial cells results in an increase in swelling-activated Cl^- current and an enhancement of endogenous expression of ClC-3 protein; (*b*) ClC-3 protein participates in the generation of $I_{Cl,swell}$ in LNCaP prostate cancer epithelial cells; and (*c*) Bcl-2 overexpression weakens SOC-mediated, Ca^{2+}-dependent inhibition of volume-regulated anion channels, underlying $I_{Cl,swell}$. These three findings are of utmost physiologic importance because they establish new mechanisms in Bcl-2-mediated volume regulation and shed light on molecular origin and Ca^{2+}-dependent modulation of volume-regulated anion channels in prostate cancer cells.

Bcl-2 and Membrane Ion Channels. The antiapoptotic role of Bcl-2 is mainly carried out via its predominant localization in the outer mitochondrial membrane (1, 2). Ultrastructural studies also showed extramitochondrial Bcl-2 distribution in nuclear outer membrane and endoplasmic reticulum (ER) membrane (3) but not, to our knowledge, in the plasma membrane. Special attention recently has been paid to new antiapoptotic roles of Bcl-2 associated with its localization in the ER membrane (5). Consistent with such localization, the role of Bcl-2 in the modulation of intracellular Ca^{2+} homeostasis and the expression of ER Ca^{2+}-handling proteins, which undergo substantial alterations during apoptosis, is well recognized (6). Accordingly, there also is extensive literature on Bcl-2-dependent modulation of store-operated Ca^{2+} entry (7–9), which occurs via plasma membrane store-operated Ca^{2+} channels, the functional state of which is determined by the filling status of the ER Ca^{2+} store (34). In our recent article, we directly demonstrated that I_{SOC} in LNCaP/Bcl-2 cells is reduced (13), and we attributed this phenomenon to the diminishing number of functional SOCs occurring as an adaptive response to the long-term reduction in the ER Ca^{2+} content associated with Bcl-2 overexpression.

The literature on specific Bcl-2-dependent modulation of other types of membrane ion channels is mainly focused on K^+ ones because they are implicated in two other hallmark features of apoptotic cell death: cell shrinkage (16) and decay of the resting membrane potential (35). Because cell shrinkage is primarily associated with the loss of cytoplasmic ions, of which K^+ is the dominant one, the increase in K^+ efflux via membrane K^+ channels during the early stage of apoptosis is well documented (36, 37). Consistent with the requirement for K^+ conductance to increase during AVD, it is logical that one of the modes of antiapoptotic action of Bcl-2 consists of the down-regulation of voltage-gated K^+ channels (10). Such down-regulation may occur because of Bcl-2-induced inhibition of Cytochrome C release from mytochondria because there is evidence that this apoptotic factor *per se* is capable of activating K^+ channels (38). Standing somewhat apart from this reasoning is the observation that another antiapoptotic member of the Bcl-2 family, mcl-1, enhances K^+ channel activity as part of the prevention of murine myeloblastic FDC-P1 cell death (11). Such enhancement was accompanied by hyperpolarization of membrane resting potential, which was considered to be the key event in the protective mechanism.

Bcl-2 and Volume-Regulated Anion Channels: What Is the Link? Although Cl^- channels in general and volume-regulated ones in particular are implicated in the modulation of resting membrane potential in some cell types (39) and in apoptotic volume decrease (16–18, 40), thus far there is only one work documenting the link between swelling-activated Cl^- current and RVD process with the level of Bcl-2 expression (9).

In our experiments in LNCaP prostate cancer cells, we find that Bcl-2 overexpression considerably enhances $I_{Cl,swell}$. Moreover, we identify the substrate underlying Bcl-2-mediated enhancement of $I_{Cl,swell}$ as a ClC-3 protein, a member of the ClC family of Cl^- channels. ClC-3 is basically the only molecular candidate for the role of endogenous VRAC, which withstood tough experimental scrutiny and is still considered to be involved in $I_{Cl,swell}$ in at least some cell types (19, 24–26). The implication of ClC-3 as the long time-searched VRAC remains under debate, according to conflicting results among cellular models and experiments. Therefore, it previously was shown that knockout experiments for ClC-3 resulted in the maintaining of $I_{Cl,swell}$ (30, 41), and heterologous expression of ClC-3 did not always lead to the recording of a volume-dependent chloride current (42, 43). Those results led several teams to consider ClC-3 as an exclusive intracellular channel. However, recent results suggested that ClC-3 might be a molecular counterpart of VRAC (24, 26–28). Therefore, we investigated the role of this channel in $I_{Cl,swell}$.

Our immunodetection experiments showed that ClC-3 is notably expressed in LNCaP cells. Intracellularly applied via patch pipette, ClC-3-specific antibody also nearly prevented $I_{Cl,swell}$ activation by hypotonic conditions, thus prompting us to conclude that ClC-3 may be a part of endogenous VRAC in these cells. The specificity of this antibody was confirmed by our experiment using intracellularly applied ClC-2-specific antibody, which was without effect on $I_{Cl,swell}$ in LNCaP/neo cells. Furthermore, the enhancement of $I_{Cl,swell}$ in response to Bcl-2 increase, irrespective of whether it was achieved by heterologous overexpression or in response to EGF treatment, was

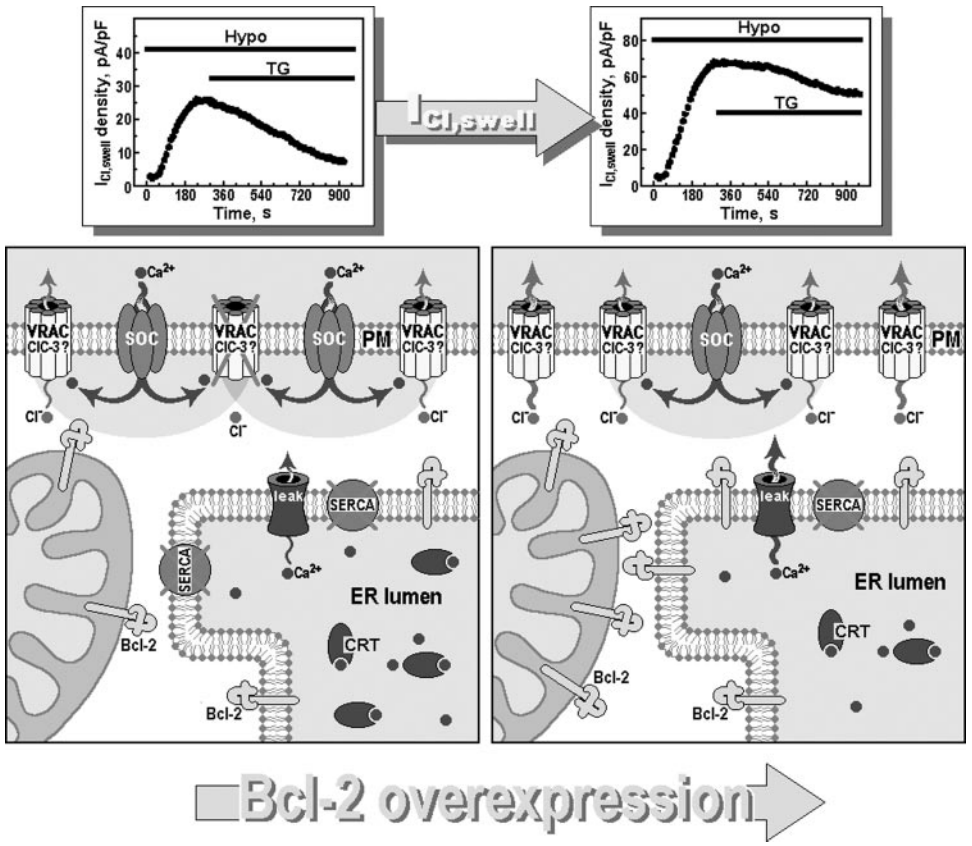

Fig. 7. Schematic diagram showing in simplified form the major effects of Bcl-2 overexpression on swelling-activated Cl^- current ($I_{Cl,swell}$) in prostate cancer epithelial cells evident from our present and previous studies (13). The *left panel* presents the control conditions characterized by low levels of expression of the mitochondria- and endoplasmic reticulum (*ER*)-localized Bcl-2, some background Ca^{2+} leak via the ER leak channels, and the basal expression of SERCA pump, intraluminal calreticulin (*CRT*), plasma membrane (*PM*), volume-regulated anion channels (*VRACs*; also designated as question marked ClC-3 to indicated uncertainty on the role of ClC-3 in VRAC), and store-operated channels (*SOCs*). Under such conditions, hypotonic stimulus evokes baseline $I_{Cl,swell}$ (see top left graph), which can be inhibited by Ca^{2+} entering via activated SOC (in response to TG-induced ER depletion caused by SERCA pump blockade). As shown in our previous work (13), Bcl-2 overexpression (*right*) results in the decreased ER intraluminal Ca^{2+} concentration, down-regulated SERCA pump and CRT expression, enhanced Ca^{2+} leak via ER leak channels, and decreased number of SOCs. Together with enhanced VRAC/ClC-3 expression demonstrated above, this results in augmented $I_{Cl,swell}$ and its weaker inhibition by SOC-transported Ca^{2+} in response to TG exposure (see the top right graph).

always paralleled by the elevation of endogenous levels of ClC-3 protein, providing additional evidence of its involvement in $I_{Cl,swell}$ and suggesting that Bcl-2 modulates $I_{Cl,swell}$ by affecting ClC-3 expression in LNCaP cells. It recently was demonstrated by Abdullaev *et al.* (44) that the activation of EGF receptors in murine mammary cells resulted in the up-regulation of VRAC sensitivity to cell volume. The authors suggested that the number of VRACs is not modified by EGF treatment. $I_{Cl,swell}$ increase observed after a 3-day EGF treatment was explained by the direct phosphorylation of VRACs by tyrosine kinase. Nevertheless, our results show that EGF treatment produces the same effects as the Bcl-2 overexpression (*i.e.*, nearly a twofold increase in ClC-3 levels and $I_{Cl,swell}$ amplitude. The correlation between ClC-3 and $I_{Cl,swell}$ observed in all of our experiments was so tight that, from our point of view, it can only be explained by ClC-3 involvement in $I_{Cl,swell}$. Moreover, our data with Bcl-2 antisense depletion in EGF-treated cells strongly support the notion of the direct relation between Bcl-2 and ClC-3/$I_{Cl,swell}$, although additional experiments are still needed to assess the possible role of tyrosine kinase-dependent regulation in the potentiating effects of EGF treatment on $I_{Cl,swell}$.

Another mechanism by which Bcl-2 may aid the up-regulation of $I_{Cl,swell}$ is by weakening its Ca^{2+}-dependent inhibition because of the decreased number of SOCs. As we showed in our recent study (13) and discussed previously, Bcl-2 overexpression in LNCaP cells causes a decrease in Ca^{2+}-carried I_{SOC}. Consistent with this and with our recent demonstration of the inhibitory action of SOCs-transported Ca^{2+} on VRACs (15), we find here that TG-conferred Ca^{2+}-dependent inhibition of $I_{Cl,swell}$ in LNCaP/Bcl-2 cells is considerably weaker than the control. Because SOCs may have some background activity, this may set some basal level of VRAC inhibition, which because of the smaller number of SOCs in Bcl-2-overexpressing cells would result in generally augmented $I_{Cl,swell}$. In this respect it should be noted that $I_{Cl,swell}$ activation and RVD in LNCaP cells are not accompanied by substantial changes in intracellular Ca^{2+} concentration (15), arguing against a critical role of Bcl-2-induced alterations in global Ca^{2+} homeostasis (other than the suppression of SOCs) in the up-regulation of $I_{Cl,swell}$. Fig. 7 demonstrates the major effects of Bcl-2 overexpression on $I_{Cl,swell}$ in prostate cancer epithelial cells as displayed our study.

One may speculate that reduced resting concentration of calcium in the ER associated with the deficiency for BAX and BAK, the two "multidomain" proapoptotic proteins with ER localization, and related increase in the antiapoptotic potential also would diminish SOC-mediated Ca^{2+} influx, thereby causing similar to Bcl-2 overexpression up-regulating effects on $I_{Cl,swell}$ (45).

Apoptosis, Bcl-2, $I_{Cl,swell}$, and RVD: How They All Relate to Each Other. The question now arises of how Bcl-2-induced up-regulation of $I_{Cl,swell}$ via an enhancement of ClC-3 and decreased Ca^{2+}-dependent inhibition translates into higher resistance of prostate cancer cells to apoptosis.

It recently was suggested that normotonic AVD and hypotonic RVD processes are somehow tightly coupled via the function of VRACs because the inhibitors of these channels were able to prevent apoptotic events (17). Although attractive, this hypothesis seems to be in conflict with the results of Bcl-2 overexpression in LNCaP cells presented previously and also recently reported for MDCK cells (9), which is characterized by an up-regulation of swelling-activated Cl^- current and an enhancement of the RVD process. In the framework of the RVD and AVD direct coupling hypothesis, which implies that facilitation of RVD must promote induction of AVD, such an outcome would mean that excessive Bcl-2 would enhance AVD instead of preventing it, as one might expect from its antiapoptotic functions.

We believe that in this respect the protective role of Bcl-2 on cell survival can be better understood, not in terms of the prevention of

apoptosis, but in terms of shifting the balance toward stabilizing cell proliferation. On one hand, Bcl-2 is known to contribute to cell survival by decreasing the rate of cell proliferation caused by prolongation of the G_1 phase of the cell cycle (46), and, conversely, cell proliferation caused by mitogenic factors is usually associated with cell volume increase (16) and intense Ca^{2+} signaling, necessarily involving ER Ca^{2+} store depletion and the activation of SOCs (47, 48). Under such conditions, Bcl-2-induced up-regulation of $I_{Cl,swell}$ caused by increased expression of ClC-3, a likely contributor to the endogenous VRAC in the prostate cancer epithelial cells, and weaker negative control of VRACs from SOCs-transported Ca^{2+} caused by decreased number of SOCs would enhance the ability of the cells to handle proliferative volume perturbations and thereby increase their survival rate and decrease their proapoptotic potential. Three experimental facts—recently demonstrated stimulation of LNCaP cell proliferation (32), inhibition of apoptosis (33) by EGF, and EGF-dependent increase of endogenous Bcl-2 levels demonstrated here—agree nicely with such a hypothesis.

An alternative explanation may rely on the fact that certain ion fluxes, and not cell shrinkage *per se*, are important for apoptosis. For example, it recently has been shown that sodium influx is necessary for cell shrinkage but not for the activation of cell death effectors, whereas potassium efflux is critical for apoptosis regardless of changes in cell size (49). Thus, it may well be that antiapoptotic significance of up-regulated $I_{Cl,swell}$ in Bcl-2-overexpressing cells is not related to the alterations in cell volume homeostasis but is rather caused by specific effects of the chloride ions on apoptotic events.

ACKNOWLEDGMENTS

We thank Professor T. Jentsch (Institute for Molecular Neuropathobiology, Hamburg University, Germany) for providing us with the hClC-3 clones.

REFERENCES

1. Shimizu S, Narita M, Tsujimoto Y. Bcl-2 family proteins regulate the release of apoptogenic cytochrome c by the mitochondrial channel VDAC. Nature 1999;399:483–7.
2. Shimizu S, Konishi A, Kodama T, Tsujimoto Y. BH4 domain of antiapoptotic Bcl-2 family members closes voltage-dependent anion channel and inhibits apoptotic mitochondrial changes and cell death. Proc Natl Acad Sci USA 2000;97:3100–5.
3. Akao Y, Otsuki Y, Kataoka S, Ito Y, Tsujimoto Y. Multiple subcellular localization of bcl-2: detection in nuclear outer membrane, endoplasmic reticulum membrane, and mitochondrial membranes. Cancer Res 1994;54:2468–71.
4. Ferri KF, Kroemer G. Organelle-specific initiation of cell death pathways. Nat Cell Biol 2001;3:E255–63.
5. Rudner J, Jendrossek V, Belka C. New insights in the role of Bcl-2 Bcl-2 and the endoplasmic reticulum. Apoptosis 2002;7:441–7.
6. Pinton P, Ferrari D, Rapizzi E, et al. A role for calcium in Bcl-2 action? Biochimie 2002;84:195–201.
7. Pinton P, Ferrari D, Magalhaes P, et al. Reduced loading of intracellular Ca(2+) stores and downregulation of capacitative Ca(2+) influx in Bcl-2-overexpressing cells. J Cell Biol 2000;148:857–62.
8. Williams SS, French JN, Gilbert M, et al. Bcl-2 overexpression results in enhanced capacitative calcium entry and resistance to SKF-96365-induced apoptosis. Cancer Res 2000;60:4358–61.
9. Shen MR, Yang TP, Tang MJ. A novel function of BCL-2 overexpression in regulatory volume decrease. Enhancing swelling-activated Ca(2+) entry and Cl(−) channel activity. J Biol Chem 2002;277:15592–9.
10. Ekhterae D, Platoshyn O, Krick S, et al. Bcl-2 decreases voltage-gated K+ channel activity and enhances survival in vascular smooth muscle cells. Am J Physiol Cell Physiol 2001;281:C157–65.
11. Wang L, Zhou P, Craig RW, Lu L. Protection from cell death by mcl-1 is mediated by membrane hyperpolarization induced by K(+) channel activation. J Membr Biol 1999;172:113–20.
12. Horoszewicz JS, Leong SS, Kawinski E, et al. LNCaP model of human prostatic carcinoma. Cancer Res 1983;43:1809–18.
13. Vanden Abeele F, Skryma R, Shuba Y, et al. Bcl-2-dependent modulation of Ca(2+) homeostasis and store-operated channels in prostate cancer cells. Cancer Cell 2002; 1:169–79.
14. Shuba YM, Prevarskaya N, Lemonnier L, et al. Volume-regulated chloride conductance in the LNCaP human prostate cancer cell line. Am J Physiol Cell Physiol 2000;279:C1144–54.
15. Lemonnier L, Prevarskaya N, Shuba Y, et al. Ca2+ modulation of volume-regulated anion channels: evidence for colocalization with store-operated channels. FASEB J 2002;16:222–4.
16. Lang F, Ritter M, Gamper N, et al. Cell volume in the regulation of cell proliferation and apoptotic cell death. Cell Physiol Biochem 2000;10:417–28.
17. Maeno E, Ishizaki Y, Kanaseki T, Hazama A, Okada Y. Normotonic cell shrinkage because of disordered volume regulation is an early prerequisite to apoptosis. Proc Natl Acad Sci USA 2000;97:9487–92.
18. Okada Y, Maeno E. Apoptosis, cell volume regulation and volume-regulatory chloride channels. Comp Biochem Physiol A Mol Integr Physiol 2001;130:377–83.
19. Duan D, Winter C, Cowley S, Hume JR, Horowitz B. Molecular identification of a volume-regulated chloride channel. Nature 1997;390:417–21.
20. Raffo AJ, Perlman H, Chen MW, et al. Overexpression of bcl-2 protects prostate cancer cells from apoptosis in vitro and confers resistance to androgen depletion in vivo. Cancer Res 1995;55:4438–45.
21. Okada Y. Cell volume-sensitive chloride channels. Contrib Nephrol 1998;123:21–33.
22. Eggermont J, Trouet D, Carton I, Nilius B. Cellular function and control of volume-regulated anion channels. Cell Biochem Biophys 2001;35:263–74.
23. Furst J, Gschwentner M, Ritter M, et al. Molecular and functional aspects of anionic channels activated during regulatory volume decrease in mammalian cells. Pflugers Arch 2002;444:1–25.
24. Duan D, Zhong J, Hermoso M, et al. Functional inhibition of native volume-sensitive outwardly rectifying anion channels in muscle cells and Xenopus oocytes by anti-ClC-3 antibody. J Physiol 2001;531:437–44.
25. Wang L, Chen L, Jacob TJ. The role of ClC-3 in volume-activated chloride currents and volume regulation in bovine epithelial cells demonstrated by antisense inhibition. J Physiol 2000;524(Pt 1):63–75.
26. Hermoso M, Satterwhite CM, Andrade YN, et al. ClC-3 is a fundamental molecular component of volume-sensitive outwardly rectifying Cl− channels and volume regulation in HeLa cells and Xenopus laevis oocytes. J Biol Chem 2002;277:40066–74.
27. Wang GX, Hatton WJ, Wang GL, et al. Functional effects of novel anti-ClC-3 antibodies on native volume-sensitive osmolyte and anion channels in cardiac and smooth muscle cells. Am J Physiol Heart Circ Physiol 2003;285:H1453–63.
28. Jin NG, Kim JK, Yang DK, et al. A fundamental role of ClC-3 in volume-sensitive Cl− channels function and cell volume regulation in AGS cells. Am J Physiol Gastrointest Liver Physiol 2003;285:G938–48.
29. Vazquez G, Wedel BJ, Trebak M, St. John Bird G, Putney JW Jr. Expression level of the canonical transient receptor potential 3 (TRPC3) channel determines its mechanism of activation. J Biol Chem 2003;278:21649–54.
30. Stobrawa SM, Breiderhoff T, Takamori S, et al. Disruption of ClC-3, a chloride channel expressed on synaptic vesicles, leads to a loss of the hippocampus. Neuron 2001;29:185–96.
31. Pidgeon GP, Barr MP, Harmey JH, Foley DA, Bouchier-Hayes DJ. Vascular endothelial growth factor (VEGF) upregulates BCL-2 and inhibits apoptosis in human and murine mammary adenocarcinoma cells. Br J Cancer 2001;85:273–8.
32. Legrand G, Humez S, Slomianny C, et al. Ca2+ pools and cell growth. Evidence for sarcoendoplasmic Ca2+-ATPases 2B involvement in human prostate cancer cell growth control. J Biol Chem 2001;276:47608–14.
33. Kulik G, Carson JP, Vomastek T, et al. Tumor necrosis factor α induces BID cleavage and bypasses antiapoptotic signals in prostate cancer LNCaP cells. Cancer Res 2001;61:2713–9.
34. Venkatachalam K, van Rossum DB, Patterson RL, Ma HT, Gill DL. The cellular and molecular basis of store-operated calcium entry. Nat Cell Biol 2002;4:E263–72.
35. Dallaporta B, Marchetti P, de Pablo MA, et al. Plasma membrane potential in thymocyte apoptosis. J Immunol 1999;162:6534–42.
36. Yu SP, Yeh CH, Sensi SL, et al. Mediation of neuronal apoptosis by enhancement of outward potassium current. Science 1997;278:114–7.
37. Bortner CD, Hughes FM Jr, Cidlowski JA. A primary role for K+ and Na+ efflux in the activation of apoptosis. J Biol Chem 1997;272:32436–42.
38. Platoshyn O, Zhang S, McDaniel SS, Yuan JX. Cytochrome c activates K+ channels before inducing apoptosis. Am J Physiol Cell Physiol 2002;283:C1298–305.
39. Jentsch TJ, Stein V, Weinreich F, Zdebik AA. Molecular structure and physiological function of chloride channels. Physiol Rev 2002;82:503–68.
40. Okada Y, Maeno E, Shimizu T, et al. Receptor-mediated control of regulatory volume decrease (RVD) and apoptotic volume decrease (AVD). J Physiol 2001;532:3–16.
41. Arreola J, Begenisich T, Nehrke K, et al. Secretion and cell volume regulation by salivary acinar cells from mice lacking expression of the Clcn3 Cl− channel gene. J Physiol 2002;545:207–16.
42. Li X, Shimada K, Showalter LA, Weinman SA. Biophysical properties of ClC-3 differentiate it from swelling-activated chloride channels in Chinese hamster ovary-K1 cells. J Biol Chem 2000;275:35994–8.
43. Weylandt KH, Valverde MA, Nobles M, et al. Human ClC-3 is not the swelling-activated chloride channel involved in cell volume regulation. J Biol Chem 2001; 276:17461–7.
44. Abdullaev IF, Sabirov RZ, Okada Y. Upregulation of swelling-activated Cl− channel sensitivity to cell volume by activation of EGF receptors in murine mammary cells. J Physiol 2003;549:749–58.
45. Scorrano L, Oakes SA, Opferman JT, et al. BAX and BAK regulation of endoplasmic reticulum Ca2+: a control point for apoptosis. Science 2003;300:135–9.
46. Borner C. Diminished cell proliferation associated with the death-protective activity of Bcl-2. J Biol Chem 1996;271:12695–8.
47. Golovina VA. Cell proliferation is associated with enhanced capacitative Ca(2+) entry in human arterial myocytes. Am J Physiol 1999;277:C343–9.
48. Golovina VA, Platoshyn O, Bailey CL, et al. Upregulated TRP and enhanced capacitative Ca(2+) entry in human pulmonary artery myocytes during proliferation. Am J Physiol Heart Circ Physiol 2001;280:H746–55.
49. Bortner CD, Cidlowski JA. Uncoupling cell shrinkage from apoptosis reveals that Na+ influx is required for volume loss during programmed cell death. J Biol Chem 2003;278:39176–84.

Article 3

The FASEB Journal express article 10.1096/fj.05-4714fje. Published online January 9, 2006.

Protection of TRPC7 cation channels from calcium inhibition by closely associated SERCA pumps

Loïc Lemonnier, Mohamed Trebak, Jean-Philippe Lievremont,[1] Gary S. Bird, and James W. Putney, Jr.

National Institute of Environmental Health Sciences, NIH Department of Health and Human Services, Research Triangle Park, NC 27709

[1]Present Address: Neuro3d S.A., Parc d'Innovation, ESBS, Blvd Sebastien Brandt, F-67412 Illkirch, France.

Corresponding author: James W. Putney, Jr., NIEHS, PO Box 12233, Research Triangle Park, NC 27709. E-mail: putney@niehs.nih.gov

ABSTRACT

Numerous studies have demonstrated that members of the transient receptor potential (TRP) superfamily of channels are involved in regulated Ca^{2+} entry. Additionally, most Ca^{2+}-permeable channels are themselves regulated by Ca^{2+}, often in complex ways. In the current study, we have investigated the regulation of TRPC7, a channel known to be potentially activated by both store-operated mechanisms and non-store-operated mechanisms involving diacylglycerols. Surprisingly, we found that activation of TRPC7 channels by diacylglycerol was blocked by the SERCA pump inhibitor thapsigargin. The structurally related channel, TRPC3, was similarly inhibited. This effect depended on extracellular calcium and on the driving force for Ca^{2+} entry. The inhibition is not due to calcium entry through store-operated channels but rather results from calcium entry through TRPC7 channels themselves. The effect of thapsigargin was prevented by inhibition of calmodulin and was mimicked by pharmacological disruption of the actin cytoskeleton. Our results suggest the presence of a novel mechanism involving negative regulation of TRPC channels by calcium entering through the channels. Under physiological conditions, this negative feedback by calcium is attenuated by the presence of closely associated SERCA pumps.

Keywords: calcium channels • calcium signaling • ion channels • TRPC channels

Amongst the different structures involved in the regulation of Ca^{2+} homeostasis, the TRP (transient receptor potential) channels superfamily is one of the most intensively studied. The TRPs were first cloned from *Drosophila melanogaster* as a gene necessary for normal visual signal transduction (1). Seven mammalian genes with close homology to *Drosophila* TRP proteins have been identified and cloned (2–10). Due to their high homology with the fly TRPs, these seven channels have been called “canonical” TRP or TRPC.

Despite their apparent homology, the TRPCs are apparently not all activated in the same way (11). TRPC1 was first described as activated by intracellular calcium store depletion (4, 12–14). TRPC2 has been described as a store-operated (9) or as a diacylglycerol-activated (15) channel. Similarly, TRPC4 and 5 have been shown to behave as store-operated (8, 16) or non-store-operated, receptor-operated cation channels (17, 18). Finally, TRPC3, 6, and 7 have been described as diacylglycerol-activated channels (10, 19, 20), but in some situations they behave as store-operated channels (21, 22).

Previous studies have demonstrated that in some instances, the store-operated and non-store-operated pathways mutually inhibit one another (23–25). In the current study, we used stably transfected HEK-293 cells ectopically expressing human TRPC7. These cells have previously been shown to exhibit both store-operated and non-store-operated behavior of TRPC7 channels (22). Surprisingly, we found that depletion of Ca^{2+} stores with thapsigargin inhibited receptor activation of TRPC7 channels. The structurally related channel TRPC3, was similarly inhibited. This inhibition appears to be due to a role for SERCA pump in buffering calcium near the mouth of the channel. The findings reveal a novel mode of regulation of calcium-permeable TRPC channels and may provide an explanation for previously observed inhibitory effects of SERCA inhibitors on non-store-operated channels.

MATERIALS AND METHODS

Reagents

Thapsigargin, calmidazolium, and oleyl acetyl glycerol (OAG) were purchased from Calbiochem (San Diego, CA), and 1,2-bis(2-aminophenoxy)ethane-*N*,*N*,*N*',*N*'-tetraacetic acid (BAPTA) was purchased from Calbiochem. Fura-5F-AM and free acid were from Molecular Probes. The other reagents were purchased from Sigma (St. Louis, MO).

Ca^{2+} measurements

The sources of HEK-293 cells stably expressing human TRPC3 and TRPC7 have been described previously (22, 26). Coverslips with attached cells were mounted in a Teflon chamber and incubated at room temperature for 30 min in a HEPES-buffered saline solution (in mM: 145 NaCl, 5 KCl, 2 $CaCl_2$, 1 $MgCl_2$, 10 HEPES, pH 7.3) containing 1 μM fura 5F-AM. Cells were then washed and bathed in the same solution without dye for at least 10 min before beginning the experiment. For Ca^{2+} measurements, fluorescence images of several cells were recorded and analyzed with a digital fluorescence imaging system (InCyt Im2; Intracellular Imaging, Cincinnati, OH) as described previously (20). All experiments were conducted at room temperature, and data are reported as the ratio of fluorescence due to excitation at 340 and 380 nm.

Histochemistry

HEK 293 cells expressing TRPC7 were grown to subconfluence on Lab-Tek II glass slides (Fisher Scientific) and treated with either 0.1% Me_2SO (control), 1 μM cytochalasin B, or 30 μM OAG for 45 min at 37°C in DMEM and 5% CO_2. Cells were subsequently washed with phosphate-buffered saline (PBS: 120 mM NaCl, 2.6 mM KCl, 8.1 mM Na_2HPO_4, and 1.5 mM KH_2PO_4, pH 7.4) and fixed in PBS containing 4% paraformaldehyde for 30 min at 4°C (all

incubations and rinses were performed with PBS). Cells were rinsed three times, permeabilized with 0.1% Triton X-100 for 15 min at 25°C, rinsed three times. To reduce any potential nonspecific background staining, the cell preparation was incubated with 0.5% gelatin (from 2% stock diluted in PBS) for 30 min at 25°C and then washed three times.

For labeling actin cytoskeleton, fixed and permeabilized cells were incubated with Alexa 488-phalloidin (5 U/ml, Molecular Probes) for 30 min at 25°C. Cells were then rinsed three times and then incubated for a further 5 min with DAPI (5 μM, Molecular Probes) to stain the nuclei. Stained cells were then rinsed three times with PBS. In preparation for visualization, the PBS bathing the cells was removed and the Lab-Tek II slides disassembled. The stained sample was preserved by applying 20–50 μl of SHUR/MOUNT (Triangle Biomedical Sciences, Durham, NC) and covering the glass slide with a #1 glass coverslip.

Alexa-488 phalloidin (ex 488 nm, em long-pass 505 nm) and DAPI (ex 364 nm, em bandpass 435-485 nm) were visualized using an LSM 510 confocal microscope equipped with a ×40 (1.2 NA) objective. With the confocal pinhole set at 1 Airy unit, the images represent optical slices of ~0.9 μm thick. The white bar in each image represents 20 μm.

Electrophysiology

Macroscopic membrane ion currents were recorded using the patch-clamp technique in its whole cell configuration. The currents were acquired using pCLAMP-9.2 (Axon Instruments) and analyzed offline using Origin 6 (Microcal) software. The extracellular solution (osmolarity 310 mosmol/l) contained (in mM): 145 NaCl, 5 KCl, 10 HEPES, 1 $MgCl_2$, 2 $CaCl_2$, pH, 7.3 (adjusted with NaOH). The intracellular pipette solution (osmolarity 290 mosmol/l) contained (in mM): 145 Cs-methanesulfonate, 10 BAPTA, 10 HEPES, 1 $MgCl_2$, and 2.2 $CaCl_2$ (100 nM free Ca^{2+}), pH 7.2 (adjusted with CsOH). Patch pipettes were fabricated from borosilicate glass capillaries (WPI). The resistance of the pipettes varied between 3 and 5 MΩ. Necessary supplements were added directly to the respective solutions, in concentrations that would not significantly change the osmolarity. Changes in the external solutions were carried out using a multibarrel puffing micropipette with common outflow that was positioned in close proximity to the cell under investigation. During the experiment, the cell was continuously superfused with the solution via a puffing pipette to reduce possible artifacts related to the switch from static to moving solution and vice versa. For the cell-attached experiments, the same solution was present in the bath and in the patch pipette (resistance varying between 5–10 MΩ) in mM: 150 KCl, 10 HEPES, 2 $CaCl_2$, 1 $MgCl_2$, pH 7.3 adjusted with KOH. Signals were low-pass filtered at 2 kHz, digitized at 20 kHz and then analyzed using the Clampfit 9.2 software (Axon Instruments).

RESULTS

TRPC7 inhibition by store depleting agents

In this study, we used the membrane permeant diacylglycerol, OAG as an activator of TRPC7 channels to avoid upstream effects on receptor or phospholipase C activity. We carried out Ca^{2+} imaging experiments with wild-type and TRPC7-overexpressing HEK293 cells in the presence of 2 mM Ca^{2+} and 1 μM Gd^{3+} (to block endogenous store-operated channels). In wild-type cells, we observed no increase in the fluorescence ratio in response to the addition of 30 μM OAG

(*n*=44; Fig. 1*A*). Prior addition of 5 μM thapsigargin resulted in a transient increase in the fluorescence ratio corresponding to the depletion of the ER Ca^{2+} stores (peak ratio: 0.54±0.02; *n*=57). This result confirms the previous observations that 1 μM Gd^{3+} completely inhibits capacitative Ca^{2+} entry in HEK293 cells (27). Again in the presence of thapsigargin, OAG failed to activate Ca^{2+} entry in wild-type cells (Fig. 1*A*). We then used the same experimental protocol on HEK-293 cells stably overexpressing TRPC7 (TRPC7-HEK). In this case, the addition of 30 μM OAG elicits a sustained increase in the fluorescence ratio (peak ratio: 0.58±0.01; *n*=49; Fig. 1*B*), which can be attributed to TRPC7 channel activation. Wild-type cells do not show sustained Ca^{2+} entry in the presence of 1 μM Gd^{3+}, because the store-operated channels are blocked in this condition. However, in TRPC7-expressing cells thapsigargin induced a sustained increase in $[Ca^{2+}]_i$, due to the presence of a store-operated TRPC7-dependent pathway (22). Surprisingly, subsequent addition of OAG failed to induce any Ca^{2+} entry (Fig. 1*B*).

To confirm these results with more direct measurement of membrane currents, we next used the patch-clamp technique in its whole cell configuration. The protocol involved holding the membrane potential at 0 mV, corresponding to the reversal potential for the TRPC7-associated current (I_{TRPC7}), and execution of voltage ramps from −100 mV to +100 mV every 5 s.

After establishment of the whole cell configuration, TRPC7-HEK cells present an endogenous current significantly higher at +100 mV than in wt-HEK cells, due to basal activity of TRPC7 channels in these cells (I_{TRPC7}: −6.2±1.2 and 12.5±3.6 pA/pF, *n*=5; I_{wt}: −6.3±0.5 and 6.9±0.7 pA/pF, *n*=5 data not shown; respectively at −100 and +100 mV). In control conditions, application of 30 μM OAG 75 s after break-in elicits the development of an outwardly rectifying current reaching its maximal amplitude within 100 s (I_{TRPC7} max.: −27.9±5.2 and 88.6±16.3 pA/pF, respectively, at −100 and +100 mV; *n*=5; Fig. 2*A*). The addition of 5 μM thapsigargin[1] at time 0 dramatically impairs current development (I_{TRPC7} max.: −7.5±0.9 and 26.1±7.1 pA/pF, respectively, at −100 and +100 mV; *n*=5) without affecting the endogenous current observed after establishment of the whole cell configuration (I_{TRPC7}: −5.9±0.9 and 12.7±2.4 pA/pF, respectively, at −100 and +100 mV, *n*=5). This inhibition of I_{TRPC7} by thapsigargin appears constant over a wide range of potential (73.1 and 70.5% of inhibition at −100 and +100 mV respectively, Fig. 2*B*). Significantly, no such inhibition was observed when intracellular stores were discharged by inclusion of IP_3 in the pipette solution (data not shown). A similar degree of inhibition by thapsigargin was observed when the TRPC7 channels were activated through the muscarinic receptor-phospholipase C pathway with methacholine (data not shown). For the remainder of the study, we focused on currents activated by OAG, thereby avoiding complications of effects on upstream events.

To ensure that the effects of thapsigargin did not result from unexpected pharmacological effects unrelated to inhibition of SERCA pumps, we also used cyclopiazonic acid (CPA), a structurally unrelated SERCA inhibitor (Fig. 2*C*). In this case, application of 20 μM CPA induced an inhibition of I_{TRPC7} similar to that observed with thapsigargin: in the control conditions, I_{TRPC7} max.: −24.6 ± 5.1 and 82.2 ± 14.9 pA/pF, respectively, at −100 and +100 mV, *n* = 5; in the presence of CPA: −10.8 ± 3.9 and 34.6 ± 16.3 pA/pF, respectively at −100 and +100 mV, *n*=5.

I_{TRPC7} inhibition by calcium entry

It has been recently shown by Shi et al. (28) that the murine TRPC7 is complexly regulated by both intra- and extracellular calcium. Thapsigargin would be expected to alter intracellular Ca^{2+} buffering and to activate store-operated channels, and thus we considered the possibility that the effect of thapsigargin could be related to Ca^{2+} regulation of TRPC7 channels. Therefore, we first assessed the sensitivity of I_{TRPC7} to different intracellular free Ca^{2+} concentrations in the patch pipette. As shown in Fig. 3*A*, the currents elicited by the application of 30 μM OAG with 0 (*n*=5) or 100 nM (*n*=7) free Ca^{2+} in the intracellular solution do not exhibit any significant difference (I_{TRPC7} max.: −28.3±6.1 and 85.5±15.6 pA/pF for 0 nM Ca^{2+}; −24.6±5.1 and 82.2±14.9 pA/pF for 100 nM Ca^{2+}, respectively, at −100 and +100 mV). However, when we increased the free Ca^{2+} concentration to 500 nM, we observed substantial inhibition of OAG-activated I_{TRPC7} (I_{TRPC7} max.: −9.1±1.6 and 34.7±5.8 pA/pF, respectively, at −100 and +100 mV, *n*=4). These results are summarized in Fig. 3*B*, which also indicates that changing the free Ca^{2+} concentration has little effect on the endogenous current present in the cells after the whole cell configuration was established. If thapsigargin were inhibiting TRPC7 by raising intracellular Ca^{2+}, this could result either from Ca^{2+} release from intracellular stores or from entry across the plasma membrane. To distinguish between these possibilities, we repeated our experiments with thapsigargin in the presence of different extracellular Ca^{2+} concentrations (Fig. 4*A*). In the absence of Ca^{2+} in the bath, but in the presence of thapsigargin, I_{TRPC7} was not diminished as compared with control conditions (see Fig. 2*A*; I_{TRPC7} max.: −40.5±10.7 and 135.2±10.9 pA/pF, respectively, at −100 and +100 mV, *n*=5; I_{TRPC7} max.: −64.4±16.7 and 89.8±16.1 pA/pF). When we added increasing concentrations of Ca^{2+}, we observed a graded decrease in I_{TRPC7} amplitude (I_{TRPC7} max.: −25.4±4.2 and 62.9±12.1 pA/pF for 1 mM Ca^{2+}, respectively, at −100 and +100 mV, *n*=5; −7.5±0.9 and 26.1±7.1 pA/pF for 2 mM Ca^{2+}, respectively, at −100 and +100 mV, *n*=4). Addition of 0.1 mM EGTA to the Ca^{2+} free solution further reduces extracellular Ca^{2+} from a low μM concentration to submicromolar concentration. With this condition, we not only observed a lack of effect of thapsigargin (Fig. 4*B*) but also a robust increase in I_{TRPC7} amplitude when compared with that obtained with a standard solution containing 2 mM Ca^{2+} (I_{TRPC7} max.: −133.4±39.5 and 255.1±72.3 pA/pF for 0.1 mM EGTA, *n*=4; −111.9±29.1 and 194.8±27.6 3 pA/pF for 0.1 mM EGTA + Tg, respectively, at −100 and +100 mV, *n*=4). We replaced Ca^{2+} in the standard external solution with 2 mM Ba^{2+} (Fig. 4*C*). In this case, thapsigargin still failed to inhibit the development of I_{TRPC7} in response to an OAG application (I_{TRPC7} max.: −65.1±11.1 and 101.3±19.6 −133.4 pA/pF for 2 mM Ba^{2+}, *n*=6; −73.5±15.2 and 116±19.6 for 2 mM Ba^{2+} + Tg, respectively, at −100 and +100 mV, *n*=6).

These results indicate that extracellular Ca^{2+} is required for thapsigargin to inhibit TRPC7 activity. To distinguish between an action at an extracellular site from an action depending on Ca^{2+} entry, we increased the holding potential, thus decreasing the driving force for Ca^{2+} entry without changing extracellular [Ca^{2+}] (Fig. 4*D*). As described previously in Fig. 2*A*, at a holding potential of 0 mV, thapsigargin induces a substantial decrease in I_{TRPC7} amplitude (I_{TRPC7} max.: −27.9±5.2 and 88.6±16.3 pA/pF for the control, *n*=5; −7.5±0.9 and 26.1±7.1 pA/pF in the presence of thapsigargin, respectively, at −100 and +100 mV; *n*=5). When repeated with a holding potential of +50 mV, a value close to E_{Ca}, the current in the control conditions exhibited a small increase compared with the one observed at 0 mV (I_{TRPC7} max.: −27.4±4.9 and 109.2±25.1 pA/pF, respectively, at −100 and +100 mV, *n*=5), and thapsigargin now failed to inhibit the OAG-induced current (I_{TRPC7} max.: −36.1±9.3 and 140.6±17.2 pA/pF, respectively, at

−100 and +100 mV, *n*=4). Collectively then, the dependence of the thapsigargin effect on holding potential and extracellular Ca^{2+}, as well as the failure of Ba^{2+} to substitute for Ca^{2+}, indicates that Ca^{2+} entry rather than release of Ca^{2+}, extracellular Ca^{2+} binding, or some other consequence of store depletion inhibits TRPC7 channel activity.

By using the ability to change driving force for Ca^{2+} entry through changing holding potential, we were able to examine the reversibility of the Ca^{2+}-dependent inhibitory effect of thapsigargin. In the experiment shown in Fig. 5*A*, pretreatment with thapsigargin inhibited the ability of OAG to activate TRPC7 (I_{TRPC7} max.: −11.1±2.1 and 43.2±11.9 pA/pF, respectively, at −100 and +100 mV, *n*=5). As shown in the figure, when the holding potential was switched from 0 mV to 50 mV, OAG-activated current rapidly developed (I_{TRPC7} max.: −24.7±8.6 and 124.7±35.9 pA/pF, respectively, at −100 and +100 mV, *n*=5). This indicates that the effects of thapsigargin, and vide infra Ca^{2+}, do not reflect nonspecific structural effects or loss of proteins but are indicative of a rapidly reversible regulatory mechanism.

We also used the reciprocal protocol in which OAG-activated current was allowed to develop in the presence of thapsigargin by holding at +50 mV; once the current was developed, the holding potential was switched to 0 mV to permit Ca^{2+} entry. As a control, we also examined the effects of holding potential on the OAG-activated current in the absence of external Ca^{2+}. As seen in Fig. 5*B*, in the absence of Ca^{2+} OAG-activated currents were large (see also Fig. 4*B*) and were not affected by holding potential (I_{TRPC7} max. at +50 mV: −111.2±32.2 and 182.7±67.1 pA/pF, respectively, at −100 and +100 mV; I_{TRPC7} at 0 mV: −110.9± 9.4 and 185.6±76.6 pA/pF, respectively, at −100 and +100 mV, *n*=5). In the presence of Ca^{2+}, after development of the OAG-activated current at a holding potential of +50 mV, switching to 0 mV caused a rapid decrease in both inward and outward current (I_{TRPC7} max. at +50 mV: −29.1±5.4 and 114.7±25.8 pA/pF, respectively, at −100 and +100 mV; I_{TRPC7} at 0 mV: −18. ±3.7 and 64.1±18.4 pA/pF, respectively, at −100 and +100 mV, *n*=5). However, surprisingly, there was no significant difference in the final current level in the presence or absence of thapsigargin (I_{TRPC7} max. at +50 mV: −43.8±10.8 and 160.9±19.5 pA/pF, respectively, at −100 and +100 mV; I_{TRPC7} at 0 mV: −24.5±7.6 and 78.6±18.9 pA/pF, respectively, at −100 and +100 mV, *n*=4). This result indicates that once the current is fully activated by OAG, it functions independently of SERCA status. This may suggest that the effect of Ca^{2+} that depends on SERCA pumps involves the activation mechanism by OAG, rather than a more direct effect on the channel properties.

I_{TRPC7} is inhibited by calcium entry through TRPC7 channels

The most obvious mechanism for Ca^{2+} entry associated with the use of store-depleting agents is capacitative calcium entry, which involves activation of SOCs in response to depletion of ER Ca^{2+} stores. We therefore investigated the potential involvement of capacitative calcium entry in the thapsigargin-induced I_{TRPC7} inhibition. We added 1 μM Gd^{3+} to the extracellular solution to completely block SOC activity (see Fig. 1*A*; see also ref 29). However, this concentration of Gd^{3+} did not prevent thapsigargin inhibition of I_{TRPC7}, which effectively rules out the involvement of endogenous SOC in this phenomenon (I_{TRPC7} max.: −32±8.8 and 92.7±16.9 pA/pF for the control, *n*=5; −7±1.5 and 24.8±7.2 pA/pF for the Tg, respectively, at −100 and +100 mV, *n*=4; Fig. 6*A*). Surprisingly, we observed that an increase in Gd^{3+} concentration to 10 μM almost completely reversed the inhibitory effect of thapsigargin on I_{TRPC7} (I_{TRPC7} max.: −24.4±5.6 and 65.4±7.3 pA/pF for the control, *n*=4; −12.3±3.7 and 50.6±15.8 pA/pF for the Tg,

respectively, at −100 and +100 mV, *n*=5; Fig. 6*B*). We noted that at this concentration, Gd^{3+} appears to act as a partial inhibitor of TRPC7, as indicated by a decrease in I_{TRPC7} amplitude between the control conditions in the Fig. 6*A* and *B*. We also found that 2-APB, a potent inhibitor of the SOC (30, 31), but a partial inhibitor of TRPC channels (27), also reduced the inhibitory effect of thapsigargin (I_{TRPC7} max.: −23.4±8.5 and 69.2±19.4 pA/pF for the control, *n*=4; −14.9±1.9 and 49.7±8.7 pA/pF for the Tg, respectively, at −100 and +100 mV, *n*=5; Fig. 6*C*). As shown for 10 μM Gd^{3+}, 2-APB is also a partial inhibitor of I_{TRPC7} (see I_{TRPC7} amplitude in the control conditions of Fig. 6*A* and *C*).

Ca^{2+} entry via the endogenous SOC pathway cannot account for I_{TRPC7} inhibition by thapsigargin, as 1 μM Gd^{3+} does not prevent it. However, in stable TRPC7-expressing cells, there is also a thapsigargin-activated SOC that is not blocked by 1 μM Gd^{3+} (22). To determine if this pathway is involved, we examined the effects of thapsigargin on OAG-activated currents in TRPC3-expressing cells. TRPC3 is regulated similarly to TRPC7, but we have never observed any Gd^{3+}-insensitive store-operated Ca^{2+} entry in TRPC3-expressing HEK293 cells (20, 26, 27). As shown in Fig. 7, the OAG-activated current was substantially inhibited by thapsigargin pretreatment in the TRPC3-expressing cells (I_{TRPC3} max.: −13.1±1.7 and 48.6±9.1 pA/pF for the control, *n*=6; −8.4±1.1 pA and 29.4±2.6 pA/pF for the Tg, respectively, at −100 and +100 mV, *n*=6), and this effect was largely prevented by 10 μM Gd^{3+} (I_{TRPC3} max.: −11.7±2.9 and 46.5±13.6 pA/pF for the control, *n*=4; −11.1±1.3 and 55.9±9.6 pA/pF for the Tg, respectively, at −100 and +100 mV, *n*=4). This indicates that Ca^{2+} does not need to enter through store-operated TRPC channels to mediate the inhibition seen with SERCA inhibitors.

A moderate concentration of Gd^{3+} and the multifunction channel inhibitor 2-APB, were able to restore I_{TRPC7} in the presence of thapsigargin. Both of these conditions are expected to produce partial inhibition of TRPC7 channels, suggesting that the critical Ca^{2+} entry leading to I_{TRPC7} inhibition may result from Ca^{2+} entering directly through the TRPC7 channels. While it may seem strange to propose that an inhibitor of a channel prevents the action of another inhibitor, it is important to consider the microscopic consequences of the actions of direct channel inhibitors. In this case, the protective effect of the Gd^{3+} and 2-APB could result from a reduction of the quantity of Ca^{2+} entering through the channels during each channel opening, thereby reducing the range or distance from the channel at which Ca^{2+} could act. That is to say, these inhibitors should cause an apparent partial reduction of the single channel conductance. To test this hypothesis, we used the patch-clamp technique in its cell-attached configuration. Cells were held at 0 mV, and a step to +60 mV was applied every second. The results of these experiments are presented in Fig. 8 as all-points histograms reporting the single channel activity detected at +60 mV. The single channels analyzed were due to TRPC7 channel openings, because no such openings were detected in wild-type HEK293 cells (not shown). All-points histograms show a large peak at 0 pA, thus indicating the amount of time the channels were closed during each trace. Under control conditions, the mean amplitude of a single channel event was 4.301 ± 0.006 pA, which corresponds to a single channel conductance (γ) of 71.7 pS (Fig. 8*A*). By adding 10 μM Gd^{3+} or 30 μM 2-APB in the patch pipette, we observed, respectively, a 18.4 and 20.3% decrease in the single channel conductance (Gd^{3+}: 3.511±0.014 pA, γ=58.5 pS, Fig. 8*B*; 2-APB: 3.430±0.021 pA, γ=57.2 pS, Fig. 8*C*). There were also slight effects on dwell times [control, 0.635±0.020 ms; Gd^{3+}: 0.578±0.019 ms (9% inhibition); 2APB: 0.547±0.0175 ms (14% inhibition)].

Role of the cytoskeleton

The findings to this point indicate that SERCA pumps modulate inhibition of TRPC7 by Ca^{2+} entering through the channels by providing a Ca^{2+} buffer in the immediate vicinity of the sites of entry. The SERCA pumps are likely to be located very close to the channels, because this dependence on SERCA activity is seen with intracellular solutions containing 10 mM (7 mM free) BAPTA. This implies that SERCA pumps and TRPC7 channels may be maintained in close association through cellular structures, perhaps involving the cytoskeleton. To test this idea, we treated TRPC7-expressing cells with the actin depolymerizing agent, cytochalasin B. As shown in Fig. 9*A*, cytochalasin B inhibited the activation of TRPC7 channels by OAG (I_{TRPC7} max.: −20.8±4.3 and 71.1±10.3 pA/pF for the control, *n*=6; −7.5±0.1 and 28.6±1.5 pA/pF for the cytochalasin B, respectively, at −100 and +100 mV, *n*=4), as expected if the cytoskeleton is responsible for maintaining close association between TRPC7 and SERCA pumps. However, cytochalasin B had no effect in the absence of extracellular Ca^{2+} (Fig. 9*B*; I_{TRPC7} max.: −64.4±16.7 and 89.8±16.1 pA/pF for the control, *n*=4; −85.2±16.7 and 116.3±21.9 pA/pF for the cytochalasin B, respectively at −100 and +100 mV, *n*=4), as expected since in this condition close association of SERCA pumps does not modulate channel activity. This latter observation rules out nonspecific effects of cytochalasin B, for example, direct inhibitory effects on TRPC7 channels. Histochemical examination of TRPC7-expressing cells showed the expected loss of actin filament integrity and dramatic change in cell shape after treatment with cytochalasin B, while actin filament structure was unaffected by OAG (Fig. 9*D*).

To further assess the specificity of the effects of cytochalasin B, we also examined the effects of jasplakinolide, a drug known to act by stabilizing and promoting actin filament formation (32). As shown in Fig. 9*C*, this drug had no effect on the ability of OAG to activate TRPC7 current (control: I_{TRPC7} max.: −14.5±1.9 and 59.9±7.9 pA/pF, respectively, at −100 and +100 mV; jasplakinolide: I_{TRPC7} max.: −15.6±4.8 and 54.1±18.1 pA/pF, respectively, at −100 and +100 mV; *n*=5 each).

Involvement of calmodulin

Taken together, our results suggest that inhibition of SERCA pumps leads to an inhibition of I_{TRPC7} due to a local accumulation of Ca^{2+} entering the cell via the TRPC7 channels. However, this inhibition could result either from a direct interaction between the Ca^{2+} and the channels or from interaction with a Ca^{2+}-sensitive protein mediating this effect. Shi et al. (28) have recently proposed that calmodulin is involved in the Ca^{2+} sensitivity of mouse TRPC7, so we examined the effect of a calmodulin inhibitor, calmidazolium, in our model. Figure 10*A* shows I_{TRPC7} development in control cells or cells pretreated for 5 min with 3 μM calmidazolium in the presence or absence of thapsigargin. In all cases, the OAG-induced currents exhibited similar amplitudes as summarized in Fig. 10*B* (−21±5.4 and 79±11.5 pA/pF for the control, *n*=5; −21.9±5.6 and 69.1±16.1 pA/pF in the presence of calmidazolium, *n*=5; −24.9±5.7 and 67±15.4 pA/pF in the presence of calmidazolium and thapsigargin, respectively, at −100 and +100 mV, *n*=5).

DISCUSSION

In this study, we have shown that *1*) OAG-induced I_{TRPC7} is almost completely inhibited by the SERCA pump inhibitors, thapsigargin, and CPA; *2*) this inhibition results from an increase in the intracellular Ca^{2+} concentration due to Ca^{2+} entering the cell through the TRPC7 channels themselves; *3*) 2-APB and Gd^{3+} at concentrations decreasing the single-channel conductance of TRPC7 restore the OAG-induced I_{TRPC7}; *4*) disruption of the actin cytoskeleton similarly causes a Ca^{2+}-dependent inhibition of I_{TRPC7}; and *5*) calmidazolium, an inhibitor of calmodulin, completely prevents the effect of thapsigargin on I_{TRPC7}. We note that regulation of Ca^{2+} channels by Ca^{2+} entering through the channels is a well known phenomenon, demonstrated for example for store-operated TRPC1 channels (33, 34). However, almost complete dependence on SERCA, even in the face of mM buffering by BAPTA, as shown in this study for TRPC7 is without precedence; if this were the case for store-operated channels, thapsigargin would not produce sustained Ca^{2+} rises, or even detectable activation of I_{crac}. Likewise, no previous study has demonstrated that simple reduction of single channel conductance can rescue channels from inhibition by entering Ca^{2+}.

SERCA inhibitors are known to induce passive depletion of ER Ca^{2+} stores via leak channels, which results in subsequent capacitative Ca^{2+} entry. Although both phenomena induce an elevation of $[Ca^{2+}]_i$, our results demonstrate that neither of these processes is responsible for the thapsigargin-induced inhibition of TRPC7 activity. We found that store depletion alone and the accompanying transient elevation in $[Ca^{2+}]_i$, have no significant effect on I_{TRPC7} when there is no Ca^{2+} in the bath. Likewise, inhibition of capacitative Ca^{2+} entry by 1 μM Gd^{3+} did not restore I_{TRPC7} in cells exposed to thapsigargin. Discharge of intracellular stores by inclusion of IP_3 in the patch pipette did not inhibit TRPC7 [also note previous studies showing robust activation of TRPC7 by phospholipase C activation (10, 22)] or TRPC3 (20), indicating that it is SERCA activity and not store content that regulates the channels. Although a general increase in cytoplasmic Ca^{2+} can inhibit TRPC7 activity (Fig. 3*A* and ref 28), this does not seem to be the case for the inhibitory action of thapsigargin. Results shown in Fig. 1 demonstrate that in the presence of thapsigargin, no global increase in Ca^{2+} occurs in response to OAG. Rather, our results indicate that regulation of TRPC7 channels in intact cells involves Ca^{2+} entering specifically through TRPC7 channels and apparently acting at a site very close to the mouth of the channel. Furthermore, our results suggest the presence of a spatially organized structure including TRPC7 channels and closely associated SERCA pumps, and depending on an organized actin cytoskeleton. In this model, Ca^{2+} entering the cell through TRPC7 channels is sequestered in the ER via SERCA pumps, and this sequestration occurs at a rate sufficient to buffer Ca^{2+} near sites where it could act to inhibit TRPC7 channels. When these pumps are inhibited, an increased local elevation of the Ca^{2+} concentration leads to inhibition of the TRPC7 channels. This hypothesis is supported by two observations. First, 7 mM of free BAPTA in the intracellular solution are unable to prevent inhibition of I_{TRPC7} when the SERCA pumps are blocked, indicating that SERCA pumps provide a highly efficient buffering system close to the channels. Second, in the presence of 2-APB or Gd^{3+} at concentrations that inhibit the single-channel conductance of TRPC7 by ~20%, we observed restoration of I_{TRPC7} in cells exposed to thapsigargin: in this case, the reduction of Ca^{2+} entry resulting from a decrease in the TRPC7 single channel conductance is sufficient to keep the intracellular Ca^{2+} concentration below a critical threshold that would otherwise lead to channel inhibition. According to our whole cell experiments, this threshold could lie between 100 and 500 nM Ca^{2+}, values close to those given

by Shi et al. (28). Inhibition of TRPC3 by Ca^{2+} entering through the channels has been described by Zhang et al. (35). In the current study, we demonstrate that in intact cells, this modulation by Ca^{2+} is substantially tempered by closely associated SERCA pumps. Interestingly, thapsigargin did not inhibit the basal, constitutive activity of TRPC7 channels, indicating that it is the signaling mechanism by which OAG activates, rather than fundamental properties of the channels that is affected. This is consistent with our previous conclusion that OAG activation of TRPC channels is unlikely to result from a direct action on the channel molecule (36).

Our data suggest that the inhibition of TRPC7 activity by Ca^{2+} results from an indirect regulation involving calmodulin. Modulation of TRP channels by calmodulin has been described previously for TRPC3 (35), TRPC6 (28, 37), and TRPC7 channels (28). In the case of TRPC3, calmodulin was shown to inhibit the TRP channels when binding to a conserved CaM/IP_3R binding site (CIRB; ref 38) in a Ca^{2+}-dependent manner. Shi et al. (28) proposed that calmodulin constitutively binds to the TRPC7 channel and regulates it negatively. This hypothesis was supported by their observation that the application of calmidazolium increased TRPC7 activity. However, in our hands, calmidazolium had no effect on either constitutive or OAG-induced I_{TRPC7}, yet the inhibitory effect of thapsigargin was prevented. This would indicate that there is minimal calmodulin-mediated inhibitory effect of Ca^{2+} entering through the channels, due to efficient buffering by the associated SERCA pumps. Consistent with this interpretation is the finding that I_{TRPC7} is not augmented by buffering Ca^{2+} to very low levels in the intracellular solution (see Fig. 3*A*). In this condition, i.e., at a very low $[Ca^{2+}]_i$, calmodulin should not be bound to the channel (35). Note, however, that TRPC7 currents were substantially augmented by lowering extracellular Ca^{2+} by addition of EGTA to a Ca^{2+}-deficient solution (Fig. 4*B*). Since neither lowering intracellular Ca^{2+} nor treatment with calmidazolium produced a similar effect, this likely reflects a function of extracellular Ca^{2+}, perhaps an ability of Ca^{2+} to partially block the channels by binding to a high affinity site within or near the channel pore. The differential regulation by calmodulin described by Shi et al. (28) for the mouse TRPC7 channel and that observed in this study for the human form of the channel could reflect properties of channels from different species. However, further studies are needed to assess whether or not the human and mouse forms of the TRPC7 exhibit different functions or biophysical properties.

TRPC7 has been described previously as a store-operated (39) or as a receptor-operated channel (10, 28). We have recently reported that these apparently conflicting observations could be explained by a variation in the mode of expression of the channel, i.e., TRPC7 can only function as a PLC-activated channel when transiently expressed in HEK-293 cells, while it can be activated by either Ca^{2+} store depletion or PLC when stably expressed in the same cells (22). The results in the current study confirm this bimodal function of TRPC7 when stably expressed in the HEK-293 cells. As illustrated by Fig. 1, when the endogenous capacitative Ca^{2+} entry is completely inhibited by 1 μM Gd^{3+}, TRPC7-HEK cells exposed to thapsigargin exhibit a sustained elevation in $[Ca^{2+}]_i$ that is absent in wild-type cells (compare black lines in Fig. 1*A* and *B*). However, we never observed any significant increase in current in response to either thapsigargin or CPA in either wild-type or TRPC7-transfected cells. Other studies have shown that the SOC current in the HEK-293, when detected, was small (40) and was not detectable in all cells. There is therefore a possibility that under our experimental conditions, even an increased SOC current may remain below our level of detection. This conclusion underscores the likely distinct nature of the two types of TRPC7 channels. While the magnitude of the $[Ca^{2+}]_i$ signals from the two pathways are similar, the whole cell currents are very different. This

suggests that the relative Ca^{2+} permeability of the store-operated TRPC7 channels may be greater than the receptor- or DAG-activated ones. Furthermore, the store-operated TRPC7 channel is activated by depletion of ER Ca^{2+} stores, while this same condition inhibits the receptor-operated TRPC7 channel probably via its interaction with the calmodulin. As TRP channels are known to be organized in tetramers, this might result from a differential association of TRPC7 with other TRPs or regulatory subunits leading to the formation of channels with different properties.

In summary, the findings from the present study reveal a novel mechanism of regulation for TRPC channels. In their receptor activated mode, the activity of TRPC7 channels depends on closely located SERCA pumps. When these pumps are inhibited, local accumulation of Ca^{2+} leads to a calmodulin-mediated decrease in channel activity. Previous work has demonstrated negative regulation of endogenous non-store-operated channels by thapsigargin (23), and this inhibition was prevented by 30 μM 2APB, but not by 1 μM Gd^{3+}; however, the higher, TRPC-inhibiting 10 μM Gd^{3+} was not tested. Thus, it is possible that this effect of thapsigargin occurs by this same mechanism. In addition, a new function for SERCA pumps has been revealed – the regulation of surface membrane Ca^{2+} permeable channels. Mutations in a gene encoding an isoform of a SERCA pump (ATP2A2) result in a syndrome known as Darier's disease (41). The symptoms include dyskeratosis of the skin, but patients also suffer a number of neurological abnormalities, including mild mental retardation, epilepsy, schizophrenia, and bipolar disease (41). As TRPC channels are known to be highly enriched in the brain, it is conceivable that abnormalities in SERCA function could influence neuronal ion channel signaling leading to neurological deficiencies.

NOTE

As shown in Fig. 1, TRPC7 cells exhibit an apparent store-operated Ca^{2+} entry in the presence of thapsigargin. As previously shown (22), this current differs from the endogenous one in being relatively insensitive to inhibition by Gd^{3+}. Unfortunately, we were not able to detect a significant inward current associated with this Ca^{2+} entry under these recording conditions. Thus, the store-operated Ca^{2+} current is very small and likely divalent selective and does not contribute significantly to the current measurements in this study. Thus, the current does not contribute to the much larger non-store-operated current which is the focus of the present study. This can be seen from the data in Fig. 2. We have been able to observe small store-operated cation currents in TRPC7-expressing HEK cells under divalent-free conditions (data not shown, and work in progress). Note that in our hands, and as seen by others, the endogenous store-operated current in HEK293 cells is also very difficult to detect.

ACKNOWLEDGMENTS

The TRPC7 plasmid was jointly supplied by Christine Murphy and Adrian Wolstenholm of University of Bath, and John Westwick of Novartis, Horsham, UK. Drs. Christian Erxleben and Jerel Yakel read the manuscript and provided helpful comments. This work was supported by the Intramural Program of NIEHS and NIH.

REFERENCES

1. Montell, C., and Rubin, G. M. (1989) Molecular characterization of the *Drosophila trp* locus: A putative integral membrane protein required for phototransduction. *Neuron* **2,** 1313–1323

2. Zhu, X., Chu, P. B., Peyton, M., and Birnbaumer, L. (1995) Molecular cloning of a widely expressed human homologue for the *Drosophila trp* gene. *FEBS Lett.* **373,** 193–198

3. Wes, P. D., Chevesich, J., Jeromin, A., Rosenberg, C., Stetten, G., and Montell, C. (1995) TRPC1, a human homolog of a *Drosophila* store-operated channel. *Proc. Natl. Acad. Sci. USA* **92,** 9652–9656

4. Zhu, X., Jiang, M., Peyton, M., Boulay, G., Hurst, R., Stefani, E., and Birnbaumer, L. (1996) *trp*, a novel mammalian gene family essential for agonist-activated capacitative Ca^{2+} entry. *Cell* **85,** 661–671

5. Philipp, S., Cavalié, A., Freichel, M., Wissenbach, U., Zimmer, S., Trost, C., Marguart, A., Murakami, M., and Flockerzi, V. (1996) A mammalian capacitative calcium entry channel homologous to *Drosophila* TRP and TRPL. *EMBO J.* **15,** 6166–6171

6. Boulay, G., Zhu, X., Peyton, M., Jiang, M., Hurst, R., Stefani, E., and Birnbaumer, L. (1997) Cloning and expression of a novel mammalian homolog of *Drosophila Transient Receptor Potential* (Trp) involved in calcium entry secondary to activation of receptors coupled by the G_q class of G protein. *J. Biol. Chem.* **272,** 29672–29680

7. Okada, T., Shimizu, S., Wakamori, M., Maeda, A., Kurosaki, T., Takada, N., Imoto, K., and Mori, Y. (1998) Molecular cloning and functional characterization of a novel receptor-activated TRP Ca^{2+} channel from mouse brain. *J. Biol. Chem.* **273,** 10279–10287

8. Philipp, S., Hambrecht, J., Braslavski, L., Schroth, G., Freichel, M., Murakami, M., Cavalié, A., and Flockerzi, V. (1998) A novel capacitative calcium entry channel expressed in excitable cells. *EMBO J.* **17,** 4274–4282

9. Vannier, B., Peyton, M., Boulay, G., Brown, D., Qin, N., Jiang, M., Zhu, X., and Birnbaumer, L. (1999) Mouse trp2, the homologue of the human trpc2 pseudogene, encodes mTrp2, a store depletion-activated capacitative Ca^{2+} channel. *Proc. Natl. Acad. Sci. USA* **96,** 2060–2064

10. Okada, T., Inoue, R., Yamazaki, K., Maeda, A., Kurosaki, T., Yamakuni, T., Tanaka, I., Shimizu, S., Ikenaka, K., Imoto, K., et al. (1999) Molecular and functional characterization of a novel mouse transient receptor potential protein homologue TRP7. Ca^{2+}-permeable cation channel that is constitutively activated and enhanced by stimulation of G protein-coupled receptor. *J. Biol. Chem.* **274,** 27359–27370

11. Vazquez, G., Wedel, B. J., Aziz, O., Trebak, M., and Putney, J. W., Jr. (2004) The mammalian TRPC cation channels. *Biochim. Biophys. Acta* **1742,** 21–36

12. Liu, X., Wang, W., Singh, B. B., Lockwich, T., Jadlowiec, J., O'Connell, B., Wellner, R., Zhu, M. X., and Ambudkar, I. S. (2000) Trp1, a candidate protein for the store-operated Ca^{2+} influx mechanism in salivary gland cells. *J. Biol. Chem.* **275,** 3403–3411

13. Xu, S. Z., and Beech, D. J. (2001) TrpC1 is a membrane-spanning subunit of store-operated Ca(2+) channels in native vascular smooth muscle cells. *Circ. Res.* **88,** 84–87

14. Mori, Y., Wakamori, M., Miyakawa, T., Hermosura, M., Hara, Y., Nishida, M., Hirose, K., Mizushima, A., Kurosaki, M., Mori, E., et al. (2002) Transient receptor potential 1 regulates capacitative Ca^{2+} entry and Ca^{2+} release from endoplasmic reticulum in B lymphocytes. *J. Exp. Med.* **195,** 673–681

15. Lucas, P., Ukhanov, K., Leinders-Zufall, T., and Zufall, F. (2003) A diacylglycerol-gated cation channel in vomeronasal neuron dendrites is impaired in TRPC2 mutant mice: mechanism of pheromone transduction. *Neuron* **40,** 551–561

16. Philipp, S., Trost, C., Warnat, J., Rautmann, J., Himmerkus, N., Schroth, G., Kretz, O., Nastainczyk, W., Cavalié, A., Hoth, M., et al. (2000) Trp4 (CCE1) protein is part of native calcium release-activated Ca^{2+}-like channels in adrenal cells. *J. Biol. Chem.* **275,** 23965–23972

17. Schaefer, M., Plant, T. D., Obukhov, A. G., Hofmann, T., Gudermann, T., and Schultz, G. (2000) Receptor-mediated regulation of the nonselective cation channels TRPC4 and TRPC5. *J. Biol. Chem.* **275,** 17517–17526

18. Plant, T. D., and Schaefer, M. (2003) TRPC4 and TRPC5: receptor-operated Ca2+-permeable nonselective cation channels. *Cell Calcium* **33,** 441–450

19. Hofmann, T., Obukhov, A. G., Schaefer, M., Harteneck, C., Gudermann, T., and Schultz, G. (1999) Direct activation of human TRPC6 and TRPC3 channels by diacylglycerol. *Nature* **397,** 259–262

20. Trebak, M., Bird, G., St, J., McKay, R. R., Birnbaumer, L., and Putney, J. W., Jr. (2003) Signaling mechanism for receptor-activated TRPC3 channels. *J. Biol. Chem.* **278,** 16244–16252

21. Vazquez, G., Lièvremont, J.-P., Bird, G., St, J., and Putney, J. W., Jr. (2001) Human Trp3 forms both inositol trisphosphate receptor-dependent and receptor-independent store-operated cation channels in DT40 avian B-lymphocytes. *Proc. Natl. Acad. Sci. USA* **98,** 11777–11782

22. Lievremont, J. P., Bird, G. S., and Putney, J. W., Jr. (2004) Canonical transient receptor potential TRPC7 can function as both a receptor- and store-operated channel in HEK-293 cells. *Am. J. Physiol. Cell Physiol.* **287,** C1709–C1716

23. Luo, D., Broad, L. M., Bird, G. S., and Putney, J. W., Jr. (2001) Mutual antagonism of calcium entry by capacitative and arachidonic acid-mediated calcium entry pathways. *J. Biol. Chem.* **276,** 20186–20189

24. Mignen, O., Thompson, J. L., and Shuttleworth, T. J. (2001) Reciprocal regulation of capacitative and arachidonate-regulated noncapacitative Ca^{2+} entry pathways. *J. Biol. Chem.* **276,** 35676–35683

25. Moneer, Z., and Taylor, C. W. (2002) Reciprocal regulation of capacitative and non-capacitative Ca^{2+} entry in A7r5 vascular smooth muscle cells: only the latter operates during receptor activation. *Biochem. J.* **362,** 12–21

26. McKay, R. R., Szmeczek-Seay, C. L., Lièvremont, J.-P., Bird, G., St, J., Zitt, C., Jüngling, E., Lückhoff, A., and Putney, J. W., Jr. (2000) Cloning and expression of the human transient receptor potential 4 (TRP4) gene: localization and functional expression of human TRP4 and TRP3. *Biochem. J.* **351,** 735–746

27. Trebak, M., Bird, G., St, J., McKay, R. R., and Putney, J. W., Jr. (2002) Comparison of human TRPC3 channels in receptor-activated and store-operated modes. Differential sensitivity to channel blockers suggests fundamental differences in channel composition. *J. Biol. Chem.* **277,** 21617–21623

28. Shi, J., Mori, E., Mori, Y., Mori, M., Li, J., Ito, Y., and Inoue, R. (2004) Multiple regulation by calcium of murine homologues of transient receptor potential proteins TRPC6 and TRPC7 expressed in HEK293 cells. *J. Physiol.* **561,** 415–432

29. Luo, D., Broad, L. M., Bird, G., St, J., and Putney, J. W., Jr. (2001) Signaling pathways underlying muscarinic receptor-induced $[Ca^{2+}]_i$ oscillations in HEK293 cells. *J. Biol. Chem.* **276,** 5613–5621

30. Ma, H.-T., Patterson, R. L., van Rossum, D. B., Birnbaumer, L., Mikoshiba, K., and Gill, D. L. (2000) Requirement of the inositol trisphosphate receptor for activation of store-operated Ca^{2+} channels. *Science* **287,** 1647–1651

31. Braun, F.-J., Broad, L. M., Armstrong, D. L., and Putney, J. W., Jr. (2001) Stable activation of single CRAC-channels in divalent cation-free solutions. *J. Biol. Chem.* **276,** 1063–1070

32. Patterson, R. L., van Rossum, D. B., and Gill, D. L. (1999) Store-operated Ca^{2+} entry: evidence for a secretion-like coupling model. *Cell* **98,** 487–499

33. Singh, B. B., Liu, X., Tang, J., Zhu, M. X., and Ambudkar, I. S. (2002) Calmodulin regulates Ca^{2+}-dependent feedback inhibition of store-operated Ca^{2+} influx by interaction with a site in the C terminus of TrpC1. *Mol. Cell* **9,** 739–750

34. Liu, X., and Ambudkar, I. S. (2001) Characteristics of a store-operated calcium permeable channel. Sarcoendoplasmic reticulum calcium pump function controls channel gating. *J. Biol. Chem.* **276,** 29891–29898

35. Zhang, Z., Tang, J., Tikunova, S., Johnson, J. D., Chen, Z., Qin, N., Dietrich, A., Stefani, E., Birnbaumer, L., and Zhu, M. X. (2001) Activation of Trp3 by inositol 1,4,5-trisphosphate receptors through displacement of inhibitory calmodulin from a common binding domain. *Proc. Natl. Acad. Sci. USA* **98,** 3168–3173

36. Vazquez, G., Wedel, B. J., Kawasaki, B. T., Bird, G. S., and Putney, J. W., Jr. (2004) Obligatory role of Src kinase in the signaling mechanism for TRPC3 cation channels. *J. Biol. Chem.* **279,** 40521–40528

37. Boulay, G. (2003) Ca^{2+}-calmodulin regulates receptor-operated Ca^{2+} entry activity of TRPC6 in HEK-293 cells. *Cell Calcium* **32,** 201–207

38. Tang, J., Lin, Y., Zhang, Z., Tikunova, S., Birnbaumer, L., and Zhu, M. X. (2001) Identification of common binding sites for calmodulin and inositol 1,4,5-trisphosphate receptors on the carboxy termini of Trp channels. *J. Biol. Chem.* **276,** 21303–21310

39. Riccio, A., Mattei, C., Kelsell, R. E., Medhurst, A. D., Calver, A. R., Randall, A. D., Davis, J. B., Benham, C. D., and Pangalos, M. N. (2002) Cloning and functional expression of human short TRP7, a candidate protein for store-operated Ca^{2+} influx. *J. Biol. Chem.* **277,** 12302–12309

40. Bugaj, V., Alexeenko, V., Zubov, A., Glushankova, L., Nikolaev, A., Wang, Z., Kaznacheyeva, E., Bezprozvanny, I., and Mozhayeva, G. N. (2005) Functional properties of endogenous receptor-and store-operated calcium influx channels in HEK293 cells. *J. Biol. Chem.* **17,** 16790–16797

41. Hovnanian, A. (2004) Darier's disease: from dyskeratosis to endoplasmic reticulum calcium ATPase deficiency. *Biochem. Biophys. Res. Commun.* **322,** 1237–1244

Received July 14, 2005; accepted November 10, 2005.

Fig. 1

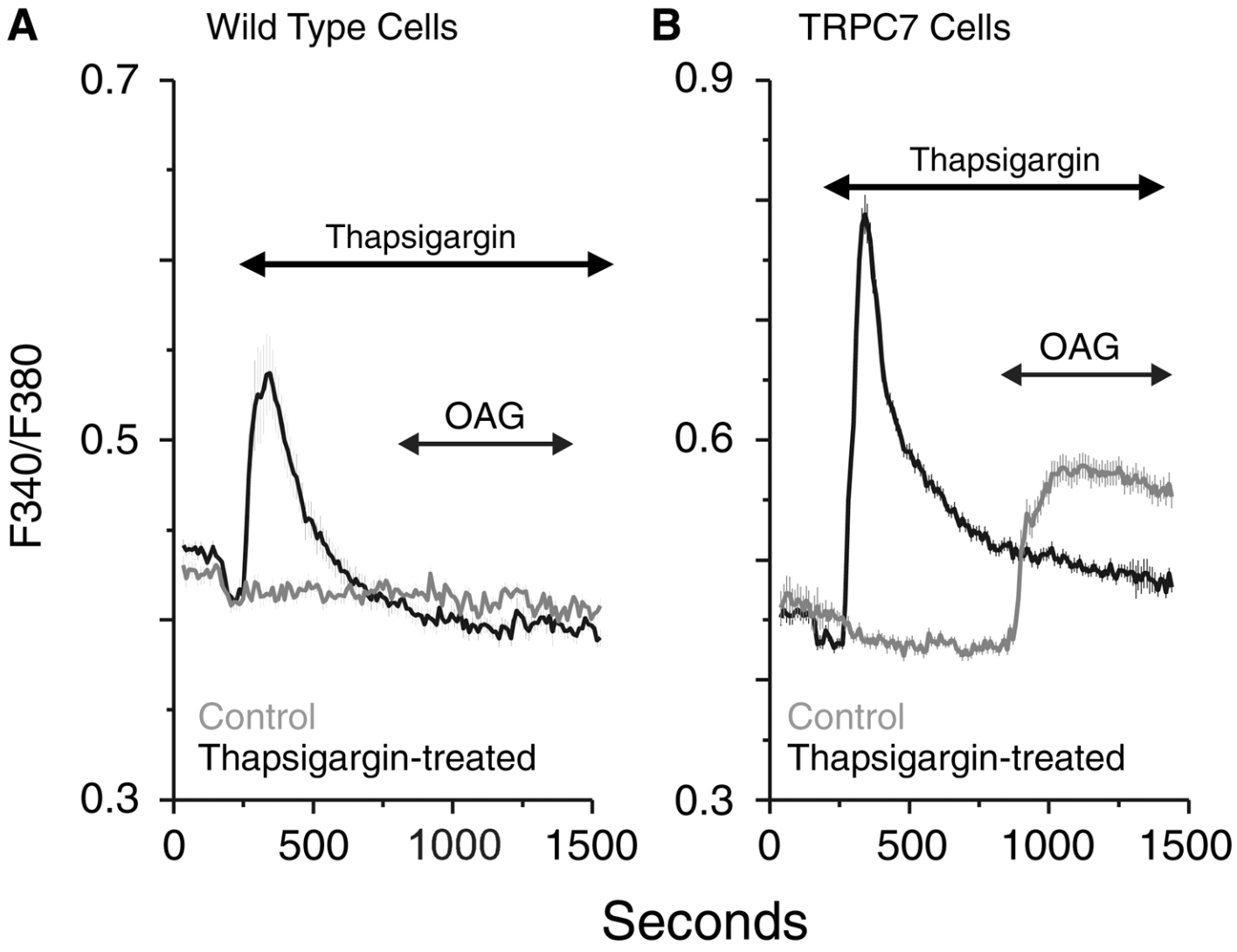

Figure 1. TOAG-induced Ca^{2+} entry in TRPC7-HEK cells is inhibited by thapsigargin. ***A*)** Time course of average fluorescence ratio in wt-HEK cells loaded with fura-5F and treated (wt Tg, black line, *n*=57, 2 independent experiments) or not (wt ctrl, gray line, *n*=40, 2 independent experiments) with 5 µM thapsigargin at the time indicated by the arrow. Cells were then exposed to 30 µM OAG as indicated. ***B*)** Same experimental protocol as in ***A*** for TRPC7-HEK cells treated (TRPC7 Tg, black line, *n*=96, 4 independent experiments) or not (TRPC7 ctrl, gray line, *n*=49, 2 independent experiments) with 5 µM thapsigargin. Experiments described in ***A*** and ***B*** were carried out in the presence of 2 mM Ca^{2+} and 1 µM Gd^{3+} in the bath; results are presented as mean ± SE.

Fig. 2

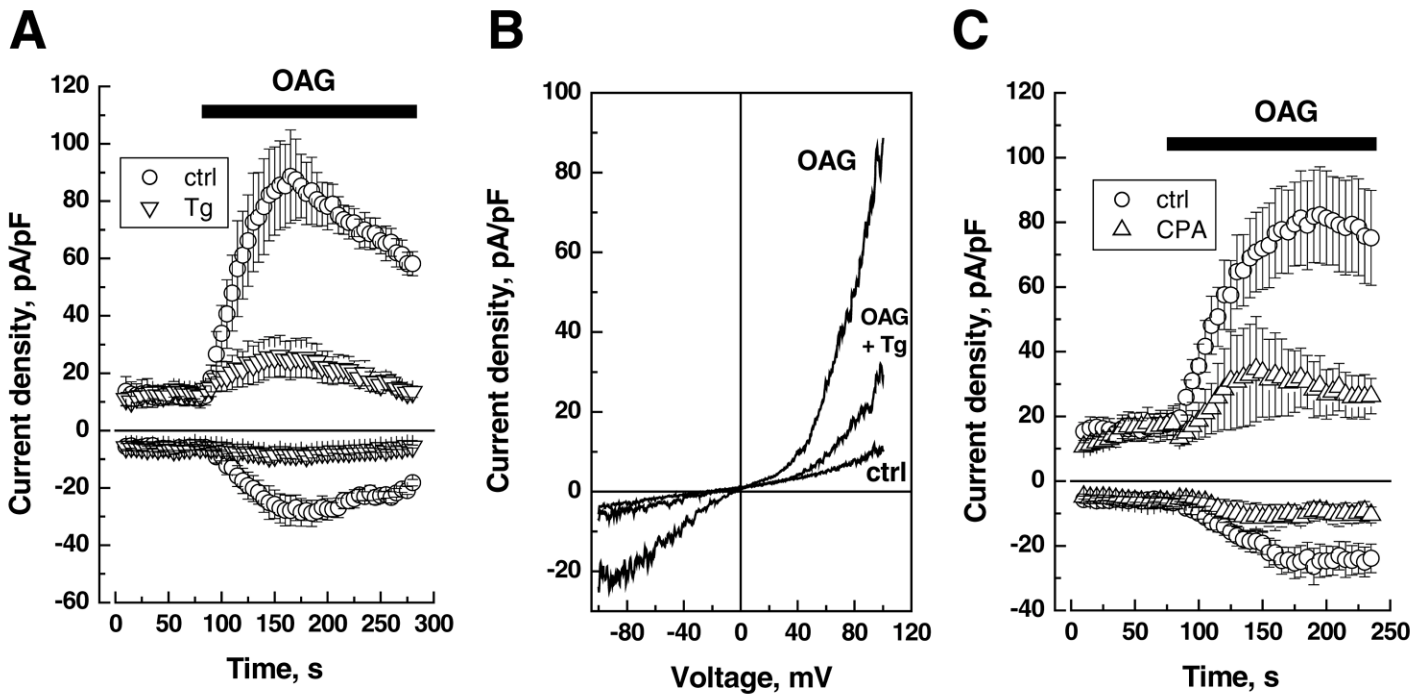

Figure 2. OAG-induced current in TRPC7-HEK cells is inhibited by SERCA inhibitors. ***A*)** Average time courses (mean±SE) of I_{TRPC7} development at −100 and +100 mV in the presence of 30 μM OAG in cells exposed (Tg, down triangle; *n*=5) or not (ctrl, circle; *n*=5) to 5 μM thapsigargin. Application of OAG is indicated by a horizontal bar; thapsigargin was added at time 0. ***B*)** I/V relationship of currents observed in a representative cell before (ctrl) and after (OAG) an application of 30 μM OAG, and in a cell exposed to thapsigargin before (+Tg, gray trace) and after OAG (OAG + Tg). ***C*)** Average time courses (mean±SE) of I_{TRPC7} development in the presence of 30 μM OAG in cells exposed (CPA, up triangle; *n*=5) or not (ctrl, circle; *n*=5) to 20 μM cyclopiazonic acid. Cyclopiazonic acid was added at time 0.

Fig. 3

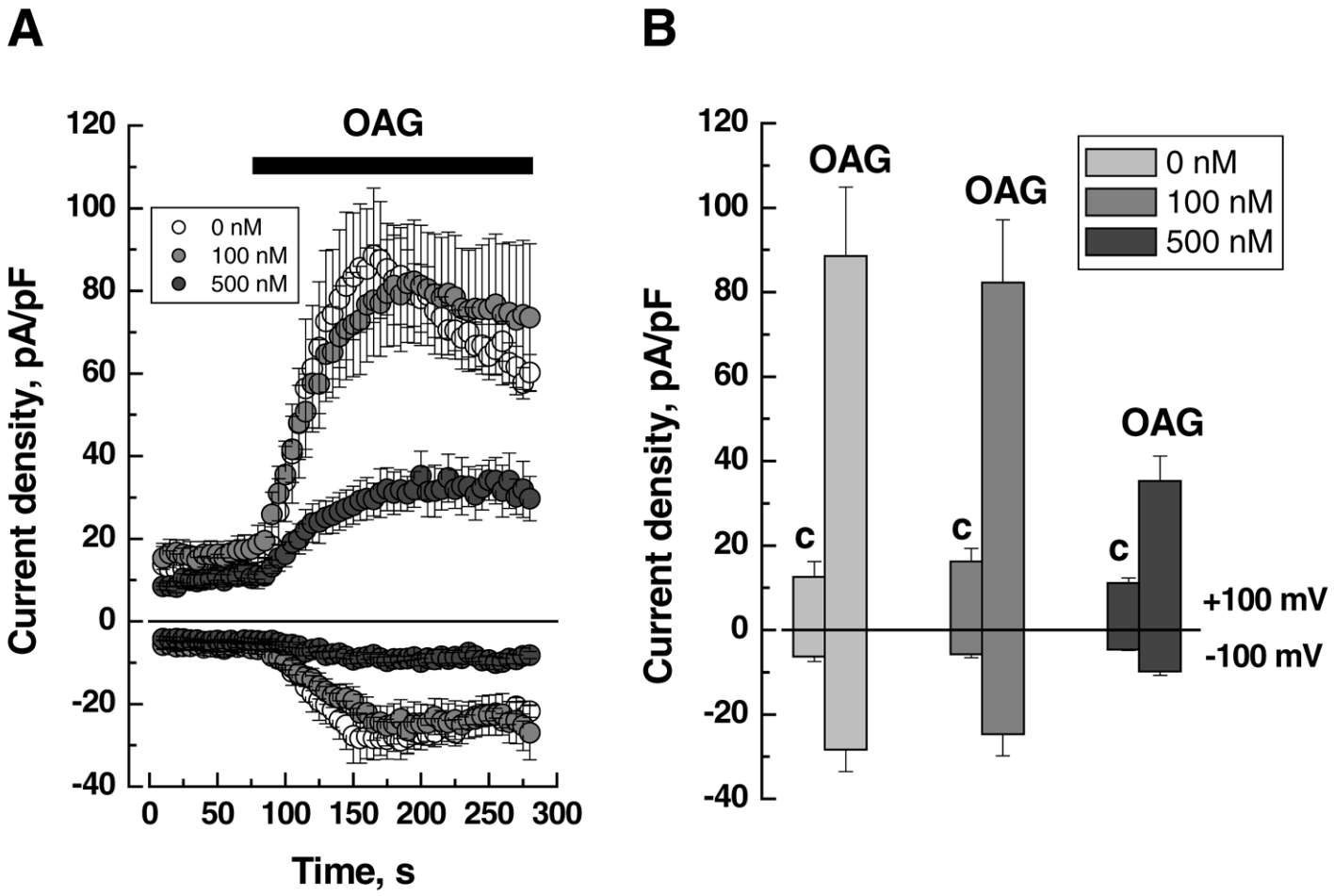

Figure 3. I_{TRPC7} is modulated by intracellular Ca^{2+} concentration. ***A***) Average time courses (mean±SE) of the OAG-induced I_{TRPC7} at −100 and +100 mV in the presence of 0 nM (10 mM BAPTA, open circle; *n*=5), 100 nM (10 mM BAPTA + 2.2 mM $CaCl_2$, gray circle; *n*=7) or 500 nM (10 mM BAPTA + 5.6 mM $CaCl_2$, dark gray circle; *n*=4) free Ca^{2+} in pipette solution. Application of OAG is indicated by a horizontal bar. ***B***) Statistical summary of the effects of intracellular Ca^{2+} concentration on currents observed before (c) and after (OAG) perfusing cells with 30 μM OAG.

Fig. 4

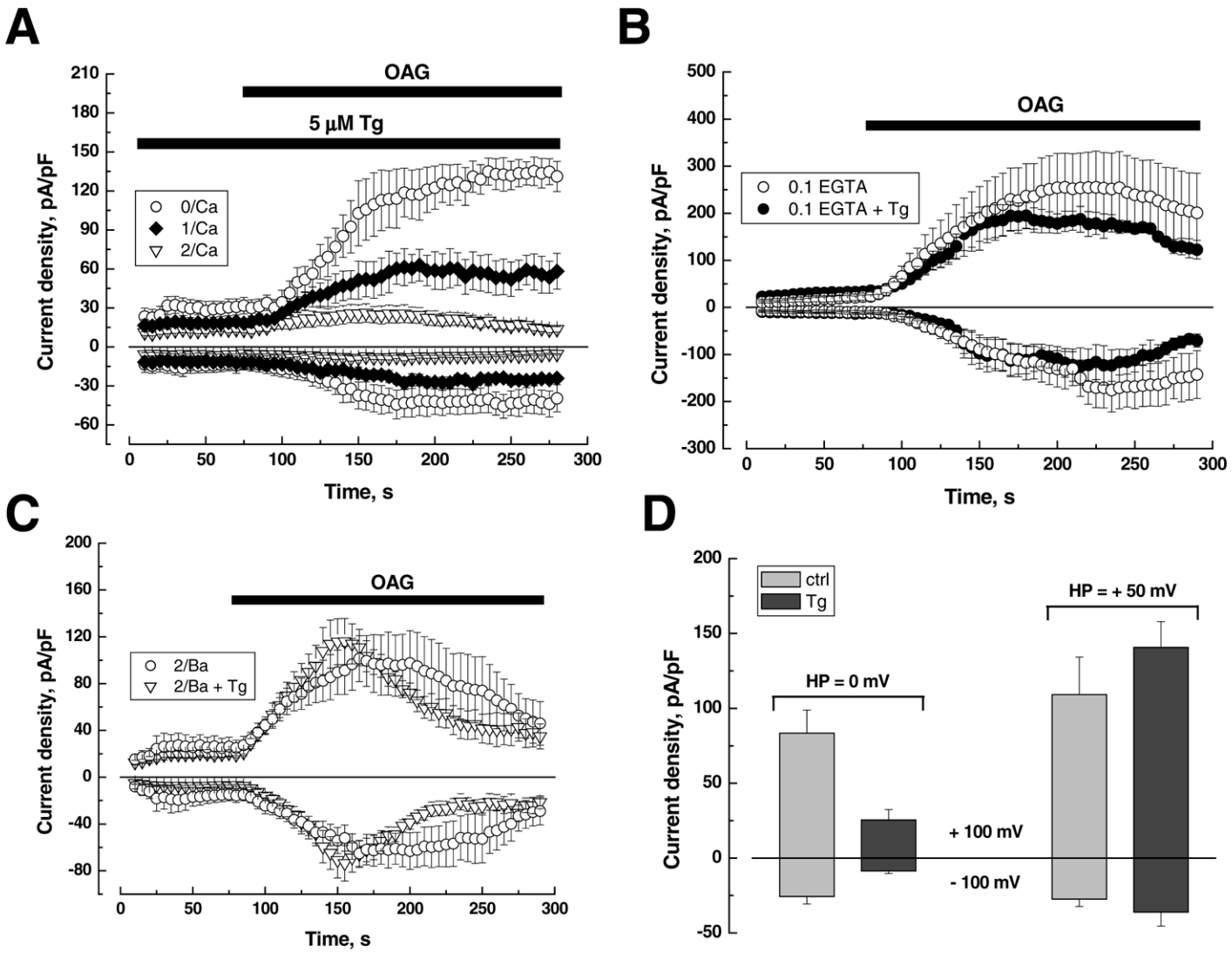

Figure 4. I_{TRPC7} inhibition depends on a Ca^{2+} entry. ***A)*** Average time courses (mean±SE) of I_{TRPC7} development at −100 and +100 mV in cells exposed to 5 µM thapsigargin in the presence of 0 mM (0/Ca, open circle; *n*=5), 1 mM (1/Ca, filled diamond; *n*=5), or 2 mM Ca^{2+} (2/Ca, down triangle, *n*=4) in the bath. Application of OAG and thapsigargin is indicated by horizontal bars. ***B)*** Average time courses (mean±SE.) of the OAG-induced I_{TRPC7} at −100 and +100 mV in cells exposed to a Ca^{2+}-free solution (0.1 mM EGTA) and treated (0.1 EGTA + Tg, filled circle; *n*=4) or not (0.1 EGTA, open circle, n=4) with 5 µM thapsigargin (added at time 0). ***C)*** Average time courses (mean±SE) of the OAG-induced I_{TRPC7} at −100 and +100 mV in cells exposed to a solution where the calcium was replaced by 2 mM Ba^{2+}. Cells were treated (2/Ba + Tg, down triangle; *n*=6) or not (2/Ba, circle; *n*=6) with 5 µM thapsigargin (added at time 0). ***D)*** Statistical summary summarizing the effect of holding the potential at 0 or +50 mV on the OAG-induced I_{TRPC7} recorded at −100 and +100 mV in cells treated (Tg, dark gray columns; *n*=5 and 4 at 0 and +50 mV, respectively) or not (ctrl, light gray columns; *n*=5 at both 0 and +50 mV) with 5 µM thapsigargin.

Fig. 5

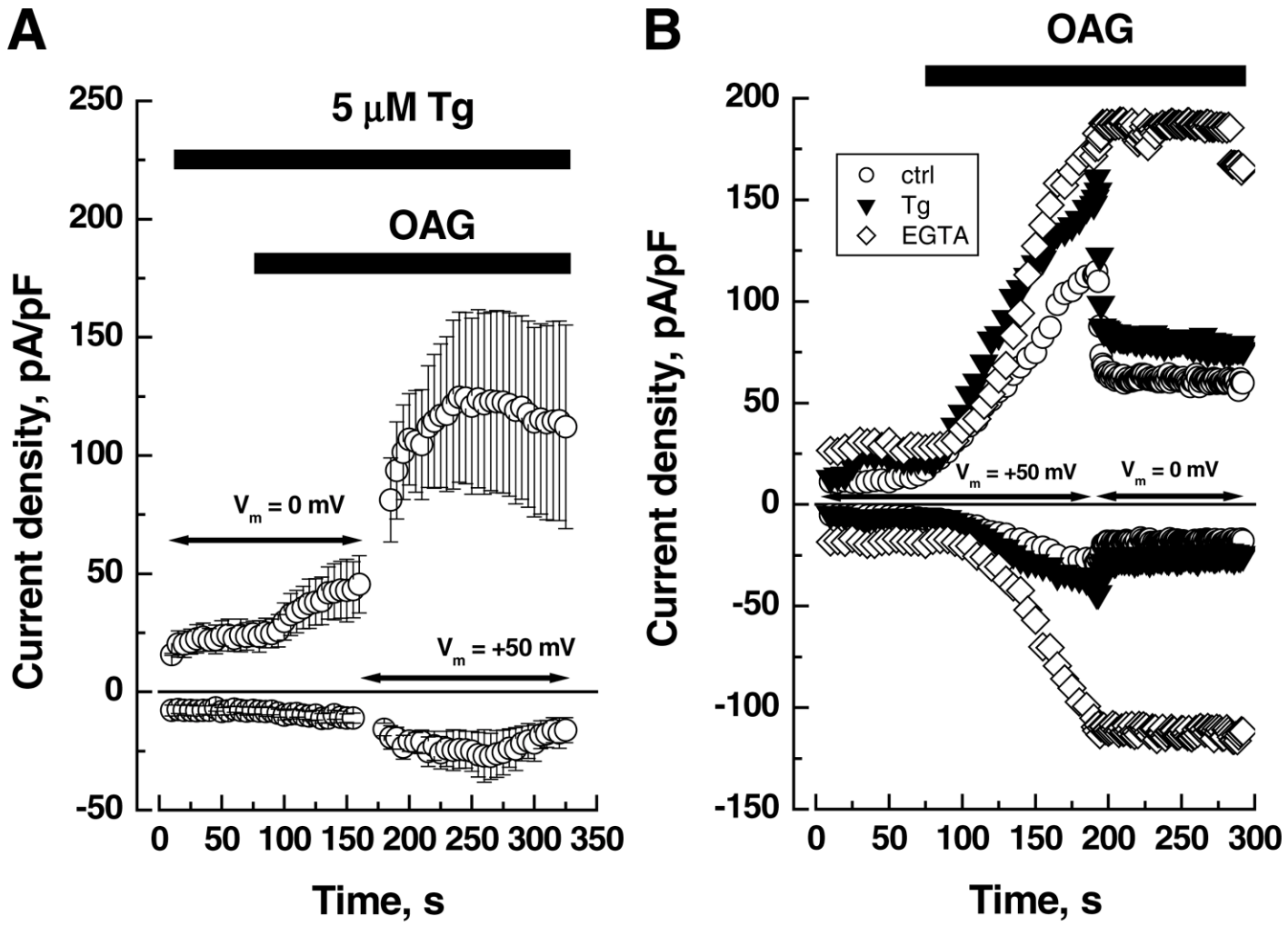

Figure 5. Ca^{2+}-dependent inhibition of TRPC7 current by thapsigargin is reversible by decreasing the driving force for Ca^{2+} entry. ***A***) Average time courses (mean±SE) of OAG-induced I_{TRPC7} at -100 and +100 mV in the presence of 5 μM thapsigargin when sequentially holding the cells at 0 and +50 mV (*n*=5). ***B***) Average time courses (mean±SE) of the OAG-induced I_{TRPC7} at −100 and +100 mV in control cells (ctrl, *n*=5), in cells exposed to 5 μM thapsigargin (Tg, *n*=4), and in the absence of external calcium (EGTA, *n*=5) when sequentially holding the cells at +50 and 0 mV.

Fig. 6

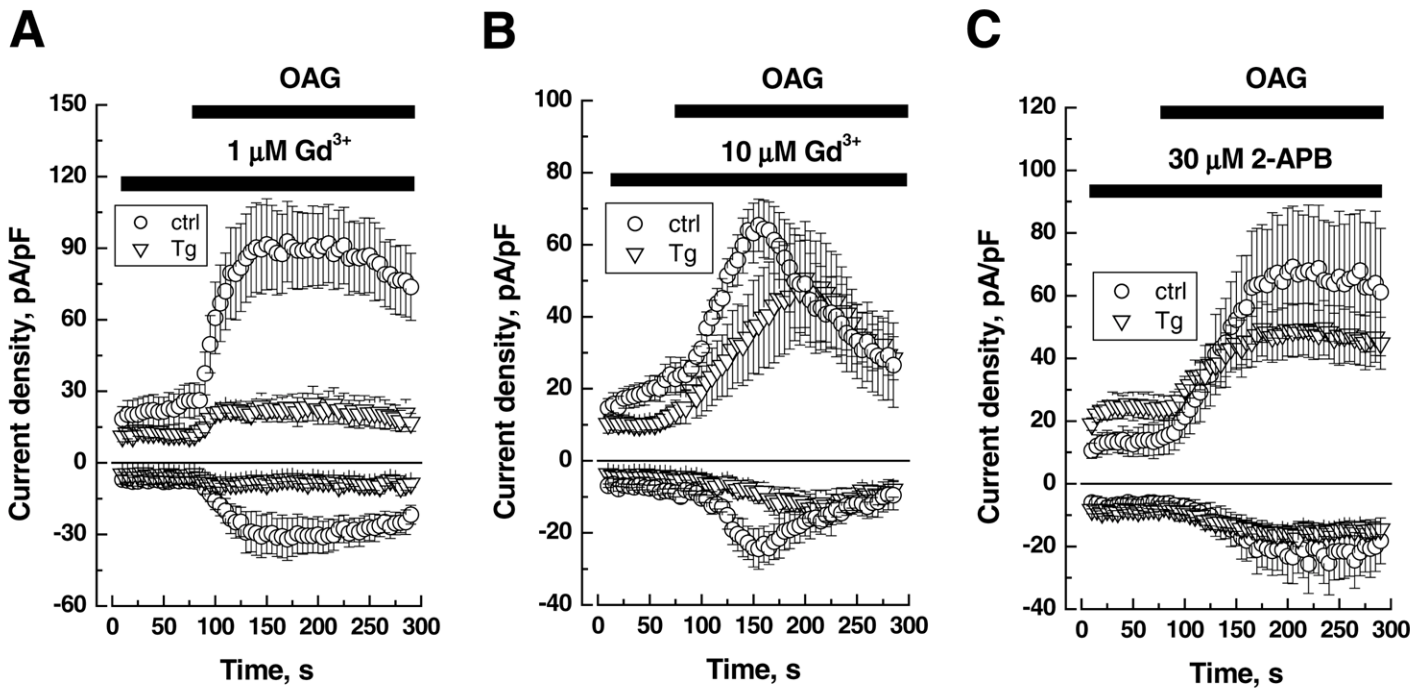

Figure 6. Thapsigargin effect on I_{TRPC7} is prevented by TRPC7 inhibitors. *A)* Average time courses (mean±SEM) of the OAG-induced I_{TRPC7} at −100 and +100 mV in the presence of 1 μM Gd^{3+} in cells treated (Tg, down triangle; *n*=4) or not (ctrl, circle; *n*=5) with 5 μM thapsigargin (added at time 0). ***B*** and ***C*)** Same experimental protocol as in ***A***, but in the presence of 10 μM Gd^{3+} (*B*; ctrl: *n*=4; Tg: *n*=5) or of 30 μM 2-APB (*C*; ctrl: *n*=4; Tg: *n*=5).

Fig. 7

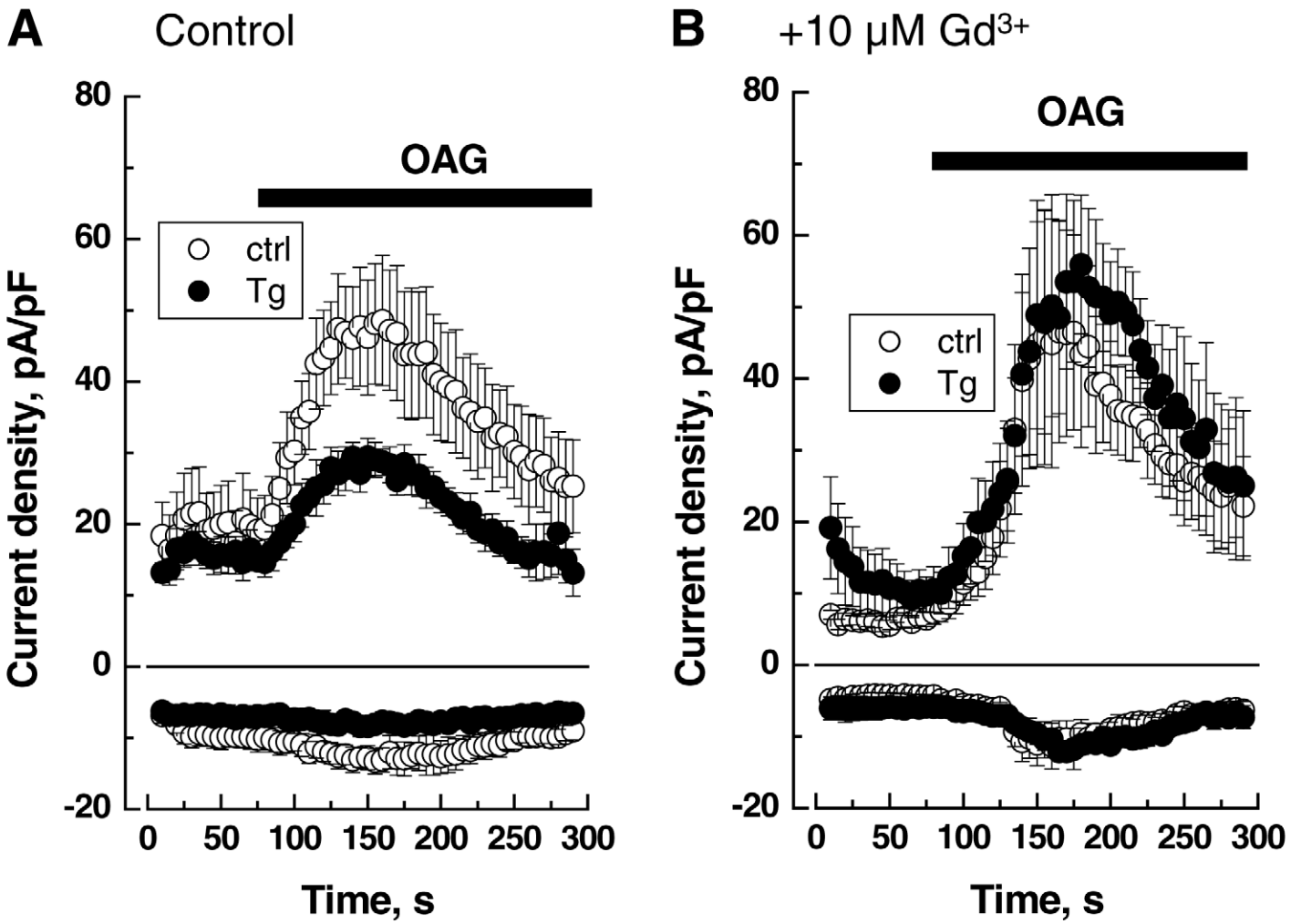

Figure 7. TRPC3 is inhibited by thapsigargin. Average time courses (mean±SE) of OAG-induced I_{TRPC3} at −100 and +100 mV in cells treated (Tg, filled circle) or not (ctrl, open circle) with 5 µM thapsigargin (added at time 0). *A)* Control (control, *n*=6; thapsigargin, *n*=6); *B)* In the presence of 10 µM Gd^{3+} (control, *n*=4; thapsigargin, *n*=4).

Fig. 8

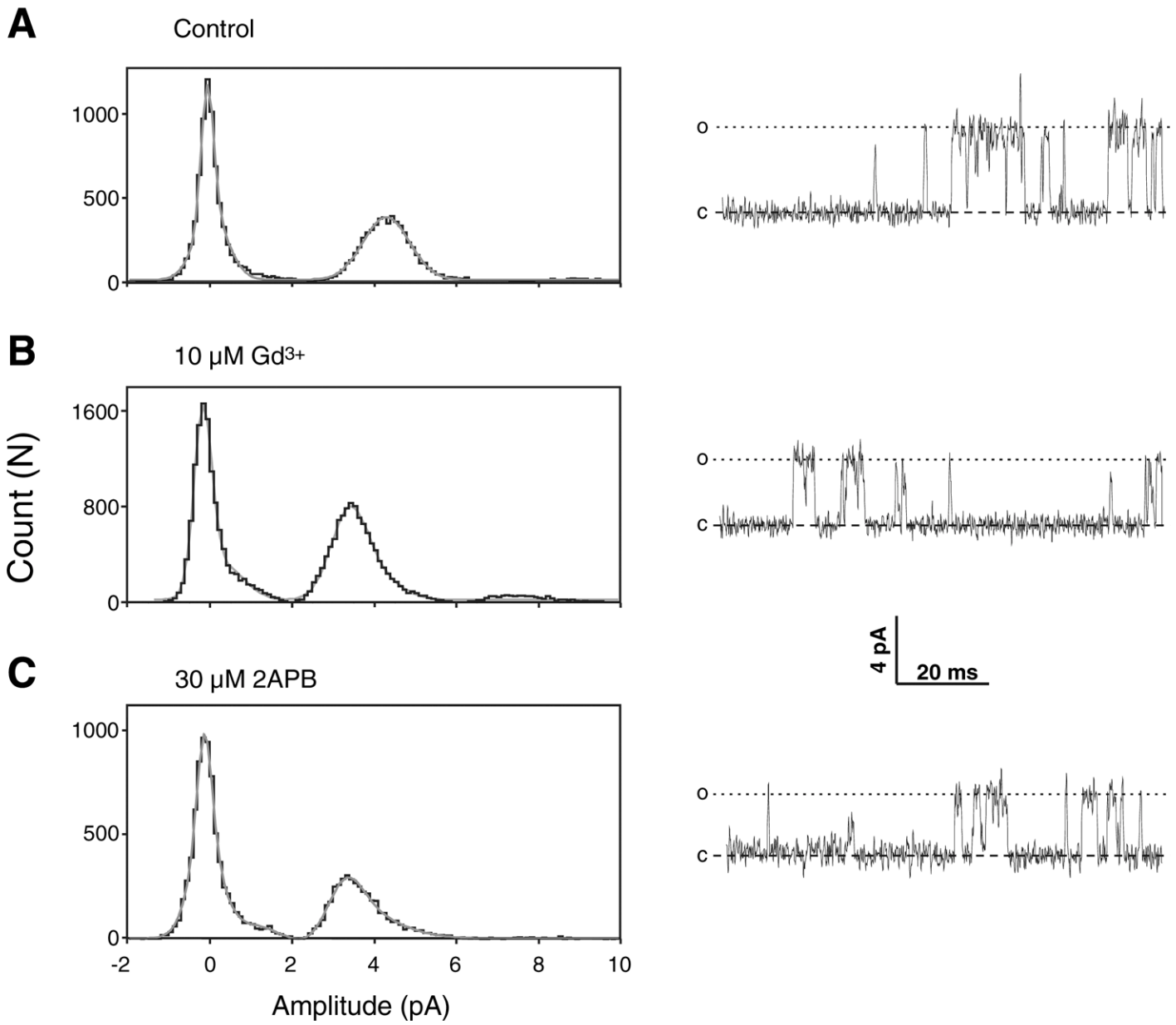

Figure 8. 2-APB and Gd^{3+} decrease the single channel conductance of TRPC7. All-points histograms summarizing single channel amplitudes at +60 mV in the cell-attached configuration. The gray curves represent fits of the data to Gaussian distributions. Representative current traces are shown on the right. ***A*)** control (30 µM OAG in the pipette, *n*=5); ***B*)** Gd^{3+} (30 µM OAG+10 µM Gd^{3+} in the pipette, *n*=5); ***C*)** 2-APB (30 µM OAG+30 µM 2-APB in the pipette, *n*=6).

Fig. 9

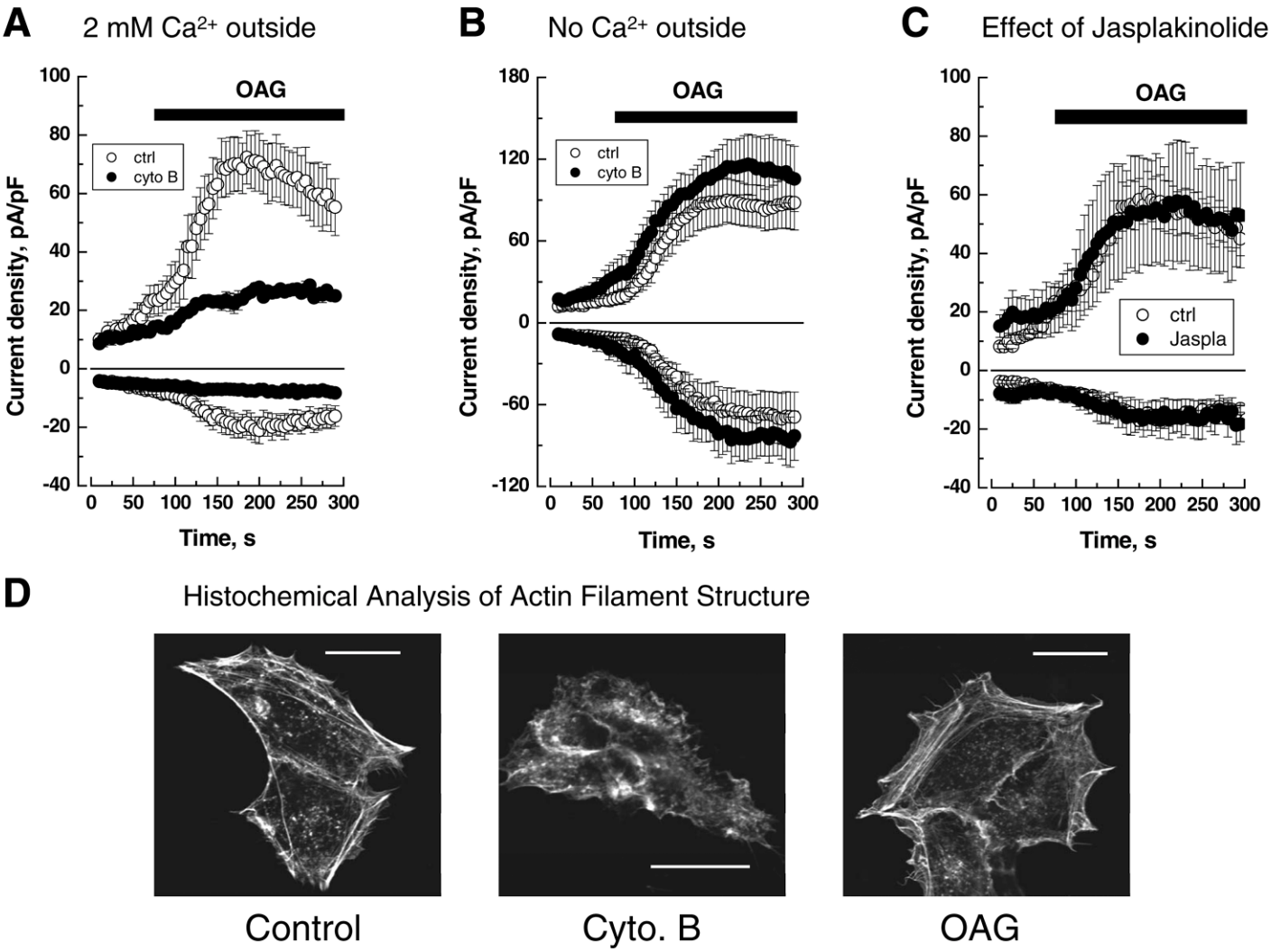

Figure 9. Inhibition of OAG-activated I_{TRPC7} by cytochalasin B. TRPC7-expressing cells were treated (filled circles) or not (open circles, control) with 1 μM cytochalasin B added 1 h before break-in. ***A***) 2 mM Ca^{2+} present in the extracellular solution, control, *n*=6, cytochalasin B, *n*=4. ***B***) No added Ca^{2+} present in the bathing solution, control, *n*=6, cytochalasin B, *n*=5. Data are presented as mean±SE. ***C***) Cells were treated (filled circles) or not (open circles, control) with 2 μM jasplakinolide at 37°C for 30 min, *n*=5 for both groups. ***D***) Actin filament network is disrupted by cytochalasin B treatment but not by OAG.

Fig. 10

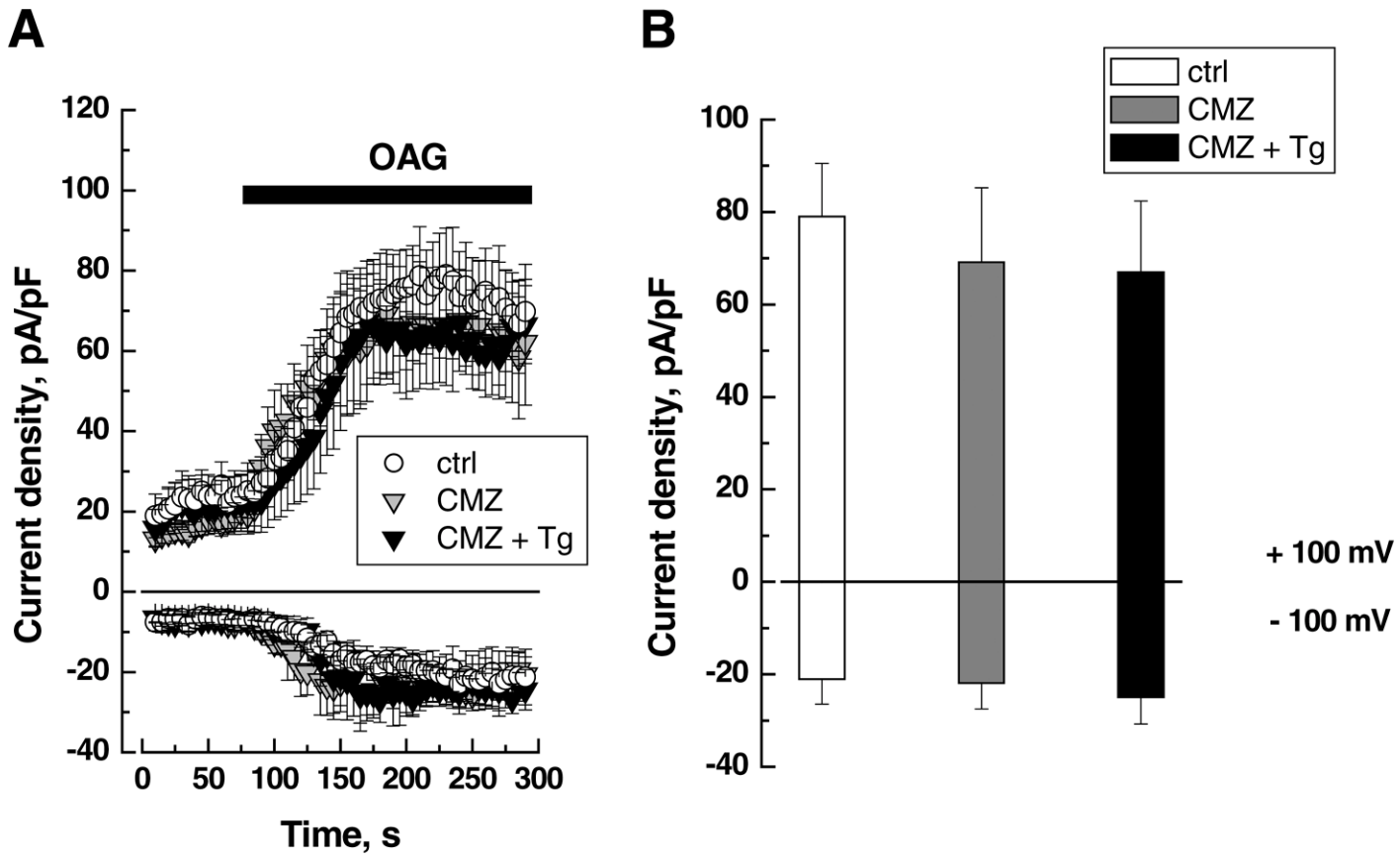

Figure 10. Thapsigargin-induced inhibition of I_{TRPC7} is mediated by calmodulin. *A)* Average time courses (mean±SE) of tOAG-induced I_{TRPC7} at −100 and +100 mV in control conditions (ctrl, circle; *n*=5) and after a 5 min pretreatment with 3 μM calmidazolium alone (CMZ, gray down triangle; *n*=5) or followed by application of 5 μM thapsigargin at time 0 (CMZ + Tg, filled down triangle; *n*=5). ***B*)** Statistical summary of average outward and inward currents from experiments in ***A***.

Article 4

Published in final edited form as:
Pflugers Arch. 2009 February ; 457(4): 757–769. doi:10.1007/s00424-008-0550-1.

Complex Functions of Phosphatidylinositol 4,5-bisphosphate in Regulation of TRPC5 Cation Channels

Mohamed Trebak[1,2], **Loic Lemonnier**[1,3], **Wayne I DeHaven**, **Barbara J. Wedel**[4], **Gary S. Bird**, and **James W. Putney Jr.**[5]
Laboratory of Signal Transduction, NIEHS/NIH, Department of Health and Human Services, P.O.Box 12233, Research Triangle Park, NC 27709

Abstract

The canonical transient receptor potential (TRPC) proteins have been recognized as key players in calcium entry pathways activated through phospholipase C-coupled receptors. While it is clearly demonstrated that members of the TRPC3/6/7 subfamily are activated by diacylglycerol, the mechanism by which phospholipase C activates members of the TRPC1/4/5 subfamily remains a mystery. Here, we provide evidence for both negative and positive modulatory roles for membrane polyphosphoinositides in the regulation of TRPC5 channels. Depletion of polyphosphatidylinositol-4-phosphate and phosphatidylinositol-4,5-bisphosphate (PIP_2) through inhibition of phosphatidylinositol 4-kinase activates calcium entry and membrane currents in TRPC5-expressing, but not in TRPC3- or TRPC7-expressing cells. Inclusion of polyphosphatidylinositol-4-phosphate or PIP_2, but not phosphatidylinositol-3,4,5-trisphosphate, in the patch pipette inhibited TRPC5 currents. Paradoxically, depletion of PIP_2 with a directed 5-phosphatase strategy inhibited TRPC5. Furthermore, when the activity of single TRPC5 channels was examined in excised patches, the channels were robustly activated by PIP_2. These findings indicate complex functions for regulation of TRPC5 by PIP_2, and we propose that membrane polyphosphoinositides may have at least two distinct functions in regulating TRPC5 channel activity.

Keywords

ion channels; non-selective cation channels; TRPC5 channels; phosphatidylinositol 4,5-bisphosphate; phospholipase C

Introduction

Calcium signaling in many cell types is initiated by stimulation of membrane receptors coupled to polyphosphoinositide-specific phospholipase C (PLC). The action of PLC on the membrane lipid phosphatidylinositol 4,5-bisphosphate (PIP_2) leads to the formation of two second messengers: inositol 1,4,5-trisphosphate (IP_3) and diacylglycerol (DAG). IP_3 activates IP_3 receptor channels in the endoplasmic reticulum and causes release of intracellular stored Ca^{2+} [1]. The fall in Ca^{2+} content within the lumen of the endoplasmic reticulum then signals the subsequent activation of plasma membrane calcium-permeable channels, a process known

5To whom correspondence should be addressed at: NIEHS, PO Box 12233, Research Triangle Park, NC 27709 USA.Phone: (919) 541-1420, Fax: (919) 541-1898, putney@niehs.nih.gov.
[1]These investigators contributed equally to this work.
[2]Present address: Cardiovascular Sciences; MC-8, Albany Medical College, 47, New Scotland Avenue, Albany, New York 12208. trebakm@mail.amc.edu
[3]Present address: Université de Lille 1, Villeneuve d'Ascq F-59650, France
[4]Present address: BASF Corporation, 26 Davis Drive, Research Triangle Park, NC 27709 USA

as capacitative Ca^{2+} entry (CCE) or store-operated Ca^{2+} entry [2,3,4]. Although CCE seems to be present ubiquitously in receptor-regulated non-excitable cells, a wide variety of Ca^{2+} permeable channels are activated downstream of the PLC pathway by mechanisms not directly related to store depletion. Examples include channels activated by mechanisms involving IP_3, cytosolic Ca^{2+}, DAG, cyclic nucleotides, phosphatidylinositol 3,4,5-trisphosphate (PIP_3), and arachidonic acid (for review see [5,6]). During the last decade, several investigations have implicated the members of the transient receptor potential (TRP) family of channel proteins as candidates for some of these Ca^{2+} entry pathways [6,7,8,9,10,11].

TRP proteins constitute a large superfamily of ion channels that are expressed in many tissues and cell types [12]. TRP channels are activated by a wide variety of external stimuli ranging from temperature and oxidative stress to hormones, growth factors and neurotransmitters [10,7,13]. TRP channels are cation permeable channels and are now fully recognized as key players in the maintenance of ion homeostasis and in cell signaling pathways. The TRP superfamily can be divided into three major families: (i) channels homologous to the vanilloid receptor called TRPV, that are activated by a variety of signals, including vanilloid compounds such as capsaicin, noxious signals, hypotonic cell swelling and heat; TRPV family consists of six Ca^{2+}-permeable channels [14,7,15,16,17]; (ii) the Melastatin-related TRP channel family (TRPM) containing eight members, with diverse functional properties such as mediating Ca^{2+} influx, controlling Mg^{2+} entry, modulating the membrane potential, and sensing cold and menthol in sensory neurons [18,19,20,13]; (iii) the canonical TRP family (TRPC), named for being structurally the closest to the superfamily founder, *Drosophila* TRP, are all activated through PLC-coupled receptors and were therefore proposed to encode components of native PLC-coupled channels, such as store-operated channels and second messenger-operated channels [8,21,11].

The TRPC family contains seven members (TRPC1 through 7). TRPC2 is a pseudogene in humans and is involved in pheromone sensing in other mammals [22]. TRPC3/6/7 represents a subfamily within TRPC family whose members can be activated by diacylglycerol produced by PLC action on PIP_2 [23,24,25,26,27]. However, the mechanism of activation *via* PLC-coupled receptors of members of the TRPC1/4/5 subfamily is still unclear. These channels are believed to play important roles in diverse physiological functions, for example in regulation of vascular tone [28] and in neurite outgrowth [29]. While most investigators agree that PLC is necessary for receptor activation of this group, the general finding is that neither IP_3 nor DAG activates these channels [27,30]. Otsuguro *et al.* [31] suggested that breakdown of PIP_2, in conjunction with inputs from G-proteins and $[Ca^{2+}]_i$, leads to activation of TRPC4. In the current study, we have investigated the role of inositol lipids in regulation and activation of TRPC5. Consistent with the findings of Otsuguro *et al.* for TRPC4, we show that in intact cells, pharmacological depletion of phosphatidylinositol 4-phosphate (PIP) and PIP_2 specifically activates TRPC5 channels while inclusion of these polyphosphoinositides in the patch pipette inhibits TRPC5 currents. However, depletion of PIP_2 by a targeted 5-phosphatase inhibited TRPC5 activity, and in excised patches, PIP_2 activated TRPC5 channels. These data suggest that PIP and/or PIP_2 exert multiple effects on TRPC5.

Material and Methods

Reagents

Methacholine, Wortmannin, LY294002 and Rapamycin were purchased from Calbiochem. D (+)-sn-1,2-di-O-octanoylglyceryl,3-O-phospholinked (DiC8) polyphosphoinositides, PIP, PIP_2 and PIP_3 were purchased from Echelon Biosciences Incorporated.

Cell culture and cell lines

Human embryonic kidney (HEK293) cells were obtained from ATCC and were transfected, using Lipofectamine 2000 reagent (Invitrogen) according to the vendor's instructions, with pcDNA3 vector containing the coding sequence of TRPC3 or TRPC5. Cells stably expressing hTRPC3-green fluorescent protein (TRPC3-GFP) fusion protein used in this study were described earlier [26,32,33]. Cells stably expressing TRPC5 (murine TRPC5 cDNA was generously donated by Dr. Lutz Birnbaumer, National Institute of Environmental Health Sciences) were generated after transfection and subsequent selection by antibiotic resistance. Several clones were selected that gave robust Ca^{2+} entry signals in response to methacholine (for example, Figure 1A). Both TRPC3-GFP and TRPC5-expressing cell lines were grown under selection with G418 at 37 °C in Dulbecco's modified eagle's medium supplemented with 10% heat-inactivated fetal bovine serum and 2 mM glutamine in a humidified 95% air, 5% CO_2 incubator.

Ca^{2+} measurements

Ca^{2+} measurements were carried out with either Fura-2-AM or Fluo-4-AM and a cell imaging system (Intracellular Imaging, Inc., Cincinnati, OH) as described previously [34]. For Fura-2 measurements, the ratio obtained by dividing the emitted fluorescence from excitation at 340 nm by the emitted fluorescence measured after excitation at 380 nm is reported as in indicator of changes in intracellular Ca^{2+} concentration. For experiments using wortmannin, which is UV sensitive, Ca^{2+} measurements were carried out with the visible wavelength dye, Fluo-4. Briefly, cells were loaded with either 1 μM of Fura-2/AM (for 30 minutes) or 4 μM of Fluo-4/AM (for 1 hour), then washed and bathed in Hepes-buffered saline solution (HBSS; in mM, 140 NaCl, 4.7 KCl, 10 CsCl, 2 $CaCl_2$, 1.13 $MgCl_2$, 10 glucose, and 10 Hepes, pH 7.4) for at least 10 min before Ca^{2+} measurements are made. Basal cytosolic Ca^{2+} was determined in a field containing up to 100 cells and cytosolic Ca^{2+} was monitored after addition of enzyme inhibitors and/or receptor agonists.

Electrophysiology

Ion currents were recorded by using either the whole-cell or nystatin-patch configuration using an Axopatch-200B amplifier (Axon Instruments) as described previously [26]. The patch pipettes were pulled with a pipette puller (Sutter) from glass capillaries (Corning glass, 7052) and fire-polished. The finished pipettes had resistances ranging between 2–5 MΩ when filled with the following solution (for whole cell experiments, in mM): 140 CsCl, 10 BAPTA (cesium salt), 1 $MgCl_2$, 2.2 $CaCl_2$, and 10 Hepes, pH 7.2, with Tris base. In most experiments, this pipette solution was buffered to ~100 nM free Ca^{2+} calculated using WinmaxC software available from Stanford University website. For nystatin-patch experiments, the pipette contained (in mM): CsCl, 55; Cs_2SO_4, 70; $MgCl_2$, 1; $CaCl_2$, 1; Glucose, 5; HEPES, 10; nystatin concentration: 200 μg/ml. The bath solution was (in mM): 140 NaCl, 4.7 KCl, 10 CsCl, 2.0 $MgCl_2$, 10 glucose, 2.0 or 10 $CaCl_2$, and 10 Hepes, pH 7.4, with NaOH. The osmolarity of these solutions was adjusted to 290–310 mOsM with glucose. Bath solution change was accomplished by gentle perfusion. Wild type HEK cells (HEK-Wt), TRPC3-GFP- and TRPC5-expressing HEK293 cells were plated the day before on coverslips. Before starting the experiments, coverslips were mounted in a perfusion chamber and electrophysiological measurements were performed at room temperature. An agar bridge served as the electrical connection between the bath and the signal ground. Whole cell currents were elicited by voltage stimuli lasting 250 ms, delivered every 5 seconds, with voltage ramps from −100 to +100 mV. Data were sampled at 5 kHz, filtered at 1 kHz, acquired with pCLAMP 9.0 software and analyzed with CLAMPFIT 9.0 (Axon).

For the single channel measurements in the inside-out configuration, the composition of the solutions present in the bath and the pipette (resistance varying between 3–6 MΩ) were

respectively (in mM): KCl, 120; HEPES, 20; EGTA, 10; $CaCl_2$, 4.1; $MgCl_2$, 1; pH 7.3 adjusted with KOH; and KCl, 140; HEPES, 10; $CaCl_2$, 1; $MgCl_2$, 1; pH 7.3 adjusted with KOH. Signals were low-pass filtered at 2 kHz, digitized at 20 kHz and then analyzed using the Clampfit 9.2 software (Axon Instr., USA).

Depletion of PIP_2 levels using Rapamycin

PIP_2 depletion was achieved by targeting of the type IV phosphatidylinositol 5-phosphatase (PI5-phosphatase) to the plasma membrane [35]. HEK293 Cells expressing TRPC5 were transfected with either a construct (2.5 μg) encoding a membrane targeted FRB domain of mTOR tagged with monomeric red fluorescent protein (mRFP), or with a construct (2.5 μg) encoding a modified cytoplasmic type IV 5-phosphatase fused to FKBP12 and tagged with mRFP, or co-transfected with both constructs. The plasma membrane targeted FRB domain of mTOR can be heterodimerized with FKBP12-5-phosphatase using rapamycin (100 nM) as described previously [35].

Results

Activation of TRPC5 by PLC-coupled receptors

An HEK293 cell line stably expressing TRPC5 channels (described in the Methods section) was used throughout this study. After activation with the muscarinic agonist, methacholine, TRPC5-expressing cells exhibited a Ca^{2+} entry pathway that was not found in the wild type cells. As described earlier, when used at concentrations ranging between 1 and 5 μM, gadolinium (Gd^{3+}) is a potent inhibitor of CCE in HEK293 cells [32,36]. As expected, methacholine-activated CCE in HEK-Wt was completely blocked by 5 μM Gd^{3+} (Figure 1A). As previously shown for TRPC3 [32] and TRPC7 [37], TRPC5-expressing cells exhibited a receptor-activated Ca^{2+} entry pathway that was Gd^{3+}-insensitive (Figure 1A). However, TRPC5 differs from members of the TRPC3/6/7 subfamily in two significant ways. First, TRPC5 channels were shown previously to be activated by higher concentrations of Gd^{3+} (50–100 μM) [38] while TRPC3 is inhibited by lanthanides at these high concentrations [39]. These results were confirmed in the present study and we found that TRPC5-expressing HEK cells show a Ca^{2+} entry in response to exogenous addition of 50 μM Gd^{3+} (Figure 1B). Second, the DAG analog, OAG (100 μM) fully activated TRPC3 while it failed to activate TRPC5 channels (Figure 1C), in confirmation of the findings of Venkatachalam et al. [27]. Furthermore, application of OAG to TRPC5-expressing HEK293 cells in the presence of the PKC inhibitor GF-109203X (10 μM) also failed to activate TRPC5 channels (data not shown).

PI-4K inhibitors (wortmannin and LY294002) specifically activate TRPC5 but not TRPC3 channels

Since neither second messenger (IP_3 or DAG) produced after PLC breakdown of PIP_2 appears to be involved in the activation of TRPC5 channels ([40,27], this study), we asked whether PIP_2 breakdown itself might be responsible for TRPC5 activation, for example by relieving tonic PIP_2 inhibition of the channels. To test this hypothesis, we first used a pharmacological strategy to deplete polyphosphoinositides in the cells.

The membrane permeant drugs, wortmannin and LY294002 are known to inhibit the phosphatidylinositol 3-kinase when used at relatively low concentrations (~100 nM and 10 μM respectively). When used at higher concentrations (20 μM for wortmannin and 100 μM for LY294002), these drugs are known to inhibit the phosphatidylinositol 4-kinase (PI4-K) [41,42]. PI4-K catalyses the phosphorylation of phosphatidylinositol (PI) into phosphatidylinositol 4 monophosphate (PIP), which in turn is converted into the substrate of PLC, PIP_2 *via* the action of the enzyme phosphatidylinositol 4-phosphate 5-kinase. Therefore,

efficient inhibition of PI4-K leads to subsequent PIP and PIP_2 depletion [41,42,43,44,45,46, 47].

As shown in Figure 2A, treatment of TRPC5-expressing HEK293 cells with 20 μM wortmannin activates calcium entry in these cells while no effect of wortmannin was observed in wild type cells. Similar results were obtained using the drug LY294002 (Figure 2B) suggesting that this calcium entry is directly associated with TRPC5 channels and not to non-specific effects of these drugs. Concentrations of these drugs which inhibit phosphoinositide 3-kinase, but not PI4-K (10 μM LY294002, 200 nM wortmannin) did not activate entry (data not shown). When LY294002 was applied to TRPC5-expressing cells in the continuous presence of Ca^{2+}, there was a delay of about a minute before Ca^{2+} entry ensued (Figure 3A), as expected if this drug must penetrate the plasma membrane, inhibit PI4-K and cause depletion of polyphosphoinositides. Note that LY294002 caused a small release of Ca^{2+} (Figure 2B) that was not seen with wortmannin (Figure 2A). However, both drugs induced similar Ca^{2+} entry in TRPC5 cells. In addition, we also utilized another structurally dissimilar PI4-K inhibitor, phenylarsine oxide [48,44]; this agent caused a large release of Ca^{2+} stores, and thus was not employed in further experiments. However, we did note that, like wortmannin and LY294002, phenylarsine oxide activated Gd^{3+}-insensitive Ca^{2+} entry in TRPC5-expressing cells, and not in wild-type or TRPC3-expressing cells (see below).

The effects of wortmannin and LY294002 are specific to TRPC5 channels. An HEK293 cell line expressing TRPC3 channels showed no increase in calcium entry after application of 100 μM LY294002 (Figure 2C). Similar results were obtained with 20 μM wortmannin (data not shown). Rather, receptor activation of TRPC3 channels in HEK293 cells was completely abrogated after treatment with 100 μM LY294002 (Figure 2D), presumably because PIP_2 is necessary for TRPC3 activation as a source of DAG, the signal for TRPC3 activation. Similar results were obtained when TRPC3-expressing HEK293 cells were treated with 20 μM wortmannin (data not shown). In addition, TRPC7 behaved identically to TRPC3; Ca^{2+} entry was not activated by PI4-K inhibitors, and agonist-activated Ca^{2+} entry was blocked by these drugs (data not shown). Note that in Figure 2D, a smaller but still significant mobilization of Ca^{2+} is seen, yet subsequent addition of Ca^{2+} shows essentially no TRPC3 activity. This is likely due to the fact that, in the presence of PI-4 kinase inhibitors, stimulation of phospholipase C-linked receptors yields a diminished production of phospholipase C products which is transient due to rapid run down of PIP_2 levels [49,42].

The experiments in Figure 2D indicate a diminished Ca^{2+} release response, which results from partial depletion of PIP_2 by LY2942002 cells. We carried out a series of such measurements determining the magnitude of the transient Ca^{2+} release signal following methacholine addition in TRPC5-expressing cells as an indication of available PIP_2 levels. This transient response was significantly reduced in LY2942002-treated cells, indicative of a reduction in available PIP_2 (Control, 0.86 ± 0.02 ratio units, n=184; LY2942002, 0.49 ± 0.02 ratio units, n=206; $P<0.0001$). Although this is an indirect indicator of PIP_2, it has the advantage of providing information on PIP_2 specifically available for PLC-degradation. This information should be more meaningful than whole cell levels of polyphosphoinositides, which are known to reflect a number of pools of lipids, some not associated with the plasma membrane [50,51,52].

The plasma membrane calcium ATPase is known to be tightly regulated by PIP_2 [53,54,55]. Thus we considered that the rise in Ca^{2+} seen in cells treated with inhibitors of PI4-K might result, at least in part, from reduced Ca^{2+} extrusion. We examined the rate of Ca^{2+} extrusion from TRPC5-expressing cells after elevation of $[Ca^{2+}]_i$ by carbachol and by LY294002. However, there was no difference between these two stimuli in the rate of $[Ca^{2+}]_i$ decline following removal of extracellular Ca^{2+}, indicating that the elevation in Ca^{2+} due to LY294002 does not result from a reduction in Ca^{2+} extrusion (Supplemental Figure).

Wortmannin and LY2942002 activate a current in TRPC5-expressing HEK cells similar to that activated by methacholine

We have shown that drugs that deplete polyphosphoinositides such as wortmannin and LY294002 activate a calcium entry pathway in TRPC5-expressing cells but not in TRPC3- or TRPC7-expressing cells or in wild type HEK293 cells. We next carried out patch-clamp current measurements initially in the perforated-patch configuration to determine if these drugs induce an ionic current in TRPC5-expressing HEK293 cells. As shown in Figure 3, the muscarinic-cholinergic agonist, carbachol, and both PI4-K inhibitors, activated inward and outward currents in TRPC5-HEK293 cells. None of these agents induced an increased current in non-transfected cells. The currents activated by carbachol and the PI4-K inhibitors were similar in that all three gave activation of larger inward than outward currents, and all three showed the double rectification typical for TRPC channels. In all three cases, current activation appeared transient, while in Ca^{2+} experiments, the responses appeared sustained (Figure 1 and 2); the reason for this difference is not known. The only difference between the current responses to carbachol and the inhibitors is that carbachol activated a significantly larger current, and acted almost immediately upon addition to the cells, while a variable delay occurred between application of the PI4-K inhibitors and the increase in current. This is consistent with the observations from the Ca^{2+} measurements. The mean, background-subtracted inward currents (at −100 mV) were (mean pA/pF ± SEM, n): carbachol, −39.6 ± 5.9 (8); LY2942002, −9.3 ± 4.5 (4); wortmannin, −18.5 ± 7.4 (3). The outward currents (at +100 mV) were (pA/pF, n): carbachol, 21.4 ± 3.8 (8); LY2942002, 6.4 ± 2.4 (4); wortmannin, 13.4 ± 2.2 (3).

While the perforated patch technique permits current measurement under the most physiological condition, i.e., without dialysis of the cytoplasm, the whole-cell mode has the advantage of permitting introduction of reagents, such as enzymes, antibodies, and small molecules. As shown in Figure 4A, stimulation of TRPC5-expressing HEK293 cells with the muscarinic agonist methacholine activates both small inward (at −100 mV) and larger outward (at +100 mV) currents that were absent in wild type HEK293 cells (data not shown). The current-voltage (IV) relationship for TRPC5 current depicted in Figure 4B displayed the characteristic double rectification with strong outward rectification, as previously described for TRPC5 [30,56]. However, the relative magnitude of the inward current is notably smaller than that seen with perforated patch. We also found that responsiveness to muscarinic agonists appeared to wash out after a period of 5–10 minutes, after which time cells seldom responded to receptor activation.

Stimulation of TRPC5-expressing HEK293 cells with 20 μM wortmannin or LY2942002 produced inconsistent results in whole-cell experiments. In some cells, wortmannin induced an increase in both inward and outward currents, although the magnitude of the currents was somewhat smaller than that obtained with methacholine (Figure 4C). Wortmannin never induced similar currents in TRPC3-expressing HEK293 cells or HEK293 wild type cells (data not shown). The IV curve obtained after addition of wortmannin to TRPC5-expressing HEK293 cells (Figure 4D) was similar to that obtained following TRPC5 activation through muscarinic agonist stimulation. The inconsistency and tendency to washout of the responses in whole-cell configuration were disappointing because this precluded experiments requiring long dialysis times, for example with antibodies directed against PIP_2.

Wortmannin-activated TRPC5 currents are inhibited by PIP and PIP_2

Our data so far suggest an inhibitory effect of polyphosphoinositides on TRPC5 channels and that this inhibition is relieved by pharmacological procedures that deplete cellular polyphosphoinositides. We then sought to explore the ability of polyphosphoinositides to inhibit wortmannin-induced TRPC5 currents in HEK293 cells stably expressing TRPC5 cation channels. Unfortunately, as discussed above, effects of these drugs on membrane currents in

the whole-cell configuration, which could be used for introduction of phospholipids, were inconsistent. In a series of experiments in which a 30 min pretreatment with wortmannin induced a consistent increase in whole cell current (an approximate doubling of inward and outward current), cells were then dialyzed with a patch pipette containing either the pipette solution alone (described in the methods section) or the pipette solution containing 20 μM of different polyphosphoinositides. As shown in Figure 5, following break-in, dialysis of cells with PIP_2 (Figure 5A) or PIP (Figure 5B) inhibited wortmannin-activated TRPC5 currents while 20 μM of PIP_3 (Figure 5C) had no effect on TRPC5 currents. The inhibitory effects of polyphosphoinositides occurred after a delay of a minute or so, perhaps due to slow diffusion of the lipids through the patch pipette openings or in the cytoplasm.

Effects of PIP_2 on single TRPC5 channels

We next turned to measurement of the activity of TRPC5 channels in excised patches. This preparation should give rapid access to the intracellular surface of the plasma membrane and the channels in order to investigate their regulation. In excised patches, there was little apparent channel activity in control cells, or in cells that had been pre-treated with PI4-K inhibitors. Addition of PIP_2 to the patches resulted in robust activation of channels with a conductance at +60mV of 64.6 ± 0.1 pS (Figure 6), a value similar to that previously reported for TRPC5 [30]. The channels were also activated albeit to a somewhat lesser extent by PIP_3. Figure 7 summarizes a series of experiments showing that the channels were significantly activated by PIP_2, but not by wortmannin, or by the de-acylated PIP_2, glycerol-phosphoryl-inositol 4,5-bisphosphate ($GPIP_2$). The channels could also be activated by addition of ATP, possibly indicating that the phosphatidylinositol or PIP precursor and necessary kinases were present in the patches. In one series of experiments (Figure 7C) in which there was measurable spontaneous activity in the patches, this activity was decreased by the PIP_2 scavenger, polylysine (PL).

Effect of membrane targeted PIP_2 5-phosphatase

The results to this point present a paradox: pharmacological and whole-cell patch-clamp data suggest that PIP_2 exerts an inhibitory control on TRPC5, while the single channel data suggests the PIP_2 activates the channels. We consider that the PI4-K inhibitors might affect different pools of PIP_2 than those involved in positive modulation of the channels. In addition, pharmacological inhibition of PI4-K not only decreases the levels of PIP2 but also depletes, and likely to a greater extent, the levels of PI4P. Therefore, we sought to use a molecular tool to specifically deplete PIP_2 levels and assess its effect on TRPC5 activity. We adopted a strategy recently developed by Varnai et al [35] whereby a cytoplasmic form of the PIP_2 5-phosphatase is targeted to the plasma membrane by rapamycin, as described in the methods section. We confirmed that addition of rapamycin to agonist-activated wild-type cells resulted in rapid cessation of Ca^{2+} signaling, as originally shown by Varnai *et al.* [35]; addition of rapamycin to wild-type cells, or cells transfected with either of the two constructs alone had no such effect (data not shown). Surprisingly, unlike the case for 4-kinase inhibitors, addition of rapamycin to TRPC5-expressing HEK293 cells did not activate TRPC5-mediated Ca^{2+} entry nor did rapamycin potentiate TRPC5-activation in response to low doses of agonist (5 μM) (not shown). Rather, agonist-activated TRPC5-mediated Ca^{2+} entry was strongly inhibited upon addition of rapamycin (Figure 8).

The 4-kinase inhibitors would decrease levels of both PIP and PIP_2, while the targeted 5-phosphatase would decrease only PIP_2, possibly increasing PIP. We thus considered the possibility that PIP might act to inhibit TRPC5, antagonizing the activation by PIP_2. For these experiments, we determined the sensitivity of TRPC5 channels to PIP_2 (Figure 9A), and selected 1 μM PIP_2 as a submaximal concentration. Addition of a large excess of PIP (10 μM) to excised patches from TRPC5-expressing cells together with 1 μM PIP_2 caused no significant

inhibition of TRPC5 channel activity (Figure 9B, C). 10 μM PIP, when applied alone, caused only modest activation of TRPC5 channel activity as compared to PIP_2 (Figure 9C).

Discussion

The mechanism of activation *via* PLC-coupled receptor stimulation of TRPC5 and TRPC4 has remained one of the unsolved mysteries in the TRPC field [57]. TRPC5 activation was shown to depend upon PLC, but clearly did not involve DAG or IP_3 [30]. Plant and Schaefer reported that receptor-mediated activation of currents in cells transfected with TRPC4 and TRPC5 was unaffected by infusion of low molecular weight heparin [57] ruling out the involvement of IP_3 receptors in TRPC5 activation. Venkatachalam et al. [27] showed that TRPC5 could be activated *via* a muscarinic receptor in DT40 B cells lacking all three IP_3 receptor subtypes. Strübing et al. [58] showed that like homomeric TRPC4 and TRPC5, heteromers formed between TRPC1 and TRPC5 were also not activated by infusion of IP_3, but responded to subsequent muscarinic receptor activation (but see [59]). Otsuguro *et al.* [31] provided the first clues to the possible activation mechanism, demonstrating that TRPC4 activity was inhibited by polyphosphoinositides. Other findings in their study suggested that depletion of polyphosphoinositides played a role in activating TRPC4, but in conjunction with other signals such as G_i/G_o or a rise in $[Ca^{2+}]_i$ [31].

In this study, we show that drugs that are expected to deplete polyphosphoinositides activate TRPC5 cation channels expressed in HEK293 cells, consistent with the Otsuguro *et al.* results, and providing a possible mechanism of activation of TRPC5 channels through PLC-coupled receptor stimulation. We confirmed that the synthetic DAG, OAG, was incapable of activating TRPC5 channels in our TRPC5-expressing HEK293 cell line. However, pharmacological inhibition of PI4-K by wortmannin and LY294002 which causes polyphosphoinositide depletion was able to activate calcium entry and whole-cell TRPC5 current in TRPC5-expressing HEK293 cells with no effect observed in wild type HEK293 cells. We found no evidence for a role for cytoplasmic Ca^{2+} signaling, since the muscarinic agonist as well as the 4-kinase inhibitors activated TRPC5 when cytoplasmic Ca^{2+} was strongly buffered in the whole-cell configuration. Importantly, the 4-kinase inhibitors were unable to activate calcium entry and ionic currents in an HEK293 cell line stably expressing TRPC3 channels. Rather, muscarinic receptor activation of TRPC3 cation channels was completely abrogated by pre-treatment with these drugs. Finally, Activation of TRPC5 currents by wortmannin could be partially reversed by including PIP or PIP_2 but not PIP_3 in the patch pipette. We cannot relate the concentrations of these lipids in the patch pipette to physiological concentrations in the plasma membrane, nor can we determine if either of these lipids can be interconverted to the other in this experimental situation. Thus, we cannot definitively determine which (or if both) of these lipids is the critical regulator of TRPC5. Nonetheless, these findings are consistent with the proposal that receptor-mediated activation of PLC activates TRPC5 through relief of inhibition by polyphosphoinositides.

It is well known that polyphosphoinositides are key regulators of many ion channels and transporters (for reviews see [60,61,62,18]). In the majority of instances, this regulation is thought to be allosteric rather than a primary means of channel activation. Also, in the majority of instances, polyphosphoinositides either activate, or are required for activation of the channels. For most TRP superfamily members, polyphosphoinositides exert positive modulatory effects on channel activity [63,64,61], and we have shown that this is the case for one member of the TRPC family, TRPC7 [65]. Surprisingly, we found that TRPC5 channels in excised patches showed low activity until PIP_2 was added to them. PIP was only a weak activator, and did not appreciably affect the ability of PIP2 to activate the channels. Also, global depletion of PIP_2 by a membrane-targeted PIP2 5-phosphatase strongly inhibited TRPC5 activity. This may mean that the 4-kinase inhibitors target a specific pool of PIP_2, or that

components of the regulatory mechanism for TRPC5 channels is lost in the excised patch. Regardless, it seems clear that in addition to its role in the signaling pathway for TRPC5 activation, PIP_2 also plays a more fundamental positive role in TRPC5 function, similar to that shown for the majority of TRP channels that have been studied. We propose a somewhat speculative model to accommodate these two apparently opposing effects of PIP_2. We suggest that PIP_2 may be intimately associated with TRPC5 channels where it is needed for proper channel function. In addition, we propose an additional role for polyphosphoinositides (PIP_2 or PIP) in a signaling mechanism, perhaps involving a negative regulator that brakes TRPC5 in a polyphosphoinositide-dependent manner. In an excised patch, this regulator may be gone, as well as the PIP_2 necessary for channel activity. Addition of PIP_2 in this circumstance would lead to channel activation. This model is summarized in Figure 10. Note that this model implies spatially restricted pools of polyphosphoinositides fulfilling these distinct functions; consistent with this idea, unlike its precursor, PIP, PIP_2 diffusion in the plasma membrane appears to be highly restricted due to interactions with the cytoskeleton [66]. In a recent study, Lukacs *et al.* [67] presented evidence that PIP2 can dually regulate TRPV1 channels, depending on the strength of the channel stimulus.

In addition to activation by PLC-coupled receptor agonists, TRPC5 channels have been shown to be activated by store depletion [56], by augmented membrane trafficking [68], and can be activated in a direct manner by high concentrations of lanthanides [38]. Lanthanides are believed to bind to a specific site in the extracellular domain of the channel leading to TRPC5 activation. However, because of the apparent complex roles of polyphosphoinositides, additional work will be needed to identify the exact site(s) on TRPC5 channels involved in phospholipid regulation. Members of the TRPC family of cation channels are increasingly recognized as important players in native calcium entry pathways controlling a wide variety of physiological functions in many cell types. Further work is needed to better understand the regulation of TRPC channels under physiological conditions and how this regulation participates in shaping complex physiological responses.

Supplementary Material

Refer to Web version on PubMed Central for supplementary material.

Acknowledgments

We are grateful to Dr. Lutz Birnbaumer who provided the plasmid containing the cDNA for murine TRPC5, and Dr. Tamas Balla who provided the constructs for plasma membrane targeting of PIP2 phosphatase. Drs. David Armstrong, Jerrel Yakel, Guillermo Vazquez, Jason Mercer and Jeremy Smyth read the manuscript and provided useful criticism. This work was supported by the Intramural Research Program, National Institute of Environmental Health Sciences, National Institutes of Health, project number Z01 ES090087.

Reference List

1. Berridge MJ. Inositol trisphosphate and calcium signalling. Nature 1993;361:315–325. [PubMed: 8381210]
2. Putney JW. A model for receptor-regulated calcium entry. Cell Calcium 1986;7:1–12. [PubMed: 2420465]
3. Berridge MJ. Capacitative calcium entry. Biochem J 1995;312:1–11. [PubMed: 7492298]
4. Parekh AB, Putney JW. Store-operated calcium channels. Physiol Rev 2005;85:757–810. [PubMed: 15788710]
5. Barritt GJ. Receptor-activated Ca^{2+} inflow in animal cells: a variety of pathways tailored to meet different intracellular Ca^{2+} signalling requirements. Biochem J 1999;337:153–169. [PubMed: 9882611]

6. Bird GS, Aziz O, Lievremont JP, Wedel BJ, Trebak M, Vazquez G, Putney JW. Mechanisms of phospholipase C-regulated calcium entry. Curr Mol Med 2004;4:291–301. [PubMed: 15101686]
7. Nilius B, Voets T. Diversity of TRP channel activation. Novartis Found Symp 2004;258:140–149. [PubMed: 15104180]
8. Putney JW. The enigmatic TRPCs: multifunctional cation channels. Trends Cell Biol 2004;14:282–286. [PubMed: 15183184]
9. Inoue R, Hanano T, Shi J, Mori Y, Ito Y. Transient receptor potential protein as a novel non-voltage-gated Ca2+ entry channel involved in diverse pathophysiological functions. J Pharmacol Sci 2003;91:271–276. [PubMed: 12719655]
10. Clapham DE, Runnels LW, Strübing C. The TRP ion channel family. Nature Rev Neurosci 2002;2:387–396. [PubMed: 11389472]
11. Birnbaumer L, Zhu X, Jiang M, Boulay G, Peyton M, Vannier B, Brown D, Platano D, Sadeghi H, Stefani E, Birnbaumer M. On the molecular basis and regulation of cellular capacitative calcium entry: Roles for Trp proteins. Proc Nat Acad Sci USA 1996;93:15195–15202. [PubMed: 8986787]
12. Minke B, Cook B. TRP channel proteins and signal transduction. Physiol Rev 2002;82:429–472. [PubMed: 11917094]
13. Fleig A, Penner R. The TRPM ion channel subfamily: molecular, biophysical and functional features. Trends Pharmacol Sci 2004;25:633–639. [PubMed: 15530641]
14. Nilius B, Voets T. TRP channels: a TR(I)P through a world of multifunctional cation channels. Pflugers Arch. 2005
15. Van Der SM, Di M,V. Endovanilloids. Putative endogenous ligands of transient receptor potential vanilloid 1 channels. Eur J Biochem 2004;271:1827–1834. [PubMed: 15128293]
16. Hoenderop JG, Nilius B, Bindels RJ. Epithelial calcium channels: from identification to function and regulation. Pflugers Arch 2003;446:304–308. [PubMed: 12684797]
17. Caterina MJ, Julius D. The vanilloid receptor: a molecular gateway to the pain pathway. Annu Rev Neurosci 2001;24:487–517. [PubMed: 11283319]
18. Voets T, Nilius B. Modulation of TRPs by PIPs. J Physiol (Lond) 2007;582:939–944. [PubMed: 17395625]
19. Nilius B, Talavera K, Owsianik G, Prenen J, Droogmans G, Voets T. Gating of TRP channels: a voltage connection? J Physiol 2005;567:35–44. [PubMed: 15878939]
20. Perraud AL, Knowles HM, Schmitz C. Novel aspects of signaling and ion-homeostasis regulation in immunocytes. The TRPM ion channels and their potential role in modulating the immune response. Mol Immunol 2004;41:657–673. [PubMed: 15220002]
21. Beech DJ, Muraki K, Flemming R. Non-selective cationic channels of smooth muscle and the mammalian homologues of Drosophila TRP. J Physiol 2004;559:685–706. [PubMed: 15272031]
22. Zufall F. The TRPC2 ion channel and pheromone sensing in the accessory olfactory system. Naunyn Schmiedebergs Arch Pharmacol 2005;371:245–250. [PubMed: 15871013]
23. Hofmann T, Obukhov AG, Schaefer M, Harteneck C, Gudermann T, Schultz G. Direct activation of human TRPC6 and TRPC3 channels by diacylglycerol. Nature 1999;397:259–262. [PubMed: 9930701]
24. Inoue R, Okada T, Onoue H, Hara Y, Shimizu S, Naitoh S, Ito Y, Mori Y. The transient receptor potential protein homologue TRP6 is the essential component of vascular α1-adrenoceptor-activated Ca^{2+}-permeable cation channel. Circ Res 2001;88:325–332. [PubMed: 11179201]
25. Okada T, Inoue R, Yamazaki K, Maeda A, Kurosaki T, Yamakuni T, Tanaka I, Shimizu S, Ikenaka K, Imoto K, Mori Y. Molecular and functional characterization of a novel mouse transient receptor potential protein homologue TRP7. Ca^{2+}-permeable cation channel that is constitutively activated and enhanced by stimulation of G protein-coupled receptor. J Biol Chem 1999;274:27359–27370. [PubMed: 10488066]
26. Trebak M, Bird GStJ, McKay RR, Birnbaumer L, Putney JW. Signaling mechanism for receptor-activated TRPC3 channels. J Biol Chem 2003;278:16244–16252. [PubMed: 12606542]
27. Venkatachalam K, Zheng F, Gill DL. Regulation of Canonical Transient Receptor Potential (TRPC) Channel Function by Diacylglycerol and Protein Kinase C. J Biol Chem 2003;278:29031–29040. [PubMed: 12721302]

28. Freichel M, Vennekens R, Olausson J, Hoffmann M, Muller C, Stolz S, Scheunemann J, Weissgerber P, Flockerzi V. Functional role of TRPC proteins in vivo: lessons from TRPC-deficient mouse models. Biochem Biophys Res Commun 2004;322:1352–1358. [PubMed: 15336983]
29. Greka A, Navarro B, Oancea E, Duggan A, Clapham DE. TRPC5 is a regulator of hippocampal neurite length and growth cone morphology. Nat Neurosci 2003;6:837–845. [PubMed: 12858178]
30. Schaefer M, Plant TD, Obukhov AG, Hofmann T, Gudermann T, Schultz G. Receptor-mediated regulation of the nonselective cation channels TRPC4 and TRPC5. J Biol Chem 2000;275:17517–17526. [PubMed: 10837492]
31. Otsuguro K, Tang J, Tang Y, Xiao R, Freichel M, Tsvilovskyy V, Ito S, Flockerzi V, Zhu MX, Zholos AV. Isoform-specific inhibition of TRPC4 channel by phosphatidylinositol 4,5-bisphosphate. J Biol Chem 2008;283:10026–10036. [PubMed: 18230622]
32. Trebak M, Bird GStJ, McKay RR, Putney JW. Comparison of human TRPC3 channels in receptor-activated and store-operated modes. Differential sensitivity to channel blockers suggests fundamental differences in channel composition. J Biol Chem 2002;277:21617–21623. [PubMed: 11943785]
33. McKay RR, Szmeczek-Seay CL, Lièvremont J-P, Bird GStJ, Zitt C, Jüngling E, Lückhoff A, Putney JW. Cloning and expression of the human transient receptor potential 4 (TRP4) gene: localization and functional expression of human TRP4 and TRP3. Biochem J 2000;351:735–746. [PubMed: 11042129]
34. Trebak M, Hempel N, Wedel BJ, Smyth JT, Bird GS, Putney JW. Negative regulation of TRPC3 channels by protein kinase C-mediated phosphorylation of serine 712. Mol Pharmacol 2005;67:558–563. [PubMed: 15533987]
35. Varnai P, Thyagarajan B, Rohacs T, Balla T. Rapidly inducible changes in phosphatidylinositol 4,5-bisphosphate levels influence multiple regulatory functions of the lipid in intact living cells. The Journal of Cell Biology 2006;175:377–382. [PubMed: 17088424]
36. Luo D, Broad LM, Bird GStJ, Putney JW. Signaling pathways underlying muscarinic receptor-induced $[Ca^{2+}]_i$ oscillations in HEK293 cells. J Biol Chem 2001;276:5613–5621. [PubMed: 11096083]
37. Lievremont JP, Bird GS, Putney JW. Canonical transient receptor potential TRPC7 can function as both a receptor- and store-operated channel in HEK-293 cells. Am J Physiol Cell Physiol 2004;287:C1709–C1716. [PubMed: 15342342]
38. Jung S, Mühle A, Schaefer M, Strotmann R, Schultz G, Plant TD. Lanthanides potentiate TRPC5 currents by an action at extracellular sites close to the pore mouth. J Biol Chem 2003;278:3562–3571. [PubMed: 12456670]
39. Halaszovich CR, Zitt C, Jüngling E, Lückhoff A. Inhibition of TRP3 by lanthanides. Block from the cytosolic side of the plasma membrane. J Biol Chem 2000;275:37423–37428. [PubMed: 10970899]
40. Plant TD, Schaefer M. TRPC4 and TRPC5: receptor-operated Ca2+-permeable nonselective cation channels. Cell Calcium 2003;33:441–450. [PubMed: 12765689]
41. Downing GJ, Kim S, Nakanishi S, Catt KJ, Balla T. Characterization of a soluble adrenal phosphatidylinositol 4-kinase reveals wortmannin sensitivity of type III phosphatidylinositol kinases. Biochem 1996;35:3587–3594. [PubMed: 8639510]
42. Nakanishi S, Catt KJ, Balla T. A wortmannin-sensitive phosphatidylinositol 4-kinase that regulates hormone-sensitive pools of inositolphospholipids. Proc Natl Acad Sci U S A 1995;92:5317–5321. [PubMed: 7777504]
43. Linseman DA, Sorensen SD, Fisher SK. Attenuation of focal adhesion kinase signaling following depletion of agonist-sensitive pools of phosphatidylinositol 4,5-bisphosphate. J Neurochem 1999;73:1933–1944. [PubMed: 10537051]
44. Linseman DA, McEwen EL, Sorensen SD, Fisher SK. Cytoskeletal and phosphoinositide requirements for muscarinic receptor signaling to focal adhesion kinase and paxillin. J Neurochem 1998;70:940–950. [PubMed: 9489713]
45. Sorensen SD, Linseman DA, McEwen EL, Heacock AM, Fisher SK. A role for wortmannin-sensitive phosphatidylinositol-4-kinase in the endocytosis of muscarinic cholinergic receptors. Mol Pharmacol 1998;53:827–836. [PubMed: 9584208]

46. Broad LM, Braun F-J, Lièvremont J-P, Bird GStJ, Kurosaki T, Putney JW. Role of the phospholipase C - inositol 1,4,5-trisphosphate pathway in calcium release-activated calcium current (I_{crac}) and capacitative calcium entry. J Biol Chem 2001;276:15945–15952. [PubMed: 11278938]
47. Nilius B, Mahieu F, Prenen J, Janssens A, Owsianik G, Vennekens R, Voets T. The Ca2+-activated cation channel TRPM4 is regulated by phosphatidylinositol 4,5-biphosphate. EMBO J 2006;25:467–478. [PubMed: 16424899]
48. Wiedemann C, Schafer T, Burger MM. Chromaffin granule-associated phosphatidylinositol 4-kinase activity is required for stimulated secretion. EMBO J 1996;15:2094–2101. [PubMed: 8641275]
49. Nakanishi S, Catt KJ, Balla T. Inhibition of agonist-stimulated inositol 1,4,5-trisphosphate production and calcium signaling by the myosin light chain kinase inhibitor, wortmannin. J Biol Chem 1994;269:6528–6535. [PubMed: 8120005]
50. McLaughlin S, Wang J, Gambhir A, Murray D. PIP2 and proteins: Interactions, organization, and information flow. Annu Rev Biophys Biomol Struct 2002;31:151–175. [PubMed: 11988466]
51. Martin TFJ. Phosphoinositide lipids as signaling molecules: common themes for signal transduction, cytoskeletal regulation, and membrane trafficking. Annu Rev Cell Dev Biol 1998;14:231–264. [PubMed: 9891784]
52. Michell RH. Nuclear PIPs. Current Biol 1992;1:200–202.
53. Choquette D, Hakim G, Filotep AG, Plishker GA, Bostwick JR, Penniston JT. Regulation of plasma membrane Ca^{2+} ATPases by lipids of the phosphatidylinositol cycle. Biochem Biophys Res Comm 1984;125:908–915. [PubMed: 6097254]
54. Enyedi A, Flura M, Sarkadi B, Gardos G, Carafoli E. The maximal velocity and the calcium affinity of the red cell calcium pump may be regulated independently. J Biol Chem 1987;262:6425–6430. [PubMed: 3032968]
55. Missiaen L, Raeymaekers L, Droogmans G, Wuytack F, Casteels R. Role of arginine residues in the stimulation of the smooth-muscle plasma-membrane Ca2+ pump by negatively charged phospholipids. Biochem J 1991;264:609–612. [PubMed: 2557845]
56. Zeng F, Xu SZ, Jackson PK, McHugh D, Kumar B, Fountain SJ, Beech DJ. Human TRPC5 channel activated by a multiplicity of signals in a single cell. J Physiol 2004;559:739–750. [PubMed: 15254149]
57. Plant TD, Schaefer M. Receptor-operated cation channels formed by TRPC4 and TRPC5. Naunyn Schmiedebergs Arch Pharmacol 2005;371:266–276. [PubMed: 15902430]
58. Strübing C, Krapivinsky G, Krapivinsky L, Clapham DE. TRPC1 and TRPC5 form a novel cation channel in mammalian brain. Neuron 2001;29:645–655. [PubMed: 11301024]
59. Kanki H, Kinoshita M, Akaike A, Satoh M, Mori Y, Kaneko S. Activation of inositol 1,4,5-trisphosphate receptor is essential for the opening of mouse TRP5 channel. Mol Pharmacol 2001;60:989–998. [PubMed: 11641427]
60. Hilgemann DW, Feng S, Nasuhoglu C. The complex and intriguing lives of PIP2 with ion channels and transporters. Science's STKE 2001;2001(111):RE19.
61. Suh BC, Hille B. Regulation of ion channels by phosphatidylinositol 4,5-bisphosphate. Curr Opin Neurobiol 2005;15:370–378. [PubMed: 15922587]
62. Logothetis D, Nilius B. Dynamic changes in phosphoinositide levels control ion channel activity. Pflugers Arch. 2007
63. Rohacs T, Lopes CM, Michailidis I, Logothetis DE. PI(4,5)P2 regulates the activation and desensitization of TRPM8 channels through the TRP domain. Nat Neurosci 2005;8:626–634. [PubMed: 15852009]
64. Runnels LW, Yue L, Clapham DE. The TRPM7 channel is inactivated by PIP2 hydrolysis. Nature Cell Biol 2002;4:329–336. [PubMed: 11941371]
65. Lemonnier L, Trebak M, Putney JW Jr. Complex regulation of the TRPC3, 6 and 7 channel subfamily by diacylglycerol and phosphatidylinositol-4,5-bisphosphate. Cell Calcium 2008;43:506–514. [PubMed: 17942152]
66. Cho H, Kim YA, Yoon JY, Lee D, Kim JH, Lee SH, Ho WK. Low mobility of phosphatidylinositol 4,5-bisphosphate underlies receptor specificity of Gq-mediated ion channel regulation in atrial myocytes. Proc Natl Acad Sci U S A 2005;102:15241–15246. [PubMed: 16217031]

67. Lukacs V, Thyagarajan B, Varnai P, Balla A, Balla T, Rohacs T. Dual regulation of TRPV1 by phosphoinositides. J Neurosci 2007;27:7070–7080. [PubMed: 17596456]

68. Bezzerides VJ, Ramsey IS, Kotecha S, Greka A, Clapham DE. Rapid vesicular translocation and insertion of TRP channels. Nat Cell Biol 2004;6:709–720. [PubMed: 15258588]

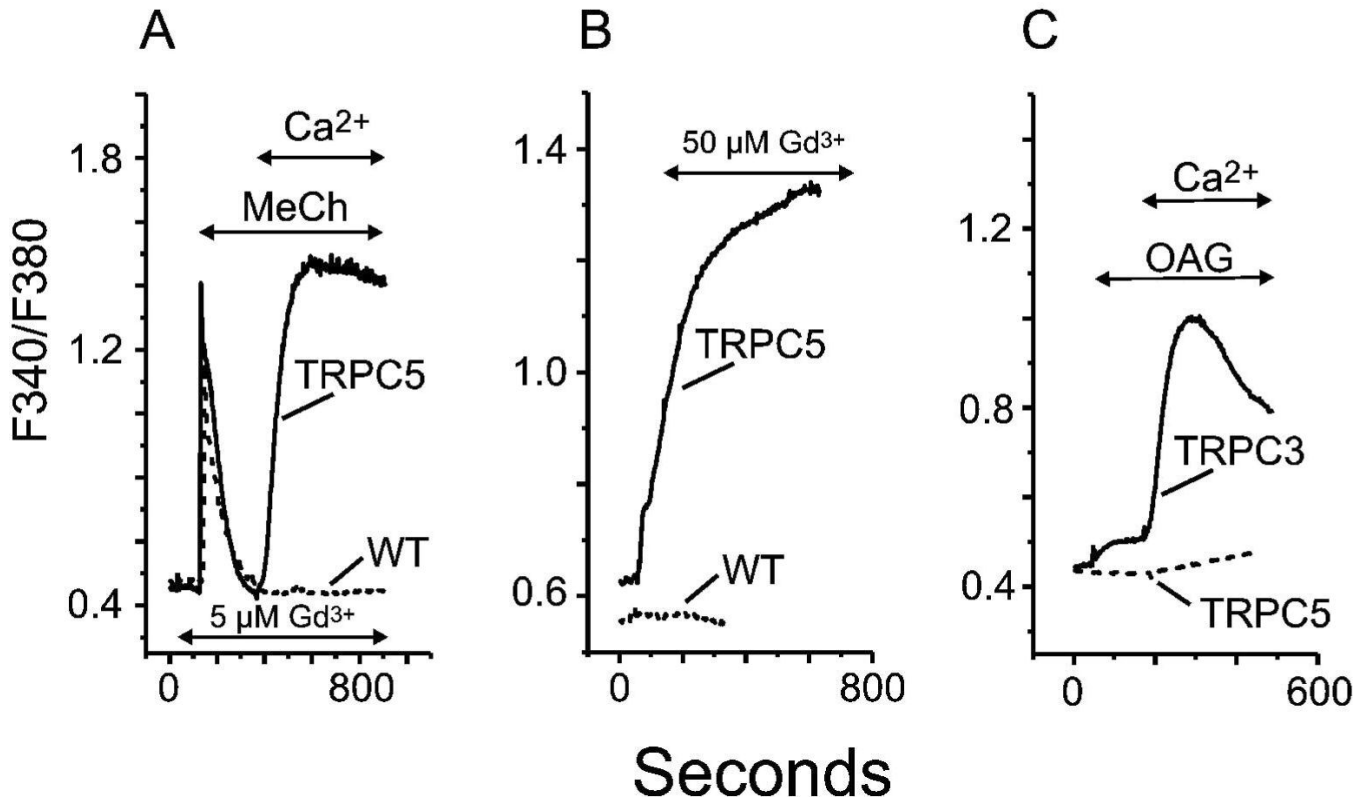

Figure 1. Modes of activation of TRPC5

A. HEK293 cells stably expressing TRPC5 channels exhibit a receptor-induced Ca^{2+} entry that is insensitive to low concentrations of Gd^{3+} (5 μM Gd^{3+}) that block the endogenous capacitative calcium entry (solid trace). Agonist-induced Ca^{2+} entry in wild type HEK293 (HEK-Wt) cells is completely abolished by 5 μM Gd^{3+} (dotted trace). B. TRPC5 channels can be activated by high concentrations of Gd^{3+} (50 μM). 50 μM Gd^{3+} induces a calcium entry in TRPC5-expressing HEK293 cells (solid trace) but not in wild type cells (dotted trace). C. Unlike TRPC3 channels that can be activated by diacylglycerol analogs (OAG, solid trace), TRPC5-expressing HEK293 cells show no calcium entry after addition of 100 μM OAG (dotted trace). OAG failed to activate TRPC5 even in the presence of protein kinase C inhibitors (data not shown). In A and C, experiments were initiated in the absence of Ca^{2+}, and Ca^{2+} restored as indicated, while in B, Ca^{2+} was present throughout. Shown are average traces from 23–58 cells, representative of a total of at least 4 independent experiments.

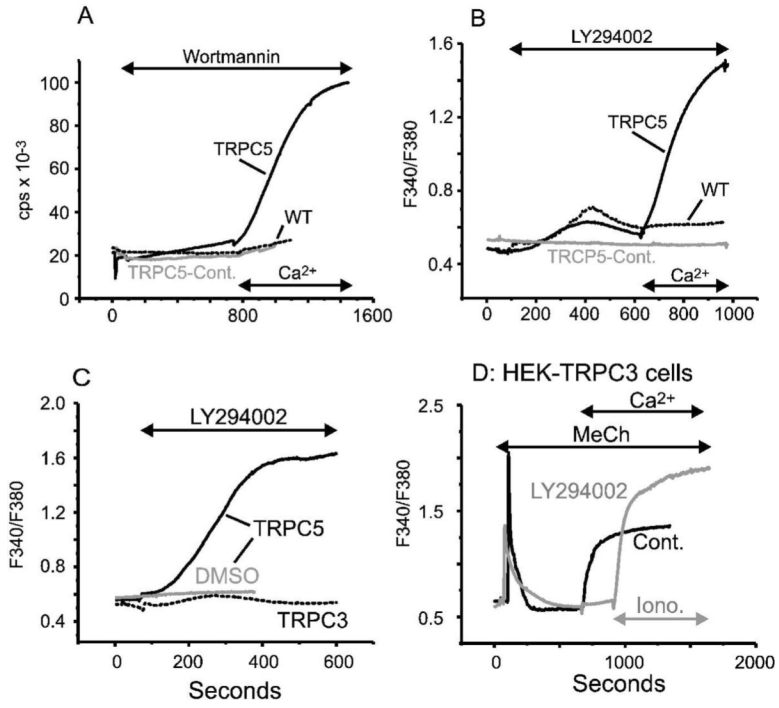

Figure 2. Phosphatidylinositol 4-kinase (PI-4K) inhibitors activate TRPC5 but not TRPC3

A. Wortmannin (20 μM) induces Ca^{2+} entry in TRPC5-expressing HEK293 cells (solid trace) but has no effect on wild type cells (dotted trace, WT). Gray trace: DMSO control for TRPC5 cells. B. Similar results are obtained for another PI-4K inhibitor, LY294002 (100 μM). C. LY294002 (100 μM) activated a robust Ca^{2+} entry in TRPC5-expressing HEK293 cells (solid trace) while it had no effect on TRPC3-expressing cells (dotted trace). Gray trace, DMSO control for TRPC5 cells. D. LY294002 (100 μM) inhibited TRPC3-mediated Ca^{2+} entry in response to agonist stimulation (methacholine, MeCh 300 μM). Black trace, absence of LY294002; gray trace, presence of LY294002; Iono., 10 μM ionomycin. Shown are average traces from at least 50 cells, representative of a total of 3–8 independent experiments.

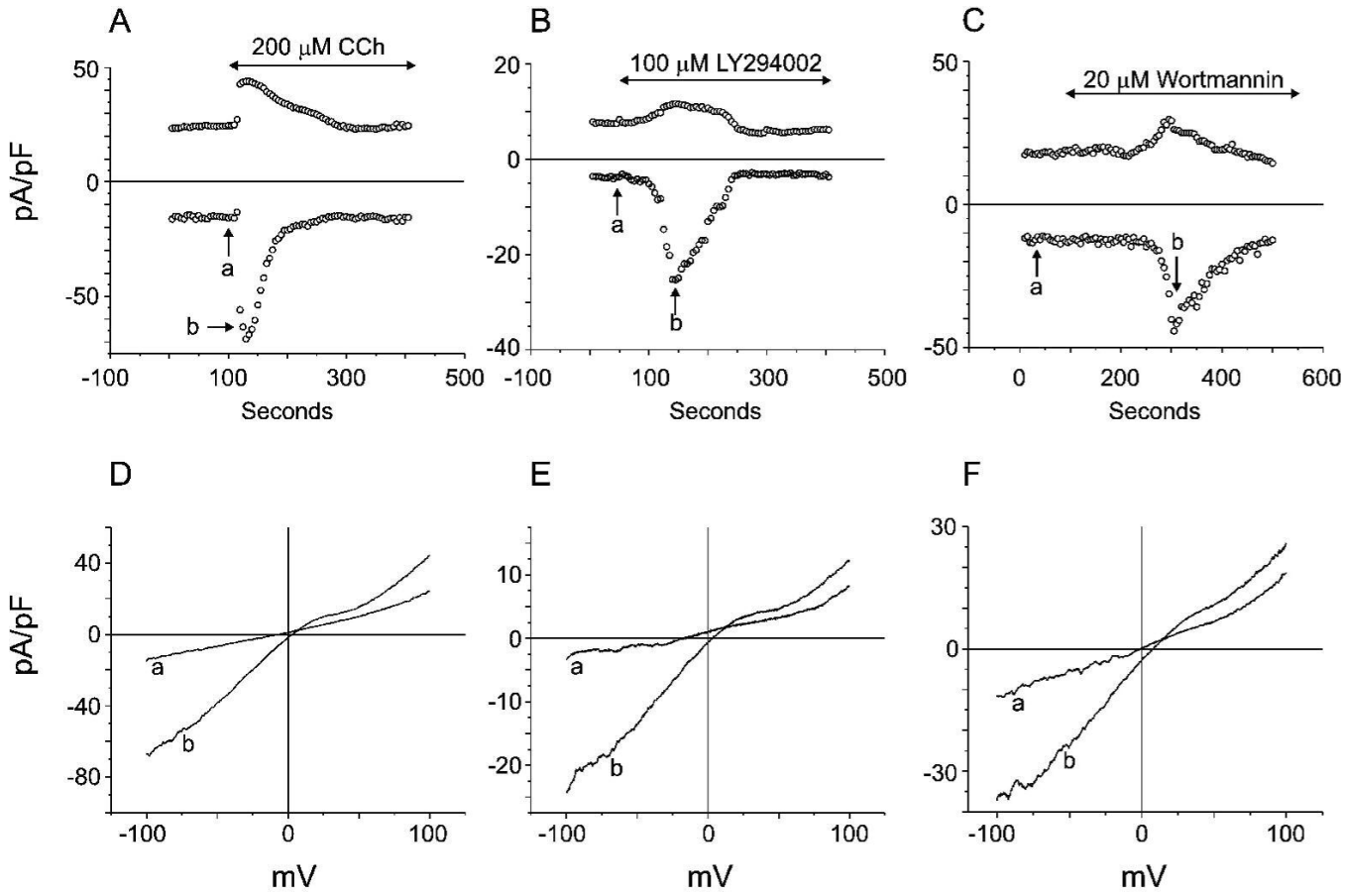

Figure 3. The muscarinic agonist carbachol (200 μM), and the PI4-K inhibitors, LY294002 (100 μM) and Wortmannin (20 μM) activate inward and outward currents measured by the perforated patch technique in TRPC5-expressing HEK293 cells

The upper panels show representative time courses of current development (at −100 and +100 mV) using the Nystatin-perforated patch mode before and after stimulation with CCh (200 μM; A), LY294002 (100 μM, B) and Wortmannin (20 μM, C). Lower panels show the corresponding current/voltage (I/V) relationship for CCh (D), LY294002 (E) and Wortmannin (F). Sweeps were taken before (a) and after (b) addition of stimuli at the times indicated in the corresponding time course traces (upper panels). In these experiments, series resistance was in the range of 33 – 50 MΩ.

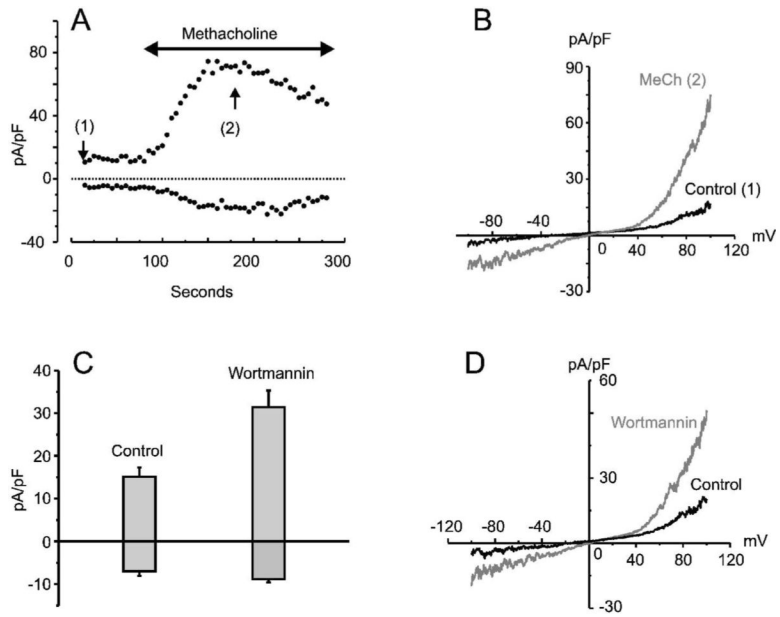

Figure 4. The muscarinic agonist methacholine (300 μM) and Wortmannin (20 μM) activate an inward and outward current measured by the whole-cell patch-clamp technique in TRPC5-expressing HEK293 cells

A. Whole cell current densities in a TRPC5-expressing cell sampled at +100 mV and −100 mV. B. Current Voltage (I/V) relationship in a TRPC5-expressing cell subjected to 250 ms voltage ramps between −100 and +100 mV, before (black trace) and after (gray trace) addition of methacholine. Representative of 6 independent experiments. C. Wortmannin (20 μM) induces an increase in both inward and outward whole cell currents in TRPC5-expressing cells, with no effect on HEK-Wt or TRPC3-expressing HEK293 cells (not shown). The data are averages of the maximum inward and outward currents before and after wortmannin addition from 17 (control) and 15 (wortmannin) experiments. D. The IV curve obtained after addition of wortmannin (20 μM) to TRPC5-expressing cells is similar to that obtained after stimulation of these cells with methacholine (see B). Representative data from a single experiment from the experiments summarized in C.

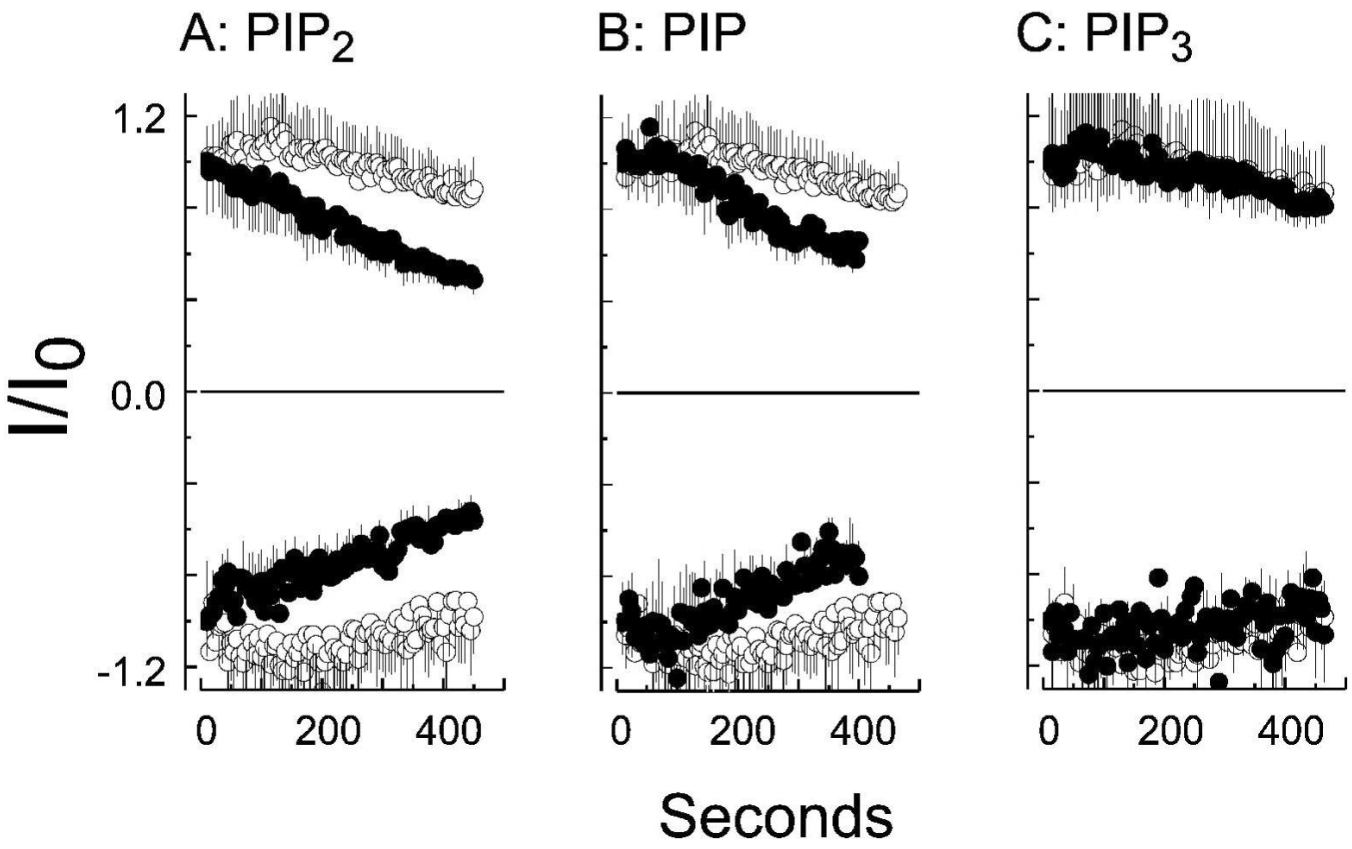

Figure 5. PIP_2 and PIP, but not PIP_3 inhibit wortmannin-activated TRPC5 currents

A. TRPC5-expressing HEK293 cells were treated with wortmannin (20 μM) for 30 minutes. Whole cell measurements were made in the absence (open circles, n=6) or presence (filled circles) of 20 μM PIP_2 (n=6, panel A), 20 μM PIP (n=5, panel B), or 20 μM PIP_3 (n=6, panel C) in the patch pipette. After break-in, there was a brief period of current run-up (~10 pA/pF). Following stabilization of the current, (~50 sec), data (outward at +100 mV, inward at −100 mV) were collected and normalized by ratio to the initial current density (I_0). The differences (control vs. lipid-treated) in inward and outward currents at the end of data collection were analyzed by t-tests; the levels of significance were: PIP_2, inward, P = 0.059 (NS), outward, P = 0.004; PIP, inward, P = 0.049, outward, P = 0.012; PIP_3, inward, P = 0.445 (NS), outward, P = 0.519 (NS).

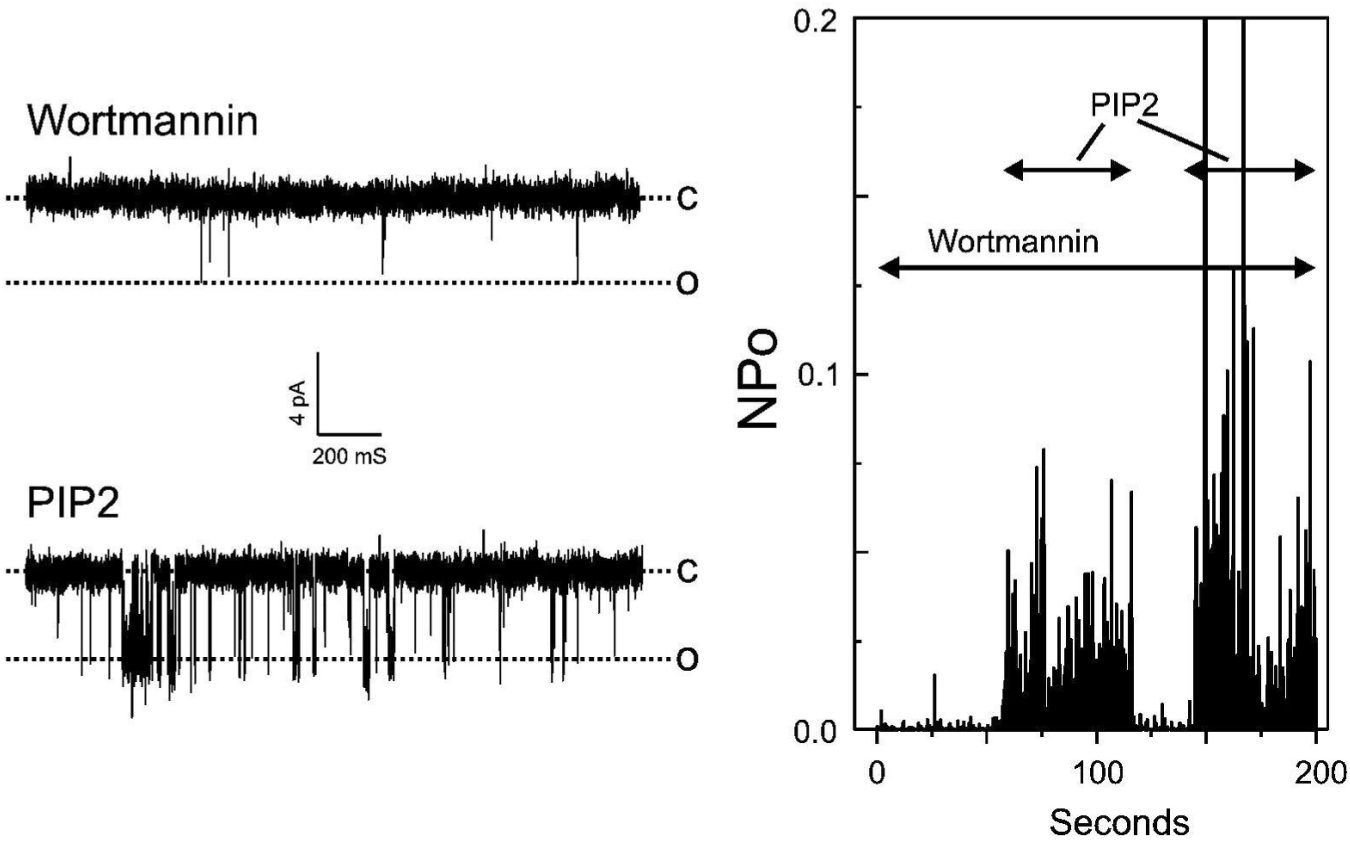

Figure 6. PIP_2 directly activates TRPC5 channels in the inside-out configuration

A: Representative traces showing TRPC5 activity at +60 mV immediately after excising a membrane patch from a cell exposed to wortmannin (top trace), and after a subsequent application of 10 μM PIP_2 (bottom trace). B: Corresponding NPo versus time plots for the same cell. Arrows indicate solution exchanges.

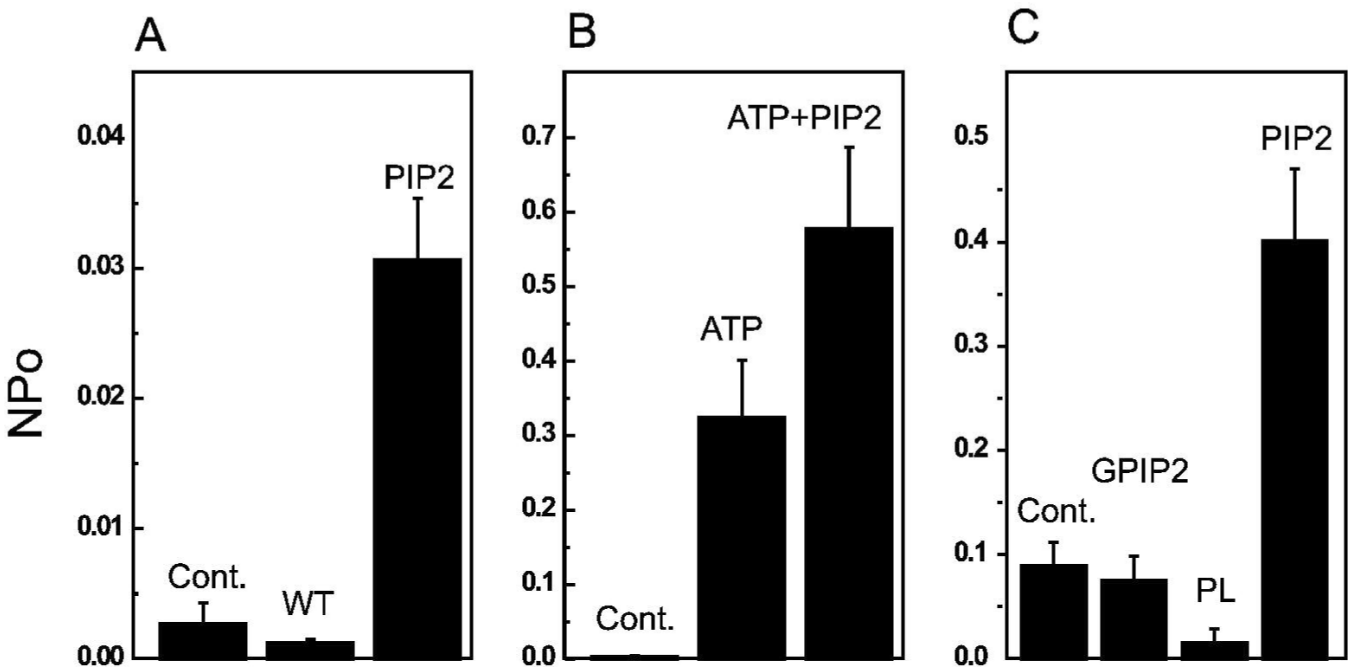

Figure 7. TRPC5 is specifically activated by PIP_2 at the single channel level

A: Histograms summarizing changes observed in NPo at +60 mV during inside-out experiments where patches were exposed to a regular external solution (cont.), and then to the same solution supplemented with 20 μM wortmannin alone (WT) or in the presence of 10 μM PIP_2; representative of 4 patches obtained in 4 independent cells. B: Same as in A, but patches were exposed to 5 mM ATP alone (ATP) or in the presence of 10 μM PIP_2 (ATP+PIP_2); representative of 4 patches obtained in 4 independent cells. C: Same as A and B, but patches were sequentially exposed to the regular external solution (Cont.), 10 μM $GPIP_2$, 0.5 μg/ml poly-L-Lysine (PL) and 10 μM PIP_2; representative of 6 patches obtained in 6 independent cells.

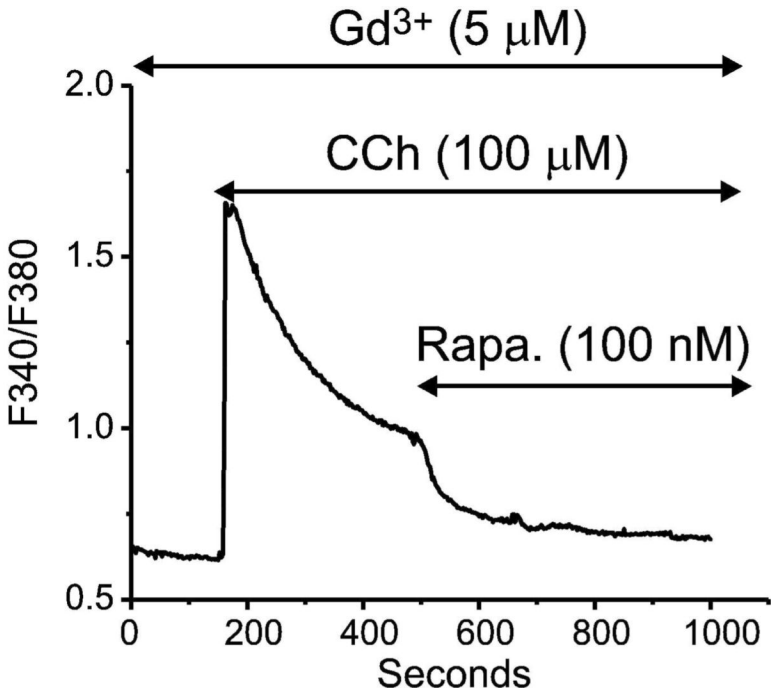

Figure 8. PIP2 depletion using plasma membrane targeted- PI5-phosphatase inhibits TRPC5

Time course of average fluorescence ratio in TRPC5-expressing HEK293 cells loaded with Fura-2. Cells were exposed to a maximal dose of Carbachol (CCh: 100 μM) in the presence of 2 mM external Ca^{2+} solution and a low dose of Gd^{3+} (5 μM) to block the endogenous store-operated Ca^{2+} entry pathway, as indicated by the horizontal arrow bars. Once the TRPC5-mediated Ca^{2+} entry fully developed, rapamycin (100 nM) was added where indicated. The trace shown represents average data of 21 cells from a recording representative of at least four separate experiments.

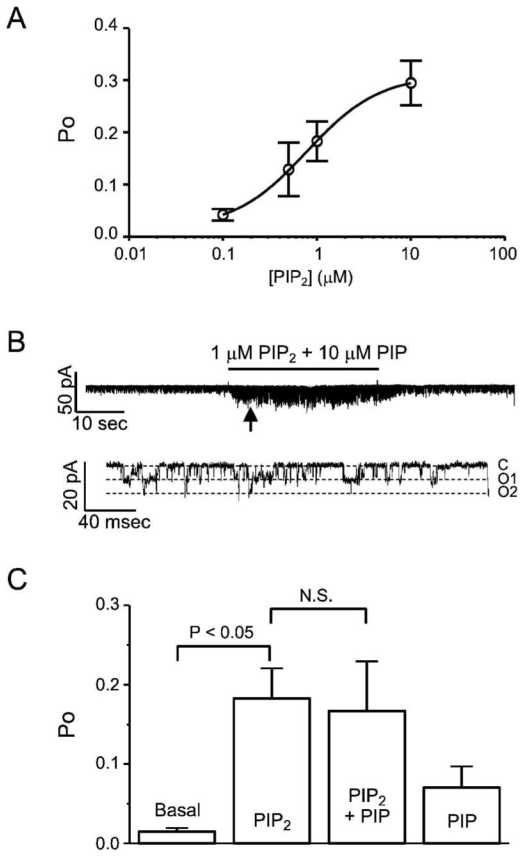

Figure 9. PIP weakly activates TRPC5 channels, but does not interfere with the ability of PIP_2 to activate the channels

A: Concentration-response curve showing the concentration-dependent effects of bath applied PIP_2 on TRPC5 channels. Single channel events were recorded at 80 mV (10 μM: n=4; 1 μM: n=10; 500 nM: n=4; 100 nM: n=4). B: Representative traces showing TRPC5 activity before, during and after the simultaneous addition of 1 μM PIP_2 and 10 μM PIP to the cytosolic side of the membrane patch through the bathing solution. Arrow on top trace indicates where the 300 msec bottom trace was taken, showing TRPC5 activity under the presence of both PIP and PIP_2. C: Bar graph indicating the effects of 1μM PIP_2 alone (n=10), 10 μM PIP alone (n=3), or PIP_2 plus PIP (n=7) (added simultaneously as seen in panel B), as well as TRPC5 basal activity recorded before the addition of PIP or PIP2 (n=8). Error bars indicate means ± SEM.

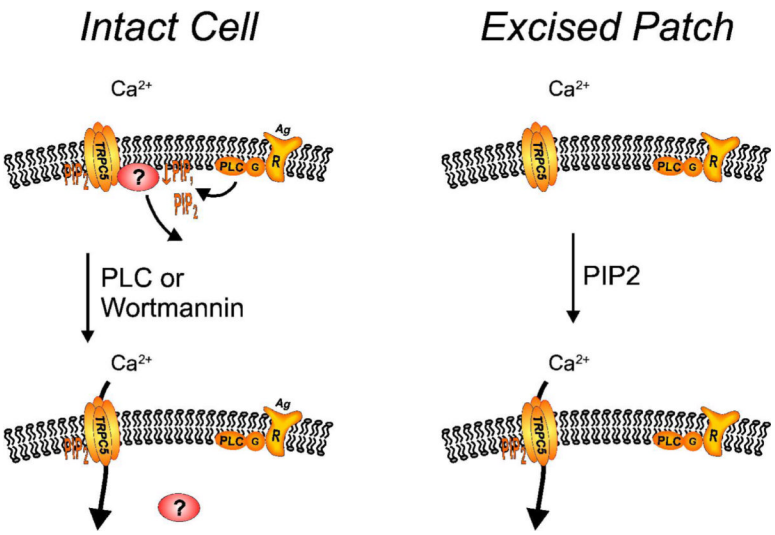

Figure 10. Model for PIP_2 regulation of TRPC5 channels

In intact cells, agonist (Ag) activation of PLC, or inhibition of PI4-K by wortmannin, leads to reduction of PIP or PIP_2, and dissociation of a polyphosphoinositide-dependent inhibitor of TRPC5. PIP_2 associated with the channel is required for activity; thus, removal of the PIP_2-dependent inhibitor leads to channel activation. In excised patches, both the PIP2 required for channel activity, as well as the inhibitor are lost; thus addition of PIP_2 leads to robust channel activation.

Article 5

TRP channel–associated factors are a novel protein family that regulates TRPM8 trafficking and activity

Dimitra Gkika,[1] Loic Lemonnier,[1] George Shapovalov,[1] Dmitri Gordienko,[1] Céline Poux,[2] Michela Bernardini,[1,6] Alexandre Bokhobza,[1] Gabriel Bidaux,[3] Cindy Degerny,[4] Kathye Verreman,[4] Basma Guarmit,[5] Mohamed Benahmed,[5] Yvan de Launoit,[4] Rene J.M. Bindels,[7] Alessandra Fiorio Pla,[1,6] and Natalia Prevarskaya[1]

[1]Inserm U1003, Equipe labellisée par la Ligue Nationale Contre le Cancer, Université des Sciences et Technologies de Lille (USTL), 59655 Villeneuve d'Ascq Cedex, France
[2]Centre national de la Recherche Scientifique (CNRS) UMR 8198 and Laboratoire de Génétique & Evolution des Populations Végétales (GEPV), Université des Sciences et Technologies de Lille (USTL), 59655 Villeneuve d'Ascq Cedex, France
[3]Laboratoire Biophotonique Cellulaire Fonctionnelle, Institut de Recherche Interdisciplinaire, USR3078 Centre National de la Recherche Scientifique, Parc scientifique de la Haute Borne, Villeneuve d'Ascq, F-59655 France
[4]CNRS UMR 8161, Institut de Biologie de Lille, Université de Lille—Nord de France, Institut Pasteur de Lille, 59019 Lille Cedex, France
[5]Inserm, Institut National de la Santé et de la Recherche Médicale U895, Centre Méditerranéen de Médecine Moléculaire, Hôpitall'Archet, 06204 Nice, France
[6]Department of Life Science and Systems Biology, University of Torino, 10123 Torino, Italy
[7]Department of Physiology, Radboud University Nijmegen Medical Centre, 6500HB Nijmegen, Netherlands

TRPM8 is a cold sensor that is highly expressed in the prostate as well as in other non-temperature-sensing organs, and is regulated by downstream receptor–activated signaling pathways. However, little is known about the intracellular proteins necessary for channel function. Here, we identify two previously unknown proteins, which we have named "TRP channel–associated factors" (TCAFs), as new TRPM8 partner proteins, and we demonstrate that they are necessary for channel function. TCAF1 and TCAF2 both bind to the TRPM8 channel and promote its trafficking to the cell surface. However, they exert opposing effects on TRPM8 gating properties. Functional interaction of TCAF1/TRPM8 also leads to a reduction in both the speed and directionality of migration of prostate cancer cells, which is consistent with an observed loss of expression of TCAF1 in metastatic human specimens, whereas TCAF2 promotes migration. The identification of TCAFs introduces a novel mechanism for modulation of TRPM8 channel activity.

Introduction

Transient receptor potential (TRP) channels form a large family of cation channels involved in a diverse range of physiological functions, and are expressed in almost all cell types (Clapham, 2003). They play important roles ranging from Ca^{2+} absorption, vasorelaxation, cell death, mechanotransduction, and hearing, to the mediation of pH, heat, taste, osmolarity, and pain sensations. Dysfunctions of TRP channels have been linked to several diseases (Nilius et al., 2007). Among members of the TRP channel family, the function of TRPM8 could be considered one of the most intriguing. Although it was initially cloned from the prostate (Tsavaler et al., 2001; Stein et al., 2004) and is expressed in tissues not affected by ambient temperature fluctuations such as the prostate, testis, and bladder (Tsavaler et al., 2001; Stein et al., 2004), this channel is mainly known as the principal detector of environmental cold (Bautista et al., 2007; Colburn et al., 2007; Dhaka et al., 2007).

TRPM8 expression is strongly up-regulated in numerous cancers such as that of the prostate, but is dramatically reduced during metastasis in androgen-independent prostate cancers (Tsavaler et al., 2001; Henshall et al., 2003; Yee et al., 2010). This pattern of variation of TRPM8 expression makes it an interesting candidate both as a diagnostic marker for the detection of certain cancers and as a prognostic marker in evaluating the

D. Gkika, L. Lemonnier, and G. Shapovalov contributed equally to this paper.
Correspondence to Dimitra Gkika: dimitra.gkika@univ-lille1.fr
D. Gordienko's present address is Laboratory of Molecular Pharmacology and Biophysics of Cell Signalling, Bogomoletz Institute of Physiology, State Key Laboratory of Molecular and Cell Biology, 01024 Kiev, Ukraine.

Abbreviations used in this paper: EAPA2, Experimental Autoimmune Prostatitis Antigen 2; FRET, Förster resonance energy transfer; HEK, human embryonic kidney; LNCaP, lymph node carcinoma of prostate; ML, maximum likelihood method; qPCR, quantitative real-time PCR; TCAF, TRP channel–associated factor; TCSPC, time-correlated single photon counting; TD FLIM, time-domain fluorescence lifetime imaging microscopy; TRP, transient receptor potential.

Supplemental material can be found at:
http://doi.org/10.1083/jcb.201402076

The Rockefeller University Press $30.00
J. Cell Biol. Vol. 208 No. 1 89–107
www.jcb.org/cgi/doi/10.1083/jcb.201402076

outcome of these cancers (Zhang and Barritt, 2006). In addition, it could play a protective role in metastatic prostate cancer (Gkika and Prevarskaya, 2011), as recent data show that it blocks the migration of prostate cancer cells (Yang et al., 2009; Gkika et al., 2010; Zhu et al., 2011). Thus, although TRPM8 is considered to be a promising target for pharmaceutical, immunological, and genetic interventions for the treatment of prostate cancer (Zhang and Barritt, 2006), it is first necessary to better understand its biological function and the physiological modulators in this organ.

Besides cool temperatures, TRPM8 is also activated by several chemical compounds that elicit a sensation of cold, of which the best known are menthol, eucalyptol, and the supercooling icilin (McKemy et al., 2002; Peier et al., 2002; Behrendt et al., 2004; Chuang et al., 2004; Beck et al., 2007; Bödding et al., 2007). Chemical agents generally serve as positive allosteric modulators. More specifically, because the activation of TRPM8 is also voltage dependent, these agonists shift the activation threshold toward more negative potentials, enabling the channel to open at higher than normal temperatures, whereas antagonists exert their effect by shifting the threshold of TRPM8 activation toward more positive potentials (Brauchi et al., 2004; Voets et al., 2004; Mälkiä et al., 2007).

In the absence of the aforementioned physical and chemical stimuli, as could be the case in non-temperature-sensing tissues, TRPM8 could be kept in readiness in a dynamic pool of vesicles under the cell surface, awaiting the appropriate signal for plasma membrane insertion and channel activation (Veliz et al., 2010; Latorre et al., 2011). This dynamic TRPM8 pool could be activated by intracellular factors known to modulate TRPM8 activity, such as second messengers generated during the activation of surface-receptor–coupled signaling pathways (Bavencoffe et al., 2010, 2011; Latorre et al., 2011; Yudin and Rohacs, 2012; Zhang et al., 2012; Shapovalov et al., 2013a). However, the intracellular elements involved in controlling the stabilization of the channel on the cell surface and the subsequent amplification of its activity are currently unknown.

Several studies show that TRP channels can be regulated by partner proteins affecting their trafficking to the plasma membrane (Vogel et al., 2007) and/or their channel activity (van de Graaf et al., 2003, 2006; Gkika et al., 2004, 2006a,b; Sinkins et al., 2004; Chang et al., 2005; Köttgen and Walz, 2005). Indeed, the regulated translocation of TRP channels appears to be a key mechanism for the gating of constitutively active subunits, as well as for enhancing the activity of stimulus-gated channels (Shapovalov et al., 2013a). Thus, the identification of the molecular components implicated in this cellular process is of great importance in understanding not only the regulatory mechanisms of TRP channels but also their function.

To identify and characterize the molecular determinants of TRPM8 regulation, we performed a screening for TRPM8 partner proteins in the prostate, where the channel is primarily expressed. As a result, we have identified a previously uncharacterized protein family as a first example of TRPM8 regulators.

Results

Identification of the TRP channel–associated factors (TCAFs): a family of TRPM8 partner proteins

To identify TRPM8 regulatory proteins, which have not been identified until now, we performed a GST pull-down assay to screen lysates of healthy mouse prostates, with the N-terminal and C-terminal cytosolic tails of TRPM8 as bait. Fourier transform ion cyclotron resonance mass spectrometry (FTMS) revealed mouse Experimental Autoimmune Prostatitis Antigen 2 (EAPA2) as a protein interacting with TRPM8. The full list of peptides interacting with TRPM8 cytosolic tails is presented in Tables S1 and S2. As EAPA2 is not known in humans, we searched for highly homologous proteins using National Center for Biotechnology Information (NCBI) Blast. Two proteins of unknown function, FAM115A, consisting of 921 amino acids (NP_055534), and FAM115C, consisting of 845 amino acids (NP_001123497), were thus identified and named TCAF1 and -2. The alignment of these two proteins with EAPA2 (hereafter renamed TCAF3) revealed 51% and 57% of identity, respectively. Once substitutions by similar residues were taken into account, the similarity between TCAF3 and TCAF1 or TCAF2 reached 69% and 66%, respectively (see Fig. 2), which suggests that they may have a common origin and belong to the same group of genes.

Indeed, a phylogenetic analysis of TCAF1, TCAF2, and TCAF3 revealed the presence of a putative gene family. Given the sequences available in GenBank, we determined two duplication events (Fig. 1 A), supported by both posterior probabilities (PP; Bayesian method) and bootstrap supports (BP; maximum likelihood method [ML]). In mammals, up to three highly similar genes were found (TCAF1, TCAF2, and TCAF3), whereas only one gene copy was seen in fish, amphibians, and birds. The mammalian TCAF1 and TCAF2 sequences are phylogenetically closer to each other than to the other vertebrate sequences. Therefore the first duplication event most likely occurred during mammalian evolution. Given the poor taxon sampling available in the database, it was not possible to precisely determine the period of duplication. A second duplication event appears to have taken place during rodent evolution to generate the TCAF3 gene (Fig. 1 A).

Although mouse TCAF3 is mainly expressed in the prostate, nothing is known about the tissue distribution of the newly identified human homologues. We thus examined TCAF1 and TCAF2 expression in several human tissue samples using quantitative real-time PCR (qPCR). Both transcripts were predominantly expressed in the prostate (Fig. 1 B), similar to TCAF3 in rodents and TRPM8 in humans and rodents.

Both TCAF1 and TCAF2 interact directly with the TRPM8 channel

To verify the association of human TCAF1 and TCAF2 proteins with TRPM8, we cloned TCAF1 and TCAF2 and studied their interaction with TRPM8 by GST pull-down assays. In vitro-translated [^{35}S]methionine-labeled TCAF1 and TCAF2 strongly interacted with the TRPM8 N-terminal tail (GST-M8N) and to

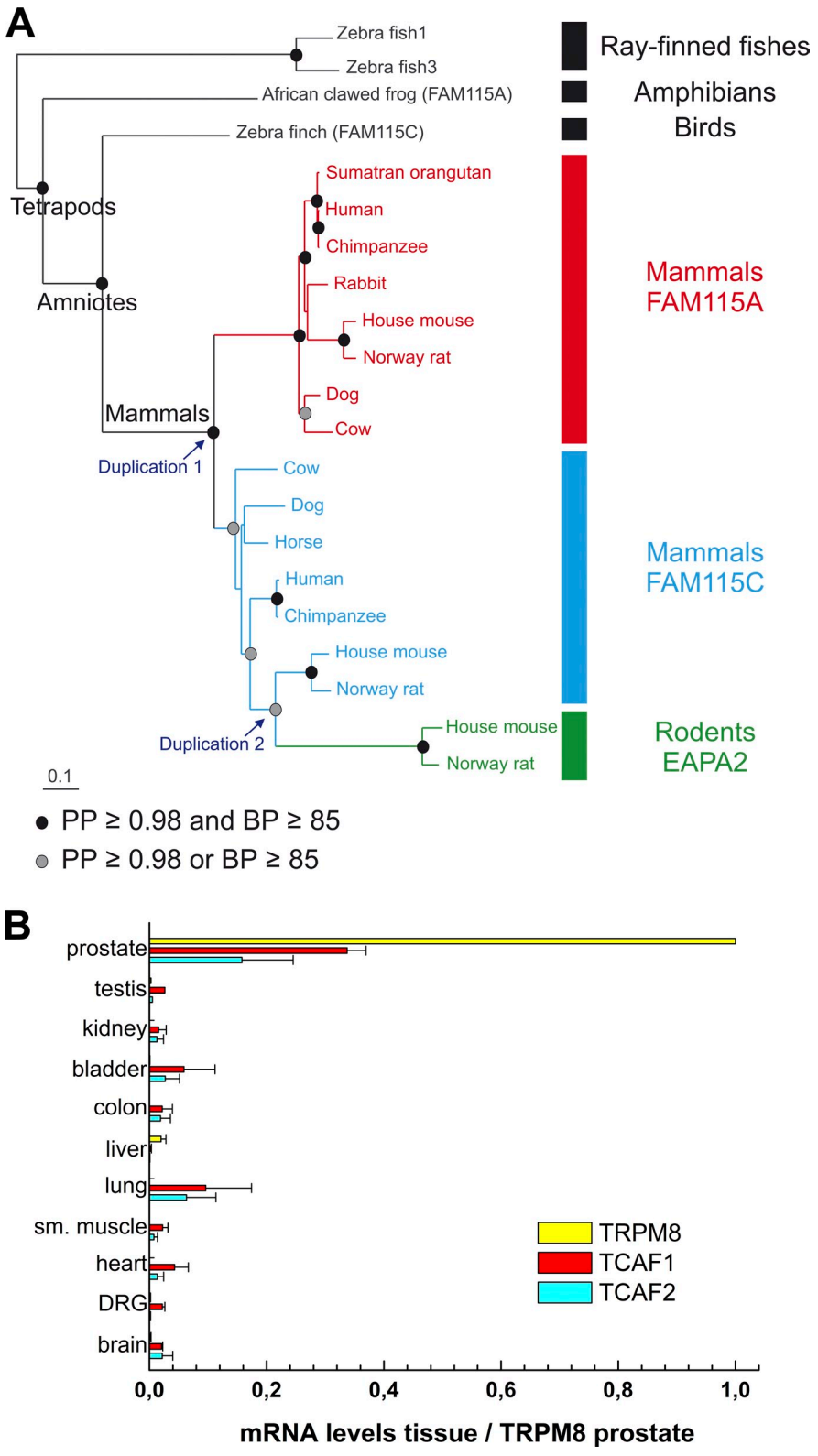

Figure 1. **Bayesian phylogenetic tree of the vertebrate *TCAF1/TCAF2/TCAF3* genes and tissue expression pattern of the human homologues.** (A) The maximum likelihood tree was similar but for one node: the cow and horse FAM115C sequences were sister groups. The phylogenetic reconstruction displays two duplication events, one during the early period of mammalian evolution and the other during rodent evolution. The scale bar represents the number of expected changes per site. (B) Analysis of TRPM8, TCAF1, and TCAF2 mRNA expression levels by qPCR in several human tissues. Values are expressed relative to 18S rRNA expression, and further normalized to TRPM8 levels in the prostate. Values are presented as means of three experimental repeats ± SEM (error bars; $n = 3$ for a single experiment).

a lesser extent with the TRPM8 C-terminal tail (GST-M8C), whereas no interaction was observed with GST alone (Fig. 3 A). This interaction was further confirmed by immunoprecipitation experiments in human embryonic kidney (HEK) 293 cells transfected with either HA-tagged TCAF1 or myc-tagged TCAF2, with or without his-tagged full-length TRPM8. TRPM8 was present on the beads and was detected in the precipitated complex (IP) with TCAF1 and TCAF2. No band was detected in precipitated complexes from cells that were not transfected with TRPM8 or cells immunoblotted for another protein such as actin, which indicates the specificity of the interaction (Fig. 3 B). TCAF interactions with additional TRP channels were also analyzed

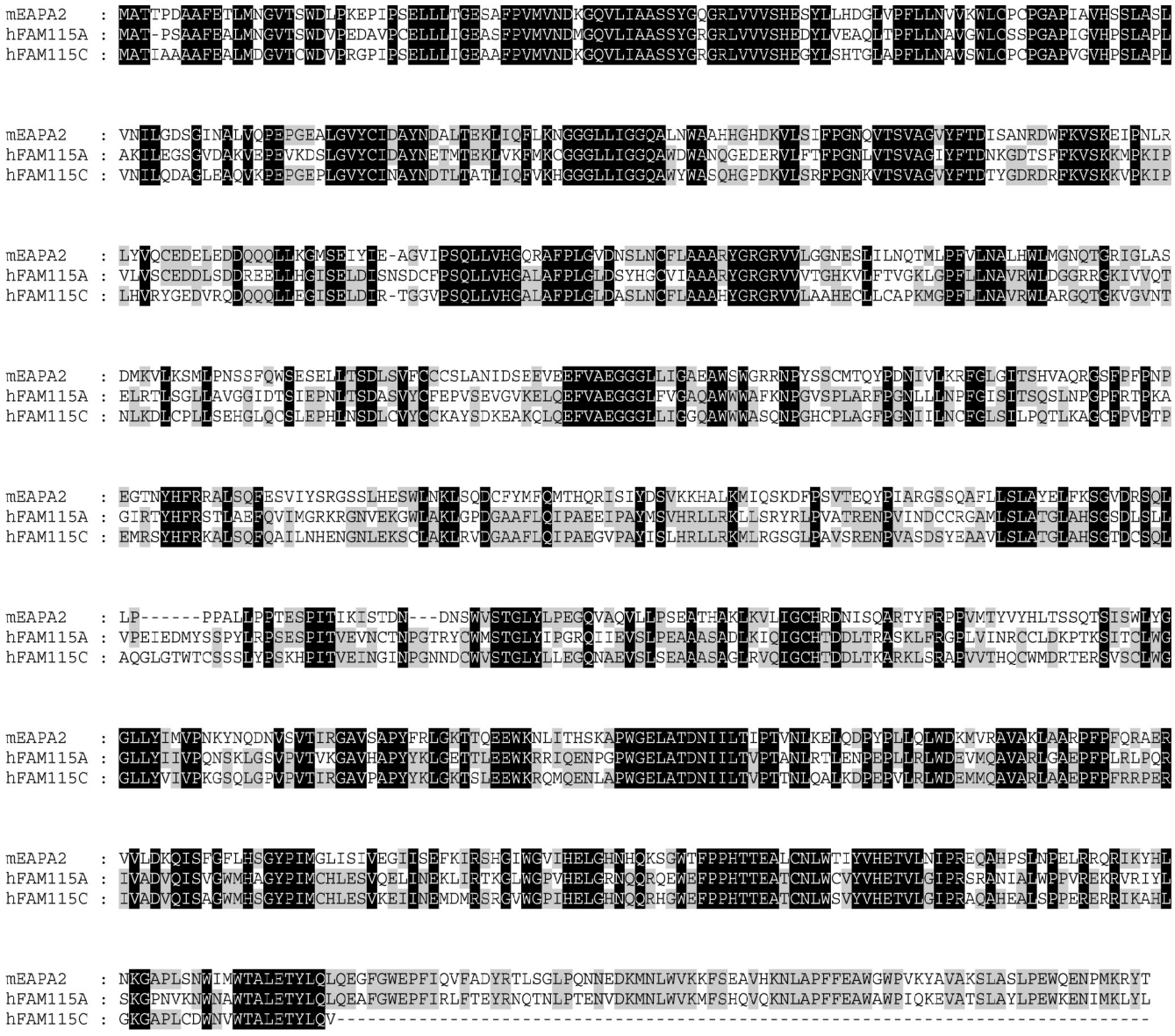

Figure 2. **Human homologues of TCAF3.** Alignment of hFAM115A (TCAF1) and hFAM115C (TCAF2) with the murine EAPA2 (TCAF3) protein. Amino acid residues are highlighted in black when present in the three proteins and in gray when they are present in only two of them.

by coimmunoprecipitation to check whether TCAF is a TRPM8-exclusive partner. Altogether, these results show that TCAFs are potential partner proteins for other TRP channels, such as TRPV6 and the short isoform of TRPM2 (Fig. S1, A and B).

Confocal imaging of the cells transfected with HA-tagged TCAF1 or myc-tagged TCAF2 and labeled with TRPM8 antibodies confirmed that both TCAFs colocalize with TRPM8 (Fig. S2, A and B). Direct interaction between the two proteins in living cells was confirmed by means of Förster resonance energy transfer (FRET) using the time-domain fluorescence lifetime imaging microscopy (TD FLIM). After the 24-h transfection, HEK cells expressing TRPM8-mTurquoise2 and TCAF-SYFP2 (Fig. 3 C) were analyzed using the time-correlated single photon counting (TCSPC) of the donor fluorescence (Fig. 3, D and E), and the lifetime of mTurquoise2 was computed on a pixel-by-pixel basis (Fig. 3, D and E). Statistical analysis revealed significant FRET between TRPM8 and TCAF1 or TCAF2 (Fig. 3 F). In control experiments on HEK cells expressing TRPM8-mTurquoise2 and free SYFP2, no significant variation of mTurquoise2 lifetime was detected (Fig. 3 F), and calculated E_{FRET} was found to be below the confidence threshold of 1%. These observations altogether with biochemical analysis of interaction confirmed in living cells that TCAFs are partners of the TRPM8 channels.

TCAFs exert opposing regulatory effects on TRPM8-mediated currents

To assess the functional effect of TCAF1–TCAF2 interactions with the TRPM8 channel in human prostate cells, we performed a series of patch-clamp experiments. The silencing of native TCAFs by siRNAs to TCAF1 or -2 was monitored by RT-PCR after 72 h, and specifically abolished TCAF1 or -2 expression

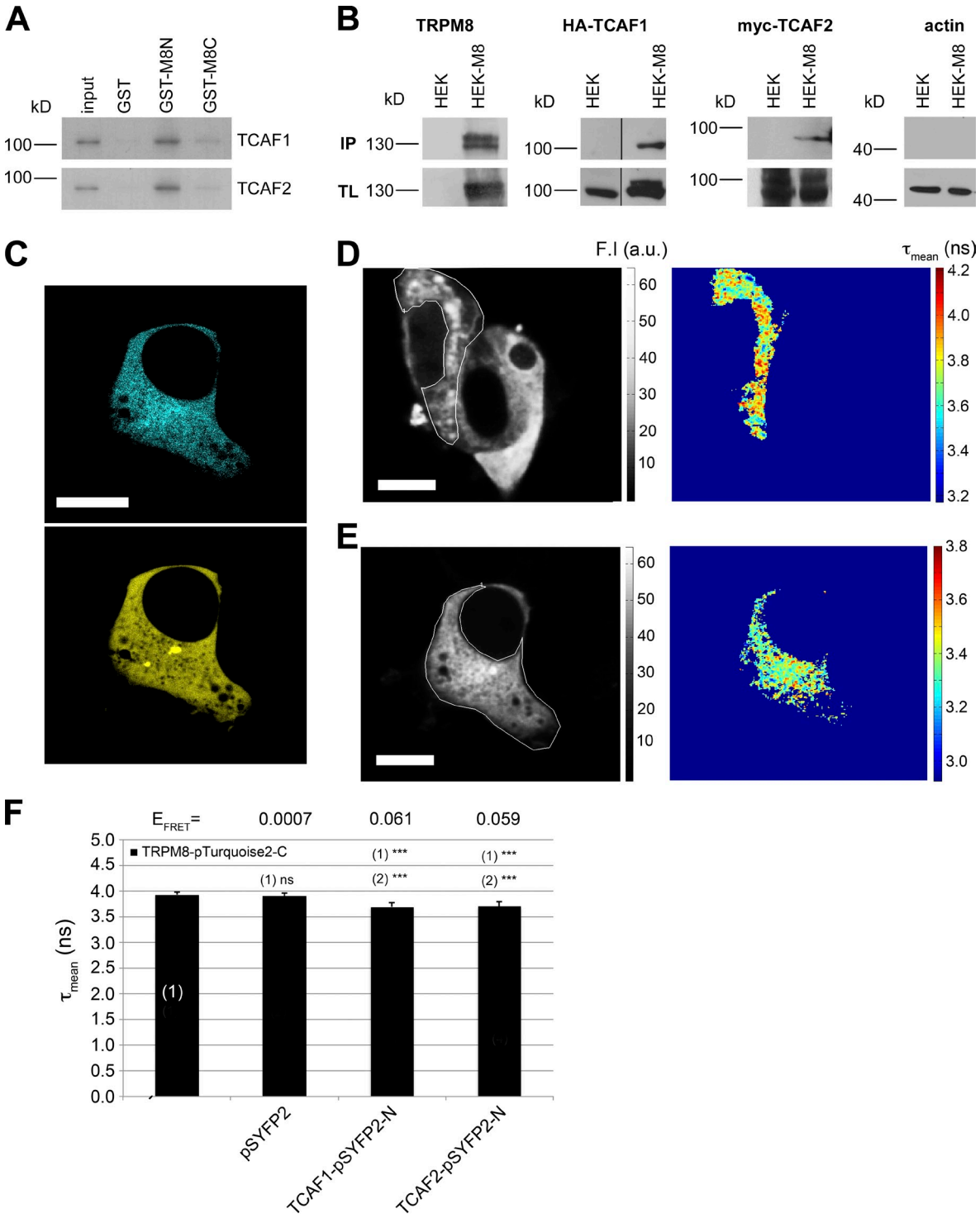

Figure 3. **TCAF1 and TCAF2 interact and colocalize with TRPM8.** (A) GST pull-down assay using [^{35}S]methionine-labeled TCAF1 or TCAF2 protein and GST or GST fused to the TRPM8 N-terminal tail (GST-M8N) or C-terminal tail (GST-M8C). (B) Cells transfected with HA-tagged TCAF1 or myc-tagged TCAF2 with (HEK-M8) or without (HEK) his-tagged full-length TRPM8, and total lysates (TL) were used for immunoprecipitation and subsequent immunoblot analysis. Immunoprecipitation of the channel was confirmed by immunoblotting for TRPM8, and the coimmunoprecipitation of TCAF1 or TCAF2 proteins was detected using an anti-HA or anti-myc antibody, respectively, on the immunoprecipitated complex (IP). No coimmunoprecipitation was detected in control immunoblots for actin. The black lines on the HA-TCAF1 blots indicate the removal of intervening lanes for presentation purposes. (C–F) TCAF1/2-to-TRPM8 binding was assessed by measuring FRET with TM FLIM in HEK293 cells after a 24-h transfection. The TCSPC approach was chosen to achieve a good spatial resolution, which would allow discriminating TRPM8-ER localization. (C) An example of concomitant expression of TRPM8-mTurquoise2 (cyan) and TCAF1-SYFP2 (yellow). (D and E) Representative FRET-FLIM images for TRPM8-mTurquoise alone and for TRPM8-mTurquoise + TCAF1-SYFP2, respectively. Grayscale-coded fluorescence images of the donor of FRET (left images in D and E; fluorescence intensity [FI] is given in arbitrary units [a.u.]) were analyzed by the phasor plot method (Phasor) to compute FLIM images (τ_{mean}) showing the mean lifetime (ns; right images of D and E). The outlines define the regions of interest for which mean lifetime of the donor of fluorescence was calculated. Bars, 10 µm. (F) Chart representing the mean lifetime of TRPM8-mTurquoise2 alone, coexpressed with the negative control SYFP2, or with TCAF1-SYFP2 or TCAF2-SYFP2. FRET efficiency (E_{FRET}) is shown on the top of the chart. Values are presented as means ± SD (error bars). ***, $P < 0.001$.

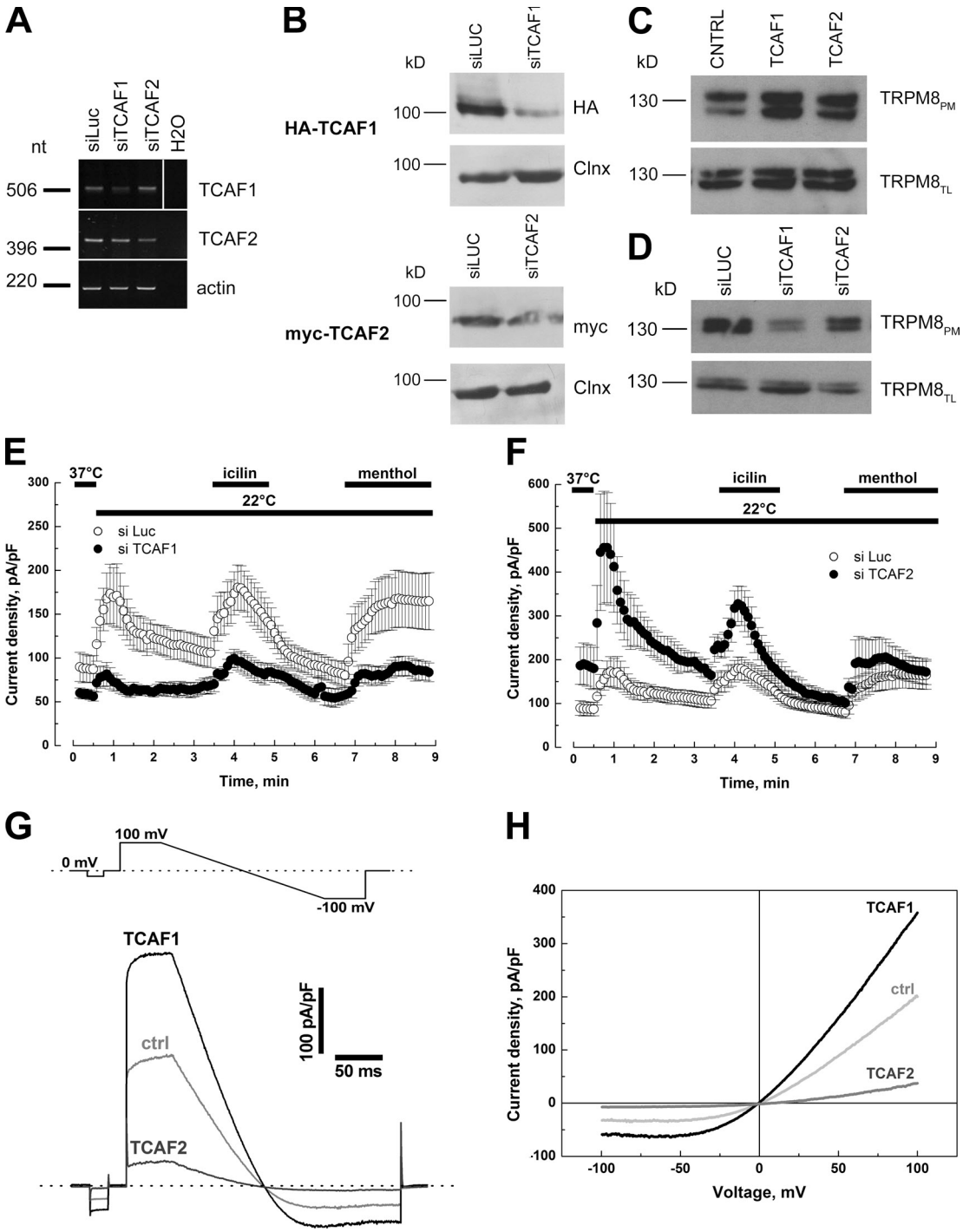

Figure 4. **TCAF1 and TCAF2 proteins have opposing effects on TRPM8 activity.** (A) Reverse-transcription PCR showing the specific decrease of TCAF1 (top) and TCAF2 (bottom) bands after cell transfection with 100 nM of the respective siRNAs. Actin was used to normalize relative expression, and siRNA to luciferase was used as a negative silencing control (siLuc). The white line on the TCAF1 gel indicates the removal of intervening lanes for presentation purposes. (B) Western blot analysis confirming the siRNA effect on HA-TCAF1– (top) and myc-TCAF2–transfected cells (bottom). Calnexin (Clnx) was used as a loading control. (C and D) Cell surface biotinylation analysis of TRPM8-transfected cells cotransfected with the empty vector (CTRL), TCAF1, or TCAF2 (C), or co-treated with siLuc, siTCAF1, or siTCAF2 (D). TRPM8 expression was analyzed by immunoblotting the plasma membrane fraction ($TRPM8_{PM}$) or total cell lysates ($TRPM8_{TL}$). Shown is the mean time course of cold- (22°C), icilin- (10 µM), and menthol-activated (500 µM) I_{TRPM8} in LNCaP cells transiently transfected with TRPM8 and treated with siLuc (open circles), siTCAF1 (E), or siTCAF2 (F; closed circles). Values are expressed as means ± SEM (error bars). (G) Single traces of menthol-evoked currents recorded in a representative LNCaP cell (out of five different cells per condition) transfected with TRPM8 and either an empty vector (ctrl), TCAF1, or TCAF2. Stimulation protocol is presented in the top panel. The corresponding IV relationships are presented in H.

at both the mRNA (Fig. 4 A) and protein levels, as seen after transfection with vectors expressing tagged proteins (Fig. 4 B). We then examined the role of the TCAFs in TRPM8 trafficking using biotin labeling. Cell-surface biotinylation experiments showed that both TCAFs enhanced channel expression in the biotinylated fraction when compared with cotransfection with

an empty vector (Fig. 4 C), whereas siRNA to TCAF1 significantly decreased channel abundance on the plasma membrane compared with control siRNAs (siLuc; Fig. 4 D).

In terms of channel activity, TCAF1 silencing in these cells at 37°C induced a decrease in basal TRPM8 activity from 88.2 ± 15.5 to 58.9 ± 5.3 pA/pF (Fig. 4 E). A similar inhibitory effect was observed on I_{TRPM8} currents evoked by cold, icilin, and menthol, which decreased from 158.1 ± 73.7, 111.6 ± 38.5, and 54.9 ± 16.4 pA/pF in control cells (n = 12) to 22.8 ± 13.3, 40.8 ± 10.1, and 32.3 ± 11.1 pA/pF, respectively, in cells transfected with TCAF1 siRNA (siTCAF1; n = 8). In contrast, TCAF2 silencing led to an increase in basal I_{TRPM8} amplitude from 88.2 ± 15.5 to 187.4 ± 47.9 pA/pF (Fig. 4 F), whereas responses to cold, icilin, and menthol were increased from 158.1 ± 73.7, 111.6 ± 38.5, and 54.9 ± 16.4 pA/pF in control cells (n = 12) to 341.3 ± 131.9, 164.2 ± 42.3, and 115.7 ± 62.2 pA/pF, respectively, in cells treated with TCAF2 siRNA (siTCAF2; n = 4). A histogram summarizing these results at both +100 and −100 mV is presented in Fig. S2 C, and shows similar effects of partner proteins silencing at both potentials. The overexpression of TCAF1 and TCAF2 had an opposite effect to that of the siRNAs, confirming the activating role of TCAF1 and the inhibitory role of TCAF2 on TRPM8 activity (n = 5; Fig. 4, G and H; and Fig. S2 D). These results clearly show that TCAF1 and -2 can modulate TRPM8 basal activity, therefore suggesting a potential role of this interaction in controlling calcium homeostasis. Moreover, TCAF1 and -2 effects on TRPM8 activity were equally observed for all tested potentials, thus precluding the existence of a voltage-dependent component to these interactions (Fig. 4 H).

The C-terminal tail of TCAF1 plays a critical role in TRPM8 regulation

TCAF1 and -2 both bind to TRPM8 and augment its targeting to the plasma membrane, while having different effects on channel activity. We therefore searched the protein sequences of TCAF1 and TCAF2 for domains that could explain this disparity. A low homology with the PI3K domain was predicted using the Conserved Domains software tool from NCBI on the C-terminal tail of TCAF1. Interestingly this domain is missing from the TCAF2 sequence, as shown in the diagram in Fig. 5 B.

To validate this putative PI3K domain in TCAF1 and assess its role in TRPM8 regulation, we first used a pharmacological approach, namely, a commonly used PI3K inhibitor wortmannin, at 1 µM. As shown in Fig. 5 A, pretreatment with wortmannin resulted in a massive decrease in I_{TRPM8} amplitude under resting conditions as well as during exposure to cold, icilin, or menthol.

Second, we generated a truncated version of TCAF1, which lacks the C-terminal tail that contains the PI3K homology domain ($TCAF1_{\Delta PI3K}$) and resembles TCAF2. The direct interaction of $TCAF1_{\Delta PI3K}$ with TRPM8 cytosolic tails was examined by GST pull-down. In vitro-translated [^{35}S]methionine-labeled TCAF1 and $TCAF1_{\Delta PI3K}$ both strongly interacted with the TRPM8 N-terminal tail (GST-M8N) and to a lesser extent with the TRPM8 C-terminal tail (GST-M8C; Fig. 5 B). The functionality of $TCAF1_{\Delta PI3K}$ was then assessed by Ca^{2+} imaging and patch-clamp experiments. Strikingly, the Ca^{2+} response to icilin application was very different between control, TCAF1-transfected, and $TCAF1_{\Delta PI3K}$-transfected cells: 270.2 ± 52.5 nM, 1,375.1 ± 174.3 nM, and 692.6 ± 178.3 nM (Fig. 5 C). These results show a dramatic halving of TCAF1 function when its PI3K homology domain is removed, proving the importance of this domain in the mediation of TCAF1's effect on TRPM8. To assess the functional role of the TCAF1 PI3K domain on TRPM8 activity, the effect of pretreatment with 1 µM wortmannin was tested on cells transfected with either wild-type TCAF1 or $TCAF1_{\Delta PI3K}$. While TCAF1-transfected cells revealed strong sensitivity to wortmannin, the TRPM8-mediated current in $TCAF1_{\Delta PI3K}$-transfected cells was wortmannin insensitive (Fig. 5, D and E). Currents elicited by cold, icilin, and menthol were, respectively, 435.2 ± 76.8, 254.7 ± 42.7, and 275.3 ± 52.2 pA/pF in control (n = 4), and 78.5 ± 22.7, 76.9 ± 16.2, and 57.1 ± 11.8 pA/pF in wortmannin-treated TCAF1-transfected cells (n = 5); and 142.7 ± 25.9, 172.7 ± 29.9, and 130 ± 23.4 pA/pF in control (n = 4), and 188.7 ± 70.8, 191.6 ± 80.1, and 135.6 ± 34.5 pA/pF in wortmannin-treated $TCAF1_{\Delta PI3K}$-transfected cells (n = 6).

We then examined the effect of this domain on TRPM8 trafficking to the plasma membrane. Cotransfection of TRPM8 with TCAF1 or $TCAF1_{\Delta PI3K}$ followed by cell-surface biotinylation showed that both TCAF1 and its truncated form enhanced channel expression in the biotinylated fraction compared with cotransfection with the empty vector (Fig. 5 F).

TCAF1 and TCAF2 exert opposing regulatory effects on endogenous TRPM8 activity

To analyze whether TCAF1 and TCAF2 are involved in the regulation of native TRPM8, we examined how the level of TCAF1 or TCAF2 expression would affect menthol-induced $[Ca^{2+}]_i$ responses in LNCaP cells, which naturally express TRPM8 (Valero et al., 2011, 2012). We first confirmed TRPM8 expression and activity in these cells by using siRNAs targeting the channel (Fig. S2, E and F). Next, we compared $[Ca^{2+}]_i$ responses to 200 µM menthol in fluo-4–loaded control LNCaP cells, LNCaP cells overexpressing either TCAF1 or TCAF2, and LNCaP cells pretreated with either control siRNA (siLuc), TCAF1 siRNA, or TCAF2 siRNA (Fig. 6). The siRNA experiments were also performed in human epithelial prostate cells, Ep156T (Fig. S3). Our results revealed that both the amplitude of the response and its temporal profile depended on the level of TCAF1 and TCAF2 expression. In control (Fig. 6 A) and TCAF1-overexpressing (Fig. 6 B) LNCaP cells, as well as in LNCaP (Fig. 6 E) and Ep156T (Fig. S3 A) cells pretreated with siLuc or siTCAF2 (Fig. 6 G and Fig. S3 C), menthol triggered a high-amplitude $[Ca^{2+}]_i$ transient. The magnitude of this oscillatory response was significantly reduced in cells overexpressing TCAF2 (Fig. 6 C) and was increased after pretreatment with siTCAF2 (Fig. 6 G and Fig. S3 C). In LNCaP cells overexpressing TCAF1, an initial phase of the menthol-induced response was followed by several long-period $[Ca^{2+}]_i$ oscillations of smaller amplitude (Fig. 6 B), whereas pretreatment with siTCAF1 virtually abolished all the response in both LNCaP (Fig. 6 F) and Ep156T (Fig. S3 B). As the temporal pattern of the $[Ca^{2+}]_i$ response to TRPM8 activation is complex, to quantify the effects of TCAF overexpression

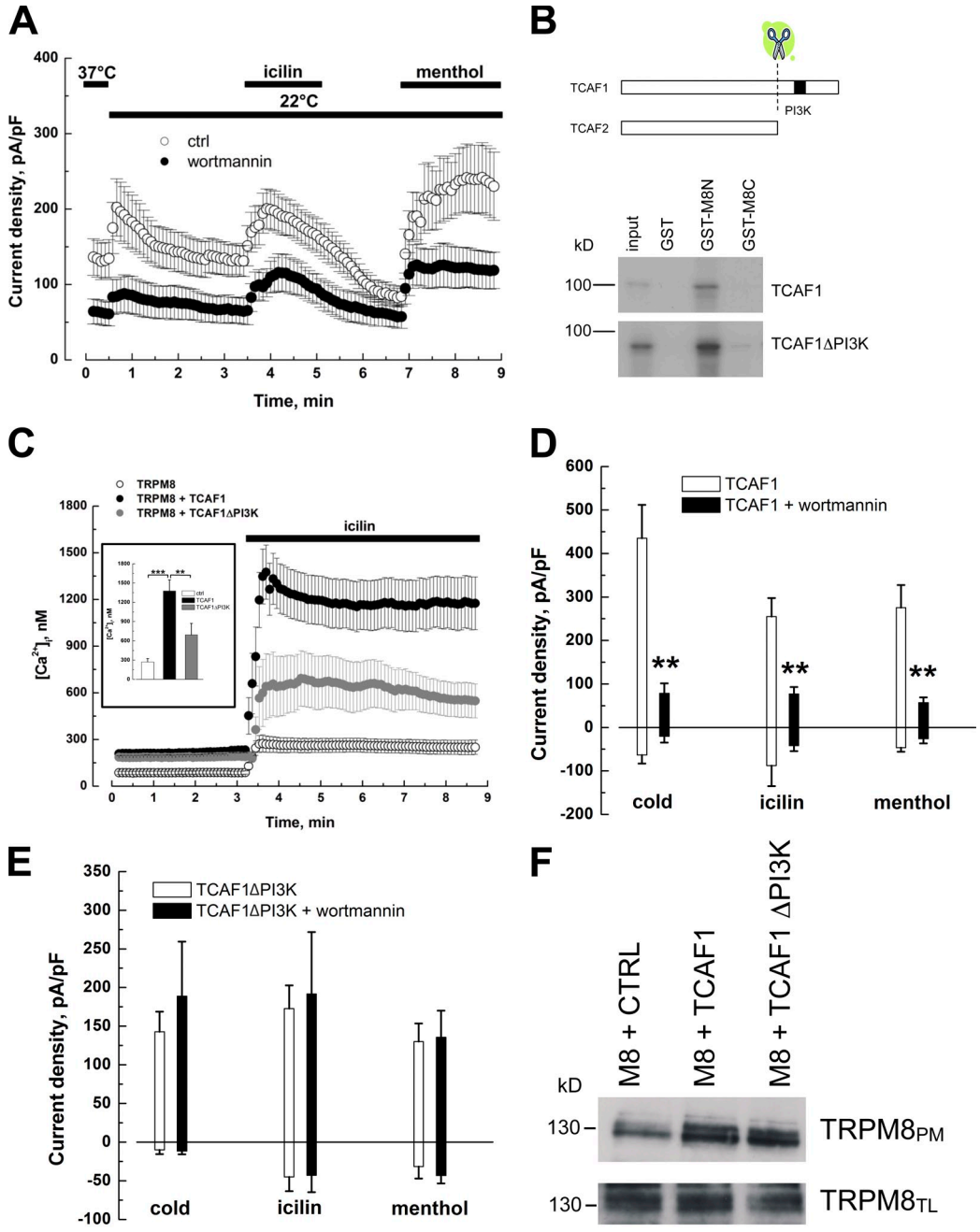

Figure 5. **TCAF1 exhibits a PI3K homology domain that is critical for the TCAF1 modulation of TRPM8 activity.** (A) Mean time course of cold- (22°C), icilin- (10 µM), and menthol-activated (500 µM) I_{TRPM8} in LNCaP cells pretreated (closed circles) or not (ctrl, open circles) for 15 min with 1 µM wortmannin. For pretreated cells, experiments were performed in the continuous presence of wortmannin at the same concentration. Currents were monitored at +100 mV, and results are presented as means ± SEM (error bars). (B) GST pull-down assay between [^{35}S]methionine-labeled TCAF1 or TCAF1$_{\Delta PI3K}$ protein and GST or GST fused to the TRPM8 N-terminal tail (GST-M8N) or C-terminal tail (GST-M8C). A schematic representation of TCAF1 and TCAF2 protein sequences and the putative PI3K site is shown. (C) Time course of mean intracellular Ca^{2+} concentration in LNCaP cells transfected with TRPM8 and an empty vector (ctrl, open circles), wild-type TCAF1 (TCAF1, black closed circles), or a truncated TCAF1 lacking the PI3K domain (TCAF1$_{\Delta PI3K}$, gray closed circles). Cells were loaded with Fura 2-AM, exposed to 10 µM icilin, and variations in [Ca^{2+}]i were monitored using an imaging system. Results are presented as means ± SEM (error bars). (inset) Histogram summarizing calcium imaging results (**, $P < 0.01$; ***, $P < 0.001$). (D and E) Histograms presenting mean cold- (22°C), icilin- (10 µM), and menthol-activated (500 µM) I_{TRPM8} in LNCaP cells transiently transfected with TRPM8 and wild-type TCAF1 (D) or TCAF1$_{\Delta PI3K}$ (E), and then treated (black columns) or not (white columns) with 1 µM wortmannin. Results at +100 and −100 mV are presented as means ± SEM (error bars; **, $P < 0.01$). (F) Cell surface biotinylation analysis of cells cotransfected with TRPM8 and the empty vector (CTRL), TCAF1, or TCAF1$_{\Delta PI3K}$. TRPM8 expression was analyzed by immunoblotting the plasma membrane fraction (TRPM8$_{PM}$) or total cell lysates (TRPM8$_{TL}$).

and siRNAs, we compared the fluo-4 signal during the first 18 min after menthol application in control LNCaP cells with that in LNCaP cells overexpressing TCAF1 or TCAF2 (Fig. 6 D), and the signal in LNCaP (Fig. 6 H) and Ep156T cells (Fig. S3 D) pretreated with siLuc with that pretreated with either siTCAF1 or siTCAF2. Menthol-induced $[Ca^{2+}]_i$ responses were directly correlated with changes in TCAF1 expression but inversely correlated with changes in TCAF2 expression, which indicates

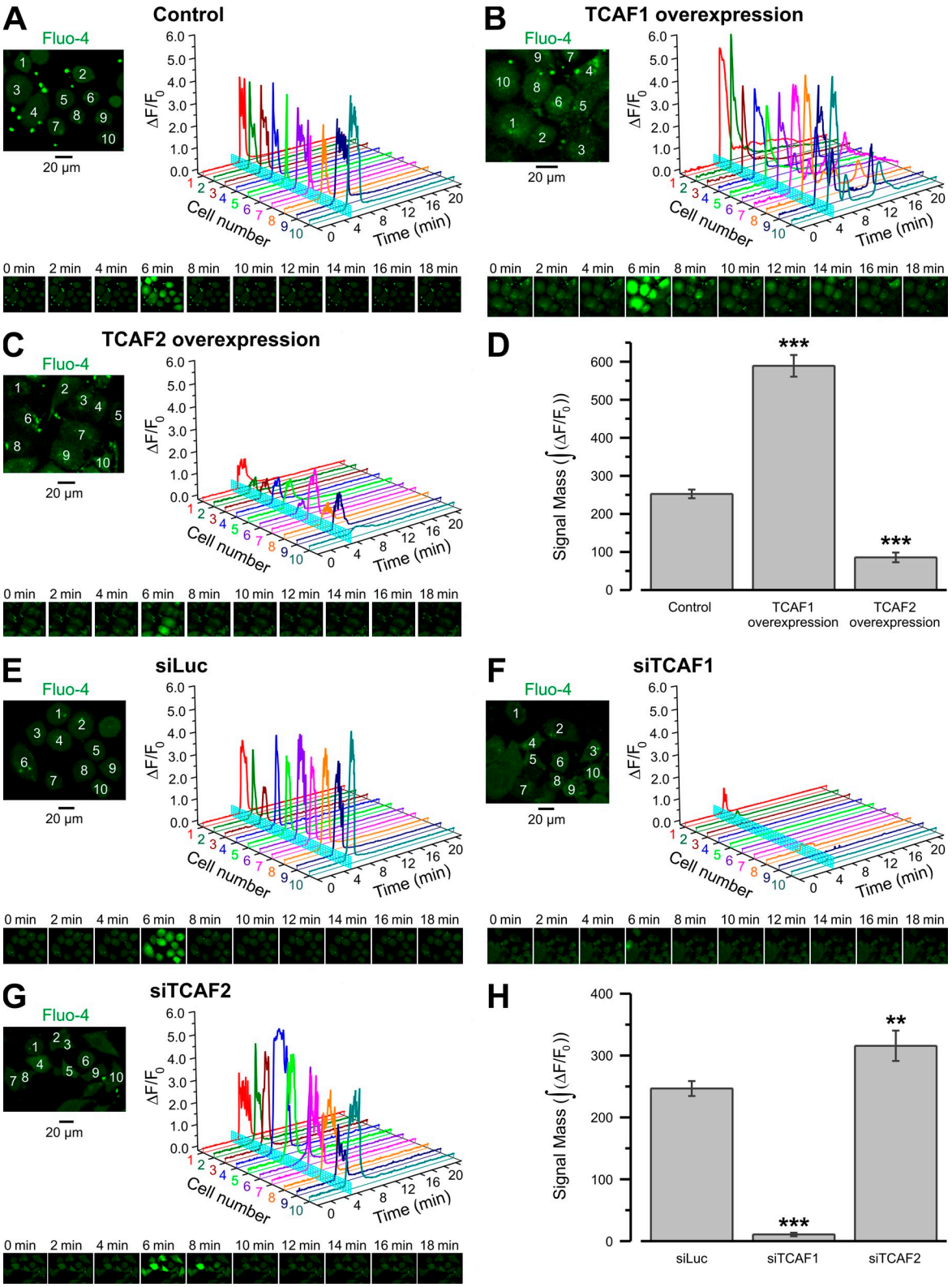

Figure 6. **The menthol-induced response of endogenous TRPM8 is modulated by TCAF1 and TCAF2.** (A–G) Changes of $[Ca^{2+}]_i$ in response to the activation of TRPM8 with 200 µM menthol were monitored using an x-y time-series imaging of fluo-4 fluorescence in control LNCaP cells (A), LNCaP cells overexpressing TCAF1 (B) or TCAF2 (C), and LNCaP cells pretreated with siLuc (E), siTCAF1 (F), or siTCAF2 (G). Images were acquired at 0.6 Hz from confocal optical slices <4 µm. The fluorescence intensity (F) was normalized to the averaged fluorescence intensity before menthol application (F_0). Relative changes in fluorescence intensity ($\Delta F/F_0$), averaged within each of 10 cells denoted by the numbers on the images (left), are plotted over time. Menthol application is depicted on the 3D plots by vertical cyan bars. The galleries below the plots demonstrate the images of fluo-4 fluorescence captured at times indicated above the images. Bar diagram plots compare masses of the fluo-4 signal, $\int(\Delta F/F_0)$, during the first 18 min after menthol application (D) in LNCaP cells overexpressing TCAF1 (n = 48) or TCAF2 (n = 51) versus control LNCaP cells (n = 62), and in LNCaP cells (H) pretreated with siTCAF1 (n = 56) or siTCAF2 (n = 42) versus LNCaP cells pretreated with siLuc (n = 52). Values are expressed as means ± SEM (error bars). ***, $P < 0.001$; **, $P < 0.01$.

that TRPM8 channel opening is facilitated by TCAF1 and suppressed by TCAF2.

TCAF1 binding introduces new kinetic states to TRPM8 single channel activity

Next, we checked for any potential effect of TCAF1/TCAF2 on TRPM8 activity at the single channel level. These experiments were performed in HEK 293 cells expressing TRPM8 under the control of a tetracycline-inducible promoter (HEK-293_{M8i}; Thebault et al., 2005) in order to limit the contamination of our recordings by the activity of other channels. Control HEK-293_{M8i} cells as well as cells transfected with TCAF1 or TCAF2 plasmids were subjected to a short tetracycline induction as described. Then, TRPM8 activity was measured in cell-attached configuration by first recording activity at room temperature followed by the application of 100 µM menthol (see Fig. S4 for sample traces). While comparing activity in control and TCAF1-transfected cells, two types of activity became apparent (Fig. 7 A). The first type, characterized by short, separate openings, was most common to control cells (19 control and 4 TCAF1-bound traces), whereas the second type exhibited the clustering of openings without any apparent increase in opening duration and was prevalent in TCAF1-transfected cells (5 control and 29 TCAF1-bound traces). In contrast, cells transfected with TCAF2 and induced according to an identical protocol exhibited virtually no TRPM8 activity (only 4 out of 31 traces exhibited TRPM8 opening), leading us to conclude that TCAF2 silences the TRPM8 channel (unpublished data).

To further study how TCAF1 binding modifies TRPM8 gating properties, the acquired traces were scrutinized for the appearance of multiple conductance levels, and those containing single-channel activity (four control and three TCAF1-bound) were individually analyzed, as described previously (Qin and Li, 2004; Fernández et al., 2011). Fig. 7 (B–D) summarizes dwell-time distributions, kinetic rates, and energy landscapes representing typical control and TCAF1-bound TRPM8 activity at room temperature and after stimulation by menthol. Interestingly, stimulation of TRPM8 activity by menthol only led to changes in the energy of the closed states, correspondingly increasing the frequency of channel openings while preserving the overall model. However, the effect of TCAF1 was qualitatively different. Although the analysis of control activity showed that the gating of TRPM8 alone could be reliably described by a relatively simple model, containing three closed and one open kinetic states (the 3c1o model; two upper panels on Fig. 7, C and D), this was not the case for the TCAF1-bound activity, suitable representation of which required a more complex model with four closed and two open states (the 4c2o model; two lower panels on Fig. 7, C and D). Fig. S5 compares the fits of the TRPM8 activity by the 4c2o and 3c1o kinetic models. Analysis of the activity of TRPM8 alone (Fig. S5, A and C) shows that both models yield identical log likelihood with additional states of the 4c2o model exhibiting virtually zero occupancy, which validates the simpler 3c1o model. On the contrary, analysis of the activity of TRPM8 interacting with TCAF1 (Fig. S5, B and D) shows significantly larger changes in log likelihood as well as a nontrivial occupancy of the additional states in the 4c2o model, emphasizing the significance of these additional kinetic states in activity of TRPM8. In other words, the binding of TCAF1 to the TRPM8 channel introduces new kinetic states that are necessary for a satisfactory description of TRPM8 gating, which implies a direct binding of TCAF1 to TRPM8.

TCAF1 but not TCAF2 shows expression patterns similar to TRPM8 during carcinogenesis, and slows down cell migration

Given the fact that TRPM8 is a marker for prostate cancer, we investigated by qPCR whether the expression of its interacting proteins, TCAF1 and TCAF2, was also associated with prostate cancer development. We initially studied TRPM8, TCAF1, and TCAF2 expression in healthy and cancerous human prostate resection samples. Patients were included in the study when both tumoral and nontumoral (healthy) tissue could be obtained from the same individual. TRPM8 and TCAF1 expression were significantly increased in cancerous samples when compared with healthy ones (10 and 5 times, respectively; $n = 7–10$ for each condition, $P < 0.05$), whereas no difference was observed for the TCAF2 transcript (Fig. 8 A).

We then assessed the variation in expression of these transcripts between localized prostate cancer and metastasis to the bone marrow of patients previously subjected to androgen ablation therapy. qPCR analysis showed a clear decrease in both TRPM8 and TCAF1 expression in metastatic samples in comparison with localized prostate cancer ($n = 7–10$ for each condition, $P < 0.01$). TCAF2 expression remained unchanged, as before (Fig. 8 B).

To verify that the similar expression patterns of TRPM8 and TCAF1 during carcinogenesis were also important at the functional level, we investigated the role of TCAF1 in prostate cell migration by performing time-lapse microscopy experiments on either PC3 or LNCaP prostate cancer cells (Fig. 9).

TRPM8 overexpression significantly decreases the cell migration speed, and this effect is exacerbated in the presence of icilin stimulation (Fig. 9, A and B), in accordance with our previous results on wound healing and transwell assays (Gkika et al., 2010). Moreover, TCAF1 overexpression significantly decreased the cell migration speed (Fig. 9, A and B) even in the absence of TRPM8 (Fig. 9 B). However, when overexpressed together with TRPM8, we observed a further significant decrease in the speed, which indicates that the TCAF1 effect is, at least partially, mediated by TRPM8 (Fig. 9, B and C). To test whether the inhibition of cell migration was due to the PI3K domain of TCAF1, we performed cell migration assay in cells overexpressing $TCAF1_{\Delta PI3K}$ (Fig. 9, A and C). We indeed observed a significant increase in the migration speed of cells transfected with $TCAF1_{\Delta PI3K}$ versus TCAF1-transfected cells (Fig. 9, A and C); this effect is further increased in the presence of TRPM8 (Fig. 9 C). These results are in agreement with modulation of TRPM8-mediated current by PI3K domain of TCAF1 (Fig. 5, D and E). Although TCAF2 inhibits the migration speed in the absence of TRPM8, it significantly increases the speed when TRPM8 is expressed (Fig. 9 C).

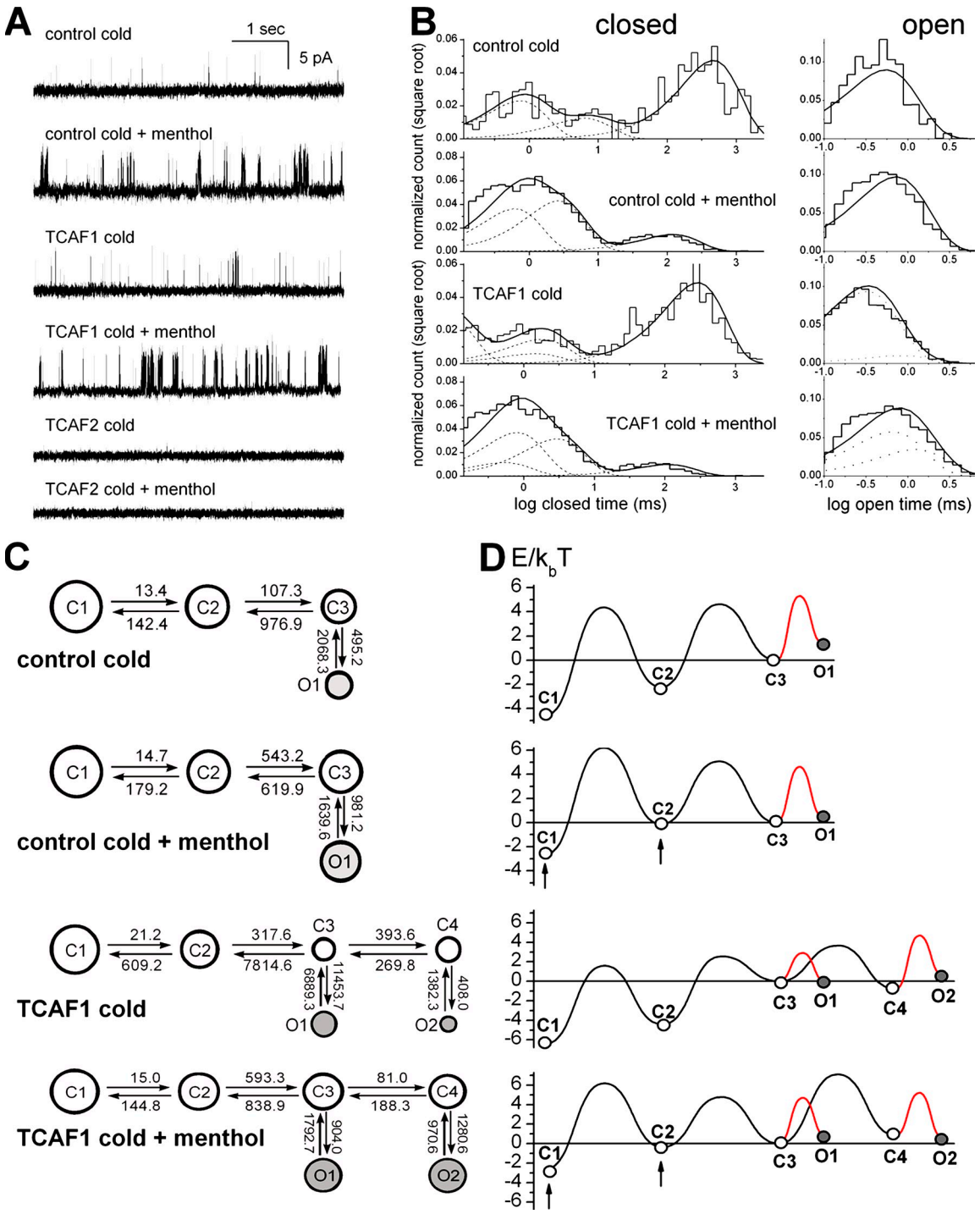

Figure 7. **TCAF1 interaction with TRPM8 introduces new kinetic states.** (A) Representative trace fragments of control and TCAF1-bound TRPM8 activity stimulated by cold (T = 20°C, controlled by room thermostat) or cold + 100 µM menthol, as indicated. (B) Representative distributions of closed (left) and open (Chetrite et al., 2000) dwell times in the traces of control and TCAF1-bound TRPM8 activity stimulated as indicated. The histogram shows the distribution of dwell times. The thick continuous line represents the cumulative best fit corresponding to the kinetic model used (C) and broken lines represent individual components of the fit. (C) Kinetic models providing the best fit to the control and TCAF1-bound TRPM8 activity. The area of each circle is proportional to the log of total time spent the corresponding state. Kinetic rates are indicated as numbers associated with the corresponding arrows. (D) Energy landscapes calculated from the corresponding kinetic models. Arrows point to significantly shifted energies in corresponding states caused by menthol stimulation. Note that contrary to the effects of different modes of TRPM8 stimulation (shifts in state energies), the interaction with TCAF1 leads to the appearance of new kinetic states.

Finally, we studied the effect of native TCAFs on cell migration with an siRNA approach. As expected, TCAF1 down-regulation increases migration, which interestingly occurs by acting on the directional persistence index (Fig. 9 E) and not on the speed (Fig. 9 D). The effect on directional migration index of siTCAF1 is exacerbated in the presence of TRPM8 (Fig. 9 E).

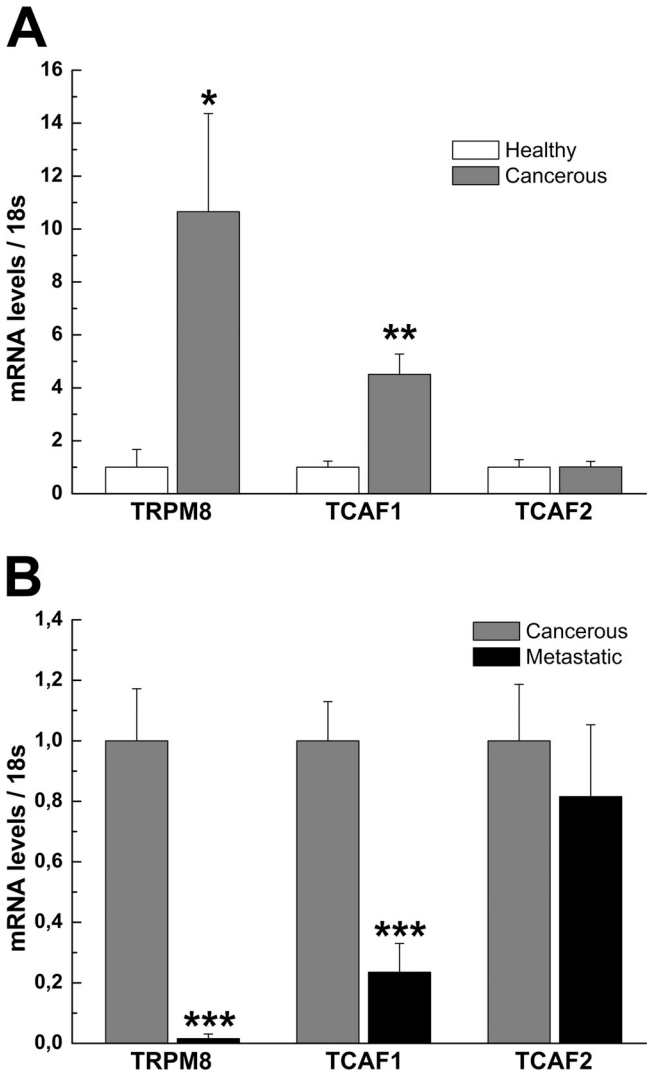

Figure 8. **TCAF expression profile in prostate cancer.** (A and B) Analysis of TRPM8, TCAF1, and TCAF2 mRNA expression levels by qPCR in healthy and cancerous human prostate samples (A), as well as in localized and metastatic human prostate cancer specimens (B). Values are calculated relative to 18S rRNA expression and presented as means ± SEM (error bars; $n = 7$–10; *, $P < 0.05$; **, $P < 0.01$; ***, $P < 0.001$).

However, we clearly show that TCAF2 has a strong promigratory effect, which is more pronounced during TRPM8 activation, as observed by the strong inhibition of cell migration in the presence of siTCAF2 and icilin (Fig. 9 F).

Discussion

Ion channels are known to have protein partners that regulate channel localization or gating, leading to important physiological consequences. In some of the better known cases, such as the T-type calcium channels, these proteins are even acknowledged as subunits of the involved ion channel (Gerster et al., 1999). Here, we present a family of proteins, the TCAFs, which regulate the trafficking as well as gating of TRPM8, the ion channel that is known to serve as a thermal sensor in peripheral neurons and to play an important role in prostate cancer. We have demonstrated by means of cellular and molecular biology as well as electrophysiological measurements that the TCAFs interact directly with TRPM8, exerting opposing effects on channel activity. We have subsequently unraveled the molecular mechanism of TCAF action on TRPM8 activity using directed mutagenesis, biochemical assays, and single-channel analysis, demonstrating: (1) a domain responsible for their distinct channel regulation activities, (2) the effect of the TCAFs on channel plasma membrane trafficking, and (3) the qualitative effect on TRPM8 activity via the introduction of new kinetic states during gating. At the cellular level, the functional TCAF1–TRPM8 interaction leads to the inhibition of cell speed, which is also supported by the loss of expression of these proteins in human metastatic specimens. Indeed these two proteins are mainly expressed in the prostate, as demonstrated by the qPCR screening of human tissues.

Addressing the molecular mechanisms responsible for the regulation of TRPM8 activity and expression by the TCAFs, we have shown that the TCAFs interact mainly with the TRPM8 N-terminal tail. Our data imply that both proteins are critical for TRPM8 function because their silencing prevents the channel's insertion into the plasma membrane. GST pull-down experiments with in vitro translated TCAFs strongly point to the direct binding of TCAFs to TRPM8, which is further supported by the introduction of new kinetic states to TRPM8 single-channel kinetics in the presence of the TCAF1 protein, whereas TCAF2 completely silences the channel while retaining it in plasma membrane. Interestingly, this situation closely resembles the role that β subunits play in regulating T-type calcium channels through the direct interaction of involved proteins (Gerster et al., 1999). To understand the opposing modulatory effects of TCAF1 and TCAF2, one has to look at sequence differences between the proteins, such as the loss of the C-terminal extremity in TCAF2. However, the removal of this region in TCAF1 ($TCAF1_{\Delta PI3K}$) did not completely mimic the behavior of TCAF2, and although $TCAF1_{\Delta PI3K}$ overexpression indeed leads to a decrease in I_{TRPM8} amplitude when compared with TCAF1, the extent of this decrease is significantly lower than that observed with TCAF2 overexpression. The presence in this region of a PI3K homology domain coupled with our observation that (1) a PI3K inhibitor (wortmannin) inhibits TRPM8 activity and that (2) this sensitivity to wortmannin is abolished in cells overexpressing $TCAF1_{\Delta PI3K}$ strongly suggest that the regulatory role of the TCAFs also involves phosphorylation. In this model, both TCAF1 and TCAF2 proteins bind to TRPM8, affecting its expression on the plasma membrane. The presence of a functional PI3K homology domain, however, is required to make the channel fully active. Moreover this domain is also critical for cell motility because $TCAF1_{\Delta PI3K}$ transfection partially reverts the inhibitory effect exerted by TCAF1. However it should be noted that because the $TCAF1_{\Delta PI3K}$ mutant implies the deletion of TCAF1 C terminus, the loss of function may not be due only to the disruption of the PI3K-specific enzymatic activity. More experiments are thus needed to characterize the respective roles of TCAF1 functional enzymatic domain and C terminus.

Our phylogenetic analysis revealed that human TCAF1 and -2 are homologues of rodent TCAF3 (EAPA2) and that these three proteins form a new protein family originating from two duplication events. TCAF3 was identified in 2006 by mass

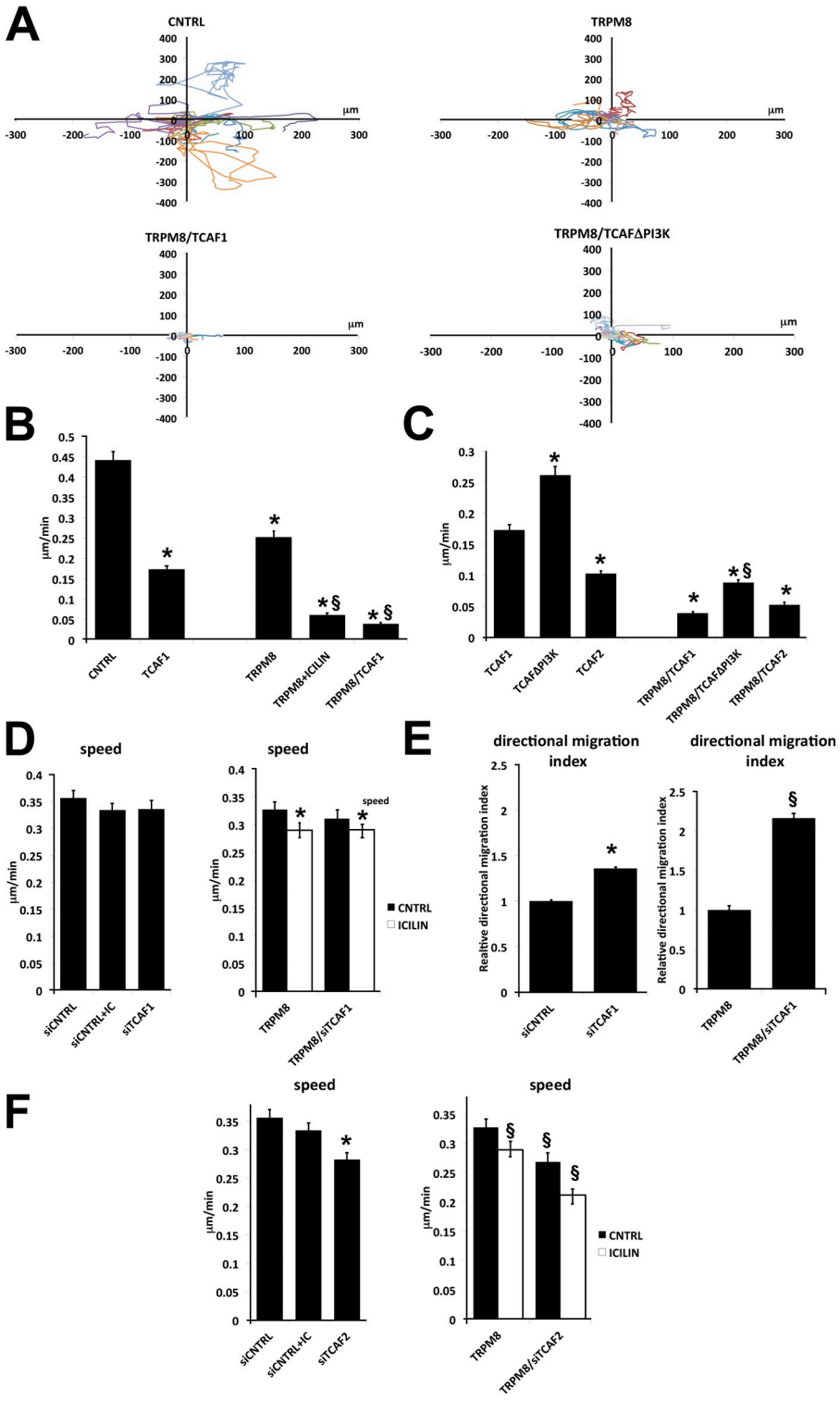

Figure 9. **TCAF functional role in prostate cancer cell migration.** (A) Representative migration plots of control (top left) and TRPM8-overexpressing cells (top right) or TRPM8 cotransfected with wild-type TCAF1 (bottom left) or truncated TCAF1 lacking the PI3K domain (TCAF1$_{\Delta PI3K,}$ bottom right). Each line represents the migration of one cell within a 10-h period. The data shown are from a single representative experiment out of three repeats. For the experiment shown: CNTRL n = 28, TRPM8 n = 58, TRPM8/TCAF1 n = 69, TRPM8/TCAF1ΔPI3K n = 98. (B and C) Bar graphs showing the quantification of cell speed in control nontransfected prostate cancer cells (CNTRL), TRPM8-overexpressing cells (TRPM8), TCAF1-overexpressing cells (TCAF1), TRPM8- and TCAF1-overexpressing cells (TRPM8/TCAF1), and TRPM8 and TCAF1 lacking the PI3K domain (TCAF1$_{\Delta PI3K}$) in the presence or absence of 10 µM icilin. (D–F) Bar graphs showing the quantification of cell speed (D) and the migratory persistence index (E, calculated as indicated in the online materials) in control cells and TRPM8-overexpressing cells in which TCAF1 or TCAF2 are down-regulated (TRPM8/siTCAF1), in the presence or absence of 10 µM icilin (F). Each graph represents the quantification of pooled independent experiments (at least three experiments for each experimental condition). For each experiment, at least 60 cells were followed per condition (*, $P < 0.05$ relative to CNTRL; § relative to TRPM8). Data are expressed as means ± SEM (error bars).

spectrometric analysis as a new prostate-specific protein regulated by androgens in mice (Fujimoto et al., 2006). At the time, the function of TCAF3 was unknown and no homologues had been identified in humans. Our discovery of the TCAF–TRPM8 interaction allows us to assign a role to this important family of proteins, often coexpressed with the TRPM8 channel. Interestingly, although TCAF1 and -2 share a common phylogenetic origin and exhibit a high degree of homology, they exert completely different regulatory effects on TRPM8. In this regard, the relative abundance of TCAFs and their competition in binding TRPM8 seems to be critical in the physiological regulation of the channel activity. This is further supported by the differences in TCAF's effect on single channel activity (the addition of one open state for TCAF1), while their binding to the channel is similar, as shown in the GST pull-down and coimmunoprecipitation assays. Moreover, the expression of TCAF1 is universally and closely

linked to TRPM8 expression, whereas the expression of TCAF2 is mostly independent and does not exhibit large variations. Although coupling with TCAF2 completely silences TRPM8 activity, its physiological role is not clear in nonoverexpressing systems. We speculate that this might be due to the loss of the C-terminal domain in the human TCAF2. This result may be different for other mammalian TCAF2s, as this domain is still present in the genes we used for the phylogenetic analysis.

The highest expression of TRPM8 is in the prostate, where it is suggested to play a role in carcinogenesis (Thebault et al., 2005; Bidaux et al., 2007; Sabnis et al., 2008; Wondergem et al., 2008). Prostate carcinogenesis is commonly associated with major alterations in TRPM8 expression and its signaling pathway (Bavencoffe et al., 2011; Gkika and Prevarskaya, 2011; Prevarskaya et al., 2011; Shapovalov et al., 2013b). In support of this hypothesis, our data reveal that TRPM8 and TCAF1 proteins show similar expression patterns in all tissues studied. Specifically, TCAF1 expression levels increase in cancerous human prostate tissue and drop in metastatic tissue, mirroring TRPM8 levels. However, the expression levels of TCAF2 remain unchanged, which suggests the differential regulation of the two transcripts and reflects their divergence at the functional level. These observations mark TCAF1 as a good candidate for inclusion in the list of well-known prognostic markers such as TRPM8, prostein, and the prostate-specific antigen (PSA), which are also deregulated in localized primary prostate cancer, whereas their overexpression is lost again at advanced tumor stages (Schmidt et al., 2006). Moreover, the increased TRPM8 activity and expression linked to the presence of TCAF1 also affects cell migration, as shown by our time lapse video microscopy experiments, and which is in accordance with previous studies linking the overactivity of TRPM8 protein with the reduced motility of prostate cancer cells (Gkika et al., 2010). More specifically, TCAF1 exerts an antimigratory effect on prostate cancer cells by acting on the cell migration persistence, thus confirming the role of TCAF1 as a TRPM8 activator. However, the complexity of interactions described and the results of our initial GST pull-down, coimmunoprecipitations, and migration assays suggest that TCAFs are partner proteins for other ion channels, such as TRPV6 and the short isoform of TRPM2, which clearly indicates the need for further studies.

Finally, although TCAFs are strongly expressed in the prostate, we show that they are also detected in other tissues, including the brain. It is therefore possible that TCAFs are not merely limited to the role of partner proteins in prostate cells, but are also required and can be therapeutically targeted in other tissues for the stabilization of the expression and modulation of the activity of this channel. For example, TCAFs and their associated molecular pathways could be targets for pain management, according to several recent studies on TRPM8 and allodynia (Chung et al., 2011; Descoeur et al., 2011; Su et al., 2011; Kawashiri et al., 2012; Shapovalov et al., 2013a).

Materials and methods

Phylogenetic analysis

For the three genes *TCAF1*, *TCAF2*, and *TCAF3*, homologous sequences were downloaded from GenBank. Sequences were aligned using Seaview version 4.2.6 (Gouy et al., 2010) and manually adjusted for amino acid alignment. A data matrix containing 2,790 bp was further used for phylogenetic analyses. Any sequence shorter than half the final matrix length was removed, yielding a total of 21 sequences (NM_203396, NM_001009534, BC000609, XM_519454, NM_001132598, NM_029930, XM_342675, XM_002711950, XM_843498, NM_001099054, NM_001130025, XM_519453, XM_539847, NM_001101924, XM_001490518, NM_146174, XM_001057103, XM_002190925, NM_001094696, NM_001089327, and NM_001089327). Phylogenetic reconstructions were performed with the maximum likelihood method (ML) using PhyML 3.0 (Guindon and Gascuel, 2003), and by Bayesian analyses using MrBAYES, version 3.1.2 (Huelsenbeck and Ronquist, 2001). The best-fit model under the ML criterion was selected from the "Akaike Criterion" output of MODELTEST, version 3.7 (Posada and Crandall, 1998). For the ML analyses, node stability was estimated by 100 nonparametric bootstrap replicates (Felsenstein, 1988). For the Bayesian analyses, the dataset was divided into three partitions according to codon positions. MODELTEST version 3.7 was used to calculate the best-fit model of sequence evolution for each partition. Two runs of four Markov chains were calculated simultaneously for 4,000,000 generations with equal initial probabilities for all trees and starting with a random tree. Tree sampling frequency was each 100 generations and the consensus tree with posterior probabilities was calculated after removal of the first 25% of the total number of trees generated, corresponding to 10,000 trees. The mean standard deviation of split frequencies between the two independent runs was <0.01.

qPCR

qPCR of mRNA transcripts was done using MESA GREEN qPCR MasterMix Plus for the SYBR Assay (Eurogentec) on the CFX96 Real-Time PCR Detection System (Bio-Rad Laboratories) and the LightCycler System (Roche). The sequences of the primers were: for TRPM8, 5′-CGGTCATCTACGAGCCCTAC-3′ and 5′-CACACACAGTGGCTTGGACT-3′; for TCAF1, 5′-TTGCCCACAGAAAATGTTGA-3′ and 5′-CAGATAGGCCAGGCTGGTAG-3′; for TCAF2, 5′-ACCACGAGAATGGGAACTTG-3′ and 5′-GAGCCTGTGCAGGGATATGT-3′; for 18S rRNA, 5′-CAGCTTCCGGGAAACCAAAGTC-3′ and 5′-AATTAAGCCGCAGGCTCCACTC-3′; for actin, 5′-TTGCTGATCCACATCTGCTG-3′ and 5′-GACAGGATGCAGAAGGAGAT-3′. β-Actin mRNA and 18S rRNA were used as endogenous controls to normalize variations in RNA extraction, the degree of RNA degradation, and the variability of reverse transcription efficiency. To quantify the results, we used the comparative threshold cycle method described by Livak and Schmittgen (2001).

For regular PCR, the following primers were used: for actin, 5′-CAGAGCAAGAGAGGCATCCT-3′ and 5′-GTTGAAGGTCTCAAACATGATC-3′; for TCAF1, 5′-ATGGCGACTCCCTCTGCTGC-3′, 5′-CCCAATCCCAGGCTTGTCCT-3′, 5′-CTACTGCTGCAAGGCGTACA-3′, and 5′-CCAGACCCTCGTAGCATCTT-3′.

Cancer tissue sampling

Prostate tissue samples (prostate adenocarcinoma) were obtained from 15 patients with a mean age of 62.4 yr (ranging from 51 to 70) who underwent radical prostatectomy between January 2004 and June 2008 at the Department of Urology at the Lyon-Sud Hospital Centre. All fragments were snap-frozen and stored in liquid nitrogen until analysis. To ascertain whether the tissue was malignant or nontumoral and to confirm the Gleason score, a histological analysis of frozen sections of each sample was performed by the same pathologist before RNA extraction. Fragments fully made up of tumoral tissue were selected and classified as "tumoral," whereas samples containing no tumoral tissue were selected and classified as "nontumoral." Fragments with a mix of normal and tumoral tissue were excluded from the study. Patients were included in the study when both a "tumoral" sample and a "nontumoral" sample could be obtained from the same individual.

In addition, we used nine samples from both localized and metastatic prostate cancer obtained after informed consent from patients with localized (T2a-b) PCa for whom a prostatectomy has been scheduled, and patients with metastatic PCa (M1), which progressed on androgen ablation therapy, were included in a clinical research program (Protocol ID 2897) sponsored by the Hôpitaux Universitaires de Strasbourg. A total volume of 3 ml of bone marrow were aspirated at a scintigraphic-indicated metastatic site. Microscopic observations were made from an aliquot of each bone marrow aspirate to confirm or rule out the presence of metastatic PCa cells. Total RNAs were extracted from small pieces of localized tumor by the use of the RNeasy midi kit (QIAGEN) and from bone marrow aspirates by the use of the Qiamp RNA blood kit (QIAGEN) according to the manufacturer's instructions.

The ethics committee of the faculty of medicine and the state medical board agreed to these investigations, and informed consent was obtained from all patients.

Cloning and siRNA

The coding sequence of the N-terminal tail of TRPM8 (690 aa, S2-K691) was amplified from the hTRPM8pcDNA4 plasmid (Thebault et al., 2005) and cloned into the pGEX6p-2 vector (tac promoter) for chemically inducible, high-level expression of GST-tagged recombinant proteins (GE Healthcare) as a BamHI–XhoI fragment using the primers 5′-CGGGATCCTCCTTTCGGGCAGCCAG-3′ and 5′-CCGCTCGAGTCACTTGGTGTCTCGGGAAATC-3′. Similarly, the C-terminal tail of TRPM8 (124 aa, G980-K1104) was cloned as a BamHI–XhoI fragment into the tac promoter pGEX6p-2 vector using the primers 5′-CGGGATCCGGCTACACGGTGGGCAC-3′ and 5′-CCGCTCGAGTCACACGAGTTTGATTTTATTAGCAATC-3′. The TCAF1 and TCAF2 genes were cloned in the pGEM-T Easy vector (T7 and SP6 RNA polymerase promoter; Promega) from normal human prostate poly(A)$^+$ RNA (Takara Bio Inc.) using the following primers: for TCAF1, 5′-ATGGCGACTCCCTCTGCTGC-3′ and 5′-TCAGTGGGGCATCTGTGTGAGG-3′; for TCAF2, 5′-ATGGCGACCATTGCTGCTGC-3′ and 5′-TCATCCCCTTCTCCCAGAATTTCTGC-3′. TCAF1 and TCAF2 were both subcloned as EcoRI fragments into the pCMV-TnT vector (CMV promotor; Promega), TCAF1 as a XhoI fragment in the pCMV-HA vector (CMV promotor; Takara Bio Inc.), and TCAF2 as an EcoRI fragment in the pCMV-myc vector (CMV promotor; Takara Bio Inc.).

For the TCAF1$_{\Delta PI3K}$ mutant, a stop codon was introduced into the pCMV-TNT-TCAF1 construct by the substitution C2162G using in vitro mutagenesis (QuikChange Site-directed Mutagenesis kit; Agilent Technologies). All long PCRs were performed with the High Fidelity Phusion DNA Polymerase (Finnzymes) and all constructs were verified by sequence analysis.

For the fluorescent *chimera*, mTurquoise2 and SYFP2 were cloned in a home-made vector derived from pEGFP-N1 (CMV promotor; Takara Bio Inc.) in which we substituted the multicloning site with a homemade counterpart that accept 5′ cloning of DNA with NheI and AgeI and 3′ cloning of DNA with Sac II and Not I. The sense linker sequence was: 5′-GCTAGCATTGAACCGGTGGAGTAGGCgCCGGtGGAGGAGGAGGGTtACCTGTTGTTGGAGGAGTTGTTGGAGGAGGAGTTGTTGGTGGTGTTGTTGGTGTTGGGTtACCTGGTGGCgCCGGtGGTGTTGGCCGCGGATTATGCGGCCGC-3′. This vector was design to normalize the size and amino acid sequence of the linker between the protein of interest and the fluorescent protein. Labels given to these vectors are intuitive: X-pSYFP2-N means that SYFP2 consists of the N terminal part of the chimera while X-pmTurquoise2-C means that mTurquoise2 is located at the C terminus of the chimera. TRPM8-pmTurquoise2-C, TCAF1-pSYFP2-N, TCAF1-pSYFP2-C, TCAF2-pSYFP2-N, and TCAF2-pSYFP2-C were constructed as described. T.W.J. Gadella (Swammerdam Institute for Life Sciences, van Leeuwenhoek Centre for Advanced Microscopy, University of Amsterdam, Amsterdam, Netherlands) provided the riginal pmTurquoise2-N1, pmTurquoise2-C1, and pSYFP2-C1 vectors. Before the clone of TCAF1 and -2 in the recipient vector, the AgeI site was suppressed by single point mutation using in vitro mutagenesis (QuikChange Site-directed Mutagenesis kit) and checked by sequencing. Fragments were amplified by the mean of PCR with the following couples of primers: for TRPM8, 5′-GATCCCGCGGTTCCTTTCGGGCAGCCAGG-3′/5′-AGTCGCGGCCGCTCAATGGTGATGGTGATGATGACCGG-3′; for TCAF1, 5′-GATCGCTAGCCGCCACCATGGCGACTCCCTCTGCTG-3′/5′-GATCACCGGTGTGGGGCATCTGTGTGA-3′ and 5′-GATCCCGCGGTGCGACTCCCTCTGCTGC-3′/5′-AGTCGCGGCCGCTCAGTGGGGCATCTGTGTGAGGA-3′; for TCAF2, 5′-GATCGCTAGCCGCCACCATGGCGACCATTGCTGC-3′/5′-GATCACCGGTTCCCCTTCTCCCAGAATTTCT-3′ and 5′-GATCCCGCGGTGCGACCATTGCTGCTGCT-3′/5′-AGTCGCGGCCGCTCATCCCCTTCTCCCAGAATTTCTGC-3′. After a 0.8%-agarose gel purification (Wizard SV gel and PCR Clean-Up System; Promega), PCR products and recipient vectors were digested with either NheI + AgeI or SacII + NotI at 37°C overnight. After DNA purification, PCR products and vectors were ligated overnight and transformed in DH5α chemo-competent bacteria (NEB). Final plasmids were extracted and sequenced before performing the experiments.

siRNAs were generated against the human sequences 5′-TTATTGGAGAGGCTTCATT-3′ (siTCAF1; Eurogentec), 5′-GGCTTCCCTGGTAACATCATCCTCA-3′ (siTCAF2; Invitrogen), and the luciferase 5′-CTTACGCTGAGTACTTCGA-3′ (siLuc; Eurogentec).

GST fusion proteins and pull-down assay

TRPM8 N- and C-terminal tail GST fusion proteins were produced and purified as per the manufacturer's instructions. In brief, BL-21 cells were transformed with the pGEX6P-2 constructs and cultured in 2XTY medium containing ampicillin (100 µg/ml) at 37°C until the OD reached 0.4–0.6. IPTG was then added to a final concentration of 0.2 mM to induce expression at 30°C for 4 h. The bacteria were pelleted and resuspended in STE buffer I (10 mM Tris-HCl,150 mM NaCl, and 1 mM EDTA, pH 8.0), and the cells were broken by lysozyme (10 mg/ml) incubation. After adequate sonication, the broken cells were pelleted at 13,000 rpm for 30 min at 4°C, and the supernatant was collected for purification. Because pGEX-6P-2 contains the coding region for GST, we used glutathione Sepharose 4B beads (GE Healthcare) to purify the TRPM8 N and C tails.

TCAF1, TCAF2, and TCAF1$_{\Delta PI3K}$ proteins were labeled with [^{35}S] methionine using a reticulocyte lysate system as per the manufacturer's instructions (Promega), added to purified GST fusion proteins, and immobilized on glutathione Sepharose 4B beads in PBS containing 1% vol/vol Triton X-100. After a 2-h incubation at room temperature, the beads were washed extensively and bound proteins were eluted with SDS-PAGE loading buffer, separated on 10% wt/vol SDS-PAGE gels, and visualized by autoradiography.

Preparation of prostate lysates, pull-down assay, and Fourier transform mass spectrometric analysis

The prostate was isolated from two 12-wk-old C57BL/6 male mice, which were sacrificed under 1.5% vol/vol isoflurane anesthesia (Nicholas Piramal Limited). The animal ethics board of the Radboud University Nijmegen approved all animal experimental procedures.

The two prostates were homogenized in homogenization buffer A (HbA; 20 mmol/liter Tris/HCl, pH 7.4, 5 mmol/liter MgCl, 5 mmol/liter NaH_2PO_4, 1 mmol/liter EDTA, 80 mmol/liter sucrose, 1 mmol/liter PMSF, and 5 g/ml leupeptin and pepstatin). The protein concentration of the homogenates was determined with the Bio-Rad protein assay (Bio-Rad Laboratories). The lysates were subjected to GST pull-down with theTRPM8 N- and C-terminal tail GST fusion proteins while GST alone and another TRP channel (TRPV6 C-tail) were used as binding controls (as described in the GST pull-down section).

GST-precipitated proteins were subjected to Fourier transform mass spectrometry (FT-MS) in the Radboud Proteomics Centre as described previously (Vogel et al., 2007). In brief, proteins were separated on a conventional 10% SDS-PAGE gel, then the gel was cut into eight slices for digestion by trypsin (two slices per lane, one for high molecular weight and one for low: S1 and S2 for GST, S3 and S4 for GST-TRPV6 C tail, S5 and S6 for GST-TRPM8 N tail, and S7 and S8 for GST-TRPM8 C tail). Peptide identification experiments were performed using a nano-HPLC 1100 nanoflow system (Agilent Technologies) connected online to a linear quadrupole ion trap-Fourier transform mass spectrometer (LTQ-FT; Thermo Fisher Scientific). Peptides and proteins were identified using the Mascot (Matrix Science) algorithm to search a local version of the NCBInr database (http://www.ncbi.nlm.nih.gov). First-ranked peptides were parsed from the Mascot database search HTML files with MSQuant (http://msquant.sourceforge.net) to generate unique first-ranked peptide lists. The full list of interacting peptides can be found in Table S1 and the summary of the number of interacting peptides in Table S2.

Cell culture and transfection

HEK 293 and lymph node carcinoma of prostate (LNCaP) C4-2 cells (provided by F. Viana, Instituto de Neurociencias de Alicante, Universidad Miguel Hernandez, CSIC, Alicante, Spain; and L.A. Pardo, Max-Planck-Institute of Experimental Medicine, Göttingen, Germany) were grown in DMEM and RPMI 1684 (Invitrogen), respectively, supplemented with 10% fetal calf serum (Poly-Labo; Seromed), L-glutamine (5 mM; Sigma-Aldrich), and kanamycin (100 mg/ml; Sigma-Aldrich). Human epithelial prostate cells, Ep156T, were a gift of V. Rotter (Weizmann Institute of Science, Rehovot, Israel) and were grown in MCDB 153 modified by Biological Industries as described previously (Kogan et al., 2006).

Cells were transfected with 2 µg of each construct or 50 nM of siRNA and 0.2 µg of pmax GFP using either Nucleofector (Amaxa) or FuGENE HD reagent (Roche) and HiPerFect Transfection Reagent (QIAGEN). Control experiments were performed by transfecting the empty vector or siRNA to Luciferase (siLuc).

Cells were used for patch-clamp experiments 24 h after nucleofection and for cell surface biotinylation 48 h after transfection.

Immunoprecipitation and immunoblotting

Cells were cotransfected with a his-tagged hTRPM8pcDNA4 plasmid and human influenza agglutinin (HA)-tagged TCAF1 or myc-tagged TCAF2, washed twice with PBS, and incubated for 60 min on ice in lysis buffer (1%

Triton X-100, 1% sodium deoxycholate, 150 mM NaCl, 10 mM $NaKPO_4$, pH 7.2, and anti-protease cocktail; Sigma-Aldrich). After centrifugation (12,000 *g* for 10 min at 4°C) of the lysates, protein concentration was determined by the BCA assay (Thermo Fisher Scientific), and equal amount of supernatants were incubated overnight at 4°C with mouse anti-his antibody (Invitrogen) immobilized on protein A/G PLUS agarose beads (Santa Cruz Biotechnology, Inc.). The pellet was washed three times, resuspended in SDS sample buffer, and heated at 37°C for 30 min, separated on 10% wt/vol SDS-PAGE gels, and analyzed by immunoblotting using rabbit anti-HA (1:2,000; Abcam), mouse anti-myc (1:500; Invitrogen), mouse anti-actin (1:5,000; Sigma-Aldrich), mouse anti-calnexin (1:2,000; EMD Millipore), rabbit anti-TRPM8 (1:1,500; Alomone Labs Ltd), and rabbit anti-TRPV6 (1:200; Santa-Cruz Biotechnology, Inc.) antibodies.

Biotinylation

Cells were washed twice with ice-cold PBS containing 1 mM $MgCl_2$ and 0.5 mM $CaCl_2$ (PBS-CM) 48 h after transfection, and surface biotinylation was performed by incubating the cells twice for 20 min at 4°C with 1 mg/ml EZ-Link Sulfo-NHS-LC-LC-Biotin (Pierce). Subsequently, cells were incubated for 5 min with quenching solution (50 mM NH_4Cl in PBS-CM) at 4°C and rinsed twice with cold PBS-CM. Cells were lysed with 1 ml of lysis buffer (1% Triton X-100, 1% sodium deoxycholate, 150 mM NaCl, 10 mM $NaKPO_4$, pH 7.2, and anti-protease cocktail; Sigma-Aldrich) for 1 h on ice. Lysates were added to 50 µl NeutrAvidin-agarose beads (Thermo Fisher Scientific). After incubation for 16 h at 4°C, the beads were washed twice with PBS-CM, twice with lysis buffer, and once with 10 mM Tris-HCl, pH 7.5. Finally, biotinylated proteins were eluted with SDS-PAGE loading buffer, separated on 10% wt/vol SDS-PAGE gel, and analyzed by immunoblotting as described for the immunoprecipitation assays with rabbit anti-TRPM8 antibody (1:1,500; Alomone Labs Ltd).

TD FLIM

TD FLIM is one of the best methods to measure FRET occurrence with a good spatial resolution and independent of the concentration of proteins (Sipieter et al., 2013). As the C termini of tetrameric TRPM8 are gathered in a restricted volume, we have chosen to fuse the recently developed cyan variant (Goedhart et al., 2012), mTurquoise2, at the C terminus of TRPM8. To optimize FRET occurrence, and because both the orientation and steric effect of TCAF were unknown, we generated both N-terminal and C-terminal SYFP2 fusion to TCAFs. Because, our preliminary experiment reported a better FRET efficiency between TRPM8-mTurquoise2 and SYFP2 fused at the N terminus of both TCAFs, we then focused on these pairs of FRET. For live-cell imaging, 120,000 HEK293 cells were placed on 35-mm glass-bottom dishes (MatTek Corporation) and transfected for 1 d. Before performing the experiment, dishes were filled with L-15 medium without phenol red (Life Technologies), and kept at 37°C using a stage incubator (Life Imaging Services). FLIM was performed with a confocal head (TCS SP5 X; Leica) with the SMD upgrade, mounted on an inverted microscope (DMI6000; Leica). A pulsed diode laser, PDL 800-B (PicoQuant GMBH), delivered 40 MHz repetitive rate pulses at 405 nm. The confocal pinhole was set to 1 Airy for a 0.921-µm optical slice. Single-photon events originated from the illuminated voxel were collected through a 63×/1.2 NA water-immersion objective lens and recorded with a TCSPC detector (HydraHarp 400; PicoQuant GMBH). Fluorescence was detected through a 483/32 single band-pass filter (Semrock) on Single Photon Avalanche Photodiodes, SPAD (MPD), set up at 256 × 256 pixels. Arrival time of single photons was measured with SymPhoTime software (PicoQuant GMBH) while the images were taken with LAS AF software (Leica). To obtain the best resolution, a fivefold zoom factor was applied, giving a pixel size of 0.193 µm and an image size of 49.21 × 49.21 µm. Because the statistical determination of the distribution of single photon arrival time requires a minimum of 100 photons per pixel, 120 frames were acquired at 200 Hz and summed in the final image.

Because interaction dynamics rely on both the K_d of the interaction and the spatial and temporal concomitance of the two proteins, measuring the interaction between a membrane-incorporated protein and a cytosol-diffusing protein is convoluted by strong divergence between their diffusion coefficients and their volume of mobility. Therefore, to test the ability of a free-diffusing protein to interact with TRPM8 for a period sufficient to generate a FRET signal, we concomitantly expressed a free SYFP2 protein with TRPM8-mTurquoise2.

The TD FLIM images have been analyzed with custom-made software named MAPI (IRI, USR 3078 Centre National de la Recherche Scientifique, BCF).

Immunocytochemistry

Cells were cotransfected with his-tagged hTRPM8pcDNA4 plasmid and HA-tagged TCAF1 or myc-tagged TCAF2, and were washed two times, fixed with 4% formaldehyde–1× PBS for 15 min, washed three times, then permeabilized in PBS-gelatin (1.2%) complemented with 0.01% Tween 20 and 100 mM glycine for 30 min at 37°C. Afterward, cells were incubated with primary antibodies: 1:200 goat polyclonal anti-TRPM8 antibody (Antibodies Online), rabbit anti-HA (1:100; Abcam), and mouse anti-myc (1:100; Invitrogen) in PBS-gelatin at 37°C for 1.5 h. After thorough washes, the slides were treated with the corresponding secondary antibodies: donkey Rhodamine Red-X–labeled anti–goat (dilution 1:300; Jackson ImmunoResearch Laboratories, Inc.) and donkey Alexa Fluor 488–labeled anti–rabbit (dilution 1/250; Jackson ImmunoResearch Laboratories, Inc.) diluted in PBS-gelatin for 1 h at room temperature. The slides were then incubated with 0.3% Sudan Black in 70% ethanol in order to reduce autofluorescence, washed two times, and mounted with Mowiol. Fluorescence analysis was performed using a confocal microscope (LSM 700; Carl Zeiss, Inc.) and ImageJ analysis software.

Total RNA extraction and reverse transcription

Total RNAs were extracted from small pieces of localized tumor using the RNeasy Midi kit (QIAGEN) and from bone marrow aspirates using the QIAamp RNA Blood kit (QIAGEN) according to the manufacturer's instructions.

Total RNA from human testis, dorsal root ganglion, prostate, bladder, colon, kidney, liver, lung, smooth muscle, heart, and brain was purchased from Takara Bio Inc., and subjected to reverse transcription as described in Bidaux et al. (2007).

Electrophysiology

Macroscopic membrane ion currents were recorded at 37°C using the patch-clamp technique in its whole cell configuration. The currents were acquired using a PC-9 amplifier (HEKA) in the case of whole-cell measurements and an Axopatch 200B amplifier (Molecular Devices), and analyzed offline using pClamp (Molecular Devices) and Origin software (OriginLab Corporation). The extracellular solution (osmolarity 310 mOsmol/liter) contained (in mM): 150 NaCl, 5 KCl, 10 TEA-Cl, 10 Hepes, 10 glucose, 1 $MgCl_2$, and 2 $CaCl_2$, pH 7.3 (adjusted with NaOH). The intracellular pipette solution (osmolarity 290 mOsmol/liter) contained (in mM): 140 CsCl, 10 Hepes, 8 EGTA, 1 $MgCl_2$, and 4 $CaCl_2$ (100 nM free Ca^{2+}), pH 7.2 (adjusted with CsOH). Patch pipettes were made from borosilicate glass capillaries (WPI). The resistance of the pipettes varied between 3 and 5 MΩ. For single-channel analysis, the extracellular and pipette solutions contained (in mM): 150 KCl, 5 glucose, 10 Hepes, 1 $CaCl_2$, and 2 $MgCl_2$, pH 7.3 (adjusted with KOH) to bring the membrane potential close to zero and minimize junction potentials. Necessary supplements were added directly to the respective solutions at concentrations that would not significantly change the osmolarity. Changes in the external solutions were performed using a multibarrel puffing micropipette with common outflow that was positioned in close proximity to the cell under investigation. During the experiment, the cell was continuously superfused with the solution via a puffing pipette to reduce possible artifacts related to the switch from static to moving solution and vice versa.

To achieve the expression of the TRPM8 channel with a plasma membrane density of one channel per patch on average, HEK-293_{M8i} cells were induced by 1 µg/ml tetracycline until the first open TRPM8 channels could be detected (typically 4 h, 20 min). To prevent the overexpression of the TRPM8 channel and avoid the appearance of multiple channels, the currents were recorded within 30 min of observation of the initial TRPM8 activity. Alternatively, HEK-293_{M8i} cells were treated with 1 µg/ml tetracycline for a short duration (typically 20 min). After this, cells were washed multiple times with fresh media and left overnight. Both approaches yielded identical TRPM8 currents.

The acquisition of TRPM8 activity was performed in cell-attached patches at room temperature (T = 20°C, controlled by a room thermostat). First, patches were subjected to a series of potentials ranging from −100 mV to 150 mV to assess the presence of the TRPM8 channel. Patches that contained TRPM8 activity were then recorded using an episodic stimulation protocol that held membrane potential at 100 mV for 10 s followed by the application of −30 mV for 2 s to prevent TRPM8 activity rundown. First, activity at room temperature was recorded, followed by the application of 100 µM menthol, to maximally stimulate TRPM8 channel.

Selection of traces suitable for single-channel analysis was performed by rejecting traces that at any point exhibited multiple simultaneous openings. Observing menthol-stimulated activity for at least 5 min

and taking mean open and closed dwell times to be 0.6 and 19 ms, respectively, the probability that two identical channels would never exhibit multiple conductance levels was $<\sim 10^{-210}$ (Baumgartner et al., 1997), which demonstrates the validity of this rejection criterion. Recorded activity was quantified by performing a single-channel search analysis using the Clampfit-10 program (pClamp software suit, Molecular Devices) and QuB 2.0 programs as described previously (Qin and Li, 2004; Fernández et al., 2011).

Imaging

Cytosolic Ca^{2+} concentrations were measured using the ratiometric dye Fura-2/AM (Invitrogen Ltd, UK) and quantified according to Grynkiewicz et al. (1985). Cells were loaded with 1 µM of Fura-2/AM for 30 min then washed and bathed in the same extracellular solution as described for whole cell recording for at least 10 min before Ca^{2+} measurements were done. Observations were performed at 37°C on an Eclipse Ti microscope using an S Fluor 20×/0.75 NA objective lens (both from Nikon). Images were collected through a Rolera EM-C^2 charge-coupled device (CCD) camera (QImaging) controlled with Metafluor software (Molecular Devices). Data were then analyzed with Origin 6.1 software (OriginLab Corporation). Unless otherwise indicated, all reagents were purchased from Sigma-Aldrich.

For the confocal Ca^{2+} imaging, changes in the $[Ca^{2+}]_i$ in LNCaP cells were imaged using the high-affinity fluorescent Ca^{2+} indicator fluo-4, which was loaded by a 50-min incubation of the cells with 5 µM fluo-4 acetoxymethyl ester followed by a 60-min wash to allow time for de-esterification. Confocal $[Ca^{2+}]_i$ imaging was performed as described previously (Povstyan et al., 2011; Shapovalov et al., 2013a). In brief, experimental chambers containing the cells were placed on the stage of an Axiovert 200M inverted microscope attached to an LSM 510 META laser-scanning unit (Carl Zeiss). x-y confocal images of fluo-4 fluorescence were acquired at 0.6 Hz using a Plan-Apochromat 40× 1.3 NA objective lens (Carl Zeiss). Fluo-4 fluorescence was excited by the 488 nm line of a 500 mW argon ion laser (Laser-Fertigung) and was captured at wavelengths >505 nm. The illumination intensity was attenuated to 0.6% with an acousto-optical tunable filter (Carl Zeiss). In all experiments, the photomultiplier gain was set at 688. To optimize signal quality, the pinhole was set to provide a confocal optical section <4 µm.

Time-lapse video microscopy

Cells were seeded at low density and kept at 37°C under 5% CO_2 in an incubator chamber for time-lapse video recording (Okolab). Cell movements were monitored with an inverted microscope (Eclipse Ti-E; Nikon) using a 10×/0.25 NA Plan objective lens.

Images were acquired every 10 min for a time lapse of 10 h with a CCD video camera (Roper Scientific) using MetaMorph software (Universal Imaging Corp.). Image stacks were analyzed with ImageJ software and at least 60 cells per condition were manually tracked using the MtrackJ plugin. We excluded dividing cells as well as cells that exited the imaged field during the time-lapse acquisition period. The parameters of speed and migratory persistence index were considered for the data analyses. The migratory persistence index was calculated as the Euclidean distance from the starting point to the final position of the cell (i.e., the shortest distance distance) divided by the accumulated distance (total path length). This value was then normalized for the total duration of the cell track duration and the value was multiplied by the square root of the cell track duration as described previously (Messina et al., 2011).

At least six fields for each condition were analyzed in each independent experiment. At least three independent experiments were done for each experimental condition.

Statistical analysis

Values are expressed as means ± SEM. The statistical significance of differences between groups was determined by analysis of variance (ANOVA) followed by pairwise comparison using Scheffe's method for patch-clamp recordings and an unpaired Student's *t* test for qPCR. A nonparametric unpaired Wilcoxon-Mann-Whitney test was used as a scoring method to assess statistical significance for migration assays. Differences in means with a $P < 0.05$ were considered statistically significant. Statistical analyses were performed using Origin 6.1 software (OriginLab Corporation) and InStat v3.06 (GraphPad Software, Inc.) or Kaleidagraph software for migration assays (Synergy Software).

Online supplemental material

Fig. S1 shows TCAF interactions with TRPV6 and TRPM2. Fig. S2 shows the expression and functional analysis of the TRPM8–TCAFs complex. Fig. S3 shows that menthol-induced responses in human prostate epithelial cells are modulated by TCAF1 and TCAF2. Fig. S4 shows a sample activity of the TRPM8 channel. Fig. S5 depicts a comparison of the fit of control and TCAF1-bound TRPM8 activity to different kinetic models. Table S1 shows the full list of interacting peptides with TRPM8 channel, a summary of which can be found in Table S2. Online supplemental material is available at http://www.jcb.org/cgi/content/full/jcb.201402076/DC1.

The authors would like to thank Prof. Varda Rotter for kindly providing the human epithelial prostate cells, Ep156T; Prof Viana and Prof. Pardo for kindly providing with prostate cell lines and input for the analysis of endogenous TRPM8 function analysis; and Prof. Theodorus W.J. Gadella for the Original pmTurquoise2-N1, pmTurquoise2-C1, and pSYFP2-C1 vectors.

This study was supported by grants from the French Ministère de l'Education Nationale and the Institut National de la Santé et de la Recherche Médicale. D. Gkika was supported by a long-term fellowship from the European Molecular Biology Organization (ALTF 161-2006) and the Institut National du Cancer Convention (07/3D1616/Pdoc-110-18/NG-NC). M. Bernardini was supported by the Vinci PhD fellowship of the Franco-Italian University (C3fr-64). D. Gordienko is supported by State Funds for Fundamental Research (F 46.2/001).

The authors declare no competing financial interests.

Submitted: 14 February 2014
Accepted: 1 December 2014

References

Baumgartner, W., K. Hohenthanner, G.F. Höfer, K. Groschner, and C. Romanin. 1997. Estimating the number of channels in patch-clamp recordings: application to kinetic analysis of multichannel data from voltage-operated channels. *Biophys. J.* 72:1143–1152. http://dx.doi.org/10.1016/S0006-3495(97)78763-0

Bautista, D.M., J. Siemens, J.M. Glazer, P.R. Tsuruda, A.I. Basbaum, C.L. Stucky, S.E. Jordt, and D. Julius. 2007. The menthol receptor TRPM8 is the principal detector of environmental cold. *Nature*. 448:204–208. http://dx.doi.org/10.1038/nature05910

Bavencoffe, A., D. Gkika, A. Kondratskyi, B. Beck, A.S. Borowiec, G. Bidaux, J. Busserolles, A. Eschalier, Y. Shuba, R. Skryma, and N. Prevarskaya. 2010. The transient receptor potential channel TRPM8 is inhibited via the α 2A adrenoreceptor signaling pathway. *J. Biol. Chem.* 285:9410–9419. http://dx.doi.org/10.1074/jbc.M109.069377

Bavencoffe, A., A. Kondratskyi, D. Gkika, B. Mauroy, Y. Shuba, N. Prevarskaya, and R. Skryma. 2011. Complex regulation of the TRPM8 cold receptor channel: role of arachidonic acid release following M3 muscarinic receptor stimulation. *J. Biol. Chem.* 286:9849–9855. http://dx.doi.org/10.1074/jbc.M110.162016

Beck, B., G. Bidaux, A. Bavencoffe, L. Lemonnier, S. Thebault, Y. Shuba, G. Barrit, R. Skryma, and N. Prevarskaya. 2007. Prospects for prostate cancer imaging and therapy using high-affinity TRPM8 activators. *Cell Calcium*. 41:285–294. http://dx.doi.org/10.1016/j.ceca.2006.07.002

Behrendt, H.J., T. Germann, C. Gillen, H. Hatt, and R. Jostock. 2004. Characterization of the mouse cold-menthol receptor TRPM8 and vanilloid receptor type-1 VR1 using a fluorometric imaging plate reader (FLIPR) assay. *Br. J. Pharmacol.* 141:737–745. http://dx.doi.org/10.1038/sj.bjp.0705652

Bidaux, G., M. Flourakis, S. Thebault, A. Zholos, B. Beck, D. Gkika, M. Roudbaraki, J.L. Bonnal, B. Mauroy, Y. Shuba, et al. 2007. Prostate cell differentiation status determines transient receptor potential melastatin member 8 channel subcellular localization and function. *J. Clin. Invest.* 117:1647–1657. http://dx.doi.org/10.1172/JCI30168

Bödding, M., U. Wissenbach, and V. Flockerzi. 2007. Characterisation of TRPM8 as a pharmacophore receptor. *Cell Calcium*. 42:618–628. http://dx.doi.org/10.1016/j.ceca.2007.03.005

Brauchi, S., P. Orio, and R. Latorre. 2004. Clues to understanding cold sensation: thermodynamics and electrophysiological analysis of the cold receptor TRPM8. *Proc. Natl. Acad. Sci. USA*. 101:15494–15499. http://dx.doi.org/10.1073/pnas.0406773101

Chang, Q., S. Hoefs, A.W. van der Kemp, C.N. Topala, R.J. Bindels, and J.G. Hoenderop. 2005. The β-glucuronidase klotho hydrolyzes and activates the TRPV5 channel. *Science*. 310:490–493. http://dx.doi.org/10.1126/science.1114245

Chetrite, G.S., J. Cortes-Prieto, J.C. Philippe, F. Wright, and J.R. Pasqualini. 2000. Comparison of estrogen concentrations, estrone sulfatase and aromatase activities in normal, and in cancerous, human breast tissues. *J. Steroid Biochem. Mol. Biol.* 72:23–27. http://dx.doi.org/10.1016/S0960-0760(00)00040-6

Chuang, H.H., W.M. Neuhausser, and D. Julius. 2004. The super-cooling agent icilin reveals a mechanism of coincidence detection by a temperature-sensitive TRP channel. *Neuron*. 43:859–869. http://dx.doi.org/10.1016/j.neuron.2004.08.038

Chung, M.K., S.J. Jung, and S.B. Oh. 2011. Role of TRP channels in pain sensation. *Adv. Exp. Med. Biol.* 704:615–636. http://dx.doi.org/10.1007/978-94-007-0265-3_33

Clapham, D.E. 2003. TRP channels as cellular sensors. *Nature*. 426:517–524. http://dx.doi.org/10.1038/nature02196

Colburn, R.W., M.L. Lubin, D.J. Stone Jr., Y. Wang, D. Lawrence, M.R. D'Andrea, M.R. Brandt, Y. Liu, C.M. Flores, and N. Qin. 2007. Attenuated cold sensitivity in TRPM8 null mice. *Neuron*. 54:379–386. http://dx.doi.org/10.1016/j.neuron.2007.04.017

Descoeur, J., V. Pereira, A. Pizzoccaro, A. Francois, B. Ling, V. Maffre, B. Couette, J. Busserolles, C. Courteix, J. Noel, et al. 2011. Oxaliplatin-induced cold hypersensitivity is due to remodelling of ion channel expression in nociceptors. *EMBO Mol. Med.* 3:266–278. http://dx.doi.org/10.1002/emmm.201100134

Dhaka, A., A.N. Murray, J. Mathur, T.J. Earley, M.J. Petrus, and A. Patapoutian. 2007. TRPM8 is required for cold sensation in mice. *Neuron*. 54:371–378. http://dx.doi.org/10.1016/j.neuron.2007.02.024

Felsenstein, J. 1988. Phylogenies from molecular sequences: inference and reliability. *Annu. Rev. Genet.* 22:521–565. http://dx.doi.org/10.1146/annurev.ge.22.120188.002513

Fernández, J.A., R. Skryma, G. Bidaux, K.L. Magleby, C.N. Scholfield, J.G. McGeown, N. Prevarskaya, and A.V. Zholos. 2011. Voltage- and cold-dependent gating of single TRPM8 ion channels. *J. Gen. Physiol.* 137:173–195. http://dx.doi.org/10.1085/jgp.201010498

Fujimoto, N., Y. Akimoto, T. Suzuki, S. Kitamura, and S. Ohta. 2006. Identification of prostatic-secreted proteins in mice by mass spectrometric analysis and evaluation of lobe-specific and androgen-dependent mRNA expression. *J. Endocrinol.* 190:793–803. http://dx.doi.org/10.1677/joe.1.06733

Gerster, U., B. Neuhuber, K. Groschner, J. Striessnig, and B.E. Flucher. 1999. Current modulation and membrane targeting of the calcium channel α1C subunit are independent functions of the β subunit. *J. Physiol.* 517:353–368. http://dx.doi.org/10.1111/j.1469-7793.1999.0353t.x

Gkika, D., and N. Prevarskaya. 2011. TRP channels in prostate cancer: the good, the bad and the ugly? *Asian J. Androl.* 13:673–676. http://dx.doi.org/10.1038/aja.2011.18

Gkika, D., F. Mahieu, B. Nilius, J.G. Hoenderop, and R.J. Bindels. 2004. 80K-H as a new Ca^{2+} sensor regulating the activity of the epithelial Ca^{2+} channel transient receptor potential cation channel V5 (TRPV5). *J. Biol. Chem.* 279:26351–26357. http://dx.doi.org/10.1074/jbc.M403801200

Gkika, D., C.N. Topala, Q. Chang, N. Picard, S. Thébault, P. Houillier, J.G. Hoenderop, and R.J. Bindels. 2006a. Tissue kallikrein stimulates $Ca^{(2+)}$ reabsorption via PKC-dependent plasma membrane accumulation of TRPV5. *EMBO J.* 25:4707–4716. http://dx.doi.org/10.1038/sj.emboj.7601357

Gkika, D., C.N. Topala, J.G. Hoenderop, and R.J. Bindels. 2006b. The immunophilin FKBP52 inhibits the activity of the epithelial Ca^{2+} channel TRPV5. *Am. J. Physiol. Renal Physiol.* 290:F1253–F1259. http://dx.doi.org/10.1152/ajprenal.00298.2005

Gkika, D., M. Flourakis, L. Lemonnier, and N. Prevarskaya. 2010. PSA reduces prostate cancer cell motility by stimulating TRPM8 activity and plasma membrane expression. *Oncogene*. 29:4611–4616. http://dx.doi.org/10.1038/onc.2010.210

Goedhart, J., D. von Stetten, M. Noirclerc-Savoye, M. Lelimousin, L. Joosen, M.A. Hink, L. van Weeren, T.W. Gadella Jr., and A. Royant. 2012. Structure-guided evolution of cyan fluorescent proteins towards a quantum yield of 93%. *Nat. Commun.* 3:751. http://dx.doi.org/10.1038/ncomms1738

Gouy, M., S. Guindon, and O. Gascuel. 2010. SeaView version 4: A multiplatform graphical user interface for sequence alignment and phylogenetic tree building. *Mol. Biol. Evol.* 27:221–224. http://dx.doi.org/10.1093/molbev/msp259

Grynkiewicz, G., M. Poenie, and R.Y. Tsien. 1985. A new generation of Ca2+ indicators with greatly improved fluorescence properties. *J. Biol. Chem.* 260:3440–3450.

Guindon, S., and O. Gascuel. 2003. A simple, fast, and accurate algorithm to estimate large phylogenies by maximum likelihood. *Syst. Biol.* 52:696–704. http://dx.doi.org/10.1080/10635150390235520

Henshall, S.M., D.E. Afar, J. Hiller, L.G. Horvath, D.I. Quinn, K.K. Rasiah, K. Gish, D. Willhite, J.G. Kench, M. Gardiner-Garden, et al. 2003. Survival analysis of genome-wide gene expression profiles of prostate cancers identifies new prognostic targets of disease relapse. *Cancer Res.* 63:4196–4203.

Huelsenbeck, J.P., and F. Ronquist. 2001. MRBAYES: Bayesian inference of phylogenetic trees. *Bioinformatics*. 17:754–755. http://dx.doi.org/10.1093/bioinformatics/17.8.754

Kawashiri, T., N. Egashira, K. Kurobe, K. Tsutsumi, Y. Yamashita, S. Ushio, T. Yano, and R. Oishi. 2012. L type Ca^{2+} channel blockers prevent oxaliplatin-induced cold hyperalgesia and TRPM8 overexpression in rats. *Mol. Pain*. 8:7. http://dx.doi.org/10.1186/1744-8069-8-7

Kogan, I., N. Goldfinger, M. Milyavsky, M. Cohen, I. Shats, G. Dobler, H. Klocker, B. Wasylyk, M. Voller, T. Aalders, et al. 2006. hTERT-immortalized prostate epithelial and stromal-derived cells: an authentic in vitro model for differentiation and carcinogenesis. *Cancer Res.* 66:3531–3540. http://dx.doi.org/10.1158/0008-5472.CAN-05-2183

Köttgen, M., and G. Walz. 2005. Subcellular localization and trafficking of polycystins. *Pflugers Arch.* 451:286–293. http://dx.doi.org/10.1007/s00424-005-1417-3

Latorre, R., S. Brauchi, R. Madrid, and P. Orio. 2011. A cool channel in cold transduction. *Physiology (Bethesda)*. 26:273–285. http://dx.doi.org/10.1152/physiol.00004.2011

Livak, K.J., and T.D. Schmittgen. 2001. Analysis of relative gene expression data using real-time quantitative PCR and the $2^{(-\Delta\Delta C(T))}$) Method. *Methods*. 25:402–408. http://dx.doi.org/10.1006/meth.2001.1262

Mälkiä, A., R. Madrid, V. Meseguer, E. de la Peña, M. Valero, C. Belmonte, and F. Viana. 2007. Bidirectional shifts of TRPM8 channel gating by temperature and chemical agents modulate the cold sensitivity of mammalian thermoreceptors. *J. Physiol.* 581:155–174. http://dx.doi.org/10.1113/jphysiol.2006.123059

McKemy, D.D., W.M. Neuhausser, and D. Julius. 2002. Identification of a cold receptor reveals a general role for TRP channels in thermosensation. *Nature*. 416:52–58. http://dx.doi.org/10.1038/nature719

Messina, A., N. Ferraris, S. Wray, G. Cagnoni, D.E. Donohue, F. Casoni, P.R. Kramer, A.A. Derijck, Y. Adolfs, A. Fasolo, et al. 2011. Dysregulation of Semaphorin7A/β1-integrin signaling leads to defective GnRH-1 cell migration, abnormal gonadal development and altered fertility. *Hum. Mol. Genet.* 20:4759–4774. http://dx.doi.org/10.1093/hmg/ddr403

Nilius, B., G. Owsianik, T. Voets, and J.A. Peters. 2007. Transient receptor potential cation channels in disease. *Physiol. Rev.* 87:165–217. http://dx.doi.org/10.1152/physrev.00021.2006

Peier, A.M., A. Moqrich, A.C. Hergarden, A.J. Reeve, D.A. Andersson, G.M. Story, T.J. Earley, I. Dragoni, P. McIntyre, S. Bevan, and A. Patapoutian. 2002. A TRP channel that senses cold stimuli and menthol. *Cell*. 108:705–715. http://dx.doi.org/10.1016/S0092-8674(02)00652-9

Posada, D., and K.A. Crandall. 1998. MODELTEST: testing the model of DNA substitution. *Bioinformatics*. 14:817–818. http://dx.doi.org/10.1093/bioinformatics/14.9.817

Povstyan, O.V., M.I. Harhun, and D.V. Gordienko. 2011. Ca2+ entry following P2X receptor activation induces IP3 receptor-mediated Ca^{2+} release in myocytes from small renal arteries. *Br. J. Pharmacol.* 162:1618–1638. http://dx.doi.org/10.1111/j.1476-5381.2010.01169.x

Prevarskaya, N., R. Skryma, and Y. Shuba. 2011. Calcium in tumour metastasis: new roles for known actors. *Nat. Rev. Cancer*. 11:609–618. http://dx.doi.org/10.1038/nrc3105

Qin, F., and L. Li. 2004. Model-based fitting of single-channel dwell-time distributions. *Biophys. J.* 87:1657–1671. http://dx.doi.org/10.1529/biophysj.103.037531

Sabnis, A.S., M. Shadid, G.S. Yost, and C.A. Reilly. 2008. Human lung epithelial cells express a functional cold-sensing TRPM8 variant. *Am. J. Respir. Cell Mol. Biol.* 39:466–474. http://dx.doi.org/10.1165/rcmb.2007-0440OC

Schmidt, U., S. Fuessel, R. Koch, G.B. Baretton, A. Lohse, S. Tomasetti, S. Unversucht, M. Froehner, M.P. Wirth, and A. Meye. 2006. Quantitative multi-gene expression profiling of primary prostate cancer. *Prostate*. 66:1521–1534. http://dx.doi.org/10.1002/pros.20490

Shapovalov, G., D. Gkika, M. Devilliers, A. Kondratskyi, D. Gordienko, J. Busserolles, A. Bokhobza, A. Eschalier, R. Skryma, and N. Prevarskaya. 2013a. Opiates modulate thermosensation by internalizing cold receptor TRPM8. *Cell Reports*. 4:504–515. http://dx.doi.org/10.1016/j.celrep.2013.07.002

Shapovalov, G., R. Skryma, and N. Prevarskaya. 2013b. Calcium channels and prostate cancer. *Recent Patents Anticancer. Drug Discov.* 8:18–26. http://dx.doi.org/10.2174/1574892811308010018

Sinkins, W.G., M. Goel, M. Estacion, and W.P. Schilling. 2004. Association of immunophilins with mammalian TRPC channels. *J. Biol. Chem.* 279:34521–34529. http://dx.doi.org/10.1074/jbc.M401156200

Sipieter, F., P. Vandame, C. Spriet, A. Leray, P. Vincent, D. Trinel, J.F. Bodart, F.B. Riquet, and L. Héliot. 2013. From FRET imaging to practical methodology for kinase activity sensing in living cells. *Prog. Mol. Biol. Transl. Sci.* 113:145–216. http://dx.doi.org/10.1016/B978-0-12-386932-6.00005-3

Stein, R.J., S. Santos, J. Nagatomi, Y. Hayashi, B.S. Minnery, M. Xavier, A.S. Patel, J.B. Nelson, W.J. Futrell, N. Yoshimura, et al. 2004. Cool (TRPM8) and hot (TRPV1) receptors in the bladder and male genital tract. *J. Urol.* 172:1175–1178. http://dx.doi.org/10.1097/01.ju.0000134880.55119.cf

Su, L., C. Wang, Y.H. Yu, Y.Y. Ren, K.L. Xie, and G.L. Wang. 2011. Role of TRPM8 in dorsal root ganglion in nerve injury-induced chronic pain. *BMC Neurosci.* 12:120. http://dx.doi.org/10.1186/1471-2202-12-120

Thebault, S., L. Lemonnier, G. Bidaux, M. Flourakis, A. Bavencoffe, D. Gordienko, M. Roudbaraki, P. Delcourt, Y. Panchin, Y. Shuba, et al. 2005. Novel role of cold/menthol-sensitive transient receptor potential melastatine family member 8 (TRPM8) in the activation of store-operated channels in LNCaP human prostate cancer epithelial cells. *J. Biol. Chem.* 280:39423–39435. http://dx.doi.org/10.1074/jbc.M503544200

Tsavaler, L., M.H. Shapero, S. Morkowski, and R. Laus. 2001. Trp-p8, a novel prostate-specific gene, is up-regulated in prostate cancer and other malignancies and shares high homology with transient receptor potential calcium channel proteins. *Cancer Res.* 61:3760–3769.

Valero, M., C. Morenilla-Palao, C. Belmonte, and F. Viana. 2011. Pharmacological and functional properties of TRPM8 channels in prostate tumor cells. *Pflugers Arch.* 461:99–114. http://dx.doi.org/10.1007/s00424-010-0895-0

Valero, M.L., F. Mello de Queiroz, W. Stühmer, F. Viana, and L.A. Pardo. 2012. TRPM8 ion channels differentially modulate proliferation and cell cycle distribution of normal and cancer prostate cells. *PLoS ONE*. 7:e51825. http://dx.doi.org/10.1371/journal.pone.0051825

van de Graaf, S.F., J.G. Hoenderop, D. Gkika, D. Lamers, J. Prenen, U. Rescher, V. Gerke, O. Staub, B. Nilius, and R.J. Bindels. 2003. Functional expression of the epithelial $Ca^{(2+)}$ channels (TRPV5 and TRPV6) requires association of the S100A10-annexin 2 complex. *EMBO J.* 22:1478–1487. http://dx.doi.org/10.1093/emboj/cdg162

van de Graaf, S.F., J.G. Hoenderop, and R.J. Bindels. 2006. Regulation of TRPV5 and TRPV6 by associated proteins. *Am. J. Physiol. Renal Physiol.* 290: F1295–F1302. http://dx.doi.org/10.1152/ajprenal.00443.2005

Veliz, L.A., C.A. Toro, J.P. Vivar, L.A. Arias, J. Villegas, M.A. Castro, and S. Brauchi. 2010. Near-membrane dynamics and capture of TRPM8 channels within transient confinement domains. *PLoS ONE*. 5:e13290. http://dx.doi.org/10.1371/journal.pone.0013290

Voets, T., G. Droogmans, U. Wissenbach, A. Janssens, V. Flockerzi, and B. Nilius. 2004. The principle of temperature-dependent gating in cold- and heat-sensitive TRP channels. *Nature*. 430:748–754. http://dx.doi.org/10.1038/nature02732

Vogel, R.O., R.J. Janssen, M.A. van den Brand, C.E. Dieteren, S. Verkaart, W.J. Koopman, P.H. Willems, W. Pluk, L.P. van den Heuvel, J.A. Smeitink, and L.G. Nijtmans. 2007. Cytosolic signaling protein Ecsit also localizes to mitochondria where it interacts with chaperone NDUFAF1 and functions in complex I assembly. *Genes Dev.* 21:615–624. http://dx.doi.org/10.1101/gad.408407

Wondergem, R., T.W. Ecay, F. Mahieu, G. Owsianik, and B. Nilius. 2008. HGF/SF and menthol increase human glioblastoma cell calcium and migration. *Biochem. Biophys. Res. Commun.* 372:210–215. http://dx.doi.org/10.1016/j.bbrc.2008.05.032

Yang, Z.H., X.H. Wang, H.P. Wang, and L.Q. Hu. 2009. Effects of TRPM8 on the proliferation and motility of prostate cancer PC-3 cells. *Asian J. Androl.* 11:157–165. http://dx.doi.org/10.1038/aja.2009.1

Yee, N.S., W. Zhou, and M. Lee. 2010. Transient receptor potential channel TRPM8 is over-expressed and required for cellular proliferation in pancreatic adenocarcinoma. *Cancer Lett.* 297:49–55. http://dx.doi.org/10.1016/j.canlet.2010.04.023

Yudin, Y., and T. Rohacs. 2012. Regulation of TRPM8 channel activity. *Mol. Cell. Endocrinol.* 353:68–74. http://dx.doi.org/10.1016/j.mce.2011.10.023

Zhang, L., and G.J. Barritt. 2006. TRPM8 in prostate cancer cells: a potential diagnostic and prognostic marker with a secretory function? *Endocr. Relat. Cancer*. 13:27–38. http://dx.doi.org/10.1677/erc.1.01093

Zhang, X., S. Mak, L. Li, A. Parra, B. Denlinger, C. Belmonte, and P.A. McNaughton. 2012. Direct inhibition of the cold-activated TRPM8 ion channel by Gαq. *Nat. Cell Biol.* 14:851–858. http://dx.doi.org/10.1038/ncb2529

Zhu, G., X. Wang, Z. Yang, H. Cao, Z. Meng, Y. Wang, and D. Chen. 2011. Effects of TRPM8 on the proliferation and angiogenesis of prostate cancer PC-3 cells in vivo. *Oncol Lett*. 2:1213–1217.

Article 6

Orai1/NFAT pathway is a gatekeeper of cancer stem cells quiescence/activation transition

Running Title: Calcium and cancer stem cell

Lucile Noyer[2*], Pilar Flamenco[1,2*], Yasmine Touil[1,3], Christian Slomianny[2], Pauline Ostyn[1], Dimitra Gkika[2,4], Raja El Machhour[1], Jerome Vandomme[1,4], Pascaline Segard[1,4], Fabien Vanden Abeele[2], Pierre Formstecher[1,4,5], Renata Polakowska[1*], Natalia Prevarskaya[2,4 *] and Loïc Lemonnier[2*#]

[1.] Inserm UMR-S 1172 Jean-Pierre Aubert Research Center, Institut pour la Recherche sur le Cancer de Lille (IRCL), 59045 Lille, France
[2.] Inserm, U1003, Laboratoire de Physiologie Cellulaire, Equipe labellisée par la Ligue contre le Cancer, Villeneuve d'Ascq, F-59650, France
[3.] SIRIC ONCOLille, Lille, France
[4.] Université Lille Nord de France, F-59000 Lille, France
[5.] CHU Lille, F-59000 Lille, France

*Equal contributors

 # Corresponding author: Loïc Lemonnier

Loïc Lemonnier
Laboratoire de Physiologie Cellulaire, INSERM U1003, Bâtiment SN3, USTL, 59655 Villeneuve d'Ascq Cedex, France; Tel.: +33-3-20-43-68-38; Fax: +33-3-20-43-40-66; E-mail: loic.lemonnier@inserm.fr

Abstract

Background

Despite the establishment of the crucial role played by cancer stem cells (CSCs) in cancer progression, the mechanisms controlling CSCs quiescence/activation states remain poorly understood. Our aim was here to investigate the potential involvement in these phenomena of calcium channels previously identified as key players in cancer progression.

Methods

Prostate cancer (PC3) and melanoma (HBL) cell lines were used to generate tumour mimicking spheres from which quiescent/slow cycling cells with CSCs properties were sorted by FACS. Control cells and CSCs were then further characterized by RT-PCR, immunofluorescence, confocal microscopy, calcium imaging and flow cytometry. Observations were confirmed with siRNAs targeting the calcium channel Orai1.

Results

We here present initial evidence that calcium channel Orai1 expression is down-regulated in prostate cancer and melanoma CSCs. The low level of Orai1 is functionally associated with a major decrease in store-operated calcium entry and cytosolic calcium concentration. This in turn down-regulates the Ca^{2+}-calcineurin-NFAT/CBP signalling pathway. Furthermore, we demonstrate that the impairment of Orai1 activity in non-stem cells effectively increases stemness-defining sphere-forming capacity and expansion of the stem cell pool in both prostate cancer and melanoma cell lines. We also show that Orai1 suppression endows CSCs with a chemotherapy-resistant phenotype.

Conclusions

Our findings uncover a previously unknown Ca^{2+}-dependent regulatory mechanism governing CSC reactivation, and potentially associated with their propagation and consequent cancer relapse.

Keywords

Melanoma, prostate cancer, cancer stem cell, Orai1 calcium channel, calcineurin/NFAT signaling

Background

Stem cells are undifferentiated, long-living cells that are unique in their ability to produce, by asymmetric division, a stem cell (SC) daughter in order to maintain the stem cell pool and a transient amplifying (TA) daughter that after several divisions is destined to differentiate. SC quiescence is crucial to protect their pool from exhaustion under conditions of diverse stresses and to ensure lifelong tissue preservation [1,2]. Increasing evidence supports the idea that cancer is driven by cancer stem cells (CSCs) [3,4]. According to this model, conventional therapies would only result in the elimination of dividing cancer cells with limited proliferation potential. These therapies would however spare the quiescent CSCs, which can be activated to proliferate and lead to metastatic tumor relapse after diverse periods of tumor dormancy [5]. When and why tumor dormancy occurs and what the mechanisms are that control activation of quiescent cells is still unclear.

Extracellular calcium and membrane channels controlling intracellular calcium concentration are known to play a crucial role in the regulation of cell proliferation and differentiation [6]. Ca^{2+} could therefore potentially control stem cell quiescence/activity transition. Although Ca^{2+} significance in the regulation of the balance proliferation/differentiation is becoming clearer, its role in regulating stem cells and their quiescence is still unknown.

One of the main calcium entry pathways into cells is Store-Operated Ca^{2+} Entry (SOCE), also known as capacitative calcium entry, mediated by Store-Operated Channels (SOCs) [7]. Molecular actors and events resulting in SOCE involve proteins from two families: STIM and Orai. STIM proteins (STIM1 and STIM2) act in the ER membrane as $[Ca^{2+}]_{ER}$ sensors, whereas Orai family members (Orai1-

3) are potential channel-forming subunits of plasma membrane SOC, which can be activated upon interaction with STIM proteins [8]. Recently, we determined that in prostate cancer, the redistribution of Orai proteins acts as an oncogenic switch mechanism [9] in response to genomic and microenvironment perturbations. Such remodeling disrupts the equilibrium of Orai channels and favors cell progression to a more aggressive pro-proliferative phenotype. The role of SOC and its molecular actors in CSCs have however only started to emerge [10,11].

Ca^{2+} signaling pathways modulate the activity of a number of Ca^{2+}-dependent enzymes, and consequently the activity of specific transcription factors, including the nuclear factor of activated T cells (NFAT). Ca^{2+} activation of the Ca^{2+}/calmodulin-dependent serine phosphatase, calcineurin, dephosphorylates NFAT. NFAT then translocates to the nucleus and activates the transcription of a number of genes [12]. Interestingly, NFAT can also be activated by Ca^{2+} nanodomains close to open SOCs [13,14]. We previously showed that the NFAT pathway controls human prostate cancer cell proliferation [15]. In contrast, NFATc1 isoform controls hair follicle stem cell quiescence by suppressing the cyclin dependent kinase 4 (CDK4) and cell cycle progression [16]. Thus, NFAT may either stimulate or inhibit cell cycle progression. The underlying mechanisms regulating NFAT's dual functions may involve a choice of co-activator usage as was demonstrated for β-catenin. When interacting with cAMP response element-binding protein (CREB)-binding protein (CBP), β-catenin controls stem cell self-renewal, but stimulates its differentiation when partnering with a CBP-related p300 transcriptional co-activator [17]. Indeed, CBP, shown to control stem cell maintenance [18,19] and to function as a tumor suppressor [20], interacts with NFAT. However, a direct mechanistic connection between Ca^{2+}/NFAT/CBP and the determination of cancer stem cell fate has not yet been documented.

Here, we investigated the expression and involvement of SOCE in the control of CSCs in two different cancer models, melanoma and prostate. We demonstrated that CSCs in both cell lines display lower SOCE than non-CSCs, which correlated with the down-regulation of Orai1. Moreover, we present evidence that CBP/calcineurin-NFAT signaling complex modulates CSCs quiescence and the size of the CSCs compartment.

Methods

Cell Culture and Spheres

The HBL human melanoma cell line was provided by Pr. Ghanem (Bruxelles, Belgium [21]). Cells were maintained in culture as previously described [22]. The androgen-independent human PC3 cells were obtained from the American Type Culture Collection and maintained in culture in RPMI 1640, GlutaMAX (Life Technologies, France) supplemented with 10% fetal bovine serum (FBS) (Lonza, Verviers, Belgium). Cells were grown at 37°C in a humidified atmosphere containing 5% CO_2.

To generate spheres, 2×10^3 cells were plated as previously described [22] and maintained in a humidified 5% CO_2 incubator at 37°C for 7 days. Spheres were counted under microscope, and dissociated mechanically for sorting experiments.

Identification of quiescent/slow cycling cells and FACS sorting

For the tracing of quiescent/slow cycling melanoma cells, the previously described stably transfected melanoma HBL-(H2B-GFP) cell line expressing the tetracycline-inducible fused histone 2B-green fluorescent protein (H2B-GFP) protein was used

[22]. In order to induce GFP, cells were treated with tetracycline (1 µg/ml) for 24 hours at 37°C in adherent cultures.

To detect quiescent/slow cycling prostate cancer cells, PC3 cells resuspended in serum-free RPMI were stained with 1 µl/10^6 cells of Vybrant DiI cell-labeling solution (Invitrogen) for 25 min at 37°C. After rinsing, the cells were re-plated for sphere formation assay. After 7 days of label dilution in HBL-H2BGFP or PC3 sphere cultures, the 5% of cells with the highest and lowest GFP or DiI staining indices were sorted by fluorescence-activated cell sorting (FACS) using a Beckman Coulter Altra instrument.

Immunofluorescence studies

Sorted cells were plated on Lab-Tek chamber glass coverslips (Millicell EZ SLIDE 8-well glass, sterile Merck Milipore, Darmstadt, Germany) at a density of 20 000 cells per well. After 24 hours the adherent cells were fixed in paraformaldehyde solution and immunocytochemistry was performed according to standard procedure [22]. The following primary antibodies were used: monoclonal anti-Melan A, anti-Ki67 and anti-CBP (Santa Cruz Biotech) at a 1:50 dilution, anti-ORAI1 (PM-5207, ProSci) and anti-CD44 (Immunotools, Germany) at 1:500 and anti-NFAT (Abcam, ab25916) at a 1:100 dilution. Positive cells were detected with secondary antibodies: Cy5® Goat anti-Rabbit IgG (H+L), Alexa 488 or AlexaFluor 594 Goat anti-mouse (Life Technologies, France) at a dilution of 1:2000. Negative controls were performed by replacing the primary antibody with an irrelevant isotype. Nuclei were counterstained with Hoescht 33342. All slides were mounted with Vectashield mounting medium (Vector Laboratories, Nanterre, France). Distribution of the labelled proteins was analyzed by confocal immunofluorescence microscopy using a Zeiss LSM 510.

Average signal intensity in selected areas was analyzed using ImageJ software. Intensity was normalized with an average of three independent background values on the same slide.

RNA Extraction and qRT-PCR

RNA extraction was performed following the manufacturer's protocol (Nucleospin® RNA XS Kit, MN Macherey Nagel). Quantitative real-time PCR of Orai1 mRNA transcript was done using MESA GREEN qPCR MasterMix Plus for SYBR Assay (Eurogentec) on the Bio-Rad CFX96 Real-Time PCR Detection System. Primers sequence is indicated in supplementary table 1. 18S rRNA gene was used as an endogenous control to normalize variations in RNA extractions, the degree of RNA degradation, and variability in RT efficiency. To quantify the results, we used the comparative threshold cycle method described by Livak and Schmittgen [23].

siRNA transfections

Cells were transfected with either 100 nM of control siRNA against Luciferase (si Luc) or 100 nM of siRNA against Orai1 (si Orai1) using HiPerFect Transfection Reagent (Qiagen SA, Courtaboeuf, France), and were observed on the 3rd day following transfection. We previously reported the efficiency of this method in down-regulating the expression of the Orai1 protein in LNCaP cells [24].

$[Ca^{2+}]_i$ measurements

Sorted cells were transferred onto glass coverslips and used for calcium fluorescence measurements after 24 hours of incubation in the standard growth medium. Cytosolic Ca^{2+} concentration was measured using ratiometric dye Fura-2

(Invitrogen Ltd, United Kingdom). Cells were loaded with 1 µM of Fura-2/AM for 45 minutes then washed and bathed for at least 10 minutes before Ca^{2+} measurements in an extracellular solution of the following composition (in mM): 150 NaCl, 10 HEPES, 10 Glucose, 5 KCl, 2 $CaCl_2$ and 1 $MgCl_2$. All reagents were purchased from Sigma (St. Louis, USA).

Flow cytometry

For cell cycle and Orai1 analysis, HBL or PC3 sphere cell suspensions were either treated as previously described [22], or stained with an anti-ORAI1 or matching isotype (PM-5207, ProSci), at a 1:100 dilution, then rinsed with PBS/BSA (2%), centrifuged, resuspended in 100 µl of PBS BSA (2%) with a secondary antibody, Cy5® Goat anti-mouse (Molecular Probes®, Life Technology™, France) at a 1:2000 dilution and incubated for 30 min on ice in the dark.

Statistical Analysis

All results are expressed as the mean +/- SEM of at least three independent experiments and three repetitions. Comparisons between means were assessed using the unpaired Student's t test. Welch's correction was applied when unequal variance was observed. Statistical analyses were performed using the GraphPad Prism 4.0 software. A p value ≤0.05 was considered as significant.

Results

Orai1 expression decreases in melanoma cells with stem cell-like properties.

Stem cells are mostly quiescent and rarely divide, displaying a slow cell cycling profile. This property has allowed their characterization as label retaining cells

(LRCs) [25]. We generated [22] a Tet-ON controlled Histone 2B-GFP (H2B-GFP)-fusion construct and labeled, isolated and characterized LRCs in HBL melanoma cell line (Supplementary Figure 1).

The importance of calcium in cell physiology has been clearly stated in many cellular models [6,26], but not in stem cells. We used qRT-PCR to evaluate the expression of Orai1, a major actor in calcium entry in non-excitable cells [27], in melanoma stem cells. We observed a 3.5 fold lower *ORAI1* expression in the subpopulation of GFP-positive (GFP^+) stem-like cells than in the GFP-negative (GFP^-) non-stem major subpopulation (Figure 1A). This variation was specific to *ORAI1* transcript, since the expression of *ORAI3*, another calcium channel pertaining to the same protein family, did not differ between these two sub-populations. Confocal fluorescent immunocytochemistry (Figure 1B and Table 1) confirmed that Orai1 level was twice as low in the GFP^+ subpopulation than in the GFP^-. The functional relevance of this decrease was examined by calcium imaging technique [28]. As presented in Figure 1C and 1D, GFP^+ HBL cells exhibited less SOCE than non-stem GFP^- cells. Values corresponding to the difference between the peak ratio and level before calcium add-back (referred to as ratio deltas) were: 1.59 ± 0.12 (GFP^-, n=144), 1.11 ± 0.12 (GFP^+, n=67). In agreement with the observed decrease in Orai1 activity, the GFP^+ HBL cells exhibited a small, albeit extremely significant, reduction in their basal calcium level when compared to GFP^- cells (Figure 1E). Ratio values were: 1.205 ± 0.001 (GFP^-, n=144) and 1.157 ± 0.001 (GFP^+, n=67). Our results therefore associate melanoma stem-like phenotype with a general decrease in calcium level and Orai1 expression.

Orai1 expression is also down-regulated in prostate CSCs.

To check whether the low Orai1/calcium is restricted to melanoma stem cells, we used an unrelated model, the androgen-independent prostate cancer PC3 cell line, labelled with a vital DiI dye to distinguish quiescent LRCs from the cycling population. Cycling cells dilute this dye by half with each cell division. After 7 days of dilution, about 15% of the population was still DiI positive (14.76 ± 3.67; n= 8; Figure 2A). In conjunction with the DiI labelling technique, we also used CD44, a well-known cell surface marker of prostate CSCs, shown to be enriched in sphere-forming cells [29,30]. The double labelling and sphere-forming capacity ensured an accurate identification of quiescent and/or slow cycling prostate CSCs. We isolated a subpopulation of $CD44^+/DiI^+$ prostate CSCs (2.90% ± 0.80; n= 7) by sorting dissociated sphere cells (Figure 2B). As in HBL cells, qRT-PCR analysis determined a 2.5 fold decrease in *ORAI1*, but not in *ORAI3* expression in $CD44^+/DiI^+$ prostate CSCs when compared to their $CD44^-/DiI^-$ counterparts (Figure 2C). The difference in *ORAI1* expression was confirmed at protein (Figure 2D, Table 2) and functional level. Ratio deltas obtained during capacitative calcium entry in non-stem (DiI^-) and stem cells PC3 (DiI^+) were respectively: 8.22 ± 0.28 (n=63) and 5.97 ± 0.17 (n=97, Figure 2E). Summarized in Figure 2F, these data demonstrate that capacitative calcium entry in CSCs was significantly lower than in non-stem PC3 cells and, as observed in melanoma cells, correlated with a significant decrease in basal calcium level (Figure 2G). Ratio values were: 1.28 ± 0.03 (DiI^-, n=63) and 1.15 ± 0.02 (DiI^+, n=97). Taken together, our data indicate that a sub-population of cells exhibiting stem cell-like properties in two unrelated cancer models express low Orai1 levels and show a decrease in SOCE and basal calcium concentration.

Inhibition of Orai1 increases a pool of cells with CSCs properties.

While Orai1 is generally accepted as being ubiquitously involved in SOCE, this has never been confirmed either in melanoma or PC3 cells. We used siRNA against Orai1 to confirm the importance of this channel for SOCE in our models. As shown in Figure 3A, a 3-day treatment with Orai1 siRNA in non-stem HBL cells significantly reduced SOCE entry when compared to cells treated with control siRNA. Ratio deltas were: 2.98 ± 0.27 (siRNA Luc, n=48) and 1.39 ± 0.2 (siRNA Orai1, n=48). Similar results were obtained in melanoma stem cells (Figure 3B), where ratio deltas were: 1.85 ± 0.13 (siRNA Luc, n=43) and 0.66 ± 0.07 (siRNA Orai1, n=88). These results, summarized in Figure 3C, confirm that Orai1 is a key element in controlling SOCE in these cells.

Having defined the involvement of Orai1 in HBL cells SOCE, we examined the effect of its inhibition on cell fate determination. As shown in Figures 3D and 3E, 10 µM BTP2 (an inhibitor of Orai1) strongly inhibited SOCE in non-stem (GFP^-) and stem (GFP^+) melanoma cells. Ratio deltas were as follows: 5.53 ± 0.21 (GFP^- ctrl, n=95), 0.06 ± 0.02 (GFP^- BTP2, n=100); 1.76 ± 0.1 (GFP^+ ctrl, n=87), 0.18 ± 0.04 (GFP^+ BTP2, n=35), Figure 3F. Subsequently to a 24 hour tetracycline-induction, BTP2 (1µM) was added to sphere- cultures. After 7 days of GFP dilution, flow cytometry analysis (Figure 4A) determined that BTP2 induced an increase in the percentage of GFP^+ cells (Figure 4B, 12.51 ± 2.33 vs. 7.17 ± 1.26; n=6, $p<0.05$). This suggests that the inhibition of Orai1 increases the number of quiescent/slow cycling cells in tumor-like melanospheres. Interestingly, spheres treated with BTP2 exhibited a greater ability to form secondary spheres than control spheres (Figures 4C, 4D), thus confirming that a decrease in Orai1 activity effectively raises the pool of stem cells. Similar results were obtained with PC3 cells (supplementary Figure 2).

In summary, our results suggest that Orai1 plays a critical role in the control of SOCE in both melanoma and prostate cancer cells, and that low Orai1 expression level and activity are linked to CSCs phenotype in both models.

Orai1 regulates quiescence via calcineurin-NFAT modulation.

Our data suggest that Ca^{2+} entry via Orai1 controls CSCs quiescence by modulating SOC currents. We have also shown that even in the absence of outside stimulation, CSCs have a lower level of basal calcium correlated to decreased Orai1 expression and activity. To explore the mechanistic relationship between Ca^{2+}, Orai1 and quiescence, we examined the calcineurin-NFAT pathway downstream of Orai1. As shown in Figures 5A and 5B, NFAT is predominantly located in the nucleus of proliferating HBL GFP^- cells, while its distribution is homogenous in GFP^+ quiescent cells. A calcineurin inhibitor, FK506 that blocks NFAT nuclear translocation (Figure 5C), augments the number of spheres (Figure 5D, 103 ± 10 vs. 60 ± 6, n=5; $p<0.01$), along with an increase in GFP expression compared to control cells (Figure 5E). This demonstrates that inactive NFAT increases the pool and quiescence of CSCs.

Chemotherapeutic stress induces quiescence and is associated with a decrease in Orai1 expression.

The CSCs hypothesis portends that CSCs possess comparable resistance to chemotherapy and thus serve as a reservoir for tumor repopulation after therapy [31]. While recent studies have provided evidence that therapy resistance relates to the ability of CSCs to enter quiescence [32–34], the underlying mechanistic relationship remains to be understood. Because our data point to the importance of Orai1 in controlling CSCs quiescence and Orai1 has been linked to apoptosis

[9,35,36], we investigated whether CSCs enter quiescence in response to DNA damage and stress-inducing chemotherapeutics, and whether this correlates with Orai1 expression levels. Melanoma cells were treated during 24h with 100 µM 5-fluorouracil (5FU) or 40 µM oxaliplatin and the proportion of G_0 cells and cells expressing low levels of Orai1 ($Orai1^{low}$) was estimated by flow cytometry analyses. As shown in Figure 6A, 5FU and oxaliplatin treatment significantly increased a quiescent G_0 subpopulation from 12.17 ± 1.53 % in controls to respectively 33.73 ± 4.50 % and 31.98 ± 5.19 % in treated cells. Simultaneously, the $Orai1^{low}$ subpopulation increased from 3.97 ± 0.78% in control to 23.56 ± 2.74% and 32 ± 2.20%, respectively in 5FU and oxaliplatin treated cells (Figure 6B). Clearly, the newly-generated $Orai1^{low}$ cells were mainly in the G_0 phase of the cell cycle (Figure 6C). These results confirm that Orai1 downregulation induces cellular quiescence and suggest that this ability endows CSCs with a chemotherapeutic-resistant phenotype.

NFAT cooperates with CBP to control quiescence and the pool of CSCs.

While investigating for molecular targets of NFAT that could control CSCs quiescence, we concentrated on NFAT-controlled [37] CBP, a transcriptional co-activator, and an important regulator of stemness in different cell types [20,38,39]. As shown in Figures 7A and 7B, CBP expression was higher in GFP^+ than in GFP^- melanoma cells and this expression was further increased by BTP2 and FK506 (Figure 7C). Similar data were obtained with PC3 cells (Figure 7D). Analysis of these data indicates that inactivation of Orai1 or NFAT by BTP2 and FK506 decreases the ratio of non-CSCs pool to CSCs pool when compared to control cells in both models. This phenomenon was accompanied by a decrease in the ratio of $NFAT^+$ to CBP^+

cells within the CSCs compartments, while not significantly affecting this ratio in the non-stem cell compartments (Figure 7, Table 3). This suggests that the balance between the self-renewing CSCs and differentiating non-CSCs is regulated by CBP. The CBP upregulation was accompanied by Orai1 and NFAT inactivation, demonstrating their inverse relationship and thereby implying that Orai1-instigated signaling negatively regulates CBP linked to melanoma and prostate CSC quiescence.

Discussion:

In this study, we present new data supporting the idea of cytoplasmic calcium presiding over CSCs' determination toward either proliferation or quiescence. Using two cancer models as different as neural crest-derived melanoma and epithelial prostate cancer, we conclude that the Orai1 calcium channel and its classic downstream calcineurin-NFAT signaling, are the key actors responsible for a Ca^{2+}-mediated switch between CSCs quiescence and activation. Furthermore, our data suggest that Orai1/calcineurin/NFAT signals exert their regulatory function by cooperating with a CBP transcriptional coactivator, which segregates with an inactive Orai1/NFAT signal. This suggests that the $CBP^{+}/Orai1^{low}/NFAT^{inactive}$ phenotype is a new marker for melanoma and prostate CSCs.

It has been suggested that calcium channels display a functional specificity in the activation of Ca^{2+}-dependent transcription factors and gene expression. Consistent with this hypothesis, NFAT translocation and NFAT-dependent gene expression have been shown to be dependent on Orai1-mediated Ca^{2+} entry [14,40]. NFAT is regulated by the Ca^{2+} concentration achieved locally near the Orai1 channel, likely due to a co-localization of calmodulin-calcineurin-NFAT within the Orai1-

associated nanodomain, in such a way that Ca^{2+} entering via Orai1 can be locally detected by the calcium sensor. It has been proposed that NFAT activation, strictly dependent on Orai1, follows an ‘‘all-or-none’’ mode. If an insufficient number of Orai1 channels are activated, NFAT dephosphorylation is not completed and nuclear translocation does not occur [40]. Our result that NFAT is predominantly localized in the nucleus of proliferating cells, whilst its distribution is mainly in the cytoplasm in quiescent CSCs, could therefore be explained by the reduced number of activated Orai1 channels in a quiescent stem cell population.

We show that when activated, NFAT cooperates with CBP to control quiescence and the pool of CSCs. The influence of CBP in a CSC’s fate decision does not appear to be exceptional. CBP and its homolog p300 protein, were shown to balance self-renewal and differentiation of hematopoietic stem cells [19], to maintain the self-renewal and pluripotency of embryonic stem cells [41] and to govern quiescence, proliferation and differentiation of normal and tumor stem cells [20,42]. Our study mechanistically links CBP to calcium signaling and suggests that CBP, interacts with the NFAT transcription factor to balance CSCs’ quiescence/activation state and determine CSCs’ or non-CSCs’ fates. Thus, we provide one possible explanation of how Ca^{2+} is capable of contributing to cellular processes as diametrically opposed as quiescence, proliferation and differentiation.

Interestingly, inhibitors of either Orai1 expression (siRNA) or activity (BTP2), as well as an inhibitor of calcineurin (FK506), all inactivated NFAT and significantly increased the CSCs compartment encompassing both quiescent G_0 and slow cycling cells at the expense of the fast proliferating/differentiating cell compartment, thus demonstrating that Orai1-signaling activates quiescent CSCs and stimulates their exit from the stem cell compartment. As these phenotypic changes are accompanied by

variations in Ca^{2+} influx and its intracellular concentration, it becomes clear that Orai1 is at the top of the signaling network that controls CSCs' cycling activity and determines their fate. Evidence corroborating this interpretation is provided by a direct relationship between Orai1/SOCE and entry into quiescence of melanoma and prostate CSCs in response to stress-inducing chemotherapeutics. This is an important observation given that Orai1 function was linked to apoptosis [9,35,36], so its downregulation may represent an important mechanism of drug resistance acquired by cellular retraction into a reversible quiescence, an attribute of stem cells [32]. This result is in agreement with a previous report [10], where it was shown that prostate cancer cells overexpressing the stem cells marker SOX2, were exhibiting a reduced expression of Orai1 as well as a decreased SOCE. As in our case, these features were associated with a higher resistance of cells to apoptotic inducers, confirming that the $Orai1^{low}$ phenotype is a new marker of CSCs, at least in melanoma and prostate cancer.

Various studies have clearly stated that inhibition of Orai1 blocks both SOCE and proliferation in cancer cells [9,43]. Our data suggest that, rather than a decrease in cell proliferation as in non-CSCs, a loss of SOCE activity in CSCs elicits an increase in their quiescence. Therefore, while targeting Orai1 would eradicate proliferating cells, it would also increase the pool of drug-resistant CSCs constituting a reservoir of dormant tumor-initiating cells underlying tumor dormancy. If controlled, Orai1-inactivation would therefore offer an anticancer therapy by chronic tumor cell dormancy, potentially preventing tumor relapse.

Conclusion

We show that Orai1 calcium channel and its downstream calcineurin-NFATc1 signaling are the key actors responsible for Ca^{2+} mediated switch between CSCs quiescence and activation. Furthermore, our data suggest that Orai1/calcineurin/NFATc1 signals exert their regulatory function by cooperating with CBP transcriptional coactivator. Our findings therefore provide new insight into the control of CSCs fate, and propose that $CBP^{+}/Orai1^{low}/NFAT^{inactive}$ phenotype is a new marker of melanoma and prostate CSCs. Furthermore, we demonstrate that the impairment of Orai1 activity in non-stem cells effectively increases stemness properties, and that it endows CSCs with chemotherapy resistant phenotype. Thus, our findings uncover a previously unknown Ca^{2+}-dependent regulatory mechanism governing CSC reactivation, potentially associated with their propagation and cancer relapse.

List of abbreviations

5FU: 5-fluorouracil; **CDK4**: cyclin dependent kinase 4; **CBP**: CREB-binding protein; **CREB**: cAMP response element-binding protein; **CSCs**: cancer stem cells; **ER**: endoplasmic reticulum; **FACS**: fluorescence-activated cell sorting; **H2B-GFP**: histone 2B-green fluorescent protein; **LRCs**: label retaining cells; **NFAT**: nuclear factor of activated T cells; **SC**: stem cell; **SOC**: Store-Operated Channels; **SOCE**: Store-Operated Ca^{2+} Entry; **TA**: transient amplifying;

Declarations

Ethics approval and consent to participate: not applicable

Consent for publication: not applicable

Availability of data and materials: all data generated or analyzed during this study are included in this published article [and its supplementary information files]

Competing interests: the authors declare that they have no competing interests

Funding: this study was supported by grants from the Institut National de la Sante et de la Recherche Medicale (INSERM), SIRIC ONCOLille, La Ligue Contre le Cancer comité du Septentrion, Université Lille and the SILAB-Jean Paufique Corporate Foundation. P. Flamenco was supported by fellowships from CPER (Contrat de Plan Etat/Région) Nord - Pas de Calais and ERASMUS Mundus. Y. Touil was supported by the Institut pour la Recherche sur le Cancer de Lille (IRCL) and by SIRIC ONCOLille. R. El Machhour was supported by Ligue Nationale Contre le Cancer.

Authors' contributions: PF and LL designed and carried out most of the experiments presented in this manuscript, and wrote it together. YT, PO, REM, JV and PS helped with cell culture (sphere formation) and subsequent CSCs sorting. CS carried out the confocal experiments. DG designed all qRT-PCR primers used in this study, and provided technical insight regarding molecular biology experiments. FVA contributed to calcium imaging experiments. PF edited the manuscript. RP and NP equally contributed to project conception, and to the manuscript edition. All the authors have read and approved the manuscript.

Acknowledgements: The authors thank N. Jouy (BiCell-IFR114) for her assistance with flow cytometry analyses and FACS sorting, and E. Richard (BioImaging Center Lille - IFR 147) for access to the instruments and technical advice.

References

1. Cheng T, Rodrigues N, Shen H, Yang Y, Dombkowski D, Sykes M, et al. Hematopoietic stem cell quiescence maintained by p21cip1/waf1. Science. 2000;287:1804–8.

2. Cheung TH, Rando TA. Molecular regulation of stem cell quiescence. Nat. Rev. Mol. Cell Biol. 2013;14:329–40.

3. Reya T, Morrison SJ, Clarke MF, Weissman IL. Stem cells, cancer, and cancer stem cells. Nature. 2001;414:105–11.

4. Nguyen LV, Vanner R, Dirks P, Eaves CJ. Cancer stem cells: an evolving concept. Nat. Rev. Cancer. 2012;12:133–43.

5. Coller HA, Sang L, Roberts JM. A new description of cellular quiescence. PLoS Biol. 2006;4:e83.

6. Clapham DE. Calcium signaling. Cell. 2007;131:1047–58.

7. Skryma R, Mariot P, Bourhis XL, Coppenolle FV, Shuba Y, Vanden Abeele F, et al. Store depletion and store-operated Ca2+ current in human prostate cancer LNCaP cells: involvement in apoptosis. J. Physiol. 2000;527 Pt 1:71–83.

8. Soboloff J, Spassova MA, Tang XD, Hewavitharana T, Xu W, Gill DL. Orai1 and STIM reconstitute store-operated calcium channel function. J. Biol. Chem. 2006;281:20661–5.

9. Dubois C, Vanden Abeele F, Lehen'kyi V, Gkika D, Guarmit B, Lepage G, et al. Remodeling of channel-forming ORAI proteins determines an oncogenic switch in prostate cancer. Cancer Cell. 2014;26:19–32.

10. Jia X, Li X, Xu Y, Zhang S, Mou W, Liu Y, et al. SOX2 promotes tumorigenesis and increases the anti-apoptotic property of human prostate cancer cell. J. Mol. Cell Biol. 2011;3:230–8.

11. Hu J, Qin K, Zhang Y, Gong J, Li N, Lv D, et al. Downregulation of transcription factor Oct4 induces an epithelial-to-mesenchymal transition via enhancement of Ca2+ influx in breast cancer cells. Biochem. Biophys. Res. Commun. 2011;411:786–91.

12. Hogan PG, Chen L, Nardone J, Rao A. Transcriptional regulation by calcium, calcineurin, and NFAT. Genes Dev. 2003;17:2205–32.

13. Kar P, Nelson C, Parekh AB. CRAC channels drive digital activation and provide analog control and synergy to Ca(2+)-dependent gene regulation. Curr. Biol. CB. 2012;22:242–7.

14. Kar P, Samanta K, Kramer H, Morris O, Bakowski D, Parekh AB. Dynamic assembly of a membrane signaling complex enables selective activation of NFAT by Orai1. Curr. Biol. CB. 2014;24:1361–8.

15. Thebault S, Flourakis M, Vanoverberghe K, Vandermoere F, Roudbaraki M, Lehen'kyi V, et al. Differential role of transient receptor potential channels in Ca2+ entry and proliferation of prostate cancer epithelial cells. Cancer Res. 2006;66:2038–47.

16. Horsley V, Aliprantis AO, Polak L, Glimcher LH, Fuchs E. NFATc1 balances quiescence and proliferation of skin stem cells. Cell. 2008;132:299–310.

17. Teo J-L, Kahn M. The Wnt signaling pathway in cellular proliferation and differentiation: A tale of two coactivators. Adv. Drug Deliv. Rev. 2010;62:1149–55.

18. Kitsos CM, Sankar U, Illario M, Colomer-Font JM, Duncan AW, Ribar TJ, et al. Calmodulin-dependent protein kinase IV regulates hematopoietic stem cell maintenance. J. Biol. Chem. 2005;280:33101–8.

19. Rebel VI, Kung AL, Tanner EA, Yang H, Bronson RT, Livingston DM. Distinct roles for CREB-binding protein and p300 in hematopoietic stem cell self-renewal. Proc. Natl. Acad. Sci. U. S. A. 2002;99:14789–94.

20. Wang F, Marshall CB, Ikura M. Transcriptional/epigenetic regulator CBP/p300 in tumorigenesis: structural and functional versatility in target recognition. Cell. Mol. Life Sci. CMLS. 2013;70:3989–4008.

21. Ghanem GE, Comunale G, Libert A, Vercammen-Grandjean A, Lejeune FJ. Evidence for alpha-melanocyte-stimulating hormone (alpha-MSH) receptors on human malignant melanoma cells. Int. J. Cancer J. Int. Cancer. 1988;41:248–55.

22. Ostyn P, El Machhour R, Begard S, Kotecki N, Vandomme J, Flamenco P, et al. Transient TNF regulates the self-renewing capacity of stem-like label-retaining cells in sphere and skin equivalent models of melanoma. Cell Commun. Signal. CCS. 2014;12:52.

23. Livak KJ, Schmittgen TD. Analysis of relative gene expression data using real-time quantitative PCR and the 2(-Delta Delta C(T)) Method. Methods San Diego Calif. 2001;25:402–8.

24. Flourakis M, Lehen'kyi V, Beck B, Raphaël M, Vandenberghe M, Abeele FV, et al. Orai1 contributes to the establishment of an apoptosis-resistant phenotype in prostate cancer cells. Cell Death Dis. 2010;1:e75.

25. Pece S, Tosoni D, Confalonieri S, Mazzarol G, Vecchi M, Ronzoni S, et al. Biological and molecular heterogeneity of breast cancers correlates with their cancer stem cell content. Cell. 2010;140:62–73.

26. Prevarskaya N, Skryma R, Shuba Y. Calcium in tumour metastasis: new roles for known actors. Nat. Rev. Cancer. 2011;11:609–18.

27. Prakriya M. Store-operated Orai channels: structure and function. Curr. Top. Membr. 2013;71.

534 28. Kondratska K, Kondratskyi A, Yassine M, Lemonnier L, Lepage G, Morabito A, et
535 al. Orai1 and STIM1 mediate SOCE and contribute to apoptotic resistance of
536 pancreatic adenocarcinoma. Biochim. Biophys. Acta. 2014;1843:2263–9.

537 29. Garraway IP, Sun W, Tran CP, Perner S, Zhang B, Goldstein AS, et al. Human
538 prostate sphere-forming cells represent a subset of basal epithelial cells capable of
539 glandular regeneration in vivo. The Prostate. 2010;70:491–501.

540 30. Patrawala L, Calhoun-Davis T, Schneider-Broussard R, Tang DG. Hierarchical
541 organization of prostate cancer cells in xenograft tumors: the CD44+alpha2beta1+
542 cell population is enriched in tumor-initiating cells. Cancer Res. 2007;67:6796–805.

543 31. Alison MR, Lin W-R, Lim SML, Nicholson LJ. Cancer stem cells: in the line of fire.
544 Cancer Treat. Rev. 2012;38:589–98.

545 32. Borst P. Cancer drug pan-resistance: pumps, cancer stem cells, quiescence,
546 epithelial to mesenchymal transition, blocked cell death pathways, persisters or
547 what? Open Biol. 2012;2:120066.

548 33. Touil Y, Igoudjil W, Corvaisier M, Dessein A-F, Vandomme J, Monté D, et al.
549 Colon cancer cells escape 5FU chemotherapy-induced cell death by entering
550 stemness and quiescence associated with the c-Yes/YAP axis. Clin. Cancer Res.
551 Off. J. Am. Assoc. Cancer Res. 2014;20:837–46.

552 34. Ehninger A, Boch T, Medyouf H, Müdder K, Orend G, Trumpp A. Loss of SPARC
553 protects hematopoietic stem cells from chemotherapy toxicity by accelerating their
554 return to quiescence. Blood. 2014;123:4054–63.

555 35. Cui W, Ma J, Wang X, Yang W, Zhang J, Ji Q. Free fatty acid induces
556 endoplasmic reticulum stress and apoptosis of beta-cells by Ca2+/calpain-2
557 pathways. PloS One. 2013;8.

558 36. Henke N, Albrecht P, Bouchachia I, Ryazantseva M, Knoll K, Lewerenz J, et al.
559 The plasma membrane channel ORAI1 mediates detrimental calcium influx caused
560 by endogenous oxidative stress. Cell Death Dis. 2013;4.

561 37. Matsubara T, Ikeda F, Hata K, Nakanishi M, Okada M, Yasuda H, et al. Cbp
562 recruitment of Csk into lipid rafts is critical to c-Src kinase activity and bone
563 resorption in osteoclasts. J. Bone Miner. Res. Off. J. Am. Soc. Bone Miner. Res.
564 2010;25:1068–76.

565 38. Ring A, Kim Y-M, Kahn M. Wnt/Catenin signaling in adult stem cell physiology
566 and disease. Stem Cell Rev. 2014;10:512–25.

567 39. Chitilian JM, Thillainadesan G, Manias JL, Chang WY, Walker E, Isovic M, et al.
568 Critical components of the pluripotency network are targets for the p300/CBP
569 interacting protein (p/CIP) in embryonic stem cells. Stem Cells Dayt. Ohio.
570 2014;32:204–15.

571 40. Ong HL, Jang S-I, Ambudkar IS. Distinct contributions of Orai1 and TRPC1 to
572 agonist-induced [Ca(2+)](i) signals determine specificity of Ca(2+)-dependent gene
573 expression. PloS One. 2012;7:e47146.

41. Fang F, Xu Y, Chew K-K, Chen X, Ng H-H, Matsudaira P. Coactivators p300 and CBP maintain the identity of mouse embryonic stem cells by mediating long-range chromatin structure. Stem Cells Dayt. Ohio. 2014;32:1805–16.

42. Kida A, Kahn M. Hypoxia selects for a quiescent, CML stem/leukemia initiating-like population dependent on CBP/catenin transcription. Curr. Mol. Pharmacol. 2013;6:204–10.

43. Umemura M, Baljinnyam E, Feske S, De Lorenzo MS, Xie L-H, Feng X, et al. Store-operated Ca2+ entry (SOCE) regulates melanoma proliferation and cell migration. PloS One. 2014;9:e89292.

Figure legends:

Figure 1: Orai1 expression and calcium signaling are down-regulated in HBL CSCs. (A): Real-time quantitative PCR showing the expression of *orai1* and *orai3* in HBL GFP^- and GFP^+ FACS-sorted subpopulations (n=4 *, $p<0.05$). (B): Confocal microscopy of HBL GFP^- and GFP^+ cells. Sorted cells were immuno-reacted with anti-Orai1 antibody (red), Hoechst 33342 stained nuclei are in blue. Scale bar = 20µm. Representative images of 4-6 fields from 3 independent experiments. Table 1: Average ± S.E.M fluorescence intensities measured in cells from three independent experiments (***$p<0.001$). (C): Time course of calcium imaging in response to SERCA pump inhibitor thapsigargin in the absence of extracellular calcium. Thapsigargin and calcium add-backs are indicated by bars. (D): Histogram summarizing deltas of ratio observed in (C) after calcium addition; $p<0.05$. (E): Histogram presenting basal calcium levels in GFP^- and GFP^+ HBL cells as observed in (C); $p<0.001$.

Figure 2: PC3 CSCs have altered calcium signaling. (A): Dilution of DiI vital dye by PC3 cells. Flow cytometry histogram overlay shows DiI^+ cells at time 0, 4 and 7 days of dilution. Vertical line indicates window for DiI^+ cells (representative experiment). (B): Two-color flow cytometry analyses of DiI^- and CD44-labelled PC3 cells. The red rectangle gates the double positive population. (C): Real-time quantitative PCR showing the expression of *orai1* and *orai3* in PC3 $DiI^-/CD44^-$ and PC3 $DiI^+/CD44^+$ FACS-sorted subpopulations (n=3 **, $p< 0.01$). (D): Confocal microscopy of PC3 cells. Live cells were labeled with DiI and after 7 days of dilution were immuno-reacted with anti-CD44 antibody and then sorted. Shown are DiI (orange) and indirect CD44 (green) and Orai1 immunofluorescence (red), Hoechst

33342 stained nuclei are in blue. Scale bar = 20µm. Representative images of 4-6 fields from 3 independent experiments. Table 2: Average ± S.E.M of fluorescence intensities measured in PC3 cells. Data from three experiments (***, $p<0.001$) (E): Time course of cellular responses observed by calcium imaging technique. Thapsigargin and calcium add-backs are indicated by bars. (F) Histogram summarizing ratio deltas observed in (E) after calcium addition; $p<0.001$. (G): Histogram presenting basal calcium levels in DiI^- and DiI^+ PC3 cells as observed in (E); $p<0.05$.

Figure 3: Orai1 is a key actor in HBL cells' SOCE. (A, B): Time courses of calcium ratios after 3 days of treatment with siRNA targeting Orai1 (siOrai1) or Luciferase (siLuc). Thapsigargin and calcium add-backs are indicated by bars. (C): Histogram summarizing deltas of ratio observed in (A) and (B) after calcium addition; $p<0.001$. (D, E): Time courses of calcium ratios in the presence or absence of 10 µM BTP2. Thapsigargin and calcium add-backs are indicated by bars. (F): -Histogram summarizing ratio deltas observed in (D) and (E) after calcium addition; $p<0.001$.

Figure 4: Inhibition of Orai1 increases stemness in CSCs (A, B): Representative experiment where HBL-H2B-GFP cells, after a 24h-long induction with tetracycline, were incubated with BTP2 (1µM) or Control. After 7 days the percentage of GFP^+ cells was determined by flow cytometry. (B): Corresponding quantitative histogram (n=5 *, $p<0.05$). (C): BTP2 increases SFU in the total population of HBL cells compared to control. Scale bar, 500µm. (D): Quantification of SFU treated with BTP2 or control, **, $p<0.01$.

Figure 5: Orai1 regulates quiescence via NFAT modulation (A): Confocal microscopy of HBL GFP^+ and GFP^- cells. Sorted cells were immuno-reacted with

anti-NFAT antibody (red), Hoescht 33342 stained nuclei (blue). Representative images of 4-6 fields from 3 independent experiments. (B): Cellular distribution of NFAT in GFP^+ cells (left) and GFP^- (right). Top: galleries show (from left to right) images of nuclei fluorescence (blue), GFP fluorescence (green), NFAT fluorescence (red) and their overlay. Bottom: spatial profiles of GFP (green curve) and NFAT (red curve) fluorescence along the yellow line, shown on the overlay images (top), respectively. Note predominant translocation of NFAT to the nuclei in GFP^- cells. (C): Confocal microscopy of HBL spheres total population treated or not (control) with FK506 10µM during 7 days. Representative images of 4-6 fields from 3 independent experiments. (D): FK506 treatment increases percentage of SFU (E) and GFP positive cells (n=6 *, $p<0.05$).

Figure 6: Chemotherapy treatment induces quiescence and is associated with a decrease in Orai1 expression (A): HBL cells were treated with 100 µM 5FU or 40 µM oxaliplatin. After 24h, quiescent cells were analyzed by the flow cytometry Ki67/IP assay, (n=5, **$p< 0.01$). (B): $Orai1^{low}$ subpopulation was analyzed by flow cytometry after 5FU and oxaliplatin treatment (24h, n=3, *$p=0.05$). (C): Cell cycle distribution gated in $Orai1^{low}$ subpopulation. 5FU and oxaliplatin 24h treatment increase the quiescent $Orai1^{low}$ subpopulation (representative experiment), n=3.

Figure 7: NFAT cooperates with CBP to control quiescence and the CSCs pool: Confocal microscopy of HBL GFP^- (A) and HBL GFP^+. (B): Sorted cells were immuno-reacted with anti-CBP antibody (red), Hoescht 33342 stained nuclei (blue). Representative images of 4-6 images from 3 independent experiments. Scale bar, 20µm. Flow cytometry histograms show the percentage of CBP positive cells in HBL-H2B GFP^- and GFP^+ (C) and PC3 $DiI^-/CD44^-$ or $DiI^+/CD44^+$ (D) subpopulations in

control conditions and after treatment with 1µM BTP2 or 10µM FK506. Table3 shows ratio between non CSCs/CSCs in both cell lines and the corresponding $NFAT^{+}/CBP^{+}$ ratio.

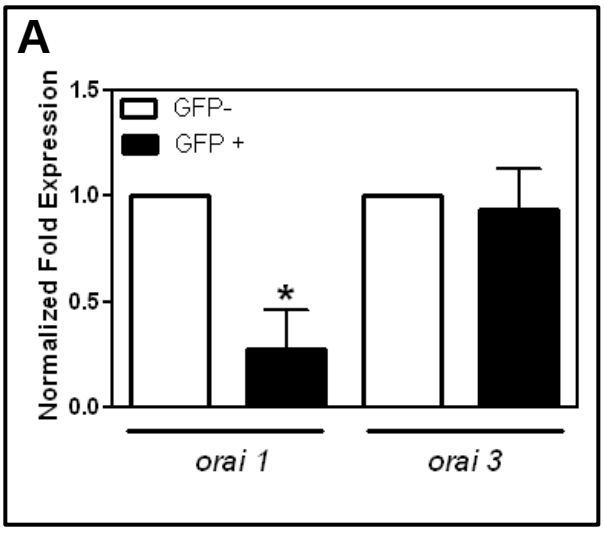

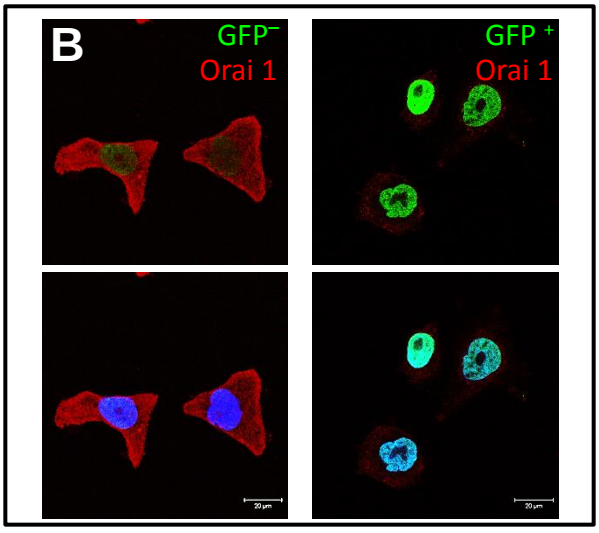

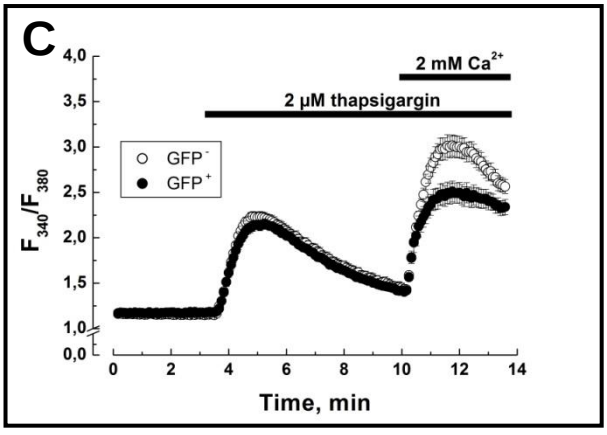

Table 1: Average Signal Intensity Orai1

GFP⁻ HBL Cells	GFP⁺ HBL Cells
15.70 ± 0.39	7.24 ± 0.56***

HDR de Loïc Lemonnier, Lille 1, 2017

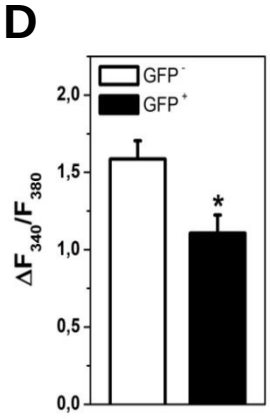

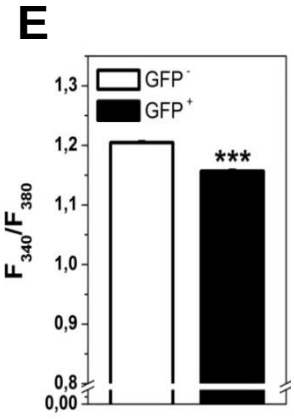

Figure 1

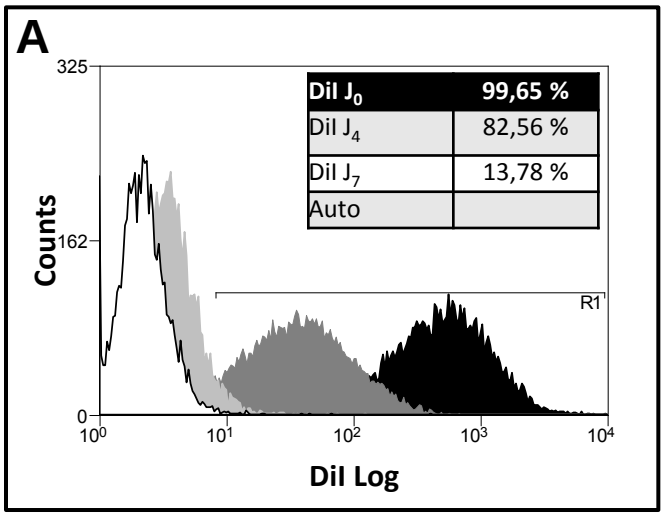

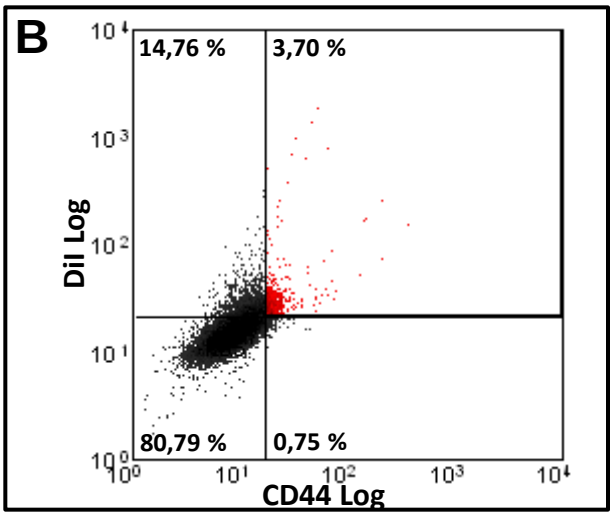

HDR de Loïc Lemonnier, Lille 1, 2017

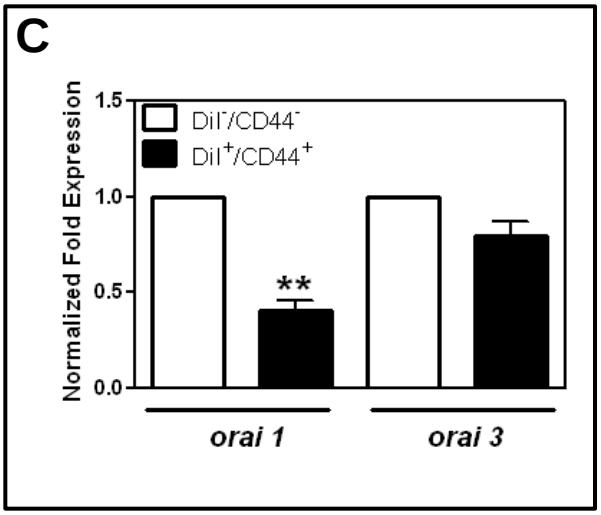

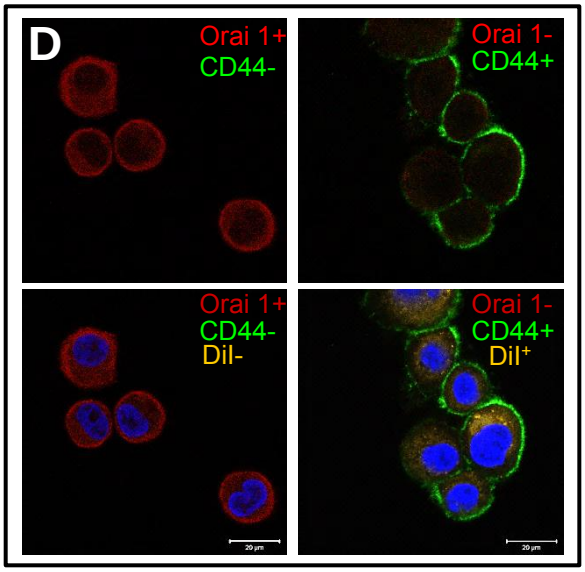

Table 2: Average Signal Intensity Orai1

Dil-/CD44- PC3 Cells	Dil+/CD44+ PC3 Cells
12.03 ± 0.67	4.13 ± 0.17 ***

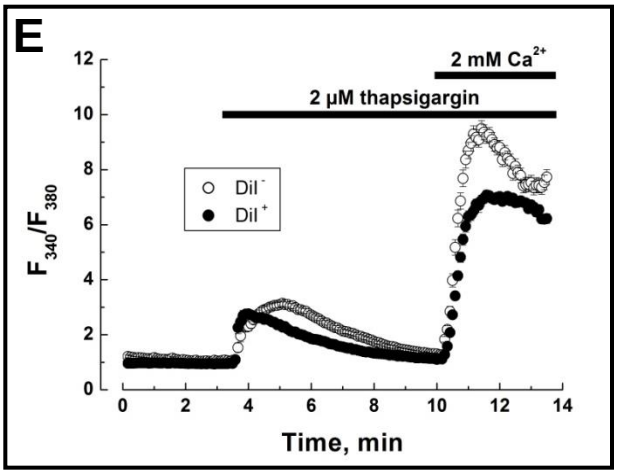

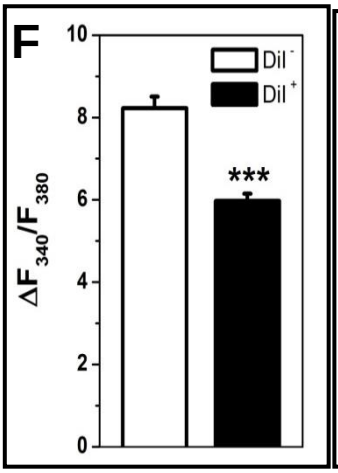

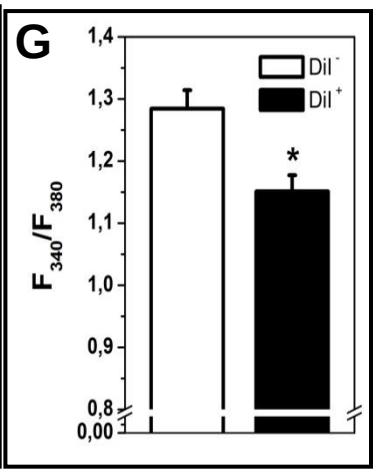

Figure 2

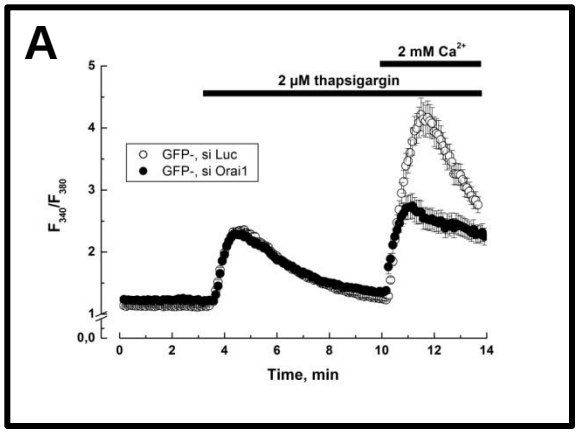

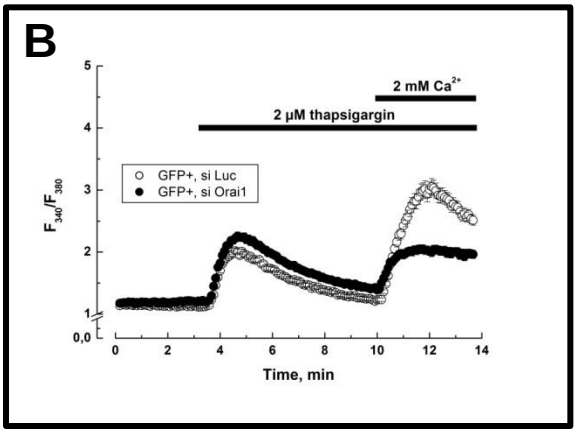

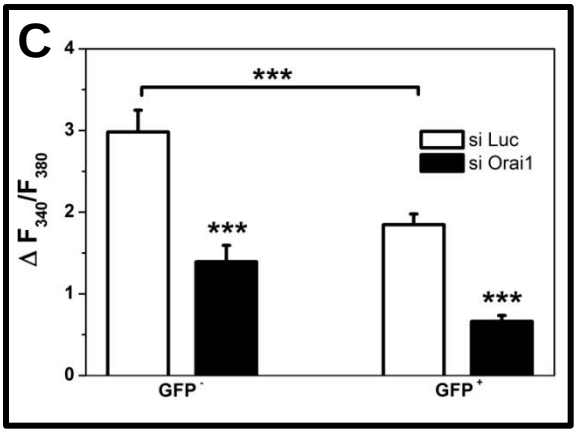

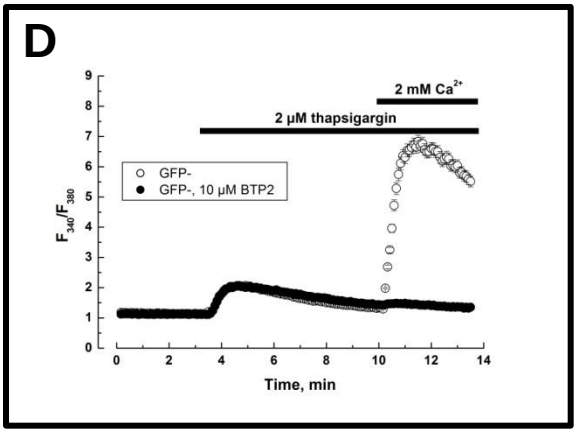

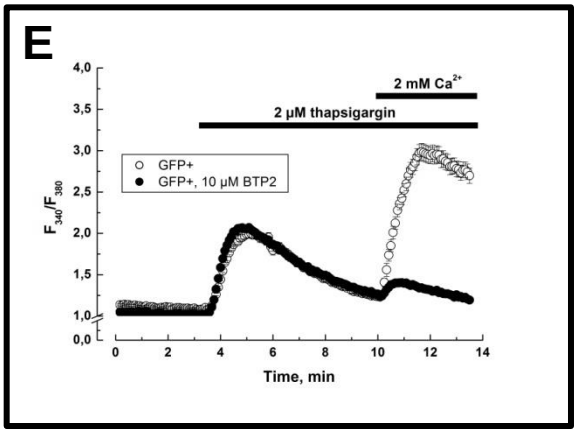

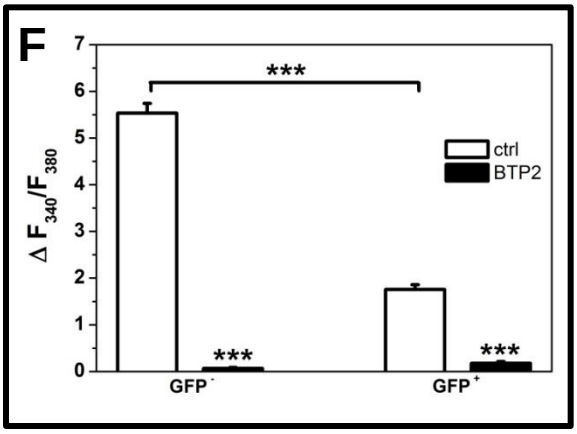

HDR de Loïc Lemonnier, Lille 1, 2017

Figure 3

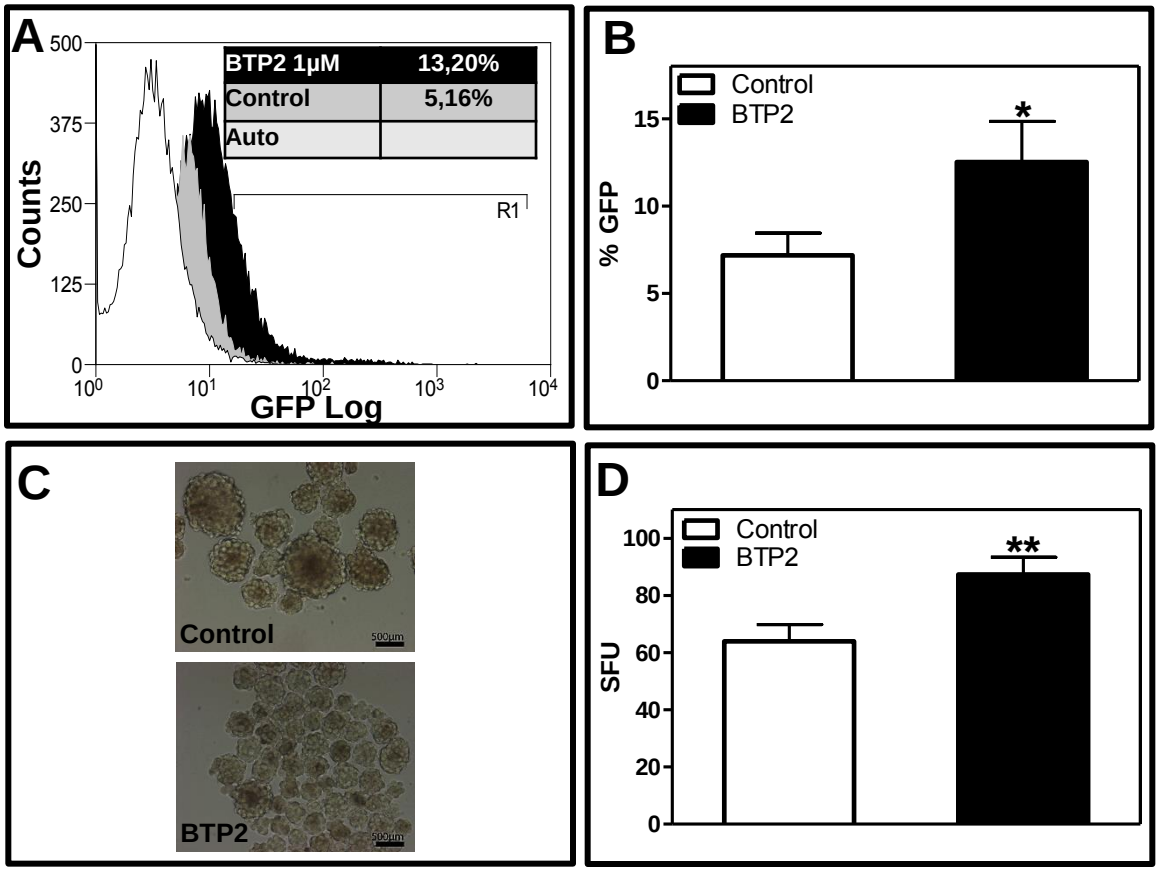

Figure 4

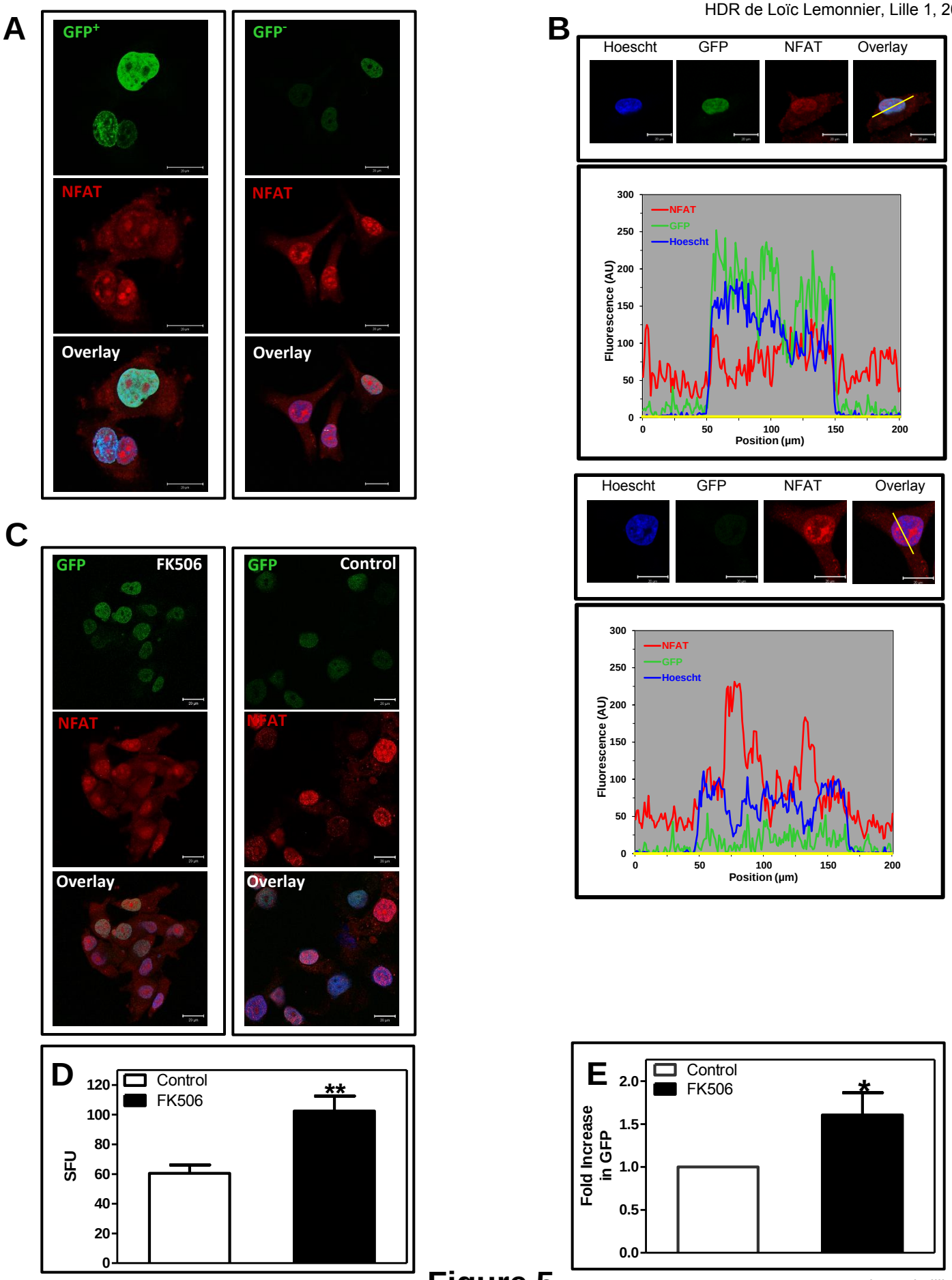

Figure 5

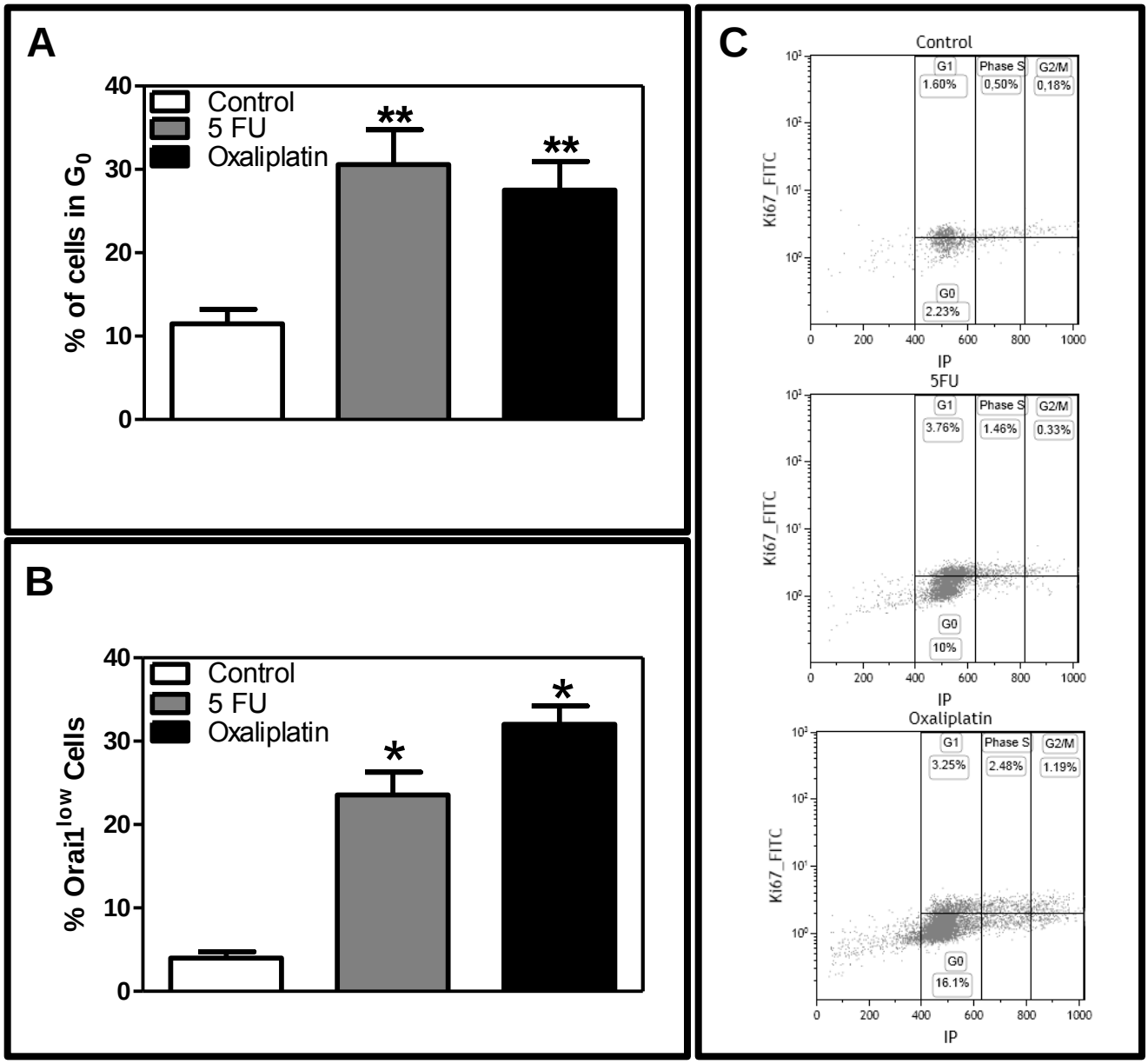

Figure 6

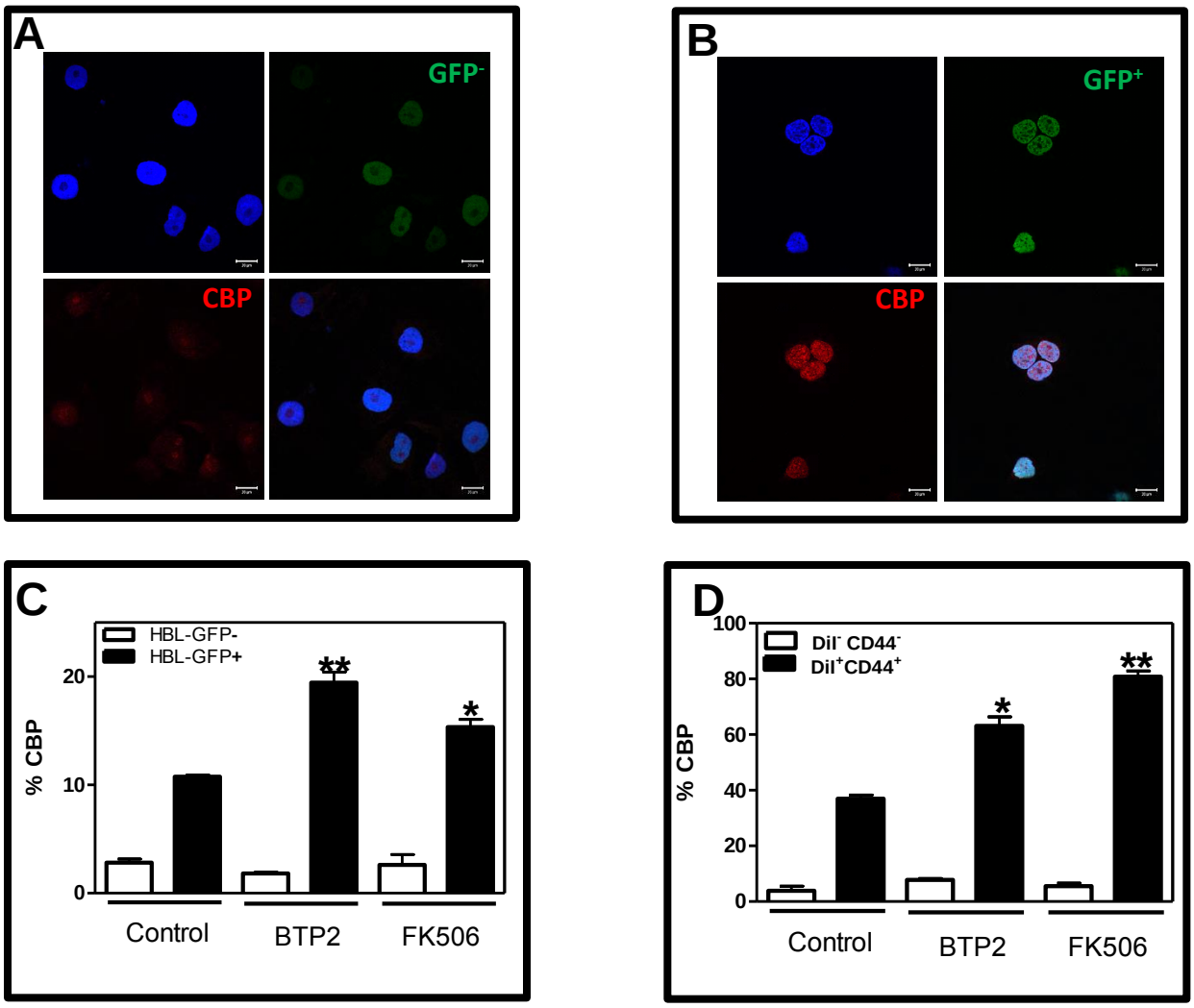

Table 3	Non CSCs / CSCs		NFAT+/CBP+ CSCs		NFAT+/CBP+ Non CSCs	
	HBL- H2B GFP	PC3	HBL- H2B GFP	PC3	HBL- H2B GFP	PC3
Control	13.9	17	4.18	1.18	5.91	1.20
BTP2	4	8.67	0.77	0.89	5.23	1.13
FK506	5.1	5.18	2.41	0.92	5.13	1.24

HDR de Loïc Lemonnier, Lille 1, 2017

Figure 7

Table S1

List of primers used for qRT-PCR.

No.	Name	Forward (5′-…-3′)	Backward (5′-…-3′)
1	hOrai1	ATGGTGGCAATGGTGGAG	CTGATCATGAGCGCAAACAG
2	hOrai3	GGCCAAGCTCAAAGCTTCC	CCTGGTGGGTACTCGTGGT
3	18s	CAGCTTCCGGGAAACCAAAGTC	AATTAAGCCGCAGGCTCCACTC

Supplementary Figure Legends:

Figure S1: GFP label retaining melanoma stem-like cells are quiescent and relatively undifferentiated. (A): HBL-H2B-GFP cells were incubated for 24h with tetracycline (pulse) to induce H2B-GFP expression. After 7 days of GFP dilution (chase) a subpopulation of slow cycling cells retains GFP (representative experiment) in monolayer cultures and (B): in cells grown under sphere-forming conditions for 7 days. Representative flow cytometry dot plot analysis. Upper right gating out GFP-negative cells (black) from the GFP positive (red) subpopulation (Auto = autofluorescence) at 0 and 7 days of dilution (C): Confocal microscopy of HBL-H2B-GFP total population after 7 days of GFP dilution in spheres. Shown are: H2B-GFP fluorescence (green) and immunofluorescence with anti-Ki67 (red) and anti-Melan A (white) antibodies, nuclei were stained with Hoechst 33342 (blue). Scale bar = 20µm.

Figure S2: Orai1 is a key actor in PC3 cells capacitative calcium entry. (A, B): Time courses of calcium ratios after 3 days of treatment with siRNA

targeting Orai1 (siOrai1) or Luciferase (siLuc) as control. Thapsigargin and calcium add-backs are indicated by bars. (C): Histogram summarizing ratio deltas observed in (A) and (B) after calcium addition to the bath; $p<0.001$. (D): Cells were labeled with DiI and after 7 days of dilution percentage of DiI LRCs was quantified by flow cytometry; **, $p<0.01$ (E): BTP2 increases SFU in PC3 total population; *, $p<0.05$.

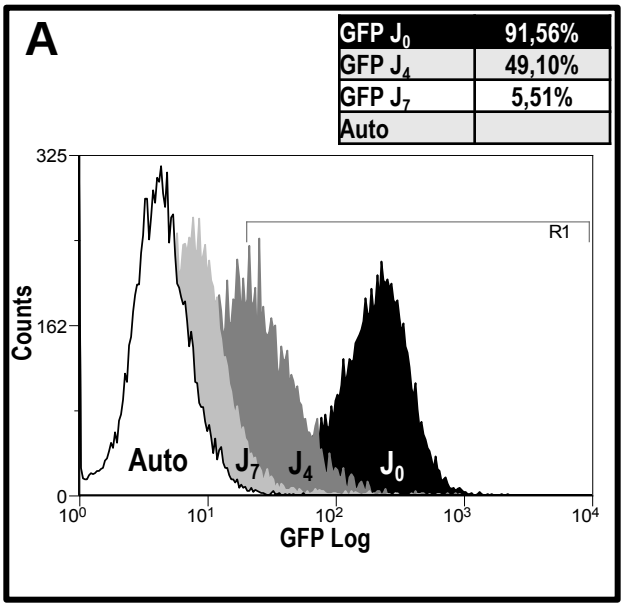

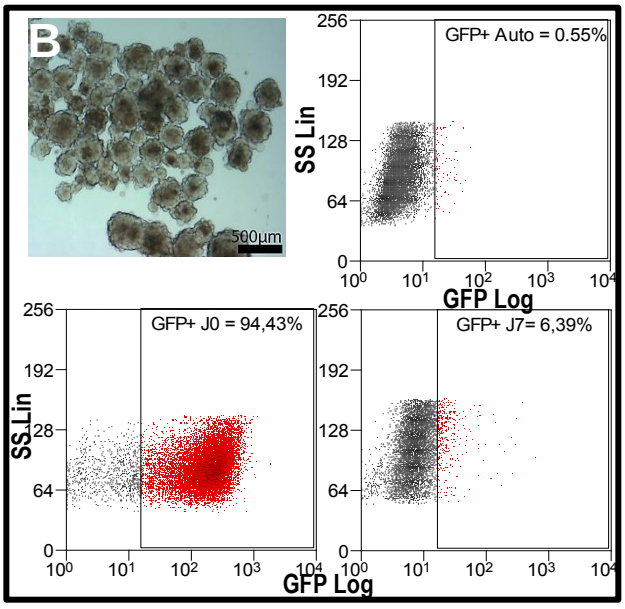

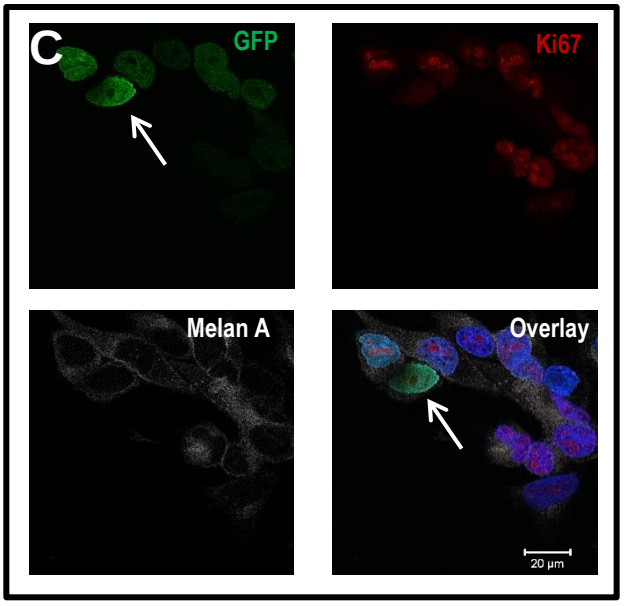

Supplementary Figure 1

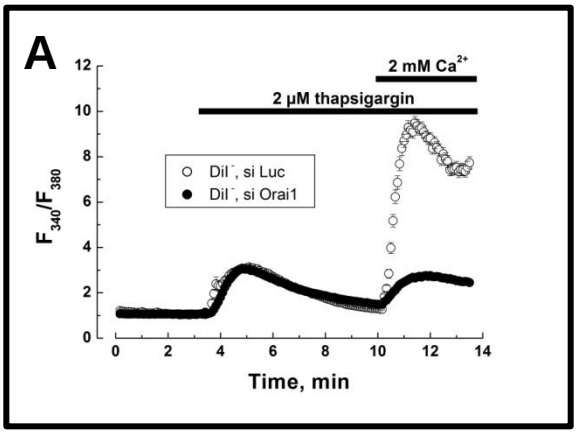

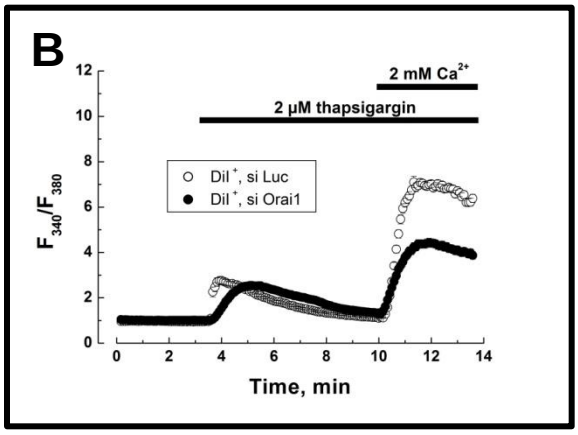

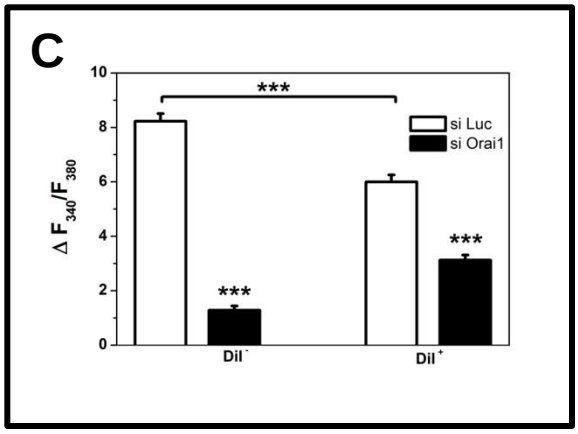

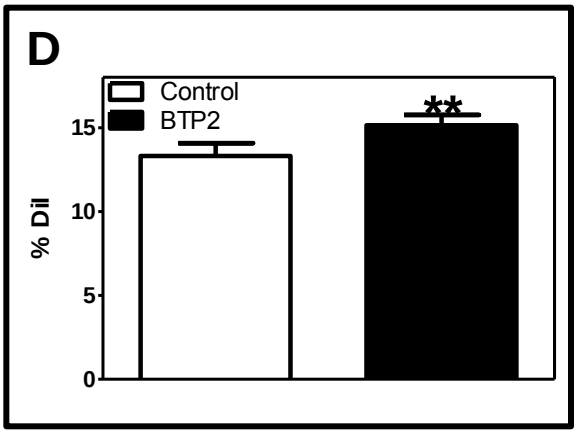

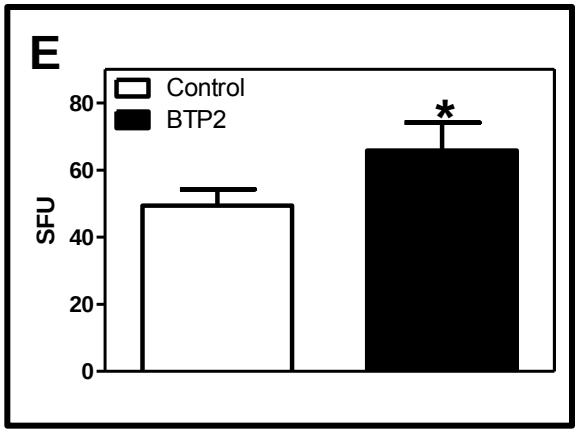

Supplementary Figure 2